Cysteine Biosynthesis in *Leishmania*

Tânia Filipa Ferreira Ramos
MPharm

Thesis submitted for the degree of Doctor of Philosophy

Institute of Infection, Immunity and Inflammation
College of Medical, Veterinary and Life Sciences
University of Glasgow

November 2013

Abstract

Every year 2 million people are diagnosed with leishmaniasis and 350 million are at risk of becoming infected. Spread throughout 88 countries in the world, leishmaniasis is a group of diseases comprising visceral, mucocutaneous and cutaneous leishmaniasis as the main forms. Visceral leishmanisis is the most severe form of the disease and is caused by *Leishmania donovani*. The parasite, *Leishmania*, is transmitted to humans by a sandfly vector. The absence of vector-control procedures and effective vaccines for humans makes chemotherapy the only weapon against leishmaniasis. Great efforts have been made to develop new drugs against these diseases, however toxic side effect and the constant cases of resistance call for new drug targets and drugs to be discovered and developed.

Cysteine is a key building block of trypanothione, an antioxidant unique to trypanosomatids that plays a pivotal role for the survival of the parasites. *Leishmania* can obtain cysteine in two ways, using the sulphydrylation and trans-sulphuration pathways. Humans lack the sulphydrylation pathway, thus this, and especially cysteine synthase (CS), of *Leishmania* could be a potential drug target. In order to determine the relative importance of these pathways, the levels of thiols at different stages of promastigote growth of wild-type, mutants lacking CS (∆*cs*), and CS episomal re-expressor parasite lines were determined. It was found that during logarithmic phase the mutant parasites have significantly reduced levels of thiols, which is reversed in the CS re-expressing parasite line. The mRNA and protein levels of cystathionine ß-synthase (CBS) were increased in ∆*cs L. donovani*, while this decrease was reversed in the CS re-expessing line. These data suggest that the reverse trans-sulphuration pathway compensates for the loss of CS to some extent but that this is not sufficient to maintain thiol levels during logarithmic growth. It was further found that ornithine decarboxylase mRNA is up-regulated while the protein levels appear to be reduced in the ∆*cs* parasite line. The latter was supported by the finding that the ∆*cs* mutant

parasites have low sensitivity to α-difluoromethylornithine, an inhibitor of ornithine decarboxylase.

The studies on the recombinant *L. major* cysteine synthase (CS) have shown that it can be inhibited by small peptides based on the C-terminal of *L. major* serine acetyltransferase. The CPM assay showed promising results to be used in high-throughput screening of CS inhibitors.

The data overall suggests that the levels of thiols are dependent on an adequate supply of cysteine through the sulphydrylation pathway. How this affects polyamine biosynthesis is yet to be investigated.

Author's declaration

I, Tânia Filipa Ferreira Ramos hereby declare that I am the sole author of this thesis and the work presented has not been submitted for any other degree. I have performed all the work apart from the following exceptions.

Chapter 3:

The construct pET21a^{+}-*Lmj*CS was provided by Dr Gareth Westrop (University of Strathclyde, UK).

Generation and characterization of the cysteine synthase crystal structure as shown on Figures 3.18 and 3.19.

Chapter 4:

Dr Lesley McCaig generated the *L. donovani* cysteine synthase knockout and re-expressor lines. These lines along with the *L. donovani* wild-type lines were used to infect hamsters. The hamsters were infected by Dr Elmarie Myburgh.

List of Publications

Fyfe, P.K., Westrop, G.D., **Ramos, T.**, Muller, S., Coombs, G.H., and Hunter, W.N. (2012). Structure of *Leishmania major* cysteine synthase. Acta Crystallographica Section F *68*.

Acknowledgements

First of all I would like to thank Professor Sylke Müller for giving me the opportunity to work in her laboratory. Thank you for all the teachings and great advice. Thank you for helping me grow as a scientist and a person. Thank you for your patience and care. I am very grateful to the past and present members of the Müller group for all the support and kind words. A special thanks goes to Dr Andy, Dr Ellie, Dr Larissa, Marco and Sonal who have helped me with my "silly questions" and to keep my spirits up! A special thanks to Dr Eva for taking the time and patience to teach everything I know about HPLC.

I would like to thank Professor Graham Coombs for allowing to work in his lab and for all the valuable advice.

I would like to thank Dr Gareth Westrop for all the valuable teaching and guidance given during my time at University of Strathclyde.

I would like to thank Dr Elmarie Myburgh for helping me recover the parasite lines from the hamsters.

I would like to thank Professor Buddy Ullman for the anti-ornithine decarboxylase antibody that allowed me to characterize the *L. donovani* lines.

I would like to thank my friends outside of University (you know who you are!). You are my family away from home. Thank you for all the laughter, cakes and chocolates! I will never forget you and I hope our friendship will last forever wherever you are or will be in the future!

And finally a very special thank you to the ones that made all this experience possible, my parents. Thank you for all the love, care, patience and education. Thank you for everything! I love you with all my heart.

Para os meus pais.

Table of contents

List of Tables

List of Figures

List of Abbreviations

3-MP	3 – mercaptopyruvate
3'13K	13 kb RNA
5'DST	*Leishmania* splice acceptor
AAT20	Amino acid transporter 20
AcoA	Acetyl Co-A
AdoMet	adenosyl methionine
AdoMetDC	Adenosyl methionine decarboxylase
AmpR	Ampicillin resistance
APS	Ammonium persulphate
APSK	5-phosphosulphate kinase
At	*Arabidopsis thaliana*
ATP	Adenosine triphosphate
ATPS	ATP sulphurylase
BSA	Bovine Serum Albumine
BSO	Buthionine sulfoximide
Cad	Cadaverine
CBL	Cystathionine β-liase
CBS	Cystathionine ß-synthase
CDC	Centers for Disease Control
CGL	Cystathionine γ-lyase
CGS	Cystathionine γ-synthase
CL	Cutaneous leishmaniasis
CPM	7-diethylamino-3-(4'maleimidylphenyl)-4-methylcoumarin
CPM	7-diethylamino-3-(4'maleimidylphenyl)-4-methylcoumarin
CS	Cysteine synthase
CSC	Cysteine synthase complex
Cys	Cysteine
dcAdoMet	Decarboxylated adenosyl methionine
ddH_2O	Double distilled water
DFMO	α-difluoromethylornithine

DMSO	Dimethyl sulphoxide
DNA	Deoxyribonucleic acid
DNPases	3'(5'),5'- diphosphonucleosidase 3'(2')-phosphorylase
dNTPs	Deoxyribonucleotide
dsDNA	Double-stranded DNA
DTPA	Diethylenetriamine pentaacetic acid
Ec	*Escherishia coli*
EDTA	Ethylenediaminetetraacetic acid
EPPS	N-[2-hydroxyethyl]-piperazine-N'[3-propanesulphonic acid]
FCS	fetal calf serum
gDNA	Genomic DNA
GIPLs	Glucoinositolphospholipids
GluDH	glutamate dehydrogenase
Gm	*Glycine max*
GPI	Glucosylphosphatidylinositol
GPI8	Glycosylphosphatidylinositol
GSH	Glutathione
HCys	Homocysteine
Hi	*Haemophilus influenza*
HIV	Human immunodeficiency virus
homoT$(SH)_2$	Homotrypanothione
HPLC	High pressure liquid chromatography
HRP	Horse radish peroxidase
hyg	Hygromicin phosphotransferase
Ig	Immunoglubulin
IPC	Inositol phosphoceramide
IPC	Inositol phosphoceramide
IPTG	Isopropyl ß-D-1-thiogalactopyranoside
Kan	Kanomycin
kDNA	Kinetoplastid DNA
L.	*Leishmania*
lacI	*lac* repressor
LB	Luria broth
Ld	*Leishmania donovani*

Lmj	*Leishmania major*
LPG	Lipophosphoglycan
ML	Mucocutaneous leishmaniasis
MOPS	3-(N-morpholino)propanesulfonic acid
MSP	Mercaptopyruvate sulphurtransferase
Mt	*Mycobacterium tuberculosis*
MTA	5'-methylthioadenosine
NADPH	Nicotinamide adenine dinucleotide phosphate
NADPH-SR	NADPH-dependent sulphite reductase
NEDA	N-1-naphthylethylenediamine
OAS	*O*-acetyl transferase
OD	Optic density
ODC	Ornithine decarboxylase
OPB	oligopeptidase B
OPS	*O*-phosphoserine
Orn	Ornithine
P-gpA	P-glycoprotein A
PAG	Propargylglycine
PAPS	3-phosphoadenosine 5-phosphosulphate
PAPS ST	3-phosphoadenosine 5-phosphosulphate sulfotransferase
PBS	Phosphate buffered saline
PCR	Polymerase chain reaction
PGA	Polyglutamate
PGDH	D-3-phosphoglycerate dehydrogenase
PLP	Pyridoxal 5'-phosphate
PPi	Pyrophosphate
PSAT	3-phosphoserine aminotransferase
PSP	3-phosphoserine phosphatase
Put	Putrescine
Put	Putrescine
RFU	Relative fluorescent units
RNA	Ribonucleic acid
RNS	Reactive Nitrogen Species
ROS	Reactive Oxigen Species

RPM	Rotation per minute
RT-PCR	Real-time PCR
RTS	Reverse transsulphuration pathway
S.D.	Standard deviation
S.E.M.	Standard error of the mean
sat	nourseothricin acetyltransferase
SAT	Serine acetyl-transferase
Sb^{III}	Trivalent sodium stibogluconate
Sb^{V}	Pentavalent sodium stibogluconate
SDS	Sodium dodecyl sulphate
SDS-PAGE	SDS-polyacrylamide gel electrophoresis
SP	Sulphydrylation pathway
Spd	spermidine
SpdS	Spermidine synthase
Spm	Spermine
SSC	Saline-sodium citrate
$T(SH)_2$	Dihydrotrypanothione
TCA	trichloroacetic acid
TCEP	*tris*(2-carboxyethyl)phosphine
TEMED	Tetramethylethylenediamine
TEV	*tabacco etch virus*
TryR	Trypanothione reductase
TryS	Trypanothione synthase
TS_2	Trypanothione disulphide
TSH	Trypanothione
TSH	Trypanothione
TXN	tryparodixyn
UMSBP	Universal minicircle sequence-binding protein
WHO	World Health Organisation

Introduction

1 Introduction

1.1 *Leishmania* parasites

Leishmania parasites are the causative agent of Leishmaniasis, a spectrum of diseases that affect people in 88 countries across four continents. About 2 million people are diagnosed every year with the disease while 350 million people are at risk of being infected with this parasite (WHO). *Leishmania* is a protozoan parasite of the order *Kinetoplastida* and family *Trypanosomatidae* (Myler, 2008). This family also comprises other known parasites, the *Trypanosoma brucei*, the causative agent of the African trypanosomiasis or sleeping sickness in humans and Nagana in cattle, and *Trypanosoma cruzi*, the causative agent of the human American trypanosomiasis or Chagas disease.

Leishmaniasis can exhibit at least three clinical forms: cutaneous, mucocutaneous, and visceral. Each condition depends on the host genetic variability and thus their immune response, the transmitting sandfly vector, environmental factors and on the species of parasite (Harhay *et al.*, 2011; McCall *et al.*, 2013; Peacock *et al.*, 2007).

Cutaneous leishmaniasis (CL), caused by *L. mexicana*, *L. major*, *L. tropica*, *L. amazonensis*, and *L. braziliensis*, mainly occurs in Afghanistan, Brazil, India, Nepal and Sudan. Mucocutaneous leishmaniasis (ML) is caused by *L. braziliensis, L. panamensis, L. guyanensis,* and *L. amazonensis*. It occurs in countries like Bolivia, Brazil and Peru. Cutaneous and mucocutaneous leishmaniasis generates slow-healing, localised ulcerations in the skin and mucosal surfaces. Visceral leishmanisis (VL) is the most severe form of the disease being lethal if left untreated. *L. donovani* and *L. infantum* are the main causative species of this disease. The countries affected are Bangladesh, Brazil, India, Nepal and Sudan. In this case the parasite disseminates through internal organs such as the liver, spleen, and bone

marrow, causing approximately 70,000 deaths per year (Harhay *et al.*, 2011; McCall *et al.*, 2013; Peacock *et al.*, 2007; WHO).

Leishmaniasis is a vector-borne disease, transmitted by 30 species of sandflies – *Phlebotomus* or *Lutzomyia* (Mishra *et al.*, 2009; Myler, 2008).

The *Leishmania* parasites are 5-14 μm long and occur as two distinctive morphologic forms: promastigote and amastigotes (Figure 1.1). The process of infection of the host starts when the phlebotomine sandfly takes its blood meal (Figure 1.2,1). In the blood stream, metacyclic promastigotes are readily captured in the dermis by cells of the host's immune system (Figure 1.2,2). Multiple cell types are involved, such as macrophages, neutrophils and/or dermal dendritic cells. Metacyclic promastigotes are the infective form with a small cell body and long flagellum that provides the parasites with the ability to swim rapidily. Inside the immune cells, the parasites undergo differentiation into aflaggelar amastigotes (Figure 1.2,3). These are located in the phagolysosome where the pH is low. Amastigotes are capable of replicating rapidly (Figure 1.2,4). This rapid replication will result in increased number of amastigotes inside the immune cell, which will lead to its death, and the release of parasites in to the blood stream (Figure 1.2,4). Here they are able to further infect more cells and to proliferate and develop the disease (Basu and Ray, 2005; Kaye and Scott, 2011; McConville *et al.*, 2007; Naderer and McConville, 2008; Sakthianandeswaren *et al.*, 2009).

When the sandfly takes a blood meal from an infected host, the proboscis of the insect captures the amastigotes (Figure 1.2,5,6). Inside the insect the parasites undergo differentiation as they migrate inside the insect gut (Figure 1.3). Amastigotes first differentiate into flagellated procyclic promastigotes (Figure 1.2,7). They are particularly resistant to the insect's digestive enzymes allowing them to multiply and proceed with their differentiation into the infective stage (metacyclic, Figure 1.2,8). Procyclic promastigotes are separated from the midgut of the insect by a type I perithrophic matrix, thus their differentiation into the next form, nectomonads (large and slender form), allows them to escape it. In the midgut, the nectomonads

differentiate into leptomonads (shorter form) and undergo a second multiplication. It is still not known if the haptomonads originate from nectomonads or from leptomonads, but they do precede the differentiation into non-dividing metacyclics parasites. Haptomonads are non-motile leaf-like parasites with short flagella and are found in the stomodeal valve (Figure 1.3). Metacyclics are found behind the stomodeal valve where they accumulate, waiting for the sandfly to take another blood meal and to re-Final Thesis 28 novstart of their life cycle (Kamhawi, 2006).

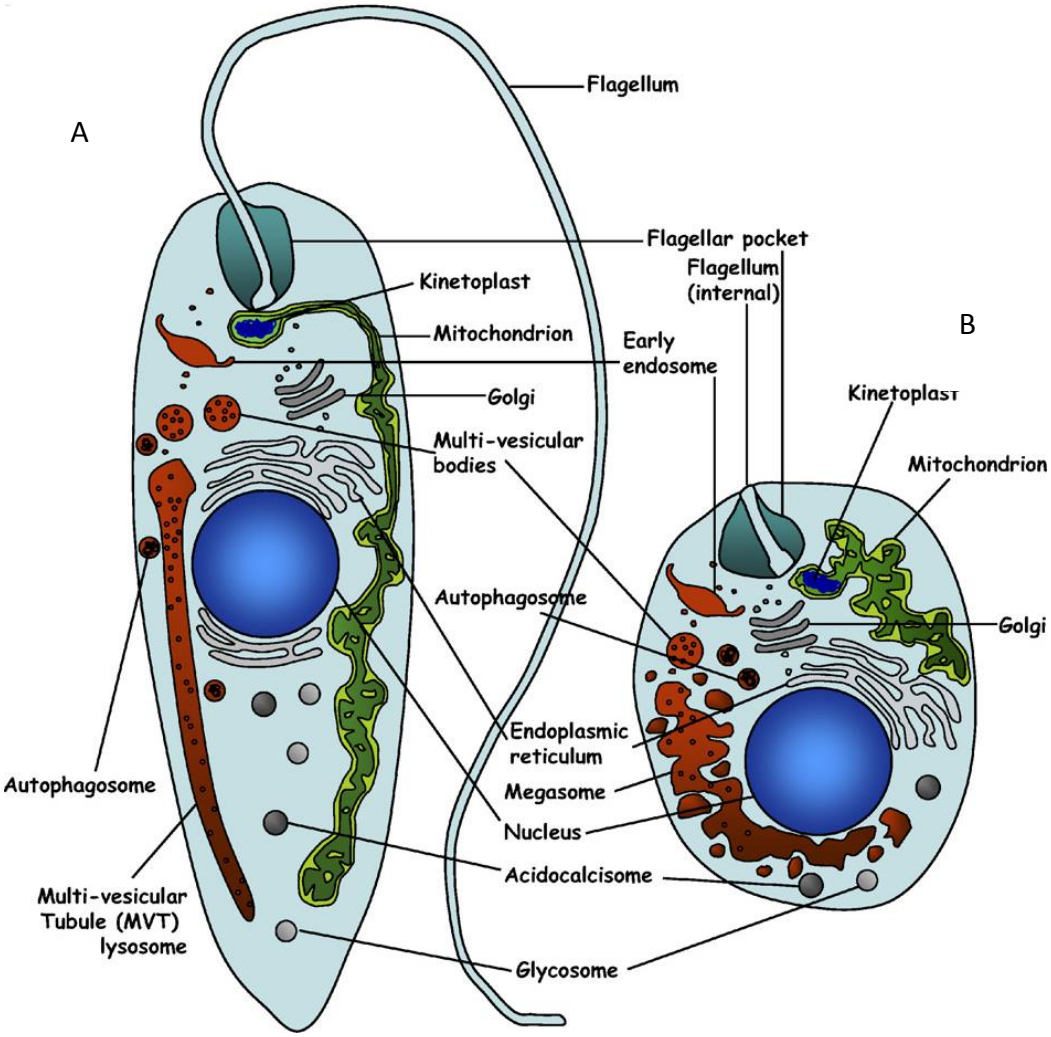

Figure 1.1 – The two forms of the *Leishmania* parasite cell.

Schematic diagram of a promastigote (a) and a amastigote (b) cell. The anterior side of the parasite is demarked by the flagellar pocket (Besteiro *et al.*, 2007).

Printed with permission from Elsevier.

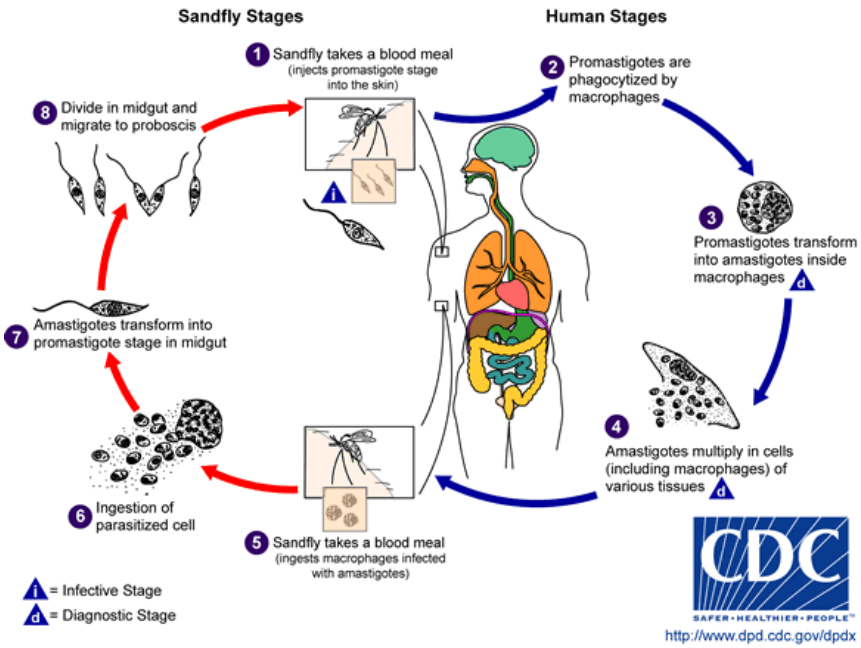

Figure 1.2 – *Leishmania* life cycle.

Schematic diagram showing each step of *Leishmania* parasite life cycle. (1) a metacyclic form-containing sandfly takes a blood meal infecting the host; (2) in the host's blood, macrophages phagocytise the promastigote parasites; (3) in the macrophage the promastigotes differentiate into amastigotes; (4) the amastigotes replicate leading to the death of the immune system cell and the spread of the amastigotes in the blood stream; (5,6) a sandfly gets infected by taking a blood meal from an infected host; (7) in the sandfly the amastigotes differentiate into promastigotes; (8) the promastigotes undergo differentiation into metacyclics, the infective stage (CDC).

Printed with permission from the Center for Disease Control.

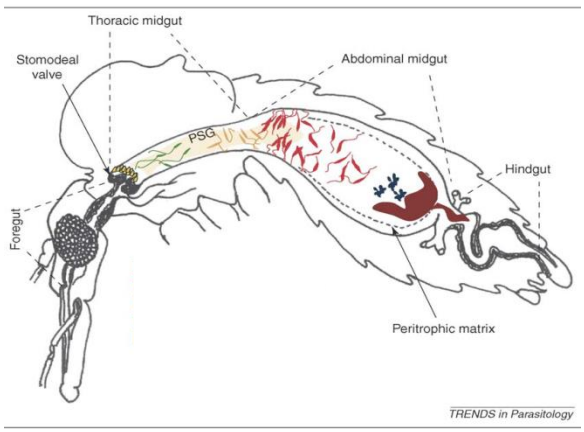

Figure 1.3 – Anatomy of a sandfly.

This schematic diagram shows the names of the compartments of a sandfly body (Kamhawi, 2006).

Printed with permission from Elsevier.

1.1.1 Interactions between *Leishmania* and macrophages

Promastigote cells are coated by a glycocalyx, which consists of glycosylphosphatidylinositol (GPI)-anchored proteins, GPI-anchored phosphoglycan, lipophosphoglycan (LPG) and a family of free GPI glycolipids termed glycoinositolphospholipids (GIPLs) (Naderer and McConville, 2008). Mutant analysis showed that LPG protects the cells from a transient rise in the reactive oxygen species (ROS) generated during phagocytosis (Naderer and McConville, 2008). Studies on *L. major* concluded that LPG is essential for their infectivity (Naderer and McConville, 2008).

On the contrary, *L. mexicana* promastigotes do not require LPG for their virulence. In fact, LPG is downregulated during the infective stage of the parasite. In terms of resistance to ROS and RNS (reactive nitrogen species), *L. mexicana* proved to be more resistant than *L. major* or *L. donovani* (Naderer and McConville, 2008).

The uptake of *L. major* promastigotes is promoted by the presence of dead parasites in the inoculums due to the high levels of surface exposed phosphatidylserine that promote the uptake of dead and live promastigotes by neutrophil receptors (Naderer and McConville, 2008).

Conversly, amastigotes have low expression levels of LPG and a less complex glycocalyx (Naderer and McConville, 2008). This coat prevents the release of parasitic peptides that could be presented to the host immune system (Naderer and McConville, 2008). Amastigotes produce inositol phosphoceramide (IPC) using sphingolipid bases taken by the host, which may complement GIPLs in their function (Naderer and McConville, 2008).

The amastigote plasma membrane is rich in phosphatidylserine which may proportionate the entrance to the cell without activating the microbicidal processes or inflammatory responses (Naderer and McConville, 2008).

1.2 Treatment

Because of the absence of vector-control measures and effective vaccines, humans rely solely on chemotherapy to treat leishmaniasis. For more than 60 years pentavalent antimonials (e.g. sodium stibogluconate and meglumine antimoniate) have been used as the primary treatment of leishmaniasis. Other drugs also available for treatment of leishmaniasis are amphotericin B and its lipid formulations, pentamidine, paramomycin, miltefosine, sitamaquine as well as imidazoles and triazoles (Croft and Coombs, 2003; Croft *et al.*, 2006). The mechanism of action of these drugs is not completely understood. The build up of resistance to antimonial drugs in the city of Bihar in India, the severe side effects of the other available drugs, and the differences in affectivity between species, and parasite stages, emphasises the need to discover new effective drugs against leishmaniasis (Coombs *et al.*, 1983; Singh *et al.*, 2012; Sundar, 2001; Sundar *et al.*, 2010; Thakur *et al.*, 2001).

Sodium stibogluconate (Sb^{V}) is a pro-drug believed to be activated (converted into trivalent form, Sb^{III}) either within macrophages or amastigotes, but not in the promastigotes. Both the trivalent and the pentavalent form have anti-*Leishmania* activity by DNA fragmentation (Cunningham and Fairlamb, 1995; Singh *et al.*, 2012). However, the pentavalent form is ineffective in the promastigote form. It has been demonstrated that the antimony drug inhibits the trypanothione reductase enzyme and affects the thiol balance in the cell by promoting the extrusion of thiols, which reduces the thiol buffering capacity and leaves the cell more susceptible to oxidative stress (Cunningham *et al.*, 1994; Mandal *et al.*, 2007; Wyllie *et al.*, 2004; Wyllie *et al.*, 2008). Thiol levels have been shown to be elevated in resistant forms of *Leishmania* parasites. Antimonials have been used in the treatment of cases of VL and CL. Although very efficient, this drug is expensive, its administration is intravenous, and there are severe cases of resistance reported in Bihar, India (Singh *et al.*, 2012; Stauch *et al.*, 2012; Sundar, 2001; Sundar *et al.*, 2010; Thakur *et al.*, 2001). Resistance to these drugs seems to be associated with efflux pumps (P-glycoprotein and multi-drug resistance protein A) that

extrude the drug outside the cell. It has also been reported that pentamonials inhibit the trypanothione reductase (Ashutosh *et al.*, 2007; Cunningham and Fairlamb, 1995; Mittal *et al.*, 2007; Mukhopadhyay *et al.*, 1996).

Amphotericin B has been used to treat cases of VL, CL, and ML, and as second choice drug to treat cases of VL resistance in Bihar, India. This drug has a high affinity for ergosterol present in *Leishmania* and fungi but absent in mammalian cells. However, it is still an expensive and difficult to administer drug (via 4 hour parenteral infusion) that has been shown to have toxic side effects (Bray *et al.*, 2003; Croft and Coombs, 2003; Croft and Olliaro, 2011; Singh *et al.*, 2012). Lipid formulations of this drug have been engineered to circumvent the side effects with success, however there are still associated with high costs (Pham *et al.*, 2013; Singh *et al.*, 2012).

Pentamidine has been used as an alternative for antimonials. It is thought to enter the *Leishmania* cell by the polyamine and arginine transporter and to accumulate in the mitochondria. Currently, due to low efficacy and toxic side effects, this drug has been withdrawn from use in India. Its side effects include nephrotoxicity, hypoglycaemia and hypotension (Basselin *et al.*, 2000; Basselin *et al.*, 1996; Bray *et al.*, 2003; Coelho *et al.*, 2007; Jha, 1983; Kandpal and Tekwani, 1997; Singh *et al.*, 2012).

Paramomycin cures both VL and CL. In bacteria its mechanism of action is inhibition of protein synthesis by binding to the 30S subunit of ribosomes. In *Leishmania* it is also known to affect the mitochondrion (Singh *et al.*, 2012; Thakur *et al.*, 2000). There are no cases of resistance, possibly due to its limited used. Nonetheless, one must not underestimate its antibiotic nature (Singh *et al.*, 2012).

Miltefosine is the first oral drug available for leishmanisis. It has been used in Bihar, India to tackle the VL resistance cases. Its oral availability makes it easy to administer as no specialised skills are required which is a necessety in poor areas of the globe. Unfortunately, there is variability of efficacy

between species. There are still no reported cases of resistance to this drug. Being an oral drug allows its miss-use in the endemic areas and therefore new drugs should be available. Its mode of action is unclear. Miltefosine is associated with teratogenicity and abortifacient side effects, thus cannot be used in pregnant women (Croft and Engel, 2006; Escobar *et al.*, 2002; Perez-Victoria *et al.*, 2006; Seifert *et al.*, 2003; Sundar *et al.*, 2006).

Sitamaquine is an oral drug developed for the treatment of VL. It inserts within biological membranes accumulating itself in *Leishmania*'s acidic compartments (Jha *et al.*, 2005; Lopez-Martin *et al.*, 2008; Sundar and Chatterjee, 2006).

Azols have been shown to have differential activity in CL and VL cases. Differences have been observed between species. The similarities between fungi and *Leishmania* regarding ergosterol content makes it possible for these drugs to be used against leishmaniasis. However, side effects affect the biosynthesis of adrenal and testicular steroids and thus limit their use. (Croft and Coombs, 2003).

The treatment of leishmaniasis depends on sensitivity variation between species, emergence of drug resistance (e.g. the city of Bihar in India), and variation of drug activity within the immune response of the patient (Croft and Coombs, 2003; Croft *et al.*, 2002; Mandal *et al.*, 2007; Seifert *et al.*, 2010; Stauch *et al.*, 2012; Sundar, 2001).

The use of combination therapy can help to decrease the length of treatment necessary and lower the drug dose needed thus avoiding drug resistance. Examples of drug combinantions that have been studied as alternatives to anti-leishmanisis therapies are the combination of miltefosine and ambisome (effective but still presenting side effects) (Singh *et al.*, 2012); the synergy of paramomycin with gentamicine has shown to be effective in CL cases (Ben Salah *et al.*, 2009); sitamaquine and miltefosine have been proposed as a possible combination as both are oral drugs, however more studies need to be done (Sangraula *et al.*, 2003); and lovastatin and miconazole, both

cholesterol lowering agents, showed some evidence of inhibition of sterol biosynthesis (Haughan *et al.*, 1992).

There are many ways to research new drugs. Drugs that are already available can be further investigated to determine their toxicity for parasites (e.g. azols, fexinidazole, tricyclics compounds). Or new drug targets can be investigated. However, new therapeutics must be low in cost; available in oral formulations; require a short therapeutical course; and have the ability to be used in drug combinations in order to avoid drug resistance and to address cases of double infection with VL and HIV virus (Chibale *et al.*, 2000; Renslo and McKerrow, 2006; Wyllie *et al.*, 2012).

The main mode of defence against antimonial drugs seams to be due to extrusion of thiols (trypanothione and glutathione) and thus imbalance of redox homeostasis. Cysteine is the active amino acid in the structure of low-molecular weight thiols and therefore its synthesis could possibly provide a good base of study for new drug targets. Drugs that target this biosynthetic pathway could be used in combination therapy with antimonials, possibly improving its efficacy or they can be used on their own to allow macrophages to win the redox battle against *leishmania*.

1.3 Cysteine biosynthesis

The cysteine biosynthetic pathway in *Leishmania* has just recently begun to be characterised. Thus this research must rely on knowledge provided by well-characterised species such as *Trymanosoma cruzi*, *Arabidopsis thaliana*, *Escherichia coli*, *Saccharomyces cerevisiae*, *Salmonella typhimurium* and *Mycobacterium turberculosis* (Becker *et al.*, 1969; Duszenko *et al.*, 1992; Gorman and Shapiro, 2004; Kredich *et al.*, 1969; Muller *et al.*, 2003; Nozaki *et al.*, 2001; Salsi *et al.*, 2010; Thomas and Surdin-Kerjan, 1997; Wirtz and Droux, 2005; Zhao *et al.*, 2006).

1.3.1 The sulphydrylation pathway and the reverse trans-sulphuration pathway

Williams *et al.* (2009), have characterised the cysteine biosynthetic pathway in *Leishmania major*. There are two cysteine biosynthetic pathways available in this parasite, the sulphydrylation pathway (SP) or *de novo* biosynthesis pathway and the reverse trans-sulphuration pathway (RTS). The essentiality of cysteine has not yet been demonstrated in *Leishmania* parasites. In members of the same family, it is an essential growth factor for *Trypanosoma brucei*, and *Trypanosoma cruzi* is able to synthesise it via the RTS pathway. *L. major* also has forward transsulphuration and thus can synthesise methionine, an essential amino acid in humans (Duszenko *et al.*, 1992; Nozaki *et al.*, 2001; Williams *et al.*, 2009).

Figure 1.4 shows a schematic diagram of the two biosynthetic pathways. Briefly, serine acetyltransferase (SAT) generates O-acetylserine (OAS) by transferring acetate from acetyl-CoA to serine. This reaction is followed by that of cysteine synthase (CS), a pyridoxal 5'-phosphate (PLP)-dependent protein that catalyses the formation of cysteine from OAS using sulphide donors (Bonner *et al.*, 2005). RTS forms homocysteine from methionine, homocysteine is converted into cysteine in two steps and is catalysed by

cystathionine ß-synthase (CBS) and cystathionine γ-lyase (CGL) (Francois *et al.*, 2006; Schnell *et al.*, 2007; Williams *et al.*, 2009).

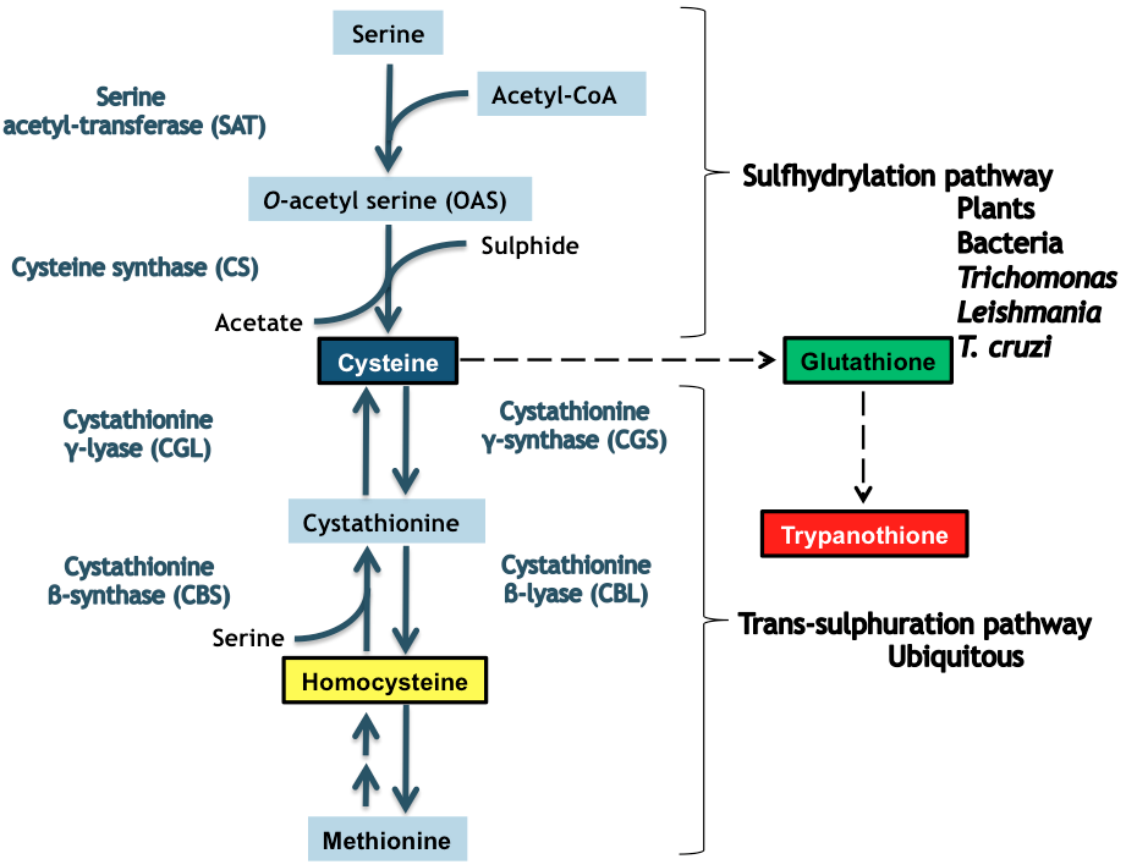

Figure 1.4 – Cysteine biosynthetic pathway.

In *Leishmania* parasites cysteine can be synthesised from serine by the sulphydrylation pathway (SP) or from methionine the reverse trans-sulphuration pathway (RTS). Apart from this parasite, *Trychomonas*, *T. cruzi*, plants and bacteria are able to use serine to synthesise cysteine. RTS is a ubiquitous pathway. For humans cysteine is an essential amino acid that is used in the synthesis of methionine. Cysteine is the building block of glutathione and trypanothione. Trypanothione is the major low-molecular weight thiol in *Leishmania* and is exclusive to trypanosomatids. The main thiols are highlighted: cysteine (blue), homocysteine (yellow), glutathione (green), and trypanothione (red).

1.3.1.2 Cysteine synthase

The sulphydrylation pathway is absent in humans, thus potentially making is a good platform from which to begin a targeted novel drug search. One important enzyme of this pathway is cysteine synthase. According to the findings of Williams *et al.* (2009), *Lmj*CS belong structurally to the type A class of CS(s). This characteristic is shared by bacteria and *A. thaliana* CS(s) who, like *Lmj*CS, are able to form a complex with SAT and accepts O-acetyl serine as a substrate (Kumaran and Jez, 2007). This is possible due to the presence of a conserved substrate-binding β8-β9 loop present in *Lmj*CS (predicted structure) and other type A CS(s). SAT binds to this motif to form a complex with CS. When bound, SAT C-terminal residues cover CS's active site, inhibiting its activity. OAS can disrupt this complex (Kumaran and Jez, 2007). As said before, type A CS(s) can accept O-acetyl serine, which is a relatively small substrate when compared with O-phosphoserine that is accepted by *Aeropyrum pernix* and *Trichomonas vaginalis* CS(s) (Mino and Ishikawa, 2003; Westrop *et al.*, 2006). This characteristic is also conferred by the substrate-binding β8-β9 loop. This loop restricts the access to the active side pocket, allowing only small positively charged substrate to bind to CS. Type B CS(s) lack this loop which allows them to accept larger and negatively charged substrates. However, they are also unable to form complex with SAT (Kumaran and Jez, 2007; Mino and Ishikawa, 2003; Schnell *et al.*, 2007; Westrop *et al.*, 2006; Williams *et al.*, 2009; Zocher *et al.*, 2007).

The enzymatic reaction of CS with OAS has been well described in both plant and bacterial enzymes. The pyridoxal 5'-phosphate (PLP) co-factor is bound to a lysine in the CS's active site forming an internal Schiff base (Figure 1.5, step 1). In the first half of the reaction, OAS binds to PLP forming an external Schiff base (Figure 1.5, step 2). Its rearrangement generates the release of one molecule of acetate and the formation of an α-amino acrylate intermediate (Figure 1.5, step 3). In the second half-reaction sulphide attacks the nucleophile ß-carbon of the aminoacrylate intermediate, and the α-carbon is re-protonated resulting in the binding of the cysteine as an external Schiff base (Figure 1.5, step 4). The final product is released via

regeneration of the external aldimine (Figure 1.5, step 1) (Bonner *et al.*, 2005; Huang *et al.*, 2005; Schnell *et al.*, 2007).

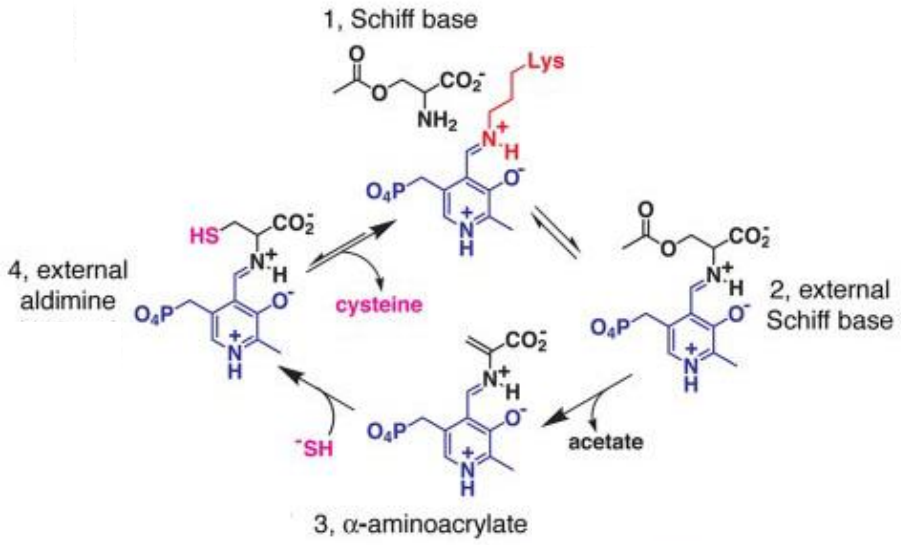

Figure 1.5 – The cysteine synthase reaction.

The reaction catalysed by cysteine synthase (red) where *O*-acetyl serine (black) is converted into cysteine (pink), in the presence of the co-factor pyridoxal 5'-phosphate (blue), in a two-step reaction that involves the formation of an α-amino acrylate intermediate.

Printed with permission from the American Society for Biochemistry and Molecular Biology.

In *Mycobacterium tuberculosis* and *Salmonella typhimurium* CS this last step is accompanied by a large conformational change that leads to the closure of the active site (Schnell *et al.*, 2007). However, in *A. thaliana* the correspondent structure remains open and the later product is assumed to mimic the external aldimine (Schnell *et al.*, 2007).

1.3.1.2.1 Cysteine synthase in plants

Plants have three types of CS: type A located in the cytosol; type B located in the chloroplast; and type C in the mitochondria. The cysteine biochemical pathway comprises three stages: the fixing of sulphate and its conversion into sulphide by assimilatory reduction; the synthesis of OAS from serine,

catalysed by serine acetyl-transferase; and the reaction of sulphide with OAS, catalysed by CS, with the formation of cysteine (Bonner *et al.*, 2005; Heeg *et al.*, 2008; Hell *et al.*, 2002; Warrilow and Hawkesford, 2002; Wirtz *et al.*, 2004).

The exclusive location of assimilatory sulphate reduction in plastids suggests that sulphide is able to reach cysteine synthesis in cytosol and mitochondria, possibly by diffusion of H_2S through membranes (Heeg *et al.*, 2008).
Cysteine synthesis is the terminal step in sulphur assimilation and is an important entry reaction of reduced sulphur into metabolism (Croft *et al.*, 2006).

The cysteine synthesis in *A. thaliana* cells shows that CS isoforms A (cytoplasm) and B (plastids) are more abundant and active than the isoform C (mitochondria). Cysteine and sulphide must be exchanged between the organelles and cytosol, the compartments can compensate for cysteine deficiency to some extent among themselves, and mitochondrial CSC is essential for normal growth (Heeg *et al.*, 2008).

In *A. thaliana* the levels of CS and SAT are not the same in the three compartments. However the quantity of cysteine and GSH is maintained in the cell with synthesis possibly being compensated by uptake (Heeg *et al.*, 2008).

1.3.1.2.2 Cysteine synthase in bacteria

S. typhimurium has one CS enzyme, whereas *M. tuberculosis* and *E. coli* have two CS enzymes, CysK and CysM. CysK uses sulphide from the sulphate reduction pathway as a source of sulphide, whereas CysM is able to use thiosulphate or larger sulphide donors. Additionally, CysK uses OAS as substrate and CysM uses O-phophoserine, which is important when the microorganism is in an anaerobic environment. CysM from *M. tuberculosis* can present as an open or closed conformations, of which there are two types, depending on the presence of substrate or a sulphur carrier. As seen in

plants, CysM has PLP bound to the lysine of the active site. In the closed conformation the surface loops are rearranged and the last five amino acids of the C-terminal of CysM are inserted in the active site. In the open conformation the active site pocket is big enough to accommodate large substrates like OPS. In the closed conformation, the C-terminal stabilises the α-amino acrylate intermediate and works as a selector for the sulphur donor and leaves space for the release of acetate. The CysM is of particular interest for the synthesis of pharmaceuticals and agrochemicals since it can accommodate larger compounds (Agren *et al.*, 2008; Agren *et al.*, 2009; Kredich *et al.*, 1969; Zhao *et al.*, 2006; Zocher *et al.*, 2007).

	Cysteine Biosynthetic pathways			Cysteine synthase			
	SP	RTS	Sulphide source	CS Substrate	Presence of β8-β9 loop	Complex with SAT	Reference
Parasites							
Leishmania major	**Yes**	**Yes**	MSP/3-MP (?)	OAS	**Yes**	**Yes**	Williams *et al.* (2009)
Trypanosoma brucei	No	**Yes**					Duszenko *et al.* (1992)
Trymanosima cruzi	No	No					Miles *et al.* (2009) Nozaki et al. (2001)
Trychomonas vaginalis			Thiosulphate	OPS	No	No	Westrop *et al.* (2006)
Entamoeba histolitica	**Yes**	No		OAS	No	No	Kumar *et al.* (2011) Chinthalapudi *et al.* (2008)
Bacteria							
Escherishia coli	**Yes**	No	Hydrogen sulphide (CysK) Thiosulphate (CysM)	OAS (CysK) OPS (CysM)			Claus *et al.* (2005) Zhao *et al.* (2006) Zocher *et al.* (2007)
Mycobacterium turberculosis	**Yes**	No	Hydrogen sulphide (CysK) Thiosulphate (CysM)	OAS (CysK) OPS (CysM)			Agren *et al.* (2008)
Salmonella typhimurium	**Yes**	No	Sulphur assimilatory pathway	OAS			Rabeh *et al.* (2004) Becker *et al.* (1969)
Yeast							
Saccharomyces cerevisiae	No	**Yes**					Thomas et al. (1997)
Plants							
Aeropyrum pernix	Yes	No	Thiosulphate	OPS	No	No	Mino *et al.* (2003)
Arabidopsis thaliana	Yes	No	Sulphur assimilatory pathway	OAS	**Yes**	**Yes**	Warrilow *et al.* (2002) Heeg *et al.* (2008) Bonner *et al.* (2005)
Humans							
Homo sapiens	No	**Yes**					Banerjee *et al.* (2005)

Table 1.1 – Cysteine biosynthetic pathways.

The table summarises the presence/absence of cysteine biosynthetic pathways, sulphur sources, CS structural characteristics, and substrate in different species (please see table for references). Humans and yeast use cysteine acquired from the exterior of the cells to synthesise methionine. (SP) sulphydrylation pathway; (TS) trans-sulfuration pathway; (CS) cysteine synthase; (SAT) serine acetyl-transferase; (OAS) O-acetyl transferase; (OPS) O-phosphoserine; (MSP) mercaptopyruvate sulfurtransferase; (3-MP) 3-mercaptopyruvate.

1.3.1.2.3 The cysteine synthase complex

SAT and CS are known to form a complex, the cysteine synthase complex (CSC) in plants and bacteria. This complex is made of one SAT and two CSs. The CSC was first described in *S. typhymurium* as a bifunctional enzyme complex by Kredich *et al.*, (1969).

In plants and bacteria the source of sulphide comes from the inorganic sulphur assimilation pathway (Figure 1.6 and 1.7). In bacteria it is important that cysteine biosynthesis is regulated because it is interlinked with nitrogen and carbon assimilation as well as sulphur assimilation (Figure 1.7). In plants cysteine biosynthesis regulates the level of sulphur in the cell (Birke *et al.*, 2012; Salsi *et al.*, 2010). In plants, cysteine is the sulphide donor for the synthesis of methionine, glutathione, phytochelatins, iron-sulphur clusters, vitamin cofactors, and multiple secondary metabolites (Bonner *et al.*, 2005; Warrilow and Hawkesford, 2002; Wirtz *et al.*, 2004).

CSC is thought to regulate sulphur assimilation and to modulate cysteine biosynthesis. When bound in the complex, the SAT activity increases and the CS activity decreases. CS activity has been reported to be much higher than SAT activity therefore cysteine biosynthesis is likely to be limited by SAT activity. SAT in the absence of CS is less active, thus the association with CS promotes the activity of SAT. Interaction between SAT and CS and cysteine synthesis depends on the sulphur status: if sulphur becomes scarce sulphide is missing to stabilize the CSC, and the OAS accumulated from SAT activity, dissociates from the complex. This results in a decrease in SAT activity, reduced acetyl-CoA consumption, and OAS formation until the cell is resupplied with sulphide (Berkowitz *et al.*, 2002; Bogdanova *et al.*, 1997; Bonner *et al.*, 2005; Droux *et al.*, 1998; Francois *et al.*, 2006; Heeg *et al.*, 2008; Kumaran *et al.*, 2007b;. Wirtz *et al.*, 2006).

At high concentrations, OAS isomerizes to N-acetylserine in an irreversible chemical process that acts as an inducer of the gene expression for sulphate permease. These genes are consequently expressed to enhance sulphate

uptake and sulphate reduction, thus providing sulphide for cysteine synthesis. Like in plants and bacteria, *Entamoeba* acquires inorganic sulphur via the sulphide reduction pathway (Berkowitz *et al.*, 2002; Bogdanova *et al.*, 1997; Bonner *et al.*, 2005; Droux *et al.*, 1998; Francois *et al.*, 2006; Heeg *et al.*, 2008; Kumaran *et al.*, 2007b;. Wirtz *et al.*, 2006). In *T. vaginalis*, Westrop *et al.* 2006 postulated that sulphide provision might be via homocysteine desulphurase (or methionine γ-lyase) because these parasites lack the *de novo* pathway to generate sulphide.

Excess of Cys inhibits SAT activity in a negative feedback loop. In plants each of the cytosolic, chloroplast and mitochondrial SAT proteins have a distinct sensitivity towards cysteine which is dependent on the cysteine available in each compartment. This feedback is critical and thought to regulate SAT activities in *A. thaliana* (Wirtz *et al.*, 2012).

In the presence of sufficient sulphur, the CS and SAT enzymes form the CSC, possibly as a mechanism for sulphur detoxification. When the intracellular levels of sulphur are low, OAS accumulates because free CS is unable to generate cysteine due to the lack of sulphide. An increase in OAS levels (concentrations of 0.1 and 1.0 mM OAS) lead to complex dissociation, which down-regulates SAT. Nonetheless, this increase activates expression of genes encoding sulphate transporters, ATP sulphurylase, CS, and SAT, leading to an increase in sulphur uptake and reduction. With sulphur levels elevated, free CS catalyses cysteine formation which reduces OAS levels. This allows association of SAT and CS, activation of SAT, and resumption of cysteine biosynthesis. Biochemical experiments show that in *A. thaliana* CSC has the same function in cytosol, mitochondria, and plastids (Birke *et al.*, 2012; Bonner *et al.*, 2005; Francois *et al.*, 2006; Heeg *et al.*, 2008; Kredich *et al.*, 1969; Kredich and Tomkins, 1966; Olsen *et al.*, 2004).

The active site pocket of CS-type A of *S. typhimurium* closes when the substrate binds. Only a small channel is left open so acetate can leave and hydrogen sulphide can enter and start the second part of the reaction. *E. coli* CS-typeB has highly conserved residues that are also present in *S.*

typhimurium. The same conformational changes are reported for this enzyme site pocket. However, there are some differences on the flexible loop located on the opposite site of the PLP binding site, which reflects the capacity of type B *E. coli* CS to use thiosulphate instead of hydrogen sulphide. The overall differences between type A and type B bacterial CS reside in a loop located between ß8 and ß9 for *S. typhimurium* CS type A, *E. coli* CS type B and *A. thaliana* CS, and located between ß13 and ß14 for *A. pernix* CS. These differences comprise the ability of type B enzymes to use thiosulphate as an alternative substrate. The type B proteins do not form complexes with SAT while the type A CS forms a regulatory complex with SAT. Type B CS contains a conserved positively charged residue (arginine), which affects substrate specificity (Kredich *et al.*, 1969; Oda *et al.*, 2005; Westrop *et al.*, 2006; Wirtz and Hell, 2006; Zhao *et al.*, 2006).

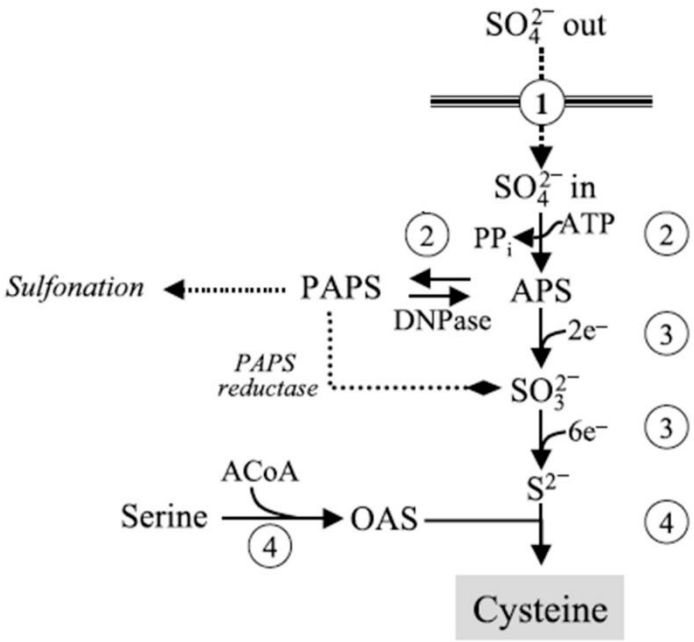

Figure 1.6 – The sulphur assimilation pathway in Plants.

The assimilation of sulphur in plants can be divided in four stages: (1) the uptake of sulphate; (2) the activation of sulphate; (3) the reduction of sulphate; and (4) the synthasis of cysteine. (PPi) pyrophosphate; (APS) adenosine 5' phosphosulphate; (DNPases) 3'(2'),5'-diphosphonucleosidase 3'(2')-phosphorylase; (PAPS) adenosine 3'-phospho 5'-phosphosulphate; (AcoA) Acetyl Co-A; (e^-) elctron.

Printed with permission from Springer.

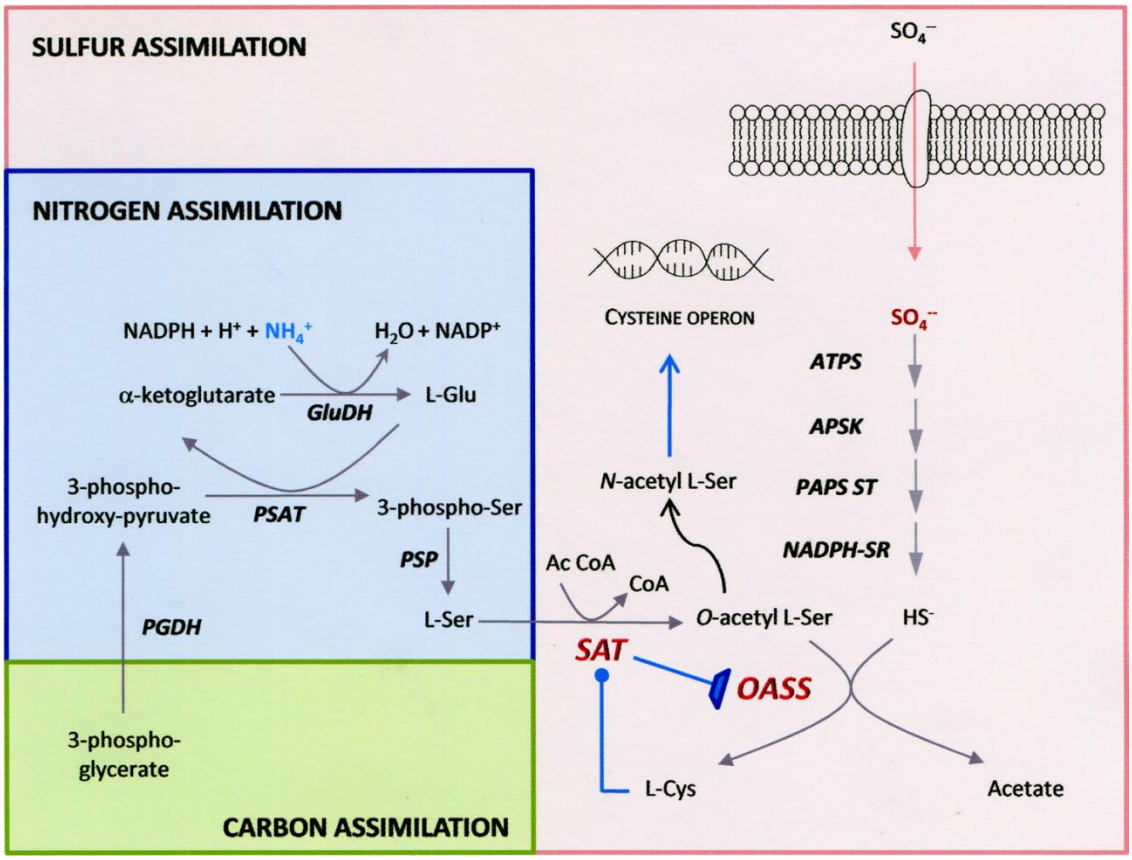

Figure 1.7 – General overview of sulphur assimilation in bacteria.

The assimilation mechanism of sulphur in bacteria. Enzymes appear in bold, except SAT and OASS (or CS, red); (ATPS) ATP sulphurylase; (APSK) 5-phosphosulphate kinase; (PAPS ST) 3-phosphoadenosine 5-phosphosulphate sulfotransferase; (NADPH-SR) NADPH-dependent sulphite reductase; (PGDH) D-3-phosphoglycerate dehydrogenase; (PSAT) 3-phosphoserine aminotransferase; (PSP) 3-phosphoserine phosphatase; (GluDH) glutamate dehydrogenase (Salsi *et al.*, 2010)

1.3.1.2.3.1 CSC in *Leishmania*

Williams *et al.* (2009) has shown that *Lmj*SAT activity was only detected when *Lmj*SAT was co-expressed with *Lmj*CS. Additionally, *Lmj*CS activity was undetectable when co-expressed with *Lmj*SAT but highly active when expressed alone (Westrop *et al.*, 2006; Williams *et al.*, 2009). In *Leishmania*, the source of sulphide is yet to be discovered but Williams *et al.* (2009) suggested possible involvement of mercaptopyruvate as a source for sulphide.

In *Leishmania*, sulphide is thought to be provided by mercaptopyruvate sulphurtransferase (MST) from 3-mercapto pyruvate (3-MP). Contrary to what is seen in plants, cysteine biosynthesis may possibly not be aimed to regulate intracellular sulphide levels but instead to generate sufficient cysteine necessary for the biosynthesis of glutathione and trypanothione, the main antioxidants found in these parasites. Williams *et al.* (2009) showed that supplementing medium with exogenous methionine resulted in elevated cysteine, glutathione and trypanothione levels, and promoted the growth of *L. major* promastigotes. Thus, cysteine might also be a source of methionine when the parasite is in a low-methionine environment (Alphey *et al.*, 2003; Williams *et al.*, 2009; Williams *et al.*, 2003). This could be accommodated by the forward reverse-transsulphuration pathway in *L. major* (Williams *et al.*, 2009).

L. major and *L. mexicana* contain single copy genes of MST. The structure of *Lmj*MST has been solved and it has a C-terminal extension of 80 amino acids (compared with other sulphurtransferases) that was shown to be essential for protein folding. Both, *LmjCS* and *Lmj*CBS can use sulphide generated by MST for cysteine synthesis (Alphey *et al.*, 2003; Williams *et al.*, 2009; Williams *et al.*, 2003).

1.3.1.3 Serine acetyl-transferase

Studies made in plants and bacteria have shown that the formation of the complex is not meant to channel the substrate between the two available CS active sites (Francois *et al.*, 2006; Huang *et al.*, 2005; Kredich *et al.*, 1969; Wirtz *et al.*, 2001; Wirtz and Hell, 2006; Zhao *et al.*, 2006). The conserved C-terminal isoleucine (Ile) residue is the only amino acid that is conserved (Table 1.2) in the C-terminal amino acids. It interacts with the protein side chain of CS through specific hydrogen bonds and hydrophobic interactions (Francois *et al.*, 2006; Raj *et al.*, 2012; Zhao *et al.*, 2006).

*Ld*SAT	MFLEGDGSGI
*At*SAT	YLTEWSDYVI
*Gm*SAT	FISEWSDYII
*Ec*SAT	NHTFEYGDGI
*Hi*SAT	GIDDGMNLNI

Table 1.2 – The amino acid sequence of SAT C-terminal.

The sequences of the last 10 amino acids of SAT(s) from *L. donovani* (*Ld*SAT), *A. thaliana* (*At*SAT), *Glycine max* (soybean) (*Gm*SAT), *E. coli* (*Ec*SAT), and *H. influenza* (*Hi*SAT). Adapted from Francois *et al.* (2006) and Raj *et al.* (2012).

The three-dimensional structure of *Haemophilus influenzae* CS complexed with a peptide that corresponds to the last 10 amino acids located in the C-terminus of *Hi*SAT, showed that the peptide binds to the active site of CS. However, with less affinity than the full length *Hi*SAT (Bonner *et al.*, 2005; Mino *et al.*, 2000b). The same phenomenon has been observed in *E. coli* where the affinity determined for the 10 amino acid peptide was much lower than of the wild-type SAT (Mino *et al.*, 2000a; Mino *et al.*, 2000b). Studies have shown that the affinity for CS complex formation varies with species. The affinity for *A. thaliana* CSC is 10-80 times higher than for *E. coli* CSC (Berkowitz *et al.*, 2002; Zhao *et al.*, 2006).

The inhibition of CS triggered by the C-terminal of SAT prompted several studies on potential small peptide inhibitors. Salsi *et al.* (2009) carried out a thorough docking study with *in silico* generated peptides in order to identify key amino acids that may play a major role in the binding to *H. influenza* CS. This study confirmed the importance of the C-terminal amino acid Ile of SAT, accounting for 50% of the binding energy. Schnell *et al.* 2007 tested the peptide DFSI, correspondent to the last four amino acids of *M. tuberculosis* SAT, against *Mt*CS. This peptide was able to form a complex and to inhibit *Mt*CS's activity (Poyraz *et al.*, 2013; Schnell *et al.*, 2007).

Salmonella CS undergoes a large-scale conformational changes between the open and closed binding conformations, which plays an important role in the recognition of the SAT C-terminal (Francois *et al.*, 2006). Wang and Leyd (2012) have proposed that the formation of *E. coli* CSC goes through three conformational stages. First the *Ec*SAT binds to one CS active site leaving the other monomer unoccupied. However, *Ec*SAT triggers a conformational change in the empty monomer that prevents a 10 amino acids peptide (last 10 amino acids of *Ec*SAT) from binding to it. Additionally, the peptide alone was not able to trigger the conformational change seen with the full length *Ec*SAT. Thus, the peptide does not contain all the necessary amino acids for the interaction between *Ec*SAT and *Ec*CS (Wang and Leyh, 2012).

1.3.1.4 Cystathionine β-synthase

L. major CBS is a PLP-dependant enzyme of the RTS pathway (Williams *et al.*, 2009). *L. major* CBS differs from human CBS because it does not have an *haem*-binding N-terminal and a C-terminal regulatory domain in the active site pocket. In mammals the haem-binding N-terminal works as a redox sensor while the C-terminal regulatory domain controls the tetrameric state of CBS and thus CBS's activity (Banerjee and Zou, 2005; Frank *et al.*, 2008; Meier *et al.*, 2001; Miles and Kraus, 2004). These groups block the entry of

the large acetyl groups of OAS (Frank *et al.*, 2008). This difference might constitute to a good base of study for new anti-*Leishmania* drugs.

CBS catalyses the production of cystathionine from serine but is also able to form cystathionine from sulphide, homocysteine and cysteine by a ß-replacement reaction (Williams *et al.*, 2009). The CBS from *T. cruzi* (lacks the C-terminal) and *S. cerevisiae* (lacks the N-terminal) can accommodate these large groups once it lacks one of them (Nozaki *et al.*, 2001; Williams *et al.*, 2009) However, the activity reported by Williams *et al.* 2009 from *Lmj*CS suggests that it lacks both terminals (Williams *et al.*, 2009).

CBS is closely related structurally to CS. In *L. major*, Williams *et al.* (2009) showed that *Lmj*CBS can also form cysteine from OAS and sulphide, however with a higher K_m than *Lmj*CS (Figure 1.8). The different sensitivity to OAS and sulphide might be relevant for adaption to different environments when differentiating between the two life-cycle stages (Williams *et al.*, 2009). This feature is also shared by *T. cruzi* CBS. In *T. cruzi* CBS only three out of eight genes have an N-terminal extension suggesting that the other five have more similarities with the biochemical proprieties of *Lmj*CS (Nozaki *et al.*, 2001) In humans, CBS lacks CS activity but with a low catalytic efficiency (Braunstein *et al.*, 1971; Nozaki *et al.*, 2001; Williams *et al.*, 2009).

(a) Homocysteine + Cysteine → Cystathionine
(b) Cysteine + Homocysteine → Cystathionine
(c) OAS + Sulphide → Cysteine
(d) Serine + Sulphide → Cysteine
(e) Cysteine + 2-mercaptoethanol → S-hydroxyethylcysteine + hydrogen sulphide

Figure 1.8 – Reactions catalysed by *Lmj*CBS.

***Lmj*CBS is able to catalyse different reactions. The activities reported by Williams *et al.* (2009) are: (a) CBS activity; (b) homocysteine sulphydrylase; (c) CS activity; (d) serine sulphydrylase; and (e) cysteine desulphurase.**

1.4 Trypanohione biosynthesis

1.5.1 Glutathione biosynthetic pathway

In humans and the majority of eukaryotes and many microorganisms, glutathione is used in the defence against xenobiotics and the detoxification of peroxides (Husain *et al.*, 2011; Krauth-Siegel and Leroux, 2012; Muller *et al.*, 2003; Pompella *et al.*, 2003; Smirnova and Oktyabrsky, 2005). In *Leishmania* and other trypanosomatids, glutathione is used for the synthesis of trypanothione, which has been proven to carry out glutathione functions in these parasites. The cysteine generated by either of the cysteine biosynthetic pathways of *Leishmania*, is converted into glutathione by two ATP-dependant steps: firstly, cysteine and glutamate form γ-glutamylcysteine in the presence of γ-glutamylcysteine synthase; and secondly, γ-glutamylcysteine is converted into glutathione by glutathione synthase (Figure 1.9) (Carter *et al.* 2003). *Entamoeba*, *Giardia* and *Trichomonas* lack the glutathione biosynthesis pathway and it has been suggested that cysteine is responsible for redox buffering (Coombs *et al.*, 2004; Husain *et al.*, 2011; Krauth-Siegel and Comini, 2008; Nozaki *et al.*, 1998; Nozaki *et al.*, 1999).

1.5.2 Polyamine biosynthetic pathway

Figure 1.10 shows a schematic diagram of the polyamine biosynthetic pathway in *Leishmania* parasites. Ornithine and urea originate from the enzymatic hydrolysis of arginine by the arginase enzyme. Ornithine is then converted into putrescine by ornithine decarboxylase, a PLP-dependent enzyme. The decarboxylase S-adenosylmethionine donates an aminopropryl group to putrescine to form spermidine. This reaction is catalysed by spermidine synthase. Decarboxylase S-adenosylmethionine is formed from S-adenosylmethinine by S-adenosylmethionine decarboxylase (Birkholtz *et al.*, 2011). *T. brucei* is able to synthesise putrescine from ornithine, whereas *T. cruzi* has to acquire polyamines from the exterior of the cell (Fairlamb *et al.*, 1987; Hunter *et al.*, 1994).

The polyamine biosynthetic pathway is essential in *Leishmania* as shown by extensive gene deletion studies (Jiang *et al.*, 1999; Reguera *et al.*, 2009; Roberts *et al.*, 2001). Polyamines are important for the stimulation of DNA and RNA synthesis. Their concentration is increased during maximal growth in prokaryotic and eukaryotic cells (Bachrach *et al.*, 1973). Bachrach *et al.* (1979) have shown that in *Leishmania* promastigotes polyamines vary with the growth stage and that blocking polyamine biosynthesis impairs growth. Thus, the polyamine biosynthetic pathway is essential for promastigotes viability and growth. Additionally Gilroy *et al.* (2011) have demonstrated that spermidine synthase is essential for a robust infection of *L. donovani* in mice, supporting the notion that polyamines are essential for parasite virulence. However, *Leishmania* parasites are able to scavenge polyamines from the exterior, which makes their biosynthesis a less attractive as drug target. A good example is that of α-difluoromethylornithine (DFMO), a suicide inhibitor of the ODC enzyme, which selectively inhibits the *Leishmania* enzyme but does not kill the parasites in the presence of exogenous polyamines (Kandpal and Tekwani, 1997)

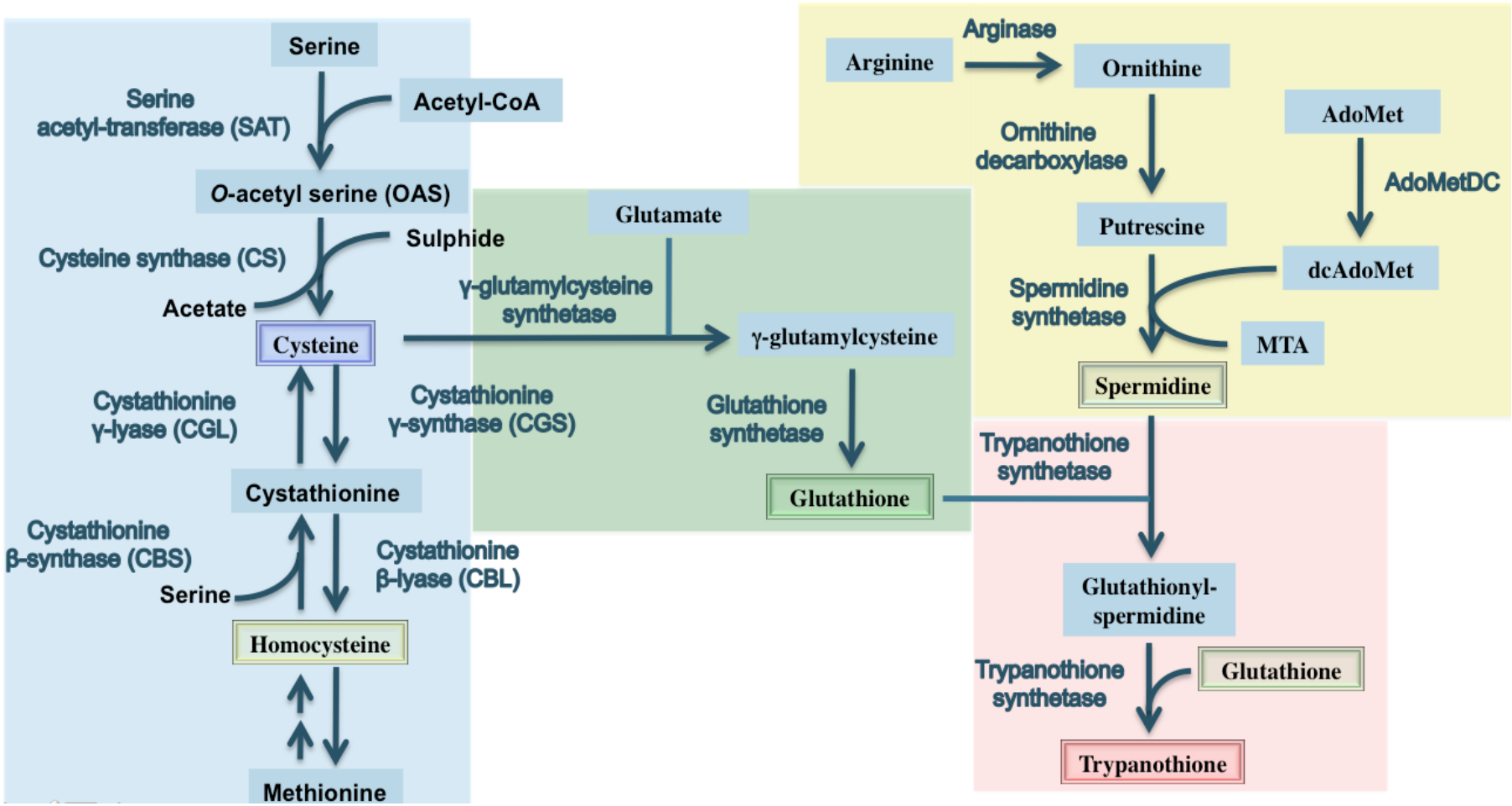

Figure 1.9 – Thiol biosynthetic pathways in *Leishmania*.

The cysteine (blue), glutathione (green), polyamine (yellow) and trypanothione (red) biosynthetic pathways are highlighted in the diagram. The thiols analysed in this study were: cysteine (blue), homocysteine (yellow), glutathione (green), and trypanothione (red). Other thiols present in these pathways are: γ-glutamylcysteine and glutathionyl-spermidine. The enzymes are in bold blue. The substrates and bi-products are in black. The arrows indicate the direction of the reaction.

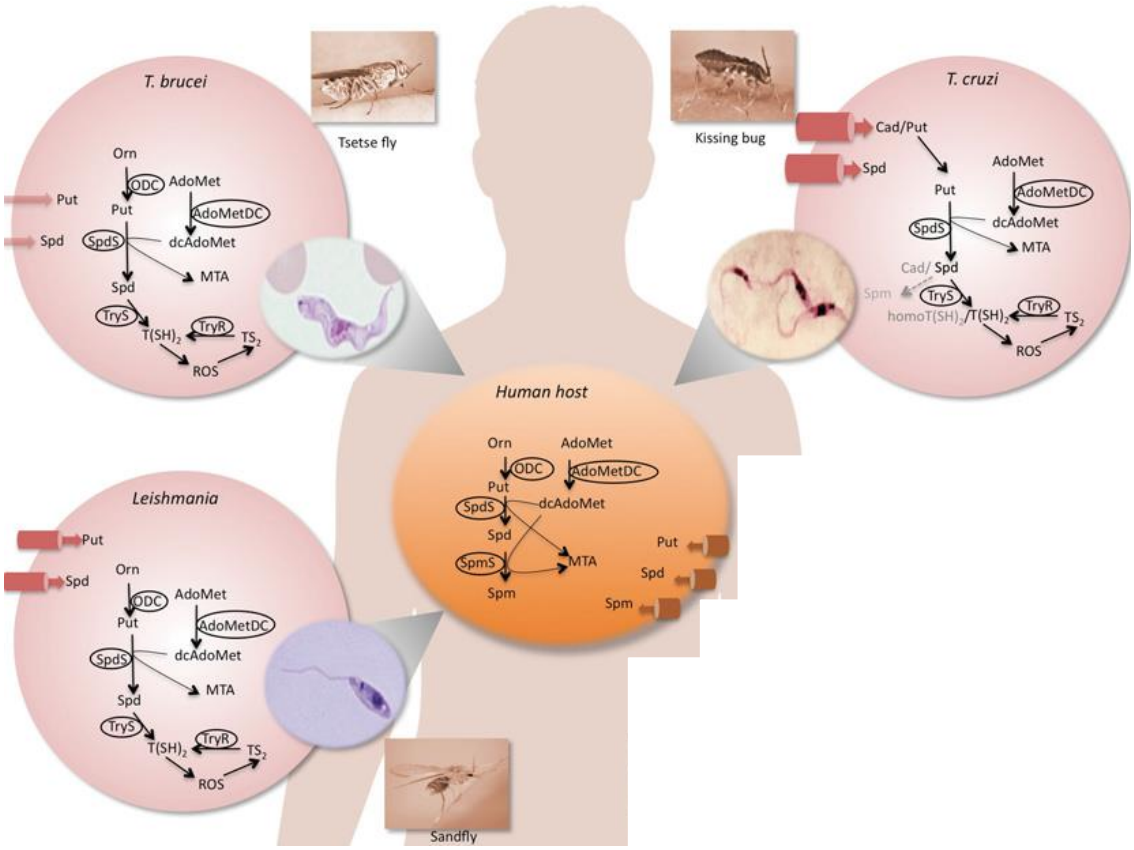

Figure 1.10 – Polyamine biosynthesis in trypanosomatids and humans.

Shematic diagram showing the major differences between trypanosomatids and human polyamine biosynthetic pathways. The major difference resides in the use of spermidine. In trypanosomatids it is used to synthesise trypanothione, their major thiol. In humans it is used to synthesise spermine. The decarboxylated adenosilmethionine supplies aminopropryl groups to the synthesis of spermidine and spermine in humans, whereas in trypanosomatids it only supplies aminopropryl groups to the synthesis of spermidine. Additionally this figure highlights the fact that polyamines can be acquired axenically in trypanosomatids and humans (cylinders). The cylinders are sized according to their efficiency. (AdoMet) adenosyl methionine; (AdoMetDC) adenosyl methionine decarboxylase; (dcAdoMet) decarboxylated adenosyl methionine; (Cad) cadaverine; (homoT$(SH)_2$) homotrypanothione; (MTA) 5'-methylthioadenosine; (ODC) ornithine decarboxylase; (Orn) ornithine; (Put) putrescine; (ROS) reactive oxygen species; (Spd) spermidine; (SpdS) spermidine synthase; (Spm) spermine; (TryR) trypanothione reductase; (TryS) trypanothione synthase; (TS_2) trypanothione disulphide; (T$(SH)_2$) dihydrotrypanothione (Birkholtz *et al.*, 2011)

Printed with permission from Biochemical Journal.

1.5.3 Trypanothione as anti-oxidant defence

Trypanothione is the major low-molecular weight thiol in trypanosomatids was discovered in 1985 by Professor Alan Fairlamb, contributing to a major advance in the development of effective therapies against trypanosomatids. This thiol plays an important role in the thiol redox balance, in the synthesis of deoxyribonucleotides, drug resistance and in the defence against chemical and oxidative stress. Its absence in humans makes its biosynthesis a good base of study for potential drug targets (Fairlamb *et al.*, 1985; Fairlamb and Cerami, 1985, 1992; Oza *et al.*, 2005)

Trypanosomatids lack genes for both glutathione reductase and thioredoxin reductase. In these organisms, trypanothione is kept in a reduced state by trypanothione reductase (structurally similar to glutathione reductase), which has been shown to be essential for this parasite (Figure 1.11) (Tovar *et al.*, 1998a; Tovar *et al.*, 1998b). Trypanothione is synthesised by trypanothione synthethase in two ATP-dependent steps that involve two molecules of glutathione and one molecule of spermidine (Ariyanayagam *et al.*, 2005; Legare *et al.*, 2001). During cell growth, trypanothione levels in *L. donovani* promastigotes decrease when the cells reach the stationary phase (Krauth-Siegel and Comini, 2008). Since trypanothione depends on the availability of spermidine, DFMO causes spermidine levels to decrease and thus trypanothione levels to be depleted (Fairlamb *et al.*, 1987). Another way to reduce trypanothione levels is to deplete trypanothione synthethase mRNA or by the down-regulation of tryparedoxin (experiments carried out in *T. brucei*) (Comini *et al.*, 2007; Dumas *et al.*, 1997). Trypanothione levels also depend on the level of glutathione, thus the inhibition of glutathionylspermidine and glutathione by buthionine sulfoximine (BSO) also lowers trypanothione levels (Faundez *et al.*, 2005). In fact, BSO is able to potentiate the toxicity of nifurtimox in *T. brucei*. However, in *L. donovani* the growth defect was not so pronounced (Weldrick *et al.*, 1999). Metal-containing drugs (*i.e.* antimonials and arsenites) induce trypanothione and glutathione efflux through Gp-glycoprotein-like protein A, a member of the

ABC (ATP-binding cassette) class of transporters (Wyllie *et al.*, 2004). In contrast, higher levels of thiols have been found in antimonial resistant *L. donovani* (Mittal *et al.*, 2007).

The trypanothione/tryparedoxin system acts as a reducing agent of enzymes (i.e. ribonucleotide reductase), and detoxification of hydroperoxides by transferring reducing equivalents from NADPH to peroxidases (Krauth-Siegel and Leroux, 2012). Wyllie *et al.*, (2010) have shown that antimonial-resistant parasites overexpress tryparedoxin and tryparedoxin peroxidase (both kept reduced by trypanothione), which resulted in a higher ability to detoxify hydropexides. Trypanosomatids have a single mitochondrion that contains the unique kinetoplastid DNA (kDNA) arranged in minicircles and maxicircles. For the replication, the parasites need a ribonucleotide reductase to reduce the deoxyribonucleotide precursors. This enzyme is kept in reduced state by trypanothione in *T. brucei*. Additionally, for the minicircle replication process to initiate, the universal minicircle sequence-binding protein (UMSBP) needs to bind the minicircles origin sequence. The trypanothione and tryparodoxin system can activate UMSBP in *C. fasciculata* (Milman *et al.*, 2007; Onn *et al.*, 2004).

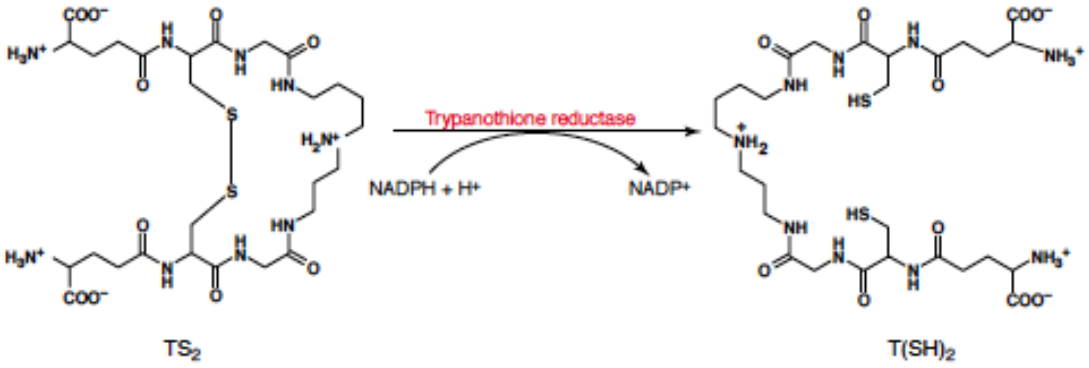

Figure 1.11 – Reduction of trypanothione.

Dithiol trypanothione (TS_2) is reduced to trypanothione ($T(SH)_2$) by trypanothione reductase with the consumption of NADPH (Muller *et al.*, 2003).

Printed with permission from Elsevier.

Aims of this study

Leishmaniasis are neglected tropical diseases that affect people worldwide. Its multiple cases of drug resistance (India and Nepal) and the absence of a vaccine for humans leaves us in desperate need to develop new drugs and to find new drug targets. Thiols are the major protectors of cells against oxidative or xenobiotic stress and have also been involved in the resistance against antimonal drugs (main treatment of visceral leishmaniasis). *Leishmania* presents two life cycle states that involve two very different hosts. Thus, adaption to different environments and oxidative challenges are crucial for the virulence and survival of these parasites. A lot of research has been done in order to find drug targets in the polyamine and trypanothione biosynthetic pathways. This work proposes to start this search at a much earlier stage, cysteine. Cysteine is the building block of glutathione and trypanothione and therefore possibly a very important piece of the puzzle. Therefore this study intends to:

- Assess the essentiality of the cysteine synthase of the sulphydrylation pathway in *L. donovani*.
- Study of the inhibition of cysteine synthase by small peptides.
- Analyse the relative contribution of the two cysteine synthase biosynthetic pathways in *L. donovani*.

Materials and Methods

2 Materials and Methods

2.1 Consumables, Biological and chemical reagents

Alpha laboratories	1.2 mL Cryovial
Ambion	RETROscript reverse transcription for real time PCR kit, Turbo DNA-free, RNaseZap
Applied Biosystems	Power Sybr® Green PCR Master Mix, Micro Amp™ Optical 96-well reaction plate
BD Plastic	50 mL syringe
Bio-Rad	Bradford protein assay reagent, Precision Plus Dual-Color Protein™ Standard
Eurogentec	Oligonucleotides, antisera generation programmes
Fisher Scientific	10 x Phosphate buffered saline (PBS), Reddy mix PCR mastermix, imidazole (low absorbance), restore western stripping buffer, 0.2 µm syringe filters, sodium hydrogen carbonate
Fluka	Dimethyl sulphoxide
Gibco	HOMEM medium
Greiner	Aspiration pipettes, 50 mL pipettes, 96 well plates
GE Healthcare	Gene images AlkPhos direct labelling and detection system, gene images CDP-Star, detection module, hypercassettes (18 x 24 cm), Hyperfilm ECL, Hybond N^+ membrane
Invitrogen	Glycogen (20µg/µL), UltraPure™ agarose, UltraPure™ low melting point agarose
Kodak	Autoradiography film
Life Technologies	Accuprime *Pfx* SuperMix, gel cassettes, glycogen, gentamycin, SYBR Safe
Lonza	Human T Nucleofector solution
Melford	Leupeptin, E64, proteinase K, ampicillin, kanamycin, isopropyl-O-dithiogalacopyranoside

Millipore	Immobilon™ western chemiluminescent HRP substrate, nylon membrane 0.20 μm of pore size
New England Biolabs	1 kb DNA ladder, 100 kb DNA ladder, T4 DNA ligase, T4 ligase buffer, 6 x DNA loading dye, restriction endonucleases and respective buffers
Novagen	Chemically competent *E. coli* BL21(DE3), pET15b vector
PAA	Fetal bovine serum gold, heat inactivated
Promega	anti-rabbit IgG (HRP conjugated), anti-mouse IgG (HRP conjugated), pGEM-T Easy vector system II
Qiagen	RNeasy Mini, QIAquick gel extraction kit, QIAamp DNA mini kit, QIAprep spin Miniprep kit, QIAquick PCR purification kit, Ni-NTA agorose
Roche	Bovine serum albumin (BSA)
Santa Cruz Biotech	Donkey anti-sheep antibody
Sartorius	Ministart syringe filter hydrophobic
Sigma	All chemicals unless otherwise stated
Stratagene	XL10-Gold® Ultracompetent Cells, StrataClone Blunt PCR cloning kit
Thermo Scientific	GelCode™ Blue Safe Protein Stain, Restore Plus western blot stripping buffer, Zeba™ desalting column
Whatman	Protran® Nictrocelulose Transfer Membrane

2.2 Equipment

Applied Systems	Micro Amp™ Optical 96-well reaction plate, 7500 real-time PCR system, 7500 real-time PCR software, primer express 3.0 for real-time PCR software
Beckman	GS-15R centrifuge, coulter Allegra™ X-12R centrifuge (rotor SX4750), Coulter Avanti J-26 XP (rotors JA25.50 and F10BCL)
Bio-Rad	TransBlot SD Semi-dry transfer cell, Gel tanks, Gene Pulser Xcell electroporator, Power Pac 300, Power Pac Basic, PowerPac HC, Transblot semi-dry transfer cell, GelDoc 2000 (Mitsubishi P91 printer) CHEF-DR-III system, Biologic DuoFlow purification system, BioFrac collector, 583 Gel dryer (KNF vacuum pump)
BMG labtech	FLUOstar OPTIMA
Constant Systems	Cell disrupter
Denver instrument	Ultra basic US-10 pH meter
Dionex	Ultimate 3000 HPLC, ultimate 3000 autosampler, ultimate 3000 variable wavelength detector, RF 2000 fluorescence detector, Chromeleon™ version 6.8 SP2 built 2284
Eppendorf	Microcentrifuge 5415D (rotor F45-24-11)
Fisher	Microcentrifuge Accuspin MicroR (rotor 13-100-515), water bath, vaccum pump FB70155, gel tanks
GE Healthcare	VaccuGene XL apparatus
G Storm	GS4 4 block PCR machine
Grant	Heat block QBT2, water bath
GraphPad	GraphPad Prism software
Hawksley	BS.748 Neubauer chamber
Heidolph	Rotamax 120 shaker

Hybaid	Mini 10 incubator
Kühner	Shaker ISF-1-W
Konica	Konica Minolta SRX-101A tabletop processor
Life Technologies	250 EX power pack, Vector NTI software
Lonza	Nucleofector® Device
Millipore	Quantum ddH_2O system
Molecular Devices	Versamax microplate reader
Phonomenex	Gemini 5 μm C-18 110Å silica column, security guard guard cartridge kit KJ0-4282
Schnakenbery	HermLe 2400k (rotor H208698033)
Sigma	1-15 microfuge (rotor 12124), 6K15 centrifuge (rotor 11150)
Sonics	Vibracell ultrasonic processor
Stuart	SB2 rotator, roller mixer SRT6
Techne	TC-412 thermocycler
Thermo Scientific	Sorvall ST-16R centrifuge (rotor TX-400), NanoDrop 1000 spectrophotometer, Holten Safe 2010 hood
UVP	HB-1000 hybridization oven, UV cross linker, 2UV™ transiluminator
VWR	Genosmart transiluminator

2.3 Buffers, solutions and media

2.3.1 DNA analysis

6x DNA loading dye	0.25% (w/v) orange-G, 0.25% (w/v) bromophenol blue, 0.25% orange-G, 40% (w/v) sucrose
1x TAE	40 mM Tris-acetate, 1 mM EDTA, pH 8.0
Southern blot:	
Depurination solution	0.25 M HCl
Denaturation solution	1.5 M NaCl, 0.5 M NaOH
Neutralisation solution	3 M NaCl, 0.5 M Tris HCl (pH 7)
20x SSC	300 mM trisodium citrate, 3 M NaCl
Primary wash buffer	2 M urea, 0.1% (w/v) SDS, 50 mM sodium phosphate pH 7.0, 150 mM NaCl, 1 mM $MgCl_2$, 0.2% (w/v) blocking reagent
Secondary wash buffer	50 mM Tris base, 100 mM NaCl, 2 mM $MgCl_2$

2.3.2 Protein analysis

Lysis buffer	0.25 M sucrose, 0.25% Triton X-100, 10 mM EDTA, 20 μM E-64, 4 μM 1,10-phenanthroline, 8 μM Pepstain A, 2 mM Phenylmethylsulfonylfluoride
Coomassie stain	GelCode™ Blue Safe Protein Stain (Thermo Scientific), or Coomassie blue stain (40% (v/v) methanol, 10% (v/v) acetic acid, 0.1% (w/v) Coomassie brilliant blue R-250)
Destaining solution	20% (v/v) methanol and 10% (v/v) acetic acid
Protein loading buffer	62.3 mM Tris-HCl pH 6.8, 2% (w/v) SDS, 10% (v/v) glycerol. 0.001% (w/v) bromophenol blue, 5% (v/v) 2-mercaptoethanol
Resolving gel buffer	1.5 M Tris base pH 8.9, 0.4% SDS
Stacking gel buffer	0.5 M Tris base pH 6.7, 0.4% SDS

1x PRB electrode buffer	2.5 mM Tris, 192 μM glycine, 0.1% (w/v) SDS
Towbin buffer	25 mM Tris base, 1.92 mM glycine, 1.3 mM SDS and 20% methanol
Purification of r*Lmj*CS:	
Lysis buffer	50 mM phosphate buffer pH8, 300 mM NaCl and 10 mM imidazole
Wash buffer	50 mM phosphate buffer pH8, 300 mM NaCl and 20 mM imidazole
Elution buffer	50 mM phosphate buffer pH8, 300 mM NaCl and 250 mM imidazole
HPLC buffer	40 mM N-[2-hydroxyethyl]-piperazine-N'[3-propanesulphonic acid] (EPPS), 4 mM of diethylenetriamine pentaacetic acid (DTPA), and pH 8 adjusted with 1 M lithium hydroxide

2.3.3 Parasites culture

PSGEMKA	0.02 M phosphate buffer, 180 mM NaCl, 55 mM glucose, 650 μM EDTA, 10 mM $MgCl_2.6H_2O$, 10 mM KCl, 0.2 g/L albumin
Freezing solution	HOMEM with 20% (V/V) heat inactivated foetal calf serum, 1% penicillin/streptomycin, 5% dimethyl sulfoxide
Medium	HOMEM, 10% (V/V) heat inactivated foetal calf serum, 1% penicillin/streptomycin

2.3.4 Bacteria culture

Ampicillin	100 μg/mL final concentration
Kanamycin	50 μg/mL concentration
Luria broth (LB) medium	10 g/L tryptone, 5 g/L yeast extract, 5 g/L NaCl
LB agar	10 g/L tryptone, 5 g/L yeast extract, 5 g/L NaCl, 1.5% (w/v) agar

TFBI	100 mM RbCl, 50 mM $MnCl_2$-$4H_2O$, 30 mM NaH_2AsO_4, 10 mM $CaCl_2$-$2H_2O$ and 15% glycerol
TFBII	0.2 M MOPS, 10 mM RbCl, 75 mM $CaCl_2$-$2H_2O$ and 15% glycerol

2.3.5 Bacterial strains

BL21 (DE3) (Novagen):
F- ompT hsdSB(rB- mB-) gal dcm (DE3)

SoloPack® (Stratagene):
Tetr Δ(mcrA)183 Δ(mcrCB-hsdSMR-mrr)173 endA1 supE44 thi-1 recA1 gyrA96 relA1 lac The [F´ proAB lacIqZΔM15 Tn10 (Tetr) Amy Camr]

XL10-Gold® Ultracompetent Cells (Stratagene):
TetrD(mcrA)183 D(mcrCB-hsdSMR-mrr)173 endA1 supE44 thi-1 recA1 gyrA96 relA1 lac Hte [F´ proAB lacIqZDM15 Tn10 (Tetr) Amy Camr]

2.3.6 *Leishmania* strains

L. donovani – BPK 206 clone 10
L. donovani - BPK206 clone 10 lacking cysteine synthase alleles
L. major – MHOM/IL/80/Friedlin

2.3.7 Oligonucleotide primers

2.3.7.1 Transfection in *Leishmania donovani*

The restriction sites are highlighted in bold and the start and termination codon are underlined:

CS forward	5' **GATATC**ATGGCGGCAGCGTCCGAC 3' (*EcoRV*)
CS reverse	5' **GGATCC**TCAGTCCTGCAGCTCCGAGG 3' (*BamHI*)

2.3.7.2 Recombinant protein expression

The restriction sites are highlighted in bold and the start and termination codon are underlined:

Lmj1	5' **GCCAT**ATGGCAGCACCGTTCGACAAGTC 3' (*NdeI*)
Lmj2	5' C**GGATCC**TCAGTCCTGCAGCTCCGAGGCATC 3' (*BamHI*)

2.3.7.3 Quantitative real-time polymerase chain reaction analysis

GPI8 forward	5' CAACAACTGGGCTGTCATTCTC 3'
GPI8 reverse	5' TGGCAGTGTGACGGTAGTTGA 3'
ODC forward	5' ACCTACGTGACGGTGGACAAC 3'
ODC reverse	5' GCATCAGGCGACTGA 3'
CS forward	5' TTTGCGTGGCAGGTGATG 3'
CS reverse	5' GCTGCGCGTGAGCTTCA 3'
CBS forward	5' TGGCGGCAGCGTCAA 3'
CBS reverse	5' TTTTCGGCGTGGAGTATCATC 3'

2.3.8 Antibodies

Antibody	Animal	Source	Dilution
Primary			
anti-*L. mexicana* cysteine synthase	Rabbit	SAPU	1:5,000
anti-*L. major* cysteine ß-synthase	Rabbit	SAPU	1:10,000
anti-*L. donovani* ornithine decarboxylase	Rabbit	Buddy Ullman (Boitz *et al.*, 2009)	1:5,000
anti-Histidine	Mouse	Clonetech	1:10,000
anti-*L. major* oligopeptidase B (OPB)	Rabbit		1:20,000
anti-mouse EF-1α clone CBP KK1	Mouse	Millipore	1:10,000
Secondary			
Donkey anti-Sheep		Santa Cruz Biotechnology	1:10,000
anti-Rabbit IgG (HRP conjugated)		Promega	1:10,000
anti-Mouse IgG (HRP conjugated)		Promega	1:10,000

2.4 Molecular methods

2.4.1 Determination of DNA and RNA concentration

DNA and RNA concentrations were determined using a Nanodrop 1000 spectrophotometer (Thermo Scientific). Optical density 260 mm (OD_{260mm}) of 1 corresponds to a double-stranded (dsDNA) concentration of 50 µg/mL. To assess the purity of each sample, the ratio of the DNA absorbance at 260 nm and at 280nm ($A_{260/280}$) was determined. For high purity DNA the expected ratio $A_{260/280}$ should be ~ 1.8, and for pure RNA, the ratio should be in the range of $A_{260/280}$ of ~ 2.

2.4.2 Ethanol precipitation

DNA was precipitated by adding three volumes of ice cold absolute ethanol absolute and 0.1 volumes of 3 M sodium acetate pH 5.4 and 2 µg of glycogen was added to the DNA before incubating it at -20 ºC overnight. The pellet was collected at 4°C, 13,000 rpm for 30 minutes. The DNA was washed with ice cold 70% ethanol, air dried and then resuspended in 50 µL of double distilled water (ddH_2O).

2.4.3 Restriction endonuclease digests

In order to verify the size of plasmid inserts, restriction endonuclease digests were carried as per manufacturer's instructions. Routinely 1 µL of plasmid DNA was digested with 1 µL of restriction enzyme and respective supplied buffer (New England Biolabs). With exception of *SmaI* (25°C), all the restriction endonuclease digests were incubated for a minimum of 2 h at 37°C. DNA fragments were analysed by gel electrophoresis (see section 2.2.4).

2.4.4 Agarose gel electrophoresis

The quality and quantity of DNA were assessed by gel electrophoresis. Agarose or low-melting point agarose was dissolved in 1 x TAE buffer at the appropriate percentage in a microwave. SYBR safe was added to 0.5 µg/mL prior to casting the gels. 6 x DNA loading dye was added to the DNA samples before these were loaded into the wells of the gel. The separation was performed in a gel tank containing 1 x TAE at 5 – 10 V/cm^2. The size of the DNA fragments was determined by comparison with a 1 kb or 100 bp ladder that was loaded and separated alongside the DNA samples. A transilluminator (2UV^{TM} transiluminator, UVP) was used to visualize (365 nm) and aid band excision for further DNA purification.

2.4.5 DNA sequencing

DNA sequencing was performed by Source Bioscience Life Sciences. The samples requirements per sequencing reaction were 1 ng/µL per 100 bp of PCR product or 100 ng/µL of plasmid and 3.2 pmol/µL of sequencing primers.

2.4.6 Southern blot analysis

To verify the genotype of the genetically-manipulated *L. donovani* lines, 2 µg of gDNA were digested with *XhoI* restriction endonuclease overnight at 37°C with the respective provided buffer. The digests analyzed by gel electrophoresis in a SYBR-safe free 0.7% agarose gel at 20V for ~22 hours. The DNA was depurinated with 0.25 M HCl, denaturated with 1.5 M NaCl, 0.5 M NaOH, and neutralised with 0.5 M Tris containing 3 M NaCl pH 7. DNA was then transferred to a Hybond-N$^+$ membrane (GE healthcare) with a 20 X SSC solution (300 mM trisodium citrate and 3 M NaCl pH 7) using a VacuGene XL apparatus (GE Healthcare) for 1.5 h. DNA was then crosslinked to the membrane using a UV crosslinker at 700 x 100 µJ/cm^2 (UVP laboratory

products). The membranes were pre-hybridized with hybridization buffer (0.5 M NaCl and 4% (w/v) of blocking reagent) at 60 °C. The probes were generated using DNA fragments excised from plasmids that were restriction endonuclease digested. The cysteine synthase (*cs*) gene was excised from the pGL102*cs* plasmid using *SmaI* and *BamHI* restriction endonucleases, hygromicin phosphotransferase (*hyg*) gene was excised from pGL345*hyg* plasmid using *SpeI* and *BamHI* restriction endonucleases; and nourseothricin acetyltransferase (*sat*) gene was excised from pGL158*sat* plasmid using *SpeI* and *BamHI* restriction endonucleases. The DNA fragments were purified using the QIAquick gel extraction kit (QIAGEN) and used to generate probes with the Gene Images AlkPhos direct labeling kit (GE Healthcare). The denatured probe was added to the hybridization buffer and left to bind overnight at 60°C. The labeled membrane was washed three times for 10 minutes with primary buffer (2 M urea, 0.1 (w/v) sodium dodecyl sulphate, 50 mM sodium phosphate pH 7, 150 mM NaCl, 1 mM $MgCl_2$ and 0.2% blocking reagent) at 60°C and then washed two times for 10 minutes with secondary buffer (1 M tris base, 2 M NaCl and 2 mM $MgCl_2$) at room temperature. The membrane was covered with CDP-Star detection reagent (GE Healthcare) for 1 minute. The excess of reagent was discarded and membrane was sealed into a plastic bag. The membrane was exposed to Hyperfilm autoradiography film (GE Healthcare) for 1.5 h and subsequently developed using a Konica Minolta SRX-101A film developer. To further analyze the DNA, the membrane was striped using 0.5% SDS at 60°C for 2 hours before being pre-hybridize and probed again as described above.

2.4.7 Synthesis of cDNA

RNA extracted from *L. donovani* lines was used to synthesize cDNA for subsequent comparative expression level analyses of a number of genes. Reactions were set up using the RETROscript® Kit (Ambion). Each reaction contained 1.5 µg total RNA, 2.5 µM of random decamers, reverse transcriptase buffer containing 30 mM $MgCl_2$, 500 µM dNTPs, 100 units of MMLV-reverse transcriptase, and 10 units of RNase inhibitor. A control

reaction contained 500 ng of the provided control template RNA (mouse liver RNA) instead of the RNA isolated from *L. donovani*. The presence of cDNA was checked by PCR reaction using the AAT20 primer set that targets the amino acid transporter 20 gene of *L. donovani*. The successful reverse transcription of the control template RNA was verified using the provided primer set. PCR products were analyzed by agarose gel electrophoresis.

2.4.8 Polymerase chain reaction

2.4.8.1 AccuPrime™ *Pfx* DNA SuperMix

AccuPrime™ *Pfx* DNA SuperMix was used to amplify genes from plasmids or *L. donovani* gDNA to be later used in transfection. The SuperMix includes 22U/mL of AccuPrime™ *Pfx* DNA polymerase, 1.1 mM $MgSO_4$ and 330 µM deoxyribonucleotide triphosphate (dNTPs). The PCR was set up with AccuPrime™ *Pfx* DNA polymerase according to manufactures instructions, 200 ng of primers, and 4 ng of gDNA, to 25 µL of final volume. The PCR thermoprofile was as follows:

Initiation	98°C for 3 minutes
30 cycles of	
Denaturation	98°C for 30 seconds
Annealing	55°C for 30 seconds
Elongation	72°C for 45 seconds
Final elongation	72°C for 10 seconds

PCR products were analyzed by agarose gel electrophoresis. When necessary DNA was quantified using the Nanodrop spectrophotometer. Fragments with the expected size were cloned into pSC-B-amp/kan Strataclone PCR cloning vector or pGEM-T easy intermediate vector.

2.4.8.2 ReddyMix PCR Master Mix

ReddyMix PCR Master Mix was used for PCR analysis of genomic/plasmid DNA. The mastermix includes 0.625 units of ThermoPrime *Taq* DNA polymerase, 1.5 mM $MgCl_2$ and 0.2 mM dNTPs. The PCR reaction was set up with ReddyMix according to manufactures instructions, 200 nM primers and bacterial colony/up to 100 ng of gDNA. The final PCR reaction volume was 10 µL and the thermoprofile was the following:

Initiation	98°C for 3 minutes
30 cycles of	
Denaturation	98°C for 30 seconds
Annealing	55°C for 30 seconds
Elongation	72°C for 45 seconds
Final elongation	72°C for 10 seconds

PCR products were analyzed by agarose gel electrophoresis.

2.4.8.3 *Taq* DNA polymerase

Taq DNA polymerase was used for PCR analysis of cDNA. The PCR reaction was set up with 0.625 units of *Taq* DNA polymerase, ThermoPol reaction buffer containing 2 mM $MgSO_4$, 200 µM dNTPs (Invitrogen), 200 nM primers and up to 100 ng of cDNA. The final PCR reaction volume was 25 µL and the thermoprofile was the following:

Initiation	95°C for 3 minutes
30 cycles of	
Denaturation	95°C for 30 seconds
Annealing	65°C for 30 seconds
Elongation	68°C for 45 seconds
Final elongation	68°C for 10 seconds

PCR products were analyzed by agarose gel electrophoresis.

2.4.9 Quantitative real-time PCR

The reactions were set up in a 96-well plate in triplicate containing 100 ng cDNA template, 400 nM primers, and Power Sybr® Green PCR Master Mix according to manufactures instructions, in a total volume of 25 µL. GPI8 gene was used as an endogenous control. The PCR reactions were run in a 7500 real time PCR system with the following thermoprofile:

1 cycle	50°C for 2 minutes
1 cycle	95°C for 10 seconds
40 cycles	95°C for 15 seconds
1 cycle	60°C for 1 minute

PCR results were gathered from the 7500 real time PCR system software (Applied Biosystems) and analysed using the $2^{-\Delta\Delta CT}$ method (Livak and Schmittgen, 2001).

2.4.10 Subcloning into intermediate vectors

2.4.10.1 StrataClone Blunt PCR Cloning Kit

The *L. donovani* cysteine synthase (*cs*) gene was amplified from gDNA and ligated into the pSC-B-amp/kan intermediate vector (Figure 2.1) to facilitate the cloning into the final vector. This kit was chosen because the PCR products generated by AccuPrime™ *Pfx* polymerase have blunt ends that allow the ligation into the blunt ended vector provided by this cloning kit. The ligation reaction was set up according to manufacturer's instructions, and contained 5 ng of the PCR product, StrataClone Blunt Cloning Buffer (Stratagene), and StrataClone Blunt Vector Mix amp/kan (Stratagene). 1 µL of ligation was transformed into StrataClone SoloPack competent cells provided by the kit and plated in agar plates containing 100 µg/mL ampicillin/kanomycin, 50 mg/mL X-gal and 0.1 M of isopropyl ß-D-1-thiogalactopyranoside (IPTG). Positive bacterial colonies were selected by

blue/white selection and were used to inoculate 5 mL of LB-medium containing 100 µg/mL ampicillin/kanomycin and incubated at 37ºC for 18 hours at 225 rounds per minute (rpm). Plasmid DNA was extracted from the bacterial cultures by alkaline lysis using the Qiagen MiniPrep method (see section 2.1.5) and subsequently digested with *Eco*RI as specified on section 2.2.3 to confirm the presence of an insert of the correct size (1,014 bp in the case of *cs*).

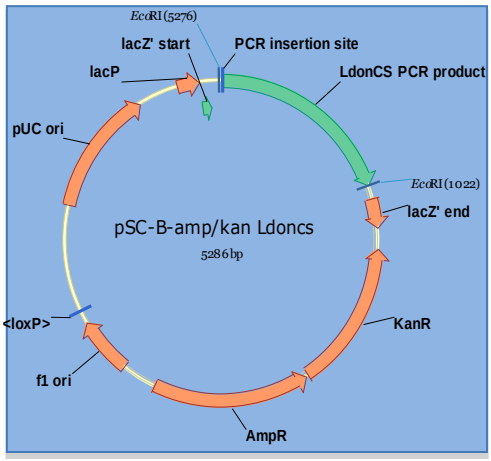

Figure 2.1 – The pSC-B-amp/kan_*Ldoncs* construct.

Vector map of the pSC-B-amp/kan intermediate vector ligated with the *Ldoncs* gene. The pSC-B-amp/kan vector is equipped with a kanomycin (KanR) and ampicillin (AmpR) resistance sequence, a lac promotor (LacP) and a ß-galactosidase α-fragment coding sequence (LacZ') to allow the blue/white bacterial colony screening, a f1 origin for single stranded DNA replication (f1 ori), a loxP recombinase recognition sequence (<loxP>) to allow the Cre-mediated recombination creating a circular DNA molecule, and a pUC origin of double stranded DNA replication (pUC ori).

2.4.10.2 pGEM-T easy

The *L. major* cysteine synthase (*Lmjcs*) gene was amplified from pET21a^{+} construct using Lmj1 and Lmj2 primers and the PCR product was analyzed by agarose gel electrophoresis (see section 2.2.4). *Lmjcs* (1,014 bp) was isolated from the agarose gel using QIAquick gel extraction kit. *Lmjcs* was subcloned into pGEM-T easy as per manufacturer's instructions. Figure 2.2 illustrates the vector map where pGEM-T vector is ligated to *Lmjcs* gene.

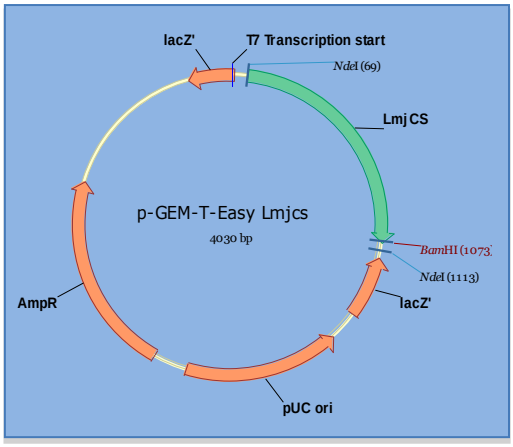

Figure 2.2 – The pGEM-T_*Lmjcs* construct.

Vector map of the pGEM-T intermediate vector ligated with the *Lmjcs* gene. The pGEM-T vector is equipped with an ampicillin (AmpR) resistance sequence, a lacZ start codon (LacZ') to allow the blue/white bacterial colony screening, and a pUC origin of double stranded DNA replication (pUC ori).

2.4.11 Cloning into transformation/ transfection vectors

2.4.11.1 Generation of pET15b_*Lmjcs* construct

Lmjcs insert was excised from pGEM-T easy using *Bam*HI and *Nde*I. The pET15b vector was linearized with the same restriction endonucleases. The ligation reaction was set up using a molar ratio of 1:3 vector to insert, T4 DNA ligase, and T4 DNA ligation reaction buffer, as per manufacturer's instructions. 3 µL of ligation was transformed into DH5α competent bacteria (see section 2.1.4) and plated onto LB-agar plates containing 100 µg/mL of ampicillin, and incubated for 18 hours at 37ºC. Bacterial colonies were used to inoculate 5 mL LB-medium and incubated for 18 hours at 37ºC at 225 rpm. Plasmid DNA was extracted using QIAprep spin Miniprep kit (QIAGEN) and digested with *Bam*HI and *Nde*I to assess the presence of an insert with the correct size before choosing at least two clones that were analysed by sequencing (Source Bioscience). Figure 2.3 depicts the vector map of the construct pET15b ligated to *Lmjcs* gene.

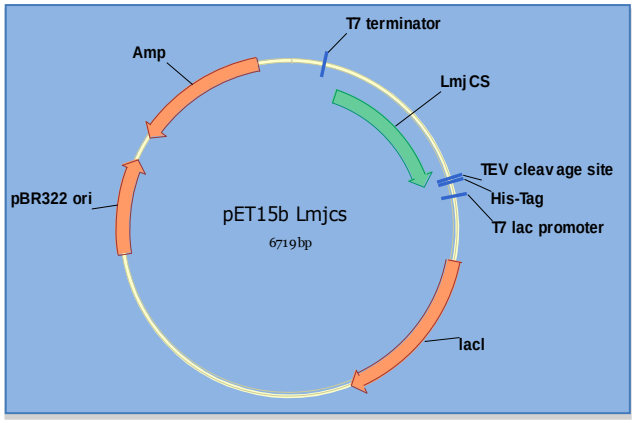

Figure 2.3 – The pET15b_*Lmjcs* construct.

Vector map of the pET15b expression vector ligated with the *Lmjcs* gene. The pET15b expression vector is equipped with an ampicillin (AmpR) resistance sequence, a T7 *lac* promoter, a *lac* repressor (*lacI*), a T7 *lac* terminator, and a pBR322 origin that confers stability to the plasmid. The TEV cleavage site allows the removal of the His-tag after the protein is expressed.

2.4.11.2 Generation of pGL102*cs* construct

Plasmid DNA was isolated from the positive bacterial clones (selected by blue/white screening) using QIAprep spin Miniprep kit (QIAGEN) and digested with *Eco*RV (generating a blunt end) and *Bam*HI (generating the 5' overhang GATCC). DNA fragments were purified as described above. The destination plasmid (pGL102) was linearized using Sma*I* (blunt end) and Bam*HI* (5' overhang GATCC), purified and used in the ligation. Colonies were tested for the presence of the insert by colony PCR. Once identified, plasmid miniprep was performed and the DNA of at least two positive clones was analyzed by DNA sequencing. Figure 2.4 shows the vector map of the final construct pGL102_*Ldoncs*.

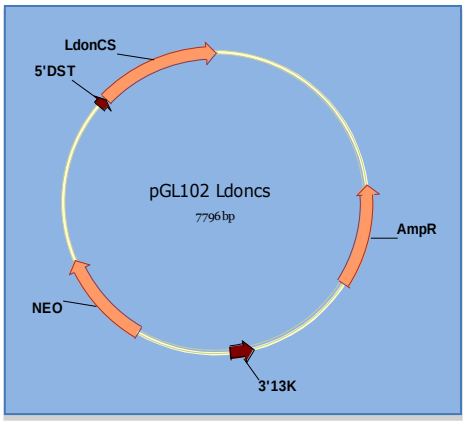

Figure 2.4 – The pGL102_*Ldoncs* construct.

Vector map of the pGL102 expression vector ligated with the *Ldoncs* gene. The pET15b expression vector is equipped with an ampicillin (AmpR) resistance sequence and a neomycin phosphotransferase (neo) resistance sequence, a *Leishmania* splice acceptor (5'DST) and a 13 kb RNA (3'13K).

2.4.12 Preparation of chemically competent *E. coli*

Competent bacteria used throughout this work were generated using either of the two methods described below.

2.4.12.1 Calcium chloride method

5 mL of LB-medium (containing the appropriate antibiotic) were inoculated with the desired bacterial strain and were incubated overnight at 37°C with at 225 rpm. From this culture, 1 mL was used to inoculate 50 mL LB-medium (containing the appropriate antibiotic) and incubated at 37°C with at 225 rpm, until OD_{600} = 0.6. The culture was transferred to a sterile microcentrifuge tube, incubated at 4°C for 10 minutes, and pelleted for 10 minutes at 4,000 rpm at 4°C. The pellet was resuspended in 50 mM $CaCl_2$ (ice cold) and incubated at 4°C for 40 minutes; and pelleted again for 10 minutes at 4,000 rpm at 4°C (AccuSpin MicroR, rotor 13-100-515). The pellet was resuspended in 1 mL of ice-cold 50 mM $CaCl_2$. Glycerol at 20% in PBS was

added to aliquots of competent cells prior to being transferred to -80°C for storage.

2.4.12.2 Rubidium chloride method

The initial steps of this method are essentially the same as described above. After pelleting the bacteria, they were resuspended in TFBI buffer (100 mM RbCl, 50 mM $MnCl_2$-$4H_2O$, 30 mM NaH_2AsO_4, 10 mM $CaCl_2$-$2H_2O$ and 15% glycerol) and incubated at 4°C for 15 minutes. The pellet was collected by centrifugation for 5 minutes at 4,000 rpm at 4°C (AccuSpin MicroR, rotor 13-100-515), and resuspended in 300 µL of ice-cold TFBII buffer (0.2 M MOPS, 10 mM RbCl, 75 mM $CaCl_2$-$2H_2O$ and 15% glycerol). Aliquots of competent cells were frozen in dry ice before being transferred to -80°C for storage.

2.4.13 Transformation of competent bacteria

Transformations of competent bacteria were set up using a 100 µL aliquot of cells and adding up to 10 µL of ligation reaction or 1 µL of plasmid DNA. The transformation reaction was incubated on ice for 30 min; heat shocked at 42°C for 45 seconds; incubated on ice for 2 min before 250 µL of LB-medium was added to the reaction. The transformation reaction was then incubated at 37°C at 225 rpm for 1 h. 100 µL of the transformation reaction was plated onto LB-agar plates containing the appropriate antibiotic.

2.4.13.1 Isolation of plasmid DNA from transformed bacteria

The isolation of plasmid DNA was performed in order to further screen for positive inserts in a plasmid. 5 mL of LB-medium supplemented with the appropriate antibiotic was inoculated with a single bacterial colony and incubated overnight at 37°C. The bacterial culture was pelleted, a single colony was picked and plasmid DNA isolation was carried using the QIAprep spin Miniprep kit according to manufacturer's recommendations.

2.5 Biochemical methods

2.5.1 Protein quantification methods

2.5.1.1 Bradford assay

A range of known concentrations (0.1 to 0.5 mg/mL) of bovine serum albumin (BSA) was used as standard for determination of the extracted protein concentration. 10 µL of either standard or sample were mixed as per manufacturer's instructions with 250 µL of filtered Bradford (Bradford, 1976) protein assay reagent (BioRad) prediluted in 1:5 in ddH_2O. The absorbance ($A_{595\ nm}$) was read.

2.5.1.2 BCA assay

The BCA (Smith *et al.*, 1985) kit provides a 2 mg/mL albumin standard from which standard concentrations (0.025 to 2 mg/mL) are prepared. The working reagent was prepared by mixing BCA reagent 1 with BCA reagent 2 in a 50:1 ratio as per manufacturer's instructions. 10 µL of either standard or sample were mixed with 200 µL of working reagent in a 96-well plate. The plate was incubated at 37°C for 30 min and the absorbance at 562 nm was read.

2.5.2 Sodium dodecyl sulphate polyacrylamide gel electrophoresis (SDS-PAGE)

Proteins were analysed by separation in a non-gradient 10% SDS-PAGE (Laemmli, 1970). Gels were prepared by first pouring 7 mL of resolving solution on a gel cassette. This solution contained 1.5 mL of resolving buffer (1.5 M Tris-HCl pH 8.9, 0.4% SDS), 2.5 mL of water, 2 mL of 30% acrylamide, and supplemented with polymerisation reagents: 20 µL of 20% ammonium persulphate (APS) and 6 µL of tetramethylethylenediamine (TEMED). The gel

was allowed to set and then 3 mL of stacking solution was added, containing 1.75 mL of water, 750 µL of stacking buffer (0.5 M Tris-HCl pH 6.7, 0.4% SDS), 0.5 mL of 30% acrylamide, and supplemented with 10 µL of 20% ammonium persulphate (APS) and 3 µL of tetramathylethylenediamine (TEMED). A comb was placed on top of the stacking solution according to the necessary number of wells. Once the gel was set, 5 to 10 µg of protein were mixed with 6 x SDS-PAGE loading buffer and boiled for 3 min. A protein ladder (Precision Plus Protein™ Dual Color Standards, Bio-Rad) was loaded onto the gel along with the samples to allow relative size determination. Gel cassettes were mounted in a gel tank (Bio-Rad) and run in PRB electrode buffer (25 mM Tris base, 1.92 mM glycine, pH 8.3 containing 1.3 mM SDS) at 20-60 mA.

SDS-PAGE gels were stained with GelCode™ Blue Safe Protein Stain (Thermo Scientific) or with Coomassie blue stain (40% (v/v) methanol, 10% (v/v) acetic acid, 0.1% (w/v) Coomassie brilliant blue R-250) for 1 hour and subsequently destained with water or 20% methanol, 10% acetic acid.

2.5.3 Western-blot analyses

After separation of proteins by SDS-PAGE they were transferred to nitrocellulose membrane using a TransBlot SD Semi-dry transfer cell (Bio-Rad). The protein containing-SDS-PAGE gel was placed on top of the nitrocellulose membrane, and both were placed between eight layers of filter papers, four on top and four at the bottom. The membrane, gel and filter papers were soaked in towbin buffer (25 mM Tris base, 1.92 mM glycine, 1.3 mM SDS and 20% methanol). The transfer occurred at 20 V, 5 mA for 1 hour. Ponceau-S (Sigma) solution was used to visualize protein on the nitrocellulose to confirm the transfer of protein. The protein-containing membrane was blocked in PBS with 5% Marvel milk powder for 1 h at room temperature or overnight at 4°C, with shaking. Primary antibodies raised against *Leishmania* recombinant proteins were diluted to the appropriate concentration (see section 2.1.6) in PBS with 1% (w/v) Marvel milk powder. The membrane was incubated at room temperature for 1 h with the diluted

antibodies and then washed three times for ten minutes with shaking in PBS with 0.1% (v/v) Tween 20. Horse radish peroxidase (HRP)-conjugated secondary antibodies were diluted to appropriate concentration (see section 2.1.6) in PBS with 1% (w/v) Marvel milk powder. Membranes were incubated for 1 h at room temperate in diluted secondary antibodies and then washed as previously explained. The detection of the secondary antibody was carried out by adding to the membrane Immobilon™ Western chemiluminescent HRP substrate (Millipore) for 5-10 seconds at room temperature. The resulting chemioluminescence was detected by Kodac Medical X-ray film (Kodac) and revealed in a Konica Minolta tabletop processor model SRX-101A (Konica).

2.5.4 Expression of recombinant C- and N-terminally 6 x His-tagged *Lmj*CS

Three types of recombinant *L. major* cysteine synthase (CS) were expressed: *Lmj*CS with a C-terminal His-tag and CS with an N-terminal His-tag. The plasmids used were pET15b*cs* (N-terminal His-tag, see section 2.1.2.1) and pET21a+*cs*[1] (C-terminal His-tag). Both plasmids were used to transform BL21/DE3 competent bacteria. 6 mL of LB-medium were inoculated with the resultant colonies from the transformation reaction (see section 2.1.4) and incubated overnight at 37°C. 1 mL of overnight culture was used to inoculate 250 mL of LB media and incubated at 37°C at 225 rpm. 1 or 2 mM IPTG was added when $O.D._{600}$ reached 0.6. The cultures induced with 1 mM IPTG were transferred to 15°C and left to express the *Lmj*CS overnight whilst the ones induced with 2 mM IPTG were transferred to 37°C.

[1] Kindly provided by Dr Gareth Westrop from University of Strathclyde.

2.5.5 Purification of recombinant C- and N-terminally 6 x His-tagged *Lmj*CS

Bacteria expressing *Lmj*CS were harvested by centrifugation (Sigma 6K15, rotor 11150) and the pellet was resuspended in lysis buffer (50 mM phosphate buffer pH8, 300 mM NaCl and 10 mM imidazole). A cell disruptor (Constant cell disruption systems) was used to mechanically lyse the cells. The cell suspension was centrifuged for 1 h at 20,000 rpm (Beckman Coulter Avanti™ J-26XP, rotor JA-25.50). The fraction that contains CS protein was identified by running both soluble and insoluble fractions in SDS-PAGE (see section 2.2.2) and staining with Coomassie (section 2.2.3). The fraction containing the protein was transferred to a Ni^{+}-agarose column. The column was then washed with wash buffer (50 mM sodium phosphate buffer pH8, 300 mM NaCl and 20 mM imidazole) to remove non-specific bound proteins. His-tagged *Lmj*CS was eluted from the column using elution buffer (50 mM sodium phosphate buffer pH8, 300 mM NaCl and 250 mM imidazole). Aliquots of all fractions were analyzed by SDS-PAGE to assess purification efficiency and purity of the recombinant protein. The concentration of *Lmj*CS was determined using the Bradford protein quantification method.

2.5.6 Removal of N-terminal His-tag

The non-tagged r*Lmj*CS was generated from the N-terminally tagged protein. The N-terminally His-tagged *Lmj*CS was used to remove the His-tag using TEV protease. After His-tag purification, N-r*Lmj*CS was passed through a Zeba™ desalt spin column to exchange the buffer that the protein was eluted in to a imidazole free buffer (50 mM sodium phosphate buffer pH8 and 300 mM NaCl) to allow a post-cleavage purification of the then non-tagged recombinant protein. The optimal conditions were assed using TEV:CS ratios 1:1, 1:50, 1:100, and 1:200 for 1 h at 30°C. The efficiency of TEV cleavage was assessed by SDS-PAGE. With the optimal cleavage conditions established, non-tagged *Lmj*CS was separated from His-tagged

*Lmj*CS by passing the reaction mixtures through the Ni^{+}-agarose column as described above.

2.5.7 Kinetic characterization of N-r*Lmj*CS, C-r*Lmj*CS and *Lmj*CS

1 mL reaction mix contained 0.4 mM sodium phosphate buffer pH 7.8, 20 mM EDTA, 10 mg/mL gelatine, 2 mM pyridoxal 5'-phosphate, 0.5-15 mM *O*-acetyl serine, and cysteine synthase (250 ng/mL N-r*Lmj*CS, 250 ng/mL C-r*Lmj*CS, and 500 ng/mL r*Lmj*CS). The reaction was initiated with when sodium sulphide (3 mM) was added. The reaction was stopped at time 2, 4 and 6 minutes. 10 µL of reaction mix were mixed with 50 µL nitrous acid (1 part sodium nitrite 0.1 M and 99 parts of sulphuric acid 0.4 M). Here the thiol of the cysteine formed is treated with an excess of nitrous acid originating a stable *S*-nitrosothiol derivative. The excess of nitrous acid is removed with 20 µL ammonium sulfamate 0.5%. Then a mixture of 1% mercuric chloride, 3.44% sulphanilamide and 0.1% N-1-naphthylethylenediamine (NEDA) is added. The mercuric ion decomposes the *S*-nitrosothiol, giving nitrous acid. The sulphanilamide diazotes the nitrous acid, which will then couple with the NEDA to give a stable azo dye ($A_{540\ nm}$).

2.5.8 Inhibition of N-r*Lmj*CS, C-r*Lmj*CS and *Lmj*CS

Thus experiment was set up as mentioned on section 2.2.8 except that the inhibitors were added to the reaction mix before the reaction was started with sodium sulphide. In addition, the inhibitor was pre-incubated for 15, 30 and 60 min at 0.1 mM with the non-tagged *Lmj*CS protein before both were added to the reaction mix. The pre-incubation times tested were 0, 15 and 30 minutes. A control with no inhibitor was setup in parallel to ensure the potential difference seen was due to the inhibitor and not because of the pre-incubation. The pre-incubation was done at room temperature and the

cysteine synthesis reaction was carried as explained on section 2.5.7 at room temperature.

2.5.9 Development of a fluorescent CS assay using 7-diethylamino-3-(4'maleimidylphenyl)-4-methylcoumarin

The standard assay conditions are similar to the assay described on section 2.5.7 (Kredich and Tomkins, 1966), only that 7-diethylamino-3-(4'maleimidylphenyl)-4-methylcoumarin (CPM) is used to detect cysteine synthesis (Chung *et al.*, 2008). High levels of background were detected using CPM and therefore a series of experiments had to be carried in order to identify the source and minimize it. The pH, sodium sulphide (Na_2S), protein stabilizer (BSA and gelatine), CPM storage and concentrations, were assessed as possible causes of background formation.

2.5.9.1 Assessing the effect of sodium sulphide on the fluorescence background at varying pH

A series of 100 µL reactions were set up containing assay buffer (0.1 mM sodium potassium phosphate pH variable, 1 mM EDTA, 10 mg/mL bovine serum albumin (BSA), and 1 mM *O*-acetyl serine (OAS) substrate. 40 µM cysteine (Cys) and 0.5 mM Na_2S substrate were tested alone or simultaneously. In a 96-well plate, 100 µL of each reaction were taken and mixed with 100 µL of 7-diethylamino-3-(4'-maleimidylphenyl)-4-methylcoumarin (CPM) in 50% DMSO. CPM reacts with the free thiol groups generating a fluorescent compound that can be measured (λexcitation = 340 nm, λemission = 465 nm). All reactions were made in triplicate for statistical analysis.

2.5.9.2 Assessing the effect of BSA and gelatine in the fluorescence background

0.1 and 1 mg/mL of gelatine and BSA were tested in order to determine their influence in the background. Five reactions were set containing assay buffer pH 7.8 only (see section 2.5.9.1) where the variable was the protein stabilizer. The first reaction contained no protein stabilizer, the second contained 1 mg/mL BSA, the thirst one contained 0.1 mg/mL BSA, the fourth one contained 1 mg/mL gelatine, and the fifth one contained 0.1 mg/mL gelatine. In a 96-well plate, 100 µL were mixed with 100 µL CPM in 50% DMSO and the fluorescence was measured (λexcitation = 340 nm, λemission = 465 nm). All reactions were made in triplicate for statistical analysis.

2.5.9.3 Assessment of the influence of CPM storage length in the fluorescence detection

To ensure the good quality of CPM stock storage length, three CPM stocks (50 µg/mL) were prepared. CPM preparations were tested on day 0, 3 and 9. Two reactions were set up per day, one containing assay buffer (see section 2.5.9.1) to be used as blank and another containing assay buffer and 40 µM cysteine. Here 100 µL of reaction were mixed with 100 µL CPM (50 µg/mL) in 50 % DMSO in a 96-well plate and the fluorescence was measured (λ excitation = 340 nm, λemission = 465 nm). All reactions were made in triplicate for statistical analysis.

2.5.9.4 Analysis of increasing CPM concentrations and its influence in the assay linearity

To determine the ideal CPM concentration, four reactions were set up containing assay buffer (see section 2.5.9.1), 40 µM cysteine and/or 0.5 mm Na_2S. The CPM concentrations tested were 25, 50 and 100 µg/mL. In a 96-well plate, 100µL of each reaction were mixed with 100µL CPM in 50% DMSO

and the fluorescence was measured (λexcitation = 340 nm, λemission = 465 nm). All reactions were performed and statistically analyzed (section 2.7.3).

2.5.9.5 Determination of the fluorescence generated by known cysteine concentrations using the CPM detection method

To determine the correlation between fluorescent read and cysteine concentration present in reaction, concentrations of cysteine (0, 20, 40, 60, 80 and 100 μM) were mixed with assay buffer (see section 2.5.9.1), 0.1mg/mL gelatine and 0.5 mM Na_2S. 100 μL of reaction were mixed with 100 μL CPM (100 μg/mL) in 50% DMSO in a 96-well plate and the fluorescence was measured (λexcitation = 340 nm, λemission = 465 nm). All reactions were made in triplicate for statistical analysis. The results were used to plot a standard curve.

2.5.9.6 Quantification of cysteine generated in an enzymatic reaction by extrapolation from a standard curve

The ideal N-r*Lmj*CS concentration was determined by setting up reactions containing increasing concentrations of N-r*Lmj*CS. 1 mL reaction contained assay buffer pH 7.8 (see section 2.2.10.1), 0.1mg/mL of gelatine, 1 mM of OAS substrate and N-r*Lmj*CS (25, 50 or 75 ng/mL). The reaction was incubated for 10 minutes at room temperature and then initiated with the addition of 0.5 mM Na_2S substrate. A reaction with no enzyme was set up as used to measure the background. The synthesis of cysteine was monitored every 2 minutes over a period of 10 minutes. 100 μL of reaction were mixed with 100 μL CPM (100 μg/mL) in 50% DMSO in a 96-well plate and the fluorescence was measured (λexcitation = 340 nm, λemission = 465 nm). All reactions were performed and statistically analyzed (section 2.7.3)

2.5.9.7 Inhibition of N-r*Lmj*CS with DYVI peptide and determination of its IC_{50} using the CPM detection method

DYVI was tested as potential *Lmj*CS inhibitor. 1 mL reaction was set with assay buffer, 0.1 mg/mL of gelatine, 1 mM of OAS substrate, 50 ng/mL N-r*Lmj*CS and 0.1 mM DYVI. The reaction was incubated for 10 minutes at room temperature and was then started with the addition of 0.5 mM Na_2S substrate. The synthesis of cysteine was monitored every 2 minutes over a period of 10 minutes. 100 μL of reaction were mixed with 100 μL CPM (100 μg/mL) in 50% DMSO in a 96-well plate and the fluorescence was measured (λexcitation = 340 nm, λemission = 465 nm). All reactions were performed and statistically analyzed (section 2.7.3)

To determine DYVI IC_{50} using the CPM detection method, several reaction were set up using increasing concentrations of this inhibitor. The assay buffer was mixed with 50 ng/mL of N-r*Lmj*CS, 0.1 mg/mL of gelatine, 1 mM of OAS substrate and DYVI (0.5, 1, 1.5, 2.5, 5, 10, 20, 50, 100 and 200 μM). The reactions were initiated with Na_2S substrate at 0.5 mM of final concentration. The fluorescence (λexcitation = 340 nm, λemission = 465 nm) was determined at minute 6 by mixing an aliquot of the reaction with CPM (100 μg/mL) in 50% DMSO in a 96-well plate.

2.5.10 HPLC methods

2.5.10.1 Detection and quantification of thiols

2.5.10.1.1 Sample preparation

Parasites were harvested as explained on section 2.6.5 and derivatized on the same day. Standard curves of the thiols of interest were set up in order to facilitate the determination of thiol concentration on parasite extracts and to determine the retention time in the HPLC column. The concentrations of the standards ranged from 50 to 250 pmol, and the thiols

derivatized were cysteine, glutathione, trypanothione and glutathione. Both sample and standard were suspended in 50 µL of HPLC buffer (40 mM N-[2-hydroxyethyl]-piperazine-N'[3-propanesulphonic acid] (EPPS), 4 mM of diethylenetriamine pentaacetic acid (DTPA), and pH 8 adjusted with 1 M lithium hydroxide) with 0.7 mM of *tris*(2-carboxyethyl)phosphine (TCEP) and incubated on ice for 45 minutes. The samples/standards were derivatized by adding 50 µL of 2 mM monobromobimane in absolute ethanol were added to each sample/ standard and heated to 70°C for 3 minutes. Then the samples/ standards were deproteinized with 100 µL of 4 M methanosulphonic acid pH 1.6 (pH adjusted with lithium hydroxide powder) and then incubated on ice for 30 minutes. Tubes were centrifuged at 13,000 rpm at 4°C for 45 minutes and the supernatant was transferred to a HPLC tube for further analysis. The samples/ standards were analyzed on the same day of preparation or stored at -20°C for no more than a week.

2.5.10.1.2 System operation

Thiol molecules were detected and quantified using reverse phase HPLC. The column used was a Gemini 5 µm C18 250 x 4.6 mm silica column (Phenomenex, UK). In order to protect the main column, the system was fitted with a pre-column (security guard column KJ0-4282, Phenomenex, UK) that would be changed when the system pressure would reach 1500 PSI. If not in use, the column was stored in 100% methanol. The instrument used was a Dionex Ultimate 3000 HPLC equipped with an auto-sampler (Ultimate 3000 autosampler), a UV detector (Dionex Ultimate 3000 Variable Wavelength Detector) and a fluorescence detector (Dionex RF 2000 Fluorescence Detector) as well as with the Chromeleon™ (Dionex) software to control the system.

The mobile phase consists of solvent A: 0.25% acetic acid; and solvent B: 100% acetonitrile.

All solvents were filtered and degassed before being applied in the HPLC system to avoid cluttering of the system tubes and column damage. The filtration and degasification process consisted in a bottle with a magnetic

stir with a filtration unit attached. A tube connects the filter unit to an electric pump. The solvents would pass through the filter (0.20 μm of pore size) to the bottle. The magnetic stir inside the bottle aids the release of the gas, which is lead out by the vacuum generated by the pump.
Before being used, the column was washed with filtered and degassed ddH_2O to remove the methanol before 50% solvent A/ 50% solvent B were applied to the column. 100% of acetonitrile would then be run over a period of 20 min to avoid the generation of high pressure. The samples/standards were placed into the autosampler and 10 or 20 μL were injected for analysis. The samples were separated using the solvent gradient shown in Table 2.1 at a flow rate of 0.55 mL/min.

Minutes	0	10	40	100	110	111	121
Solvent A (%)	100	100	92	85	50	100	100
Solvent B (%)	0	0	8	15	50	0	0

Table 2.1 - Gradient used to separate thiol-monobromobimane derivatives.

2.5.10.2 Method validation of detection and quantification of polyamines

2.5.10.2.1 Determination of the ideal solvent/ gradient

System operation was the same as explained on section 2.5.10.1.2. There were two solvent combinations tested: 100% methanol/water, and 75% Octane-1-sulfonate (20mM) + 25% acetonitrile/20% Octane-1-sulfonate (20mM) + 80% acetonitrile (Table 2.2) (Das Gupta *et al.*, 2005; Müller *et al.*, 1988; Wittich *et al.*, 1987). There were three modified gradients based on Wittich *et al.* (1987) (Table 2.2). The flow rates tested were 0.55 to 1 ml/mL and adjusted to the machine pressure.

Gradient A:

Time (minutes)	0	25	37.5	46.25	50	52.5	62.5
Solvent A (%)	42.5	32.5	17.5	0	0	42.5	42.5
Solvent B (%)	57.5	67.5	82.5	100	100	57.5	57.5

Flow rate = 0.55 mL/ min

Solvent A – Methanol

Solvent B – ddH_2O

Gradient B:

Time (minutes)	0	13	18	29	32	51	56	62.5
Solvent A (%)	75	70	35	25	0	0	75	75
Solvent B (%)	25	30	65	75	100	100	25	25

Flow rate = 1 mL/ min

Solvent A – 75% Octane-1-sulfonate (20mM) and 25% acetonitrile

Solvent B – 20% Octane-1-sulfonate (20mM) and 80% acetonitrile

Gradient C:

Time (minutes)	0	15	45	62.5
Solvent A (%)	70	0	0	70
Solvent B (%)	30	100	100	30

Flow rate = 1 mL/ min

Solvent A – 75% Octane-1-sulfonate (20mM) and 25% acetonitrile

Solvent B – 20% Octane-1-sulfonate (20mM) and 80% acetonitrile

Table 2.2 – Gradients tested for the separation of polyamines.

The tables show the gradients used in the separation of polyamines in order to quantify them. Gradients are identified as A, B and C. The solvent combination and flow rate applied is referred bellow each table.

To test gradient A, 20 pmol of 1,6-diaminohexane were run in the HPLC; to test gradient B, 20 pmol of 1,6-diaminohexane was tested; and to test gradient C, 1 nmol of putrescine was used. The referred amount of polyamines were mixed with 10% trichloroacetic acid (TCA), and perchloric acid to a final concentration of 0.2 mM. This solution was saturated with

sodium carbonate in order to bring the pH up. 2 mg/mL of dansyl chloride were added and the solution was incubated overnight at room temperature in the dark. After incubation, 25% proline was added to one of the solutions. 800 µL of solution were transferred to a 15 mL tube and 4 mL of ether were added. The tubes were gently shaken for 1 hour in order to extract the dansyl chloride derivatives. 3.5 mL of ether were transferred to a clean 15 mL tube and the tubes were placed in a heat plate at 70°C with lids removed to evaporate the ether to dryness. Dansyl chloride derivatives were resuspended in 200 µL 5% acetic acid in methanol and 150 µL were transferred to a clean HPLC tube. The sample tubes were immediately loaded in the HPLC machine otherwise they were kept at – 20°C. The above-mentioned gradients were used for each correspondent sample and the fluorescence was measured (λexcitation = 365; λemission = 485 nm). Injected volume varied from 10 to 20 µL.

2.5.10.2.2 Polyamine separation using 10 mg/mL of dansyl chloride with and without proline

When increasing the concentration of dansylchloride one has to ensure that the background will not interfere with the reading of the chromatogram. In an attempt to lower the background caused by excess of dansylchloride, 1 nmol/ 20 µL of putrescine were derivatized in the presence/ absence of proline. One solution was made without putrescine and another without proline to use as negative controls. 50 nmol of putrecine were mixed with 10% TCA, and perchloric acid to a final concentration of 0.2 mM. This solution was saturated with sodium carbonate in order to bring the pH up. 10 mg/mL of dansylchloride were added and the solution was incubated overnight at room temperature in the dark. After incubation, 25% proline was added to one of the solutions. 800 µL of solution were transferred to a 15 mL tube and 4 mL of ether were added. The tubes were gently shaken for 1 hour in order to extract the dansylchloride derivatives. 3.5 mL of ether were transferred to a clean 15 mL tube and the tubes were placed in a heat plate at 70°C with lids removed to evaporate the ether to dryness.

Dansylchloride derivatives were resuspended in 250 µL 5% acetic acid in methanol and 200 µL were transferred to a clean HPLC tube. The sample tubes were immediately loaded in the HPLC machine otherwise they were kept at –20°C. The gradient C (see section 2.5.10.2.1) was used and the fluorescence was measured (λexcitation = 365; λemission = 485 nm). Injected volume varied from 10 to 20 µL.

2.5.10.2.3 Polyamine detection and quantification in cell extracts

To quantify polyamines in cell extracts, standard curves were set up of the polyamines of interest. Putrescine standard curve was set up between 125 pmol and 500 pmol; spermidine standard curve was set up between 125 pmol and 800 pmol; and spermidine standard curve was set up between 250 pmol and 800 pmol. 1,6-diaminohexane was added to each standard at 500 pmol and used as an internal standard. Polyamines were prepared in a mix. 100 µL of polyamine mix were treated with 10% TCA, and perchloric acid to a final concentration of 0.2 mM. 500 pmol of 1,6-diaminohexane were added at this stage. The solution was saturated with sodium carbonate in order to bring the pH up. 10 mg/mL of dansylchloride were added and the solution was incubated overnight at room temperature in the dark. After incubation, 25% proline was added to one of the solutions. 800 µL of solution were transferred to a 15 mL tube and 4 mL of ether were added. The tubes were gently shaken for 1 hour in order to extract the dansylchloride derivatives. 3.5 mL of ether were transferred to a clean 15 mL tube and the tubes were placed in a heat plate at 70°C with lids removed to evaporate the ether to dryness. Dansylchloride derivatives were resuspended in 250 µL 5% acetic acid in methanol and 200 µL were transferred to a clean HPLC tube. The sample tubes were immediately loaded in the HPLC machine otherwise they were kept at –20°C. The gradient C (see section 2.5.10.2.1) was used and the fluorescence was measured (λexcitation = 365; λemission = 485 nm). Injected volume varied from 10 to 20 µL.

2.6 Culturing of *Leishmania*

2.6.1 *L. donovani* promastigote culture

L. donovani were cultured in HOMEM containing 10% fetal calf serum (FCS) and 1% penicillin/streptomycin with the appropriate antibiotics to select for the presence of selectable markers and sub-passaged weekly to a density of $5x10^5$ parasites/mL. Parasites recovered from the hamster spleen by limiting dilution assay (see section 2.6.4) or from a frozen stock (see section 2.6.2), were first cultured in the medium referred to above but containing 20% FCS. Antibiotics were added as follows when required: G418 at 50 µg/mL, hygromycin at 50 µg/mL and neurseothricin at 50 µg/mL. Cultures were incubated at 25°C.

2.6.2 Freezing/ thawing of parasites

Parasites were cryopreserved in 50% HOMEM, 20% FCS, 1% penicillin/streptomycin and 10% DMSO and transferred to -80°C for 24 hours before being transferred into liquid nitrogen.
To recover the parasites, the stabilates were quickly thawed and placed in HOMEM, 20% FCS and 1% penicillin/ streptomycin. Flasks were incubated at 25°C.

2.6.3 Analysis of *L. donovani* growth

Parasite density was determined daily by transferring an aliquot of culture to 2% formaldehyde in PBS. Parasites were counted using a Newbauer haemocytometer and observed on an inverted light microscope (Zeiss Wetzlar) using a 40x magnification. Cell growth was analyzed over a period of 6 days until the parasites reached stationary phase, and they were then sub-passaged to $5x10^5$ parasites/mL as described above.

2.6.4 Isolation of *L. donovani* from hamsters

Golden hamsters were culled six months after having being infected with *L. donovani* parasites (strain BPK 206 clone 10). Dr Elmarie Myburgh, carried out the infection. Three groups of 6 hamsters had been previously infected with *L. donovani* BPK 206 clone 10 (wild-type, WT), *L. donovani* BPK 206 clone 10 lacking the *cs* alleles (Δ*cs*), and *L. donovani* BPK 206 clone 10 lacking the cs alleles with an episomal re-expression plasmid (RE). The hamsters were dissected, and spleens and livers were removed, weighed and measured. A small portion of each organ was placed into HOMEM containing 20% FCS with 1% penicillin/streptomycin. The remainder of the organ was ground in PSGEMKA medium and used in a limiting dilution assay by liver and spleen homogenates into the first well of 96 well plates in a 1:2 dilution. From this well sequential 1:2 dilutions were made until the end of the plate.

2.6.5 Harvest of *L. donovani* from a culture

Cultures were transferred to a 15 mL Falcon tube and centrifuged at 4°C, 1,600*g* for 10 minutes. The supernatant was discarded and the parasites were washed twice with PBS with centrifuge steps in between where supernatant is discarded. Finally cells are resuspended in the intended buffer depending on the purpose.

2.6.6 Isolation of DNA

Parasites were harvested as explained on section 2.6.5. The isolation of gDNA from *L. donovani* parasites was performed using the QIAamp DNA mini kit (Qiagen) as per manufacturer's instructions. gDNA was stored at 4°C for further analysis.

2.6.7 Isolation of RNA

Parasites were harvested as explained on section 2.6.5. The isolation of genomic DNA from *L. donovani* parasites was performed using the RNeasy Mini kit (Qiagen) as per manufacturer's instructions. RNA was stored at -80°C for further analysis.

2.6.8 Isolation of protein

L. donovani promastigote parasites were pelleted and lysed using the lysis buffer (0.25 M sucrose, 0.25% Triton X-100, 10 mM EDTA, 20 μM E-64, 4 μM 1,10-phenanthroline, 8 μM pepstatin A, 2 mM phenylmethylsulfonylfluoride). The suspension was incubated on ice for 10 min and the soluble fraction, containing the total protein extract, and centrifuged at 13,000 rpm for 30 minutes at 4°C (Sigma 1-15, rotor 12124). The protein concentration of the supernatant was determined using the BCA protein quantification method.

2.6.9 Transfection of *L. donovani*

L. donovani Δ*cs* promastigotes parasites were briefly counted and $5x10^7$ parasites were pelleted at 1,000*g* for 10 minutes at 4°C (Beckman Coulter Allegra™ X-12R, rotor SX4750). 100 μL of Human T Nucleofector solution (Lonza) were added to the pellet and gently mixed. pGL102*cs* construct was ethanol precipitated (see section 2.2.2) and 10 μg were added to the pellet in a cuvette supplied by the Nucleofector® kit. Amaxa® Nucleofector® Device (Lonza). The program used was U-033 to electroporate the parasites. Electroporated parasites were transferred into 10 mL HOMEM containing 20% FCS and 1% penicillin/streptomycin. The appropriate selective drug was added to the cultures the following day.

2.6.10 Cloning by limiting dilution

Clones were isolated by a limiting dilution assay. The transfected parasites were diluted in HOMEM with 20% FCS and 1% penicillin/streptomycin. The dilutions were made as follows:

Dilution 1	4 mL of culture + 20 mL medium
Dilution 2	2 mL of dilution 1 + 22 mL medium
Dilution 3	4 mL of dilution 2 + 20 mL medium
Dilution 4	4 mL of dilution 3 + 20 mL medium

After 2 weeks incubation, clones were subpassaged into 3 mL HOMEM with 10% FCS, 1% penicillin/streptomycin, and 50 μg/mL of G-418. When the parasites reached the appropriate density, gDNA (see section 2.6.6), RNA (see section 2.6.7) and protein was extracted (see section 2.6.8).

2.6.11 Determination of IC_{50} values

The determination of *L. donovani* promastigote susceptibility to compounds was performed using resazurin dye/ Alamar Blue® (7-hydroxy-3H-phenoxazin-3-one 10-oxide) assay (Kulshrestha *et al.*, 2013; Mikus and Steverding, 2000). On a 96-well plate, 100 μL of a late-log parasite culture containing $2x10^6$ parasites/mL were transferred into each well; 100 μL of compound would be sequentially diluted in the wells rendering a final density of $1x10^6$ parasites/mL. The inhibitors tested were propargylglycine (0.3 μM to 20 mM) and α-difluoromethylornithine (0.001 μM to 20 mM); the pro-oxidants tested were hydrogen peroxide (0.02 to 30 mM), cumene hydroperoxide (1 μM to 1 mM), and *tert*-butyl hydroperoxide (1 μM to 1 mM); the metals tested were cadmium chloride (0.003 to 40 mM), and potassium arsenate (0.003 to 20 mM). The plates were incubated for 72 h before resazurin was added to each well at 125 μg/mL final concentration. The plates were incubated further for 48 h and the fluorescence using an

λemission = 620 nm and λexcitation = 544 nm. Since the assay had strong background fluorescence which varied from experiment to experiment, the values obtained from this "dead cell control" was used to assess 100% cell death. 200 μM of pentamidine was used as positive control, since the determined IC_{50} for WT was 5.6 μM, for Δ*cs* was 2.3 μM, and for RE was 3.4 μM. The percentage of viability was calculated in relation to this value.

2.7 Bioinformatic methods

2.7.1 Sequence identification

All *L. donovani* and *L. major* gene sequences identified were retrieved from the NCBI website (http://www.ncbi.nlm.nih.gov/protein/).

2.7.2 Sequence alignment

Gene sequence alignments were performed in AlignX from Vector NTI Advanced® (version 11.5.1, Invitrogen).

2.7.3 Statistical analysis

All the statistical analyses were carried using Graphpad Prism 5 software (Graphpad). Grouped data were analyzed with one-way ANOVA with Dunnett's post-test using a control sample or Tuckey's post-test. The Dunnett's post-test test allows the comparison of a mean with the mean of a control group, which has been defined for each situation, without comparing the groups between themselves. The Tuckey's test allows the comparison of the means between groups without defining a control group. All the groups are compared with each other. The data was classified according with the P-value (Table 2.3). Unless otherwise stated, all graphs were generated using the GraphPad Prism 5 software package.

P-value	Summary
> 0.05	n.s.
0.01 to 0.05	*
0.001 to 0.01	**
< 0.001	***

Table 2.3 – P-value classification.

The table shows the P-value classification according to the significance. (n.s.) not significant.

Characterization of a recombinant *L. major* cysteine synthase

3 Characterization of a recombinant *L. major* cysteine synthase

3.1 Introduction

This chapter focuses on the analysis of the recombinant cysteine synthase (CS) from *L. major* (*Lmj*CS). Previously, it was shown that *Leishmania* possess two pathways that generate cysteine, the sulphydrylation pathway and the reverse trans-sulphuration (RTS) pathway (Williams *et al.*, 2009). CS catalyses the formation of cysteine from *O*-acetyl serine (OAS) and hydrogen sulphide (H_2S). OAS is generated from serine and acetyl-CoA by serine acetyl-transferase (SAT). It was previously shown that SAT and CS forms a complex that is important to the regulation of CS activity in *Arabidopsis thaliana* (Bonner *et al.*, 2005; Francois *et al.*, 2006; Heeg *et al.*, 2008; Kumaran and Jez, 2007). This work showed that the C-terminus of SAT interacts with the active site of CS thereby inhibiting CS activity and promoting SAT activity. These observations initiated a screening of peptides and resulted in the finding that pentapeptides with C-terminal isoleucine are sufficient to inhibit CS activity of the *Haemophilus influenzae* enzyme (Salsi *et al.*, 2009). William *et al.* (2009) showed that *Leishmania* CS and SAT also form a complex. Based on these observations it was postulated that *Lmj*CS should also be susceptible to inhibition by small peptides and this hypothesis was tested in this chapter. In addition, this chapter focussed on establishing a new CS enzyme assay based on the detection of cysteine using a fluorescent dye, 7-diethylamino-3-(4-maleimidophenyl)-4-methylcoumarin (CPM) (Chung *et al.*, 2008).

3.2 Generation of the pET15b*cs* construct

To characterize *Lmj*CS, kinetically and structurally, the open reading frame of *Lmjcs* was cloned into pET15b, generating an expression construct that lead to expression of an N-terminally His-tagged *Lmj*CS protein (see section

2.4.11.1). *Lmj*CS was amplified by PCR (Figure 3.1, Lane 1) and subcloned into pGEM-T easy (Figure 3.1, Lane 2) before being excised using QIAquick gel extraction kit (QIAGEN, UK) and cloned into the destination plasmid pET15b (Figure 3.1, Lane 3). The sequence of the expression construct was verified before it was used to generate the recombinantly N-teminally His-tagged *Lmj*CS. After attempts to crystallize a C-terminally His-tagged *Lmj*CS protein by William Hunter at University of Dundee (personal communication), it was speculated that this was probably due to the presence of the His-tag. The pET15b vector, which adds an N-terminal His-tag allows the removal of the recombinant His-tag via *tabacco etch virus* (TEV) protease digest.

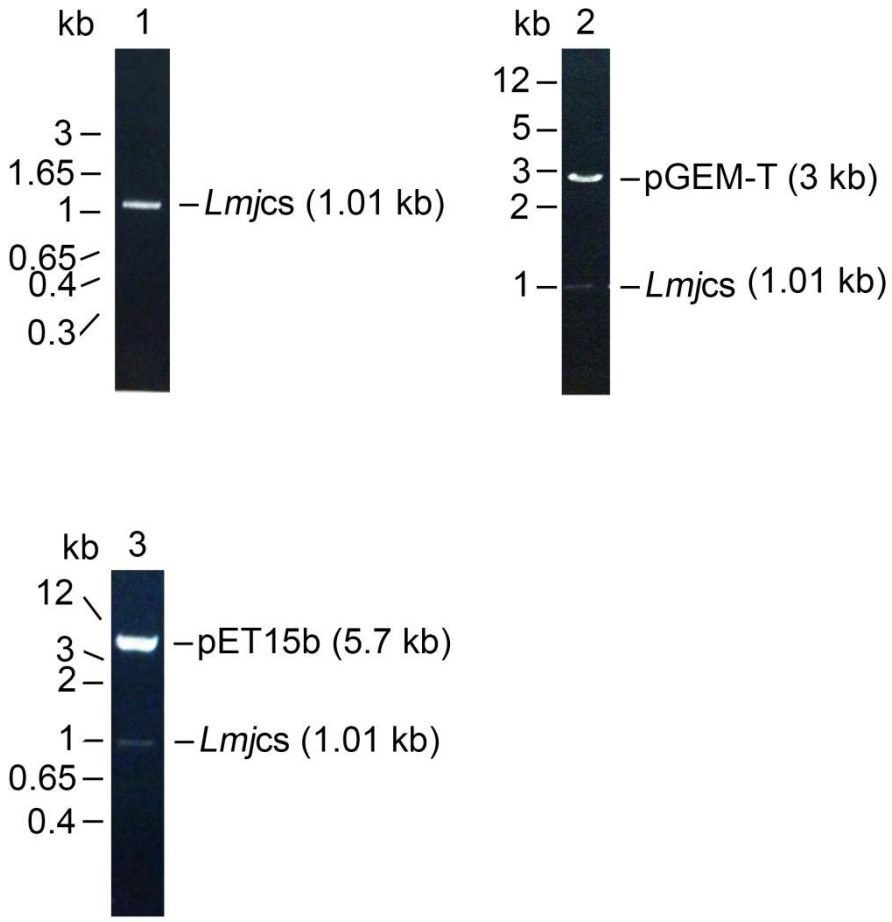

Figure 3.1 - Generation of pET15bLmjcs

(1) PCR amplification of *Lmjcs* from pET21a^{+}*Lmjcs*. (2) *Eco*RI restriction endonuclease digest of the intermediate construct pGEM-T*Lmjcs*. (3) *Bam*HI and *Nde*I restriction endonuclease digest of pET15b*Lmjcs*.

3.3 Expression and purification of N-*Lmj*CS

The expression of the N-r*Lmj*CS protein was carried by induction of the *lac*UV5 promoter with IPTG, which controls the expression of the T7 RNA polymerase gene in the *E. coli* BL21/DE3 cells. pET15b is a T7*lac* promoter containing vector and contains an N-terminal His-tag cleavable with TEV protease. Two expression conditions were tested. Bacterial cells were incubated at 37°C until optical density at 600 nm (OD_{600}) was 0.6, and then divided into two flasks. One flask was induced with 1 mM IPTG and incubated overnight at 15°C, and the other flask was induced with 2 mM IPTG and incubated for 4 h (see section 2.5.4). The bacterial pellets were lysed and the soluble and insoluble fractions were analyzed by SDS-PAGE. A prominent protein band of the expected size (37.8 kDa) of *Lmj*CS can be seen both in the soluble and the insoluble fractions (Figure 3.2). The empty pET15b vector was also transformed into *E. coli* BL21/DE3 and used as a negative control and the 37.8 kDa protein was absent in these bacterial lysates. The absence of the 37.8 kDa protein strongly suggests that the band observed in the pET15b-r*Lmj*CS transformation corresponds to N-r*Lmj*CS. At 37°C more protein is present in the insoluble fraction. At 15°C, approximately 50% of the expressed protein is found in the soluble fraction, while this proportion was lower when expression was done at 37°C.

The recombinant N-r*Lmj*CS was purified using the Ni^{+}-agarose column affinity batch method (see section 2.5.5). Figure 3.3A illustrates the purification of N-r*Lmj*CS after an expression at 37°C for 4 h with 2 mM IPTG. The yield was 6 mg/L. Figure 3.3B depicts the purification of N-r*Lmj*CS expressed at 15°C, overnight with 1 mM IPTG. The yield was 110 mg/L. Thus, it was decided to prepare a larger scale expression of N-r*Lmj*CS at 15°C induction of expression with 1 mM IPTG overnight.

In both purifications N-r*Lmj*CS was yellow, which is consistent with the presence of pyridoxal 5'-phosphate (PLP) in the active site. As seen in Figure

3.3A and B, an unidentified protein of a bigger size was co-purified with N-r*Lmj*CS.

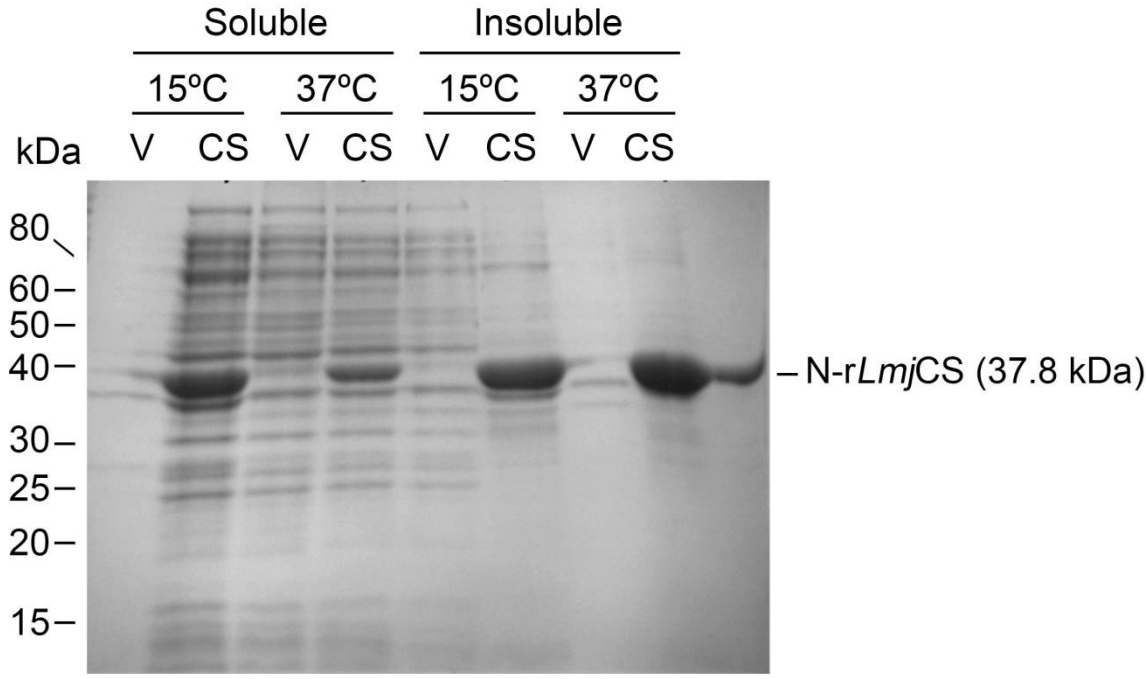

Figure 3.2 – Expression trials N-r*Lmj*CS.

Coomassie stained SDS-PAGE (10%) showing the expression trial of N-r*Lmj*CS carried at 15°C and 37°C. Soluble and insoluble fractions were screened for the presence of N-r*Lmj*CS. The bacterial lysates transformed with the empty vector was used as a negative control. (V) BL21/DE3 bacteria transformed with empty pET15b; (CS) BL21/DE3 bacteria transformed with pET15b-r*Lmj*CS construct.

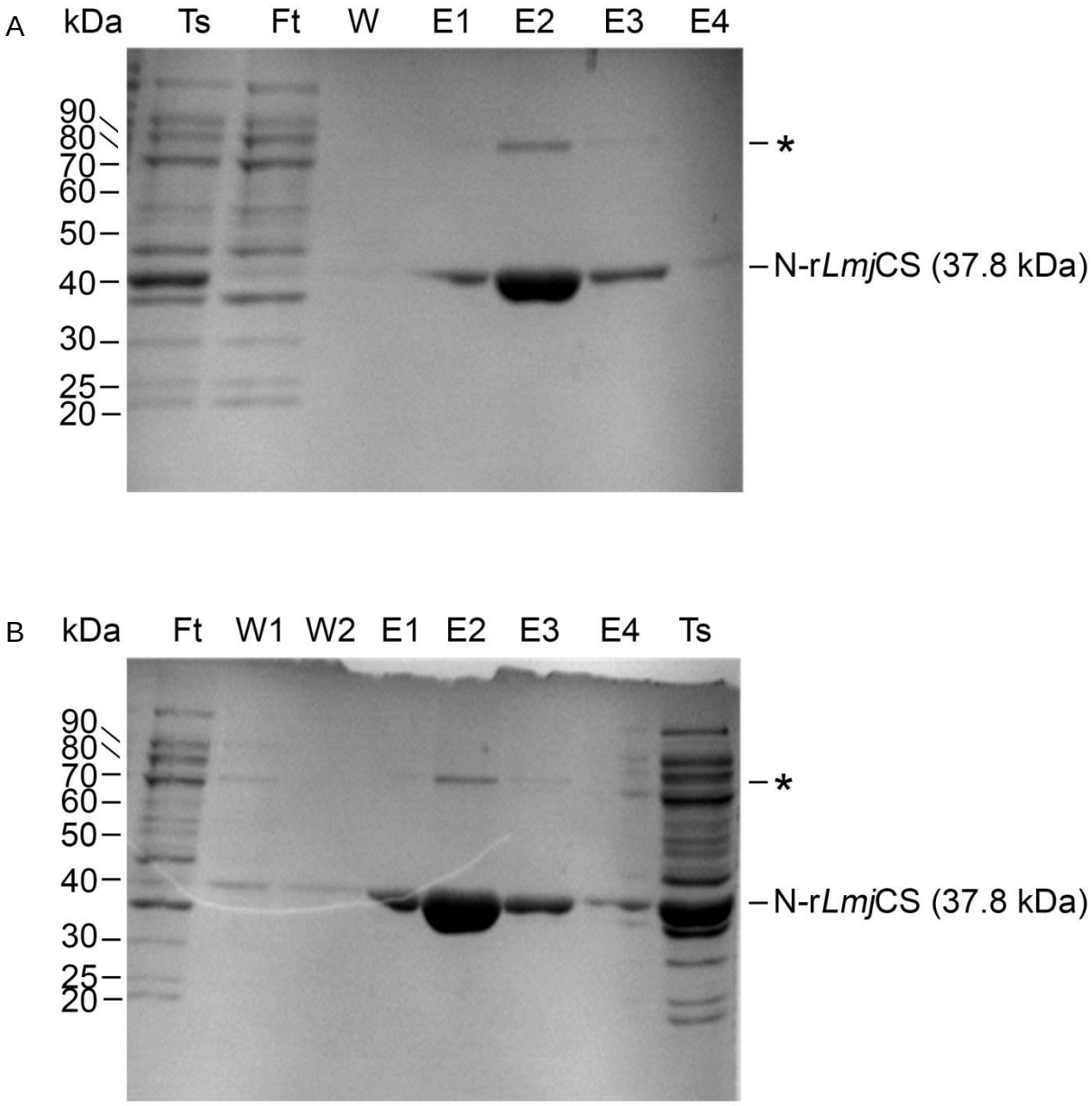

Figure 3.3 – Purification of N-r*Lmj*CS.

Panel A – Coomassie stained SDS-PAGE (10%) showing the protein purification of N-r*Lmj*CS expressed at 37°C and induced with 2 mM IPTG. Panel B - Coomassie stained SDS-PAGE (10%) showing the protein purification of N-r*Lmj*CS expressed at 15°C and induced with 1 mM IPTG. N-r*Lmj*CS expected size is 37.8 kDa. (Ts) Total protein from the soluble fraction; (Ft) flow-through; (W) wash with 20 mM imidazole; (E) elution with 250 mM imidazole. (*) Co-purifiyed unidentified protein.

3.4 Purification of the recombinant C-terminally His-tagged *L. major* cysteine synthase in *E. coli*

A C-terminally His-tagged recombinant *Lmj*CS protein was expressed as previously described by Williams et al. (2009). The expression pET21a^{+}-*Lmjcs* construct was provided by Dr Westrop, Strathclyde University. The C-r*Lmj*CS (37.8 kDa) was purified with 250 mM imidizale. The C-r*Lmj*CS yield was ~140 mg/L.

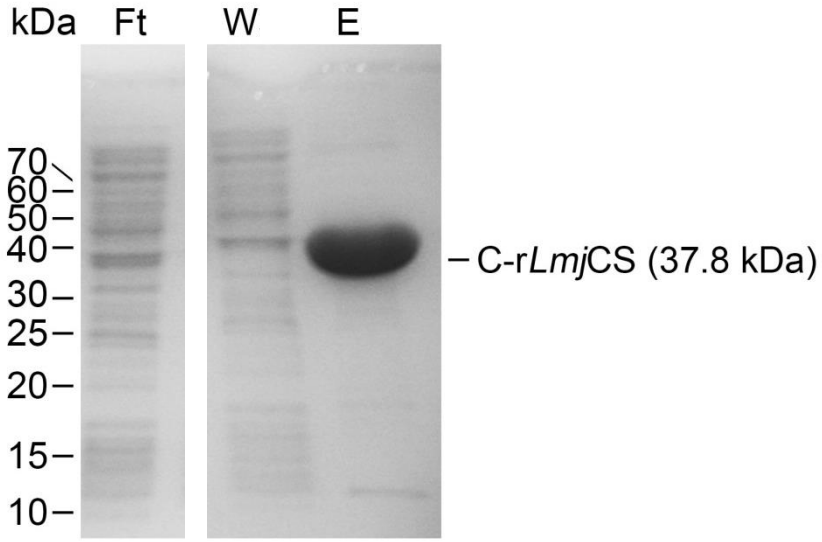

Figure 3.4 – Purification of C-r*Lmj*CS.

Coomassie stained SDS-PAGE showing the purification of C-r*Lmj*CS. The expected size of C-r*Lmj*CS is 37.8 kDa. (Ft) flow-through; (W) wash with 20 mM imidazole; (E) elution with 250 mM imidazole.

3.5 Generation of native r*Lmj*CS

The non-tagged r*Lmj*CS was generated by cleaving of the His-tag from N-r*Lmj*CS with TEV protease (see section 2.5.6). To determine the optimal cleavage conditions, ratios and incubation times were determined (see section 2.2.7). The optimal TEV:CS ratio was found to be 1 µg:0.8 µg which resulted in a good cleavage of the His-tag. The times tested were 2 h, 4 h, and overnight incubation at 37°C (Figure 3.5A). Having established the conditions, N-r*Lmj*CS (37.8 kDa) was successfully cleaved, and purified using Ni^{+}-agarose column (Figure 3.5B).

A reaction containing N-r*Lmj*CS (37.8 kDa) alone was used to distinguish the size of the non-cleaved N-r*Lmj*CS (Figure 3.5B, lane –TEV; 37.8 kDa) and cleaved r*Lmj*CS (Figure 3.5B, lane +TEV; 35.5 kDa). TEV protein size is 52 kDa and can be seen on Figure 3.5B (lane +TEV) where the digest of N-r*Lmj*CS (37.8 kDa) is depicted showing the cleaved r*Lmj*CS which is 35.5 kDa. The digest was further purified using a Ni^{+}-agarose column (Figure 3.5B, Pure) after imidazole was removed from the solution.

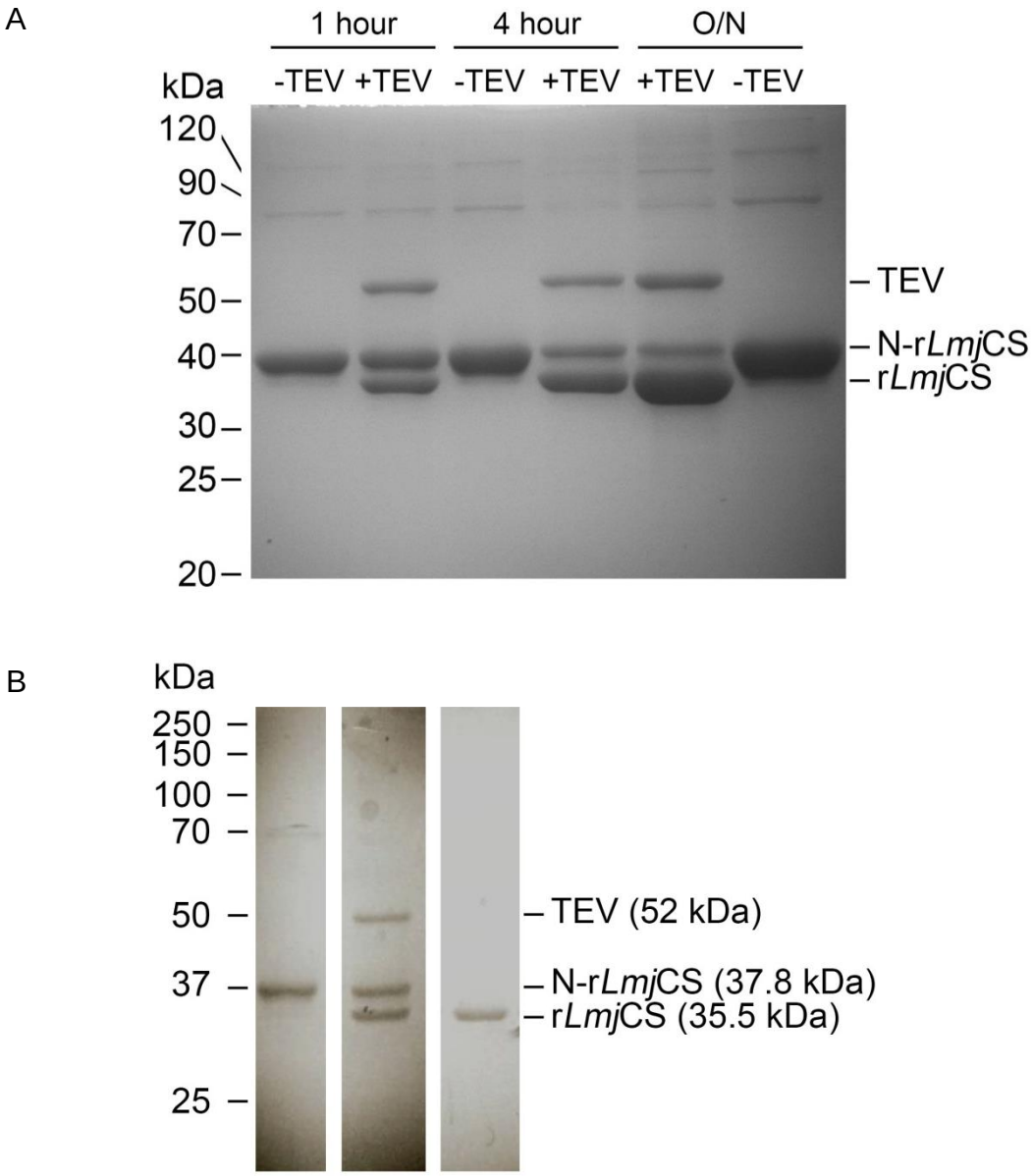

Figure 3.5 – Generation and purification of r*Lmj*CS.

Panel A – Coomassie stained SDS-PAGE showing the determination of the optimal TEV digest (+TEV). A digest without TEV (-TEV) was used as negative control. Panel B – Coomassie stained SDS-PAGE showing the purification of r*Lmj*CS after digest with TEV protease. A digest without TEV was used as negative control. N-r*Lmj*CS expected size is 37.8 kDa; r*Lmj*CS expected size is 35.5 kDa; TEV expected size is 52 kDa.

3.6 Kinetic characterization of N-r*Lmj*CS, C-r*Lmj*CS and *Lmj*CS

3.6.1 Quantification of cysteine synthesis

The kinetic characterization of the various forms of r*Lmj*CS was performed using an enzyme assay for the detection of aliphatic thiols described by Kredich and Tomkins, (1966). Briefly, the thiol of the cysteine formed reacts with an excess of nitrous acid originating a stable *S*-nitrosothiol derivative. The excess of nitrous acid is quenched by ammonium sulfamate. The *S*-nitrosothiol derivative is decomposed in the presence of mercuric ion giving nitrous acid. The nitrous acid diazotes the sulphanilamide, and the latter reacts with the naphthylethylenediamine, forming a stable azo dye (chromophore) which can be detected by spectrophotometry at 540 nm (A_{540nm}).

3.6.2 Kinetic characterization of recombinant *Lmj*CS enzymes

In order to quantify the cysteine formed in an assay, a standard curve was generated using increasing cysteine concentrations (1 to 20 nmol), 0.1 M potassium phosphate buffer pH 7.8, 1 mM EDTA, 0.5 mM Na_2S, and 1 mg/mL gelatine (Figure 3.6) (see section 2.5.7). A regression curve was plotted with the results and the resultant equation of the curve (A_{540nm} = 0.082 x cysteine (nmol)) was used to quantify cysteine synthesis in the forthcoming assays.

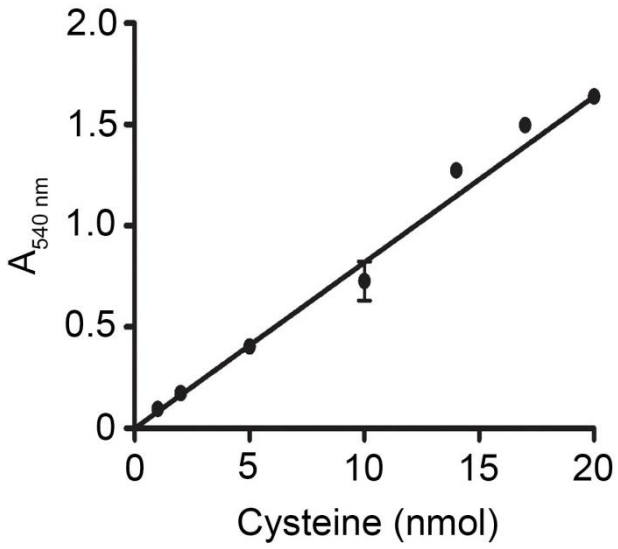

Figure 3.6 – Cysteine standard curve for the mercury chloride assay.

Graph showing the absorbance (540 nm) generated by increasing concentrations of cysteine. The linear regression curve was plotted and the absorbance was used to quantify cysteine synthesis in enzyme reactions. Values depicted represent means with S.E.M. from five experiments performed in different days.

The three forms of r*Lmj*CS were compared kinetically by their ability to synthesise cysteine. Different enzyme concentrations were tested as depicted in Figure 3.7. Each reaction contained the enzyme, 0.1 M potassium phosphate buffer pH 7.8, 1 mM EDTA, 0.5 mM Na_2S, 10 mM OAS, and 1 mg/mL gelatine. The optimal enzyme concentration should result in proportionally increasing product (Cys) formation over time without saturating the detection system. Figure 3.7 shows the resultant regression curves. 250 ng/mL of C-r*Lmj*CS was used in future assays because it gives more flexibility to do a substrate saturation assay. The same concentration was chosen for N-r*Lmj*CS. For r*Lmj*CS, 500 ng/mL were chosen instead. The rates of reaction (Table 3.1) for these concentrations were 2 nmol/min for C-r*Lmj*CS; 3.4 nmol/min for N-r*Lmj*CS; and 1.3 nmol/min for r*Lmj*CS. Although a higher concentration of r*Lmj*CS was used compared with two forms of *Lmj*CS, the rate was about half.

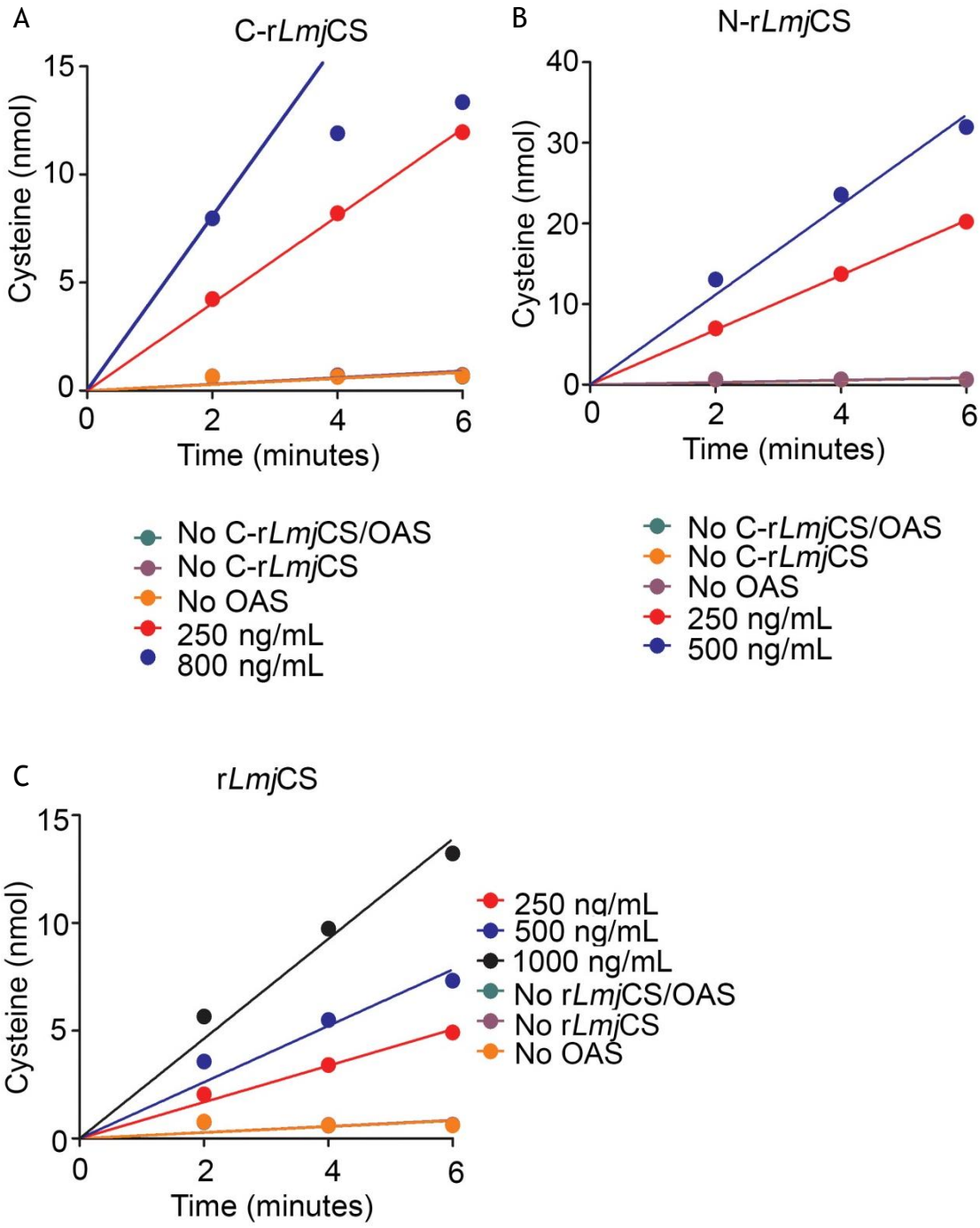

Figure 3.7 – Enzyme concentrations test.

The graphs illustrate cysteine generated by the different r*Lmj*CS enzymes at different enzyme concentrations as indicated. The OAS concentration was 10 mM. The experience was performed once. Panel A – C-r*Lmj*CS enzyme; Panel B – N-r*Lmj*CS enzyme; Panel C – r*Lmj*CS enzyme.

Enzyme	[Enzyme] ng/mL	Rate (nmol/min)
C-r*Lmj*CS	250	2.0
	800	4.0
N-r*Lmj*CS	250	3.4
	500	5.6
r*Lmj*CS	250	0.8
	500	1.3
	1000	2.3

Table 3.1 – Enzyme activity.

Table showing the reaction rate (nmol/min) for each tested enzyme concentration.

To determine the kinetic parameters, a substrate saturation curved was plotted. Increasing concentrations of OAS (0.5 to 5 mM) were tested with the previously chosen enzyme concentrations mixed with 0.1 M potassium phosphate buffer pH 7.8, 1 mM EDTA, 0.5 mM Na_2S, and 1 mg/mL gelatine. The cysteine levels were measured every two minutes, up to six minutes (Figure 3.8A, B and C). The rates of reaction increase with the increase of OAS concentration (Table 3.2). The rates along with the enzyme concentration were used to calculate the specific activity (µmol/min/mg) for each OAS concentration (Table 3.3). All the experiments were performed in triplicate.

	[N-r*Lmj*CS]	**[C-r*Lmj*CS]**	**[r*Lmj*CS]**
	250 ng/mL	250 ng/mL	500 ng/mL
OAS (mM)	Rate (pmol/min ± S.E.M.) in 10 µL of reaction, n=3		
0.5	284 ± 25	225 ± 37	387 ± 114
1	558 ± 22	358 ± 8	624 ± 96
2	1011 ± 4	603 ± 13	1006 ± 130
3	1284 ± 26	752 ± 28	1372 ± 180
5	1539 ± 84	983 ± 29	1883 ± 182
8	1995 ± 31	1246 ± 41	2160 ± 207
15	2318 ± 48	1335 ± 43	2431 ± 170

Table 3.2 – Rates of cysteine synthesis for each enzyme.

The average rate (pmol/min) of cysteine synthesis was measured with increasing concentrations of OAS substrate (0.5-15 mM). The absorbance (540 nm) was determined in 10 µL of reaction at 2, 4 and 6 minutes. The experiment was performed in triplicate and the concentration of each enzyme is shown (please refer to the table).

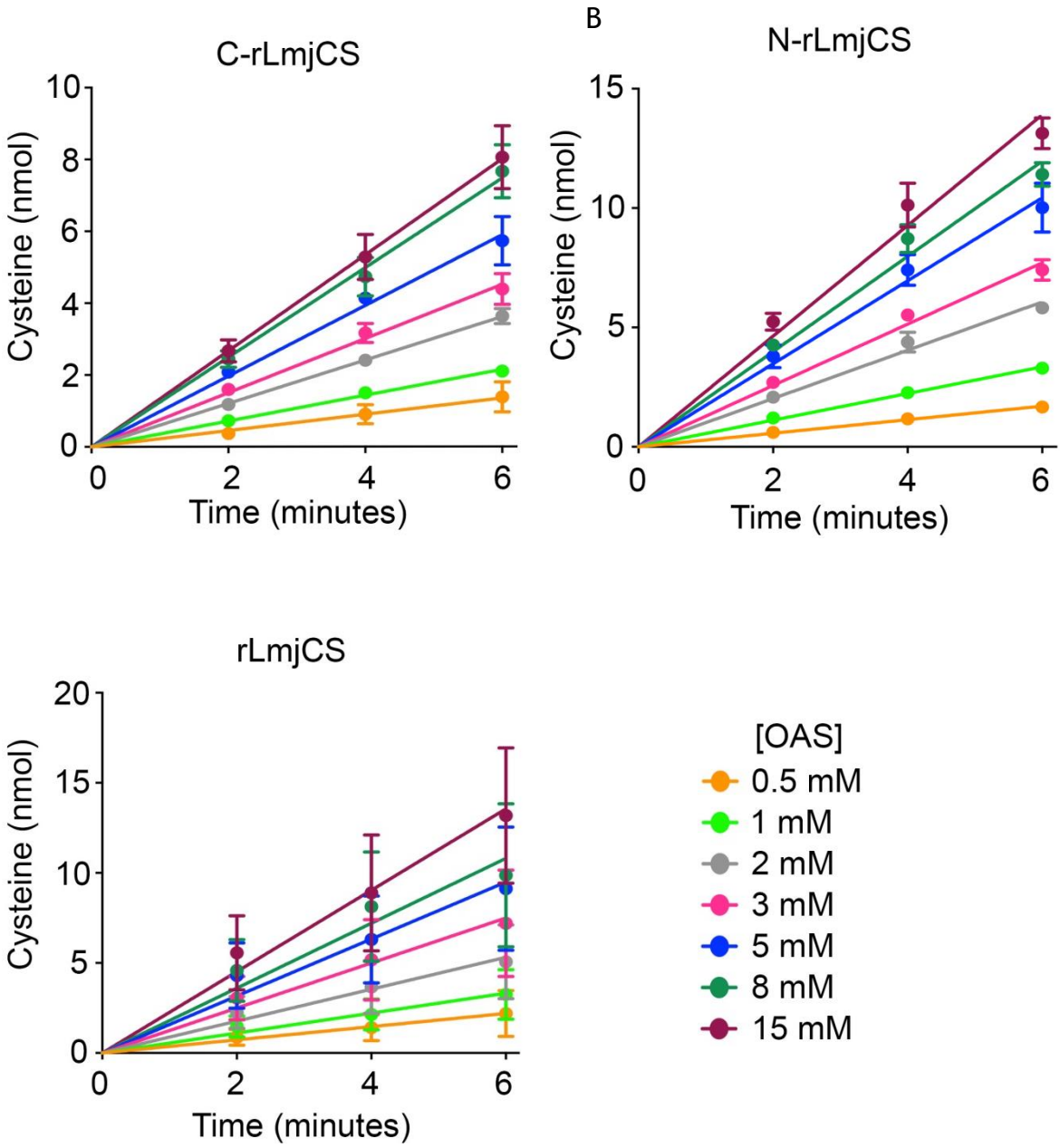

Figure 3.8 – Substrate saturation curves.

Graphs showing cysteine synthesis generated when increasing concentrations are used. Panel A – C-r*Lmj*CS enzyme (250 ng/mL); Panel B – N-r*Lmj*CS enzyme (250 ng/mL); Panel C – r*Lmj*CS enzyme (500 ng/mL). The numbers are means and S.E.M. of three independent experiments performed in triplicate.

	Specific activity (µmol/min/mg ± S.E.M.), n=3		
OAS (mM)	N-r*Lmj*CS	C-r*Lmj*CS	r*Lmj*CS
0.5	114 ± 10	90 ± 15	77 ± 23
1	223 ± 9	143 ± 3	125 ± 19
2	404 ± 2	241 ± 5	201 ± 26
3	514 ± 10	301 ± 11	274 ± 36
5	615 ± 34	393 ± 12	377 ± 36
8	798 ± 12	498 ± 17	432 ± 41
15	927 ± 19	534 ± 17	486 ± 34

Table 3.3 – Specific activity.

Table displaying the specific activities calculated from the rates (pmol/min) of the reactions with increasing OAS concentrations. The data are means ± S.E.M. of three independent experiments.

Two plots were used to analyse enzyme kinetic parameters: the Michaelis-Menten plot (Figure 3.9A); and the Lineweaver-Burk plot (Figure 3.9B). Kinetic parameters are summarised in Table 3.4.

The K_m value (or Michaelis-Menten constant) is the concentration of the substrate, here OAS, that leads to half of the maximum velocity (V_{max}) of the enzyme (Cornish-Bowden, 2004; Segel, 1993). This constant is independent of the enzyme concentration. The K_m values of all three recombinant enzymes were the same for N-r*Lmj*CS, C-r*Lmj*CS, and r*Lmj*CS, 4 mM (Figure 3.9A and B and Table 3.4).

V_{max} is specific to the enzyme concentration and is the limiting velocity for high substrate concentrations, meaning the velocity will not increase even if the substrate concentration increases (Cornish-Bowden, 2004; Segel, 1993). The V_{max} for C-r*Lmj*CS and r*Lmj*CS (696 and 630 µmol/min/mg, respectively) were lower than for N-r*Lmj*CS (1192 µmol/min/mg) (Figure 3.9A and B and Table 3.4).

k_{cat}, or turnover number, is the number of substrate molecules that are converted into product per active site of an enzyme, per unit of time, when

the enzyme is completely saturated (Cornish-Bowden, 2004; Segel, 1993). k_{cat} is expressed in sec^{-1} and the results can be seen on Table 3.4. The k_{cat} values (Table 3.4) for the C-r*Lmj*CS and r*Lmj*CS (438 sec^{-1} and 373 sec^{-1}, respectively) are lower than for the N-r*Lmj*CS (751 sec^{-1} for r*Lmj*CS).

And finally, k_{cat}/K_m is the measure of the enzymes catalytic efficiency and it can be calculated by dividing k_{cat} by K_m. The k_{cat} /K_m is expressed in M^{-1}/sec^{-1} (Cornish-Bowden, 2004; Segel, 1993). The efficiency of the N-r*Lmj*CS (Table 3.4) is the nearly double ($1.9x10^5$ M^{-1}/sec^{-1}) than the C-r*Lmj*CS ($1.1x10^5$ M^{-1}/sec^{-1}). The k_{cat} /K_m of r*Lmj*CS ($9.3x10^4$ M^{-1}/sec^{-1}) is the lowest of the three enzymes but closer to the C-r*Lmj*CS k_{cat} /K_m.

The N-r*Lmj*CS enzyme is more efficient then the C-r*Lmj*CS and r*Lmj*CS enzymes. The k_{cat}/K_m magnitude of these enzymes (~10^5 M^{-1}/sec^{-1}) is the half of the k_{cat}/K_m of other known super-efficient enzyme such as superoxide dismutase (10^{10} M^{-1}/sec^{-1}) (Folcarelli *et al.*, 1999). The tag can influence the activity of an enzyme if it is located close to the substrate binding site (Ledent *et al.*, 1997). In this case the His-tag does not cause a loss in the enzyme efficiency. Conversely, the N-r*Lmj*CS enzyme is two times more efficient than the non-tagged enzyme but still in the same order of magnitude (10^5 M^{-1}/sec^{-1}).

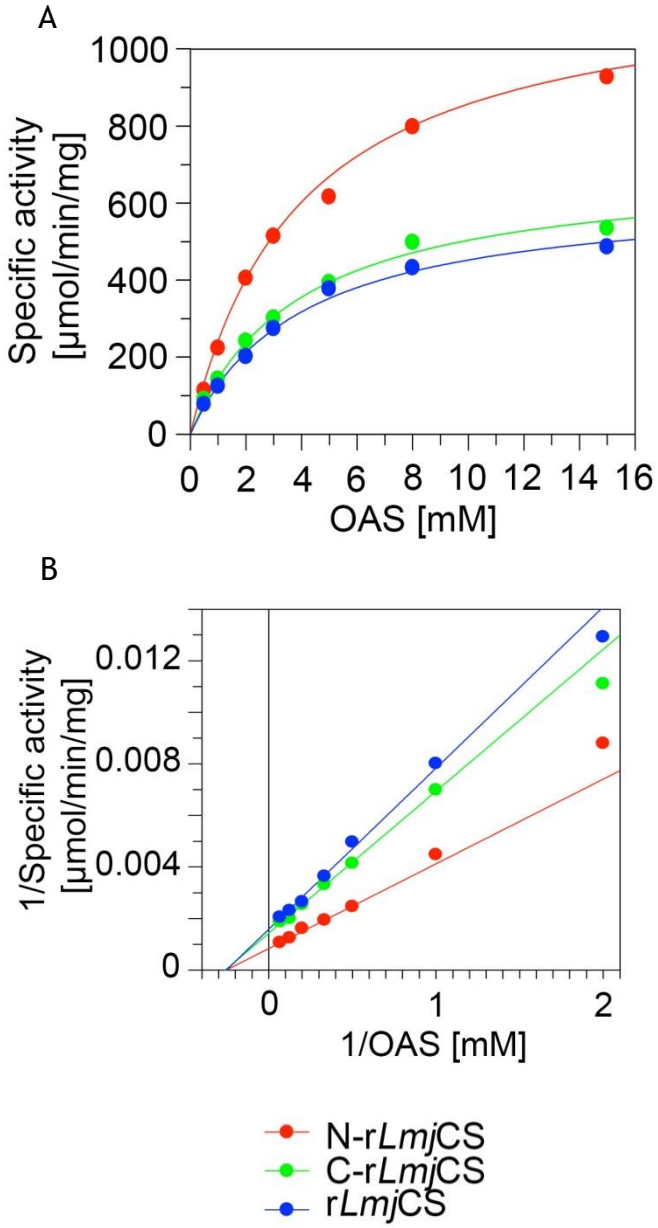

Figure 3.9 – Comparative kinetic analysis.

The specific activities are illustrated in a Michaelis-Menten (Panel A) and Linweaver-Burk (Panel B) plots for comparative kinetic analysis between the three forms of r*Lmj*CS (Software used - GraFit5).

Cysteine synthase	K_m (mM)	V_{max} (µmol/min/mg)	k_{cat} (sec^{-1})	k_{cat}/K_m (M^{-1}/sec^{-1})
N-r*Lmj*CS	4 ± 0.3	1192 ± 58	751	$1.9x10^5$
C-r*Lmj*CS	4 ± 0.2	696 ± 24	438	$1.1x10^5$
r*Lmj*CS	4 ± 0.3	630 ± 28	373	$9.3x10^4$

Table 3.4 – Analysis of kinetic parameters.

Table showing the kinetic parameters calculated or extrapolated from the Michaelis-Menten and Linweaver-Burk plots.

3.7 Inhibition of N-r*Lmj*CS, C-r*Lmj*CS and r*Lmj*CS

Peptide analogues of the *Lmj*SAT and *At*SAT C-terminus were tested as putative inhibitors of the three forms of r*Lmj*CS enzyme (see section 2.5.8). DYVI (0.1 mM), an *At*SAT C-terminal peptide analogue, inhibits ~90% of all three forms of *Lmj*CS activity. EGDGSGI (0.1 mM), an *Lmj*SAT C-terminal peptide analogue, inhibits ~30% of N-r*Lmj*CS and r*Lmj*CS activity and inhibits 50% of C-r*Lmj*CS activity. Enantiomeric forms of polyglutamate (0.1 mM and 0.5 mM of D-γEγEγEγE, and 0.1 Mm of L-γEγEγEγE) and also the non-chiral form EEEE (0.1 mM) were also tested as potential inhibitors. These compounds were added to the enzyme and the cysteine levels were measured every two minutes. Figure 3.10 illustrates the synthesis of cysteine over time when the reactions are performed in the presence of these compounds. Table 3.5 summarises the percentages of inhibition data. D-γEγEγEγE (0.1 mM), a polyglutamate enantiomer found bound to the active site of the crystallised *Lmj*CS (Fyfe *et al.*, 2012), inhibited 20% of C-r*Lmj*CS. When added to the reaction at a concentration five times greater (0.5 mM), D-γEγEγEγE, was not able to inhibit C-r*Lmj*CS to the same extent. No inhibition was detected for N-r*Lmj*CS and r*Lmj*CS enzyme forms. The levorotary enantiomer (L-γEγEγEγE) and the non-chiral polyglutamate (EEEE) were not able to inhibit r*Lmj*CS.

	% Inhibition		
	N-r*Lmj*CS	C-r*Lmj*CS	r*Lmj*CS
Control	0	0	0
0.1 mM DYVI	94 ± 6	91 ± 0	94 ± 3
0.1 mM EGDGSGI	36 ± 6	49 ± 4	33 ± 7
0.1 mM D-γEγEγEγE	n.d.	20 ± 4	0
0.5 mM D-γEγEγEγE	n.d.	20 ± 11	0
0.1 mM L-γEγEγEγE	-	-	0
0.1 mM EEEE	-	-	0

Table 3.5 – Inhibition of r*Lmj*CS.

Percentage of inhibition of all three forms of *Lmj*CS enzymes using peptides: 0.1 mM DYVI; 0.1 mM EGDGSGI; 0.1 mM D-γEγEγEγE; 0.5 mM D-γEγEγEγE; 0.1 mM L-γEγEγEγE; and 0.1 mM EEEE. The experiments were carried out on two separate occasions and the values are presented as means of percentage of inhibition ± standard deviation (S.D.); (-) not determined.

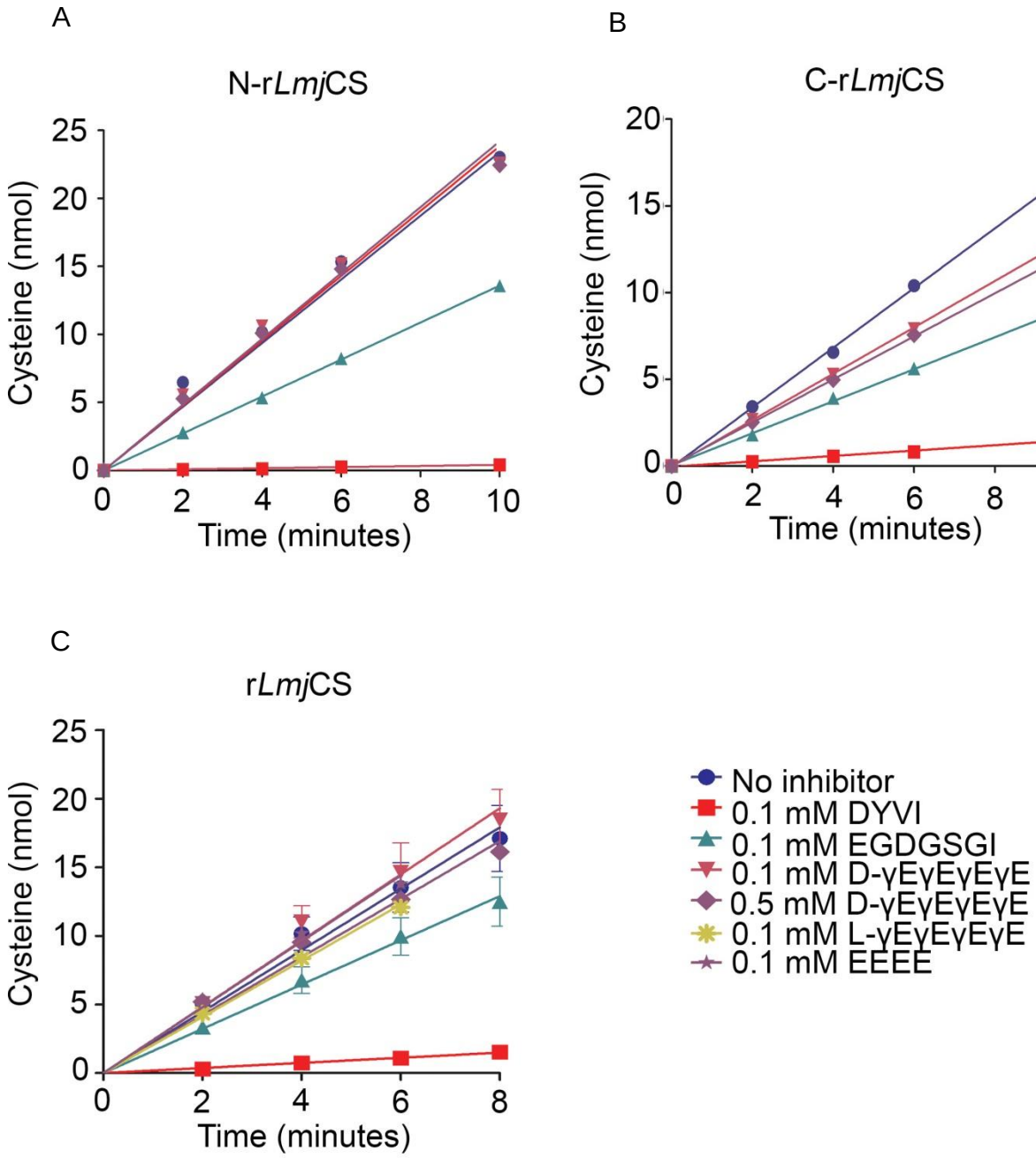

Figure 3.10 – Inhibition of r*Lmj*CS.

The graphs illustrate the inhibition of the various forms of r*Lmj*CS enzymes, using peptides: 0.1 mM DYVI; 0.1 mM EGDGSGI; 0.1 mM D-γEγEγEγE; 0.5 mM D-γEγEγEγE; 0.1 mM L-γEγEγEγE; and 0.1 mM EEEE. Panel A – C-r*Lmj*CS enzyme; Panel B – N-r*Lmj*CS enzyme; Panel C – r*Lmj*CS enzyme. The experiments were carried on two separate occasions and the values are presented as means of percentage of inhibition with standard deviation (S.D.).

3.8 Validation of a novel cysteine detection method

3.8.1 Assay validation

7-Diethylamino-3-(4'-maleimidylphenyl)-4-methylcoumarin (CPM) (Chung *et al.*, 2008) is a coumarin derivative that contains a thiol-reactive maleimide. CPM may aid to determine cysteine concentration because it forms a complex between the thiol-reactive maleimide and the sulfhydryl (-SH) group of cysteine. Once the complex is formed, the CPM fluorescence increases at a λexcitation of 340 nm and λemission of 465 nm. Being a less laborious and toxic detection method than the mercury chloride assay system (Kredich and Tomkins, 1966), the CPM detection method may be adaptable for high-throughput screening of for instance inhibition by peptide libraries or other inhibitor libraries against *Lmj*CS.

Initially, the CPM had high levels of non-specific background fluorescence (data not shown) only leaving a small window that would allow the quantification of cysteine (see section 2.5.9). Therefore, experiments were performed to optimise the assay system to maximise the signal to noise ratio. The influence of Na_2S, pH, BSA, CPM storage length, and CPM concentration were tested.

Figure 3.11 shows the result of testing the influence of pH(s) 6.5, 7.0, and 7.8 in the formation of background (see section 2.5.9.1). In this assay four reactions were set up: assay buffer (0.1 M sodium potassium phosphate pH 6.5, 7.0 or 7.8, and 1 mM EDTA) (Figure 3.11A); assay buffer with 40 µM cysteine (Figure 3.11B); assay buffer with 0.5 mM Na_2S (Figure 3.11C); and assay buffer with 40 µM cysteine and 0.5 mM Na_2S (Figure 3.11D).

The buffer with a pH of 7.8 generates a significantly (***, $P<0.001$) higher background than buffer with a pH of 7.0 and 6.5. The background fluorescence is however 2 orders of magnitude lower than the background determined when 0.5 mM Na_2S was added to the reaction. In fact, the buffer pH had no effect on background fluorescence when 0.5 mM Na_2S was present in the reaction mixture. Presumably the Na_2S in solution is converted into NaS^- (Figure 3.12), which can react with CPM generating fluorescence.

The addition 40 µM cysteine resulted in an increase of fluorescence as expected but the signal was only marginally larger (1.5 times) than the background signal determined with 0.5 mM Na_2S ($3x10^4$ vs. $2x10^4$ RFU).
When 0.5 mM Na_2S and 40 µM Cys were added to the different buffers, the signal increased further to $5x10^4$ RFU in line with the observed fluorescence of the individual reaction mixtures.
So, overall it appeared that the fluorescence of the buffer itself was negligible and that pH did not affect interaction of CPM with sulphur containing molecules.

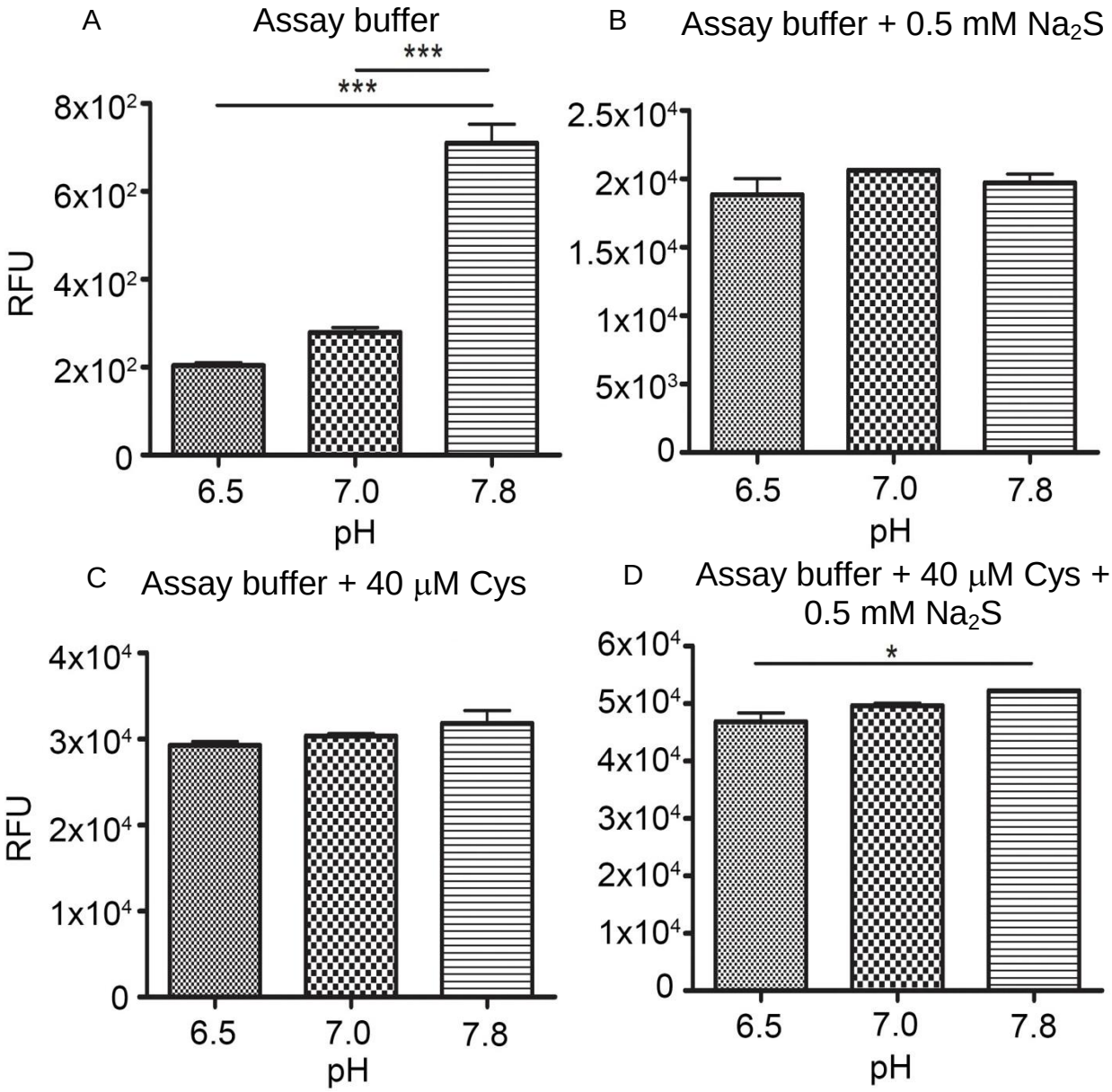

Figure 3.11 – Influence of pH in the fluorescence detection.

The graphs illustrate the fluorescence measured (λexcitation = 340 nm; λemission = 465 nm) when 40 μM of cysteine and 0.5 mM of Na_2S were added to the assay buffer, alone (Panel B and C) or together (Panel D). The assay buffer alone (Panel A) was used to determine the fluorescence background. The experiment was performed in triplicate. The results are presented in means of relative fluorescent units (RFU) ± S.E.M and were analyzed using 1-way ANOVA with Tuckey post-test. The statistical results are represented as: ***, P<0.001.

$$Na_2S + H_2O \rightarrow NaS^- + OH^- + 2Na^+$$

Figure 3.12 – Dissolution of sodium sulphide.

In the presence of water, sodium sulphide is ionised in NaS^-, OH^- and $2Na^+$. CPM reacts with the sulphide group, NaS^-, forming a complex and thus fluorescence. This fluorescence contributes to the background interfering with the detection of cysteine synthesis.

BSA is a component of the CPM assay system. However, BSA is a protein rich in cysteine residues that can react with CPM and generate background. BSA is added to the CPM reaction to prevent the adhesion of protein to the walls of the reaction tube. Gelatine, a cysteine-free molecule with a similar feature as BSA was tested as a potential replacement for BSA in order to decrease the background of the reaction. Five reactions were set up with 0.1 M potassium phosphate pH 7.8, since it helps to stabilise the *Lmj*CS enzyme, and BSA or gelatine at 1 or 0.1 mg/mL (see section 2.5.9.2). Freshly prepared CPM at 50 µg/mL was added and the fluorescence was measured. Figure 3.13 summarises the data obtained. The background fluorescence of the reaction mix when 1 mg/mL BSA was added increased from $2.2x10^3$ to $3.1x10^4$ RFU (***, $P<0.001$) while addition of 1 mg/mL gelatine only increased the background fluorescence from $2.2x10^3$ to $3.1x10^3$ RFU. Decreasing BSA to 0.1 mg/mL reduced the background fluorescence dramatically from $3.1x10^4$ to $6.5x10^3$ RFU (***, $P<0.001$), a 5 fold reduction compared to the fluorescence determined when 1 mg/mL BSA was used in the reaction mixture.

A similar reduction was not observed when gelatine was lowered to 0.1 mg/mL; this only reduced the RFU from $3.1x10^3$ to $2.7x10^3$ relative to the assay mix containing 1 mg/mL.

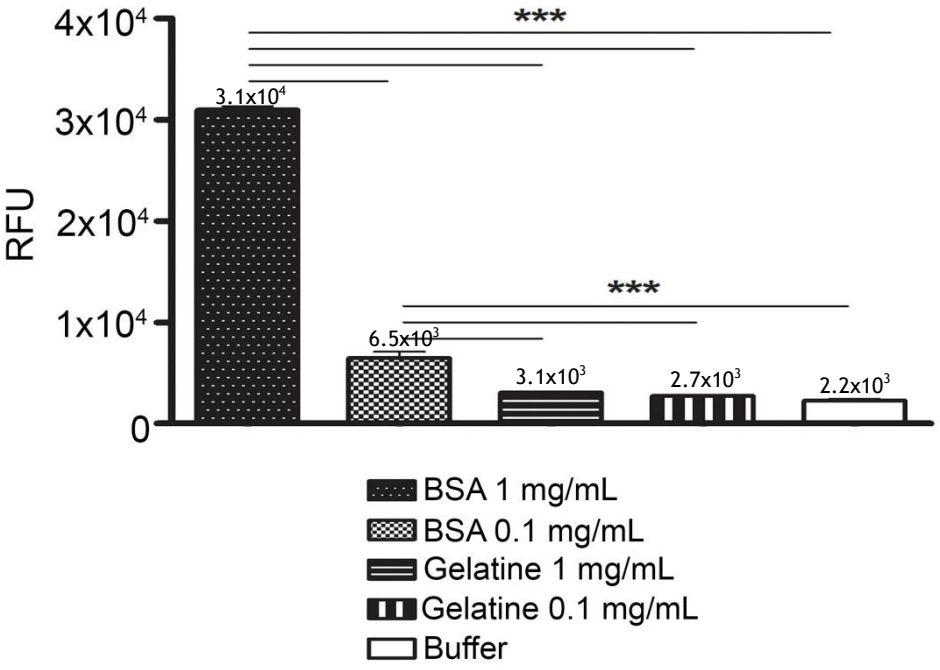

Figure 3.13 – Influence of BSA vs. gelatine on the fluorescence background.

The graphs illustrate the fluorescence measured (λexcitation = 340 nm; λemission = 465 nm) when the assay buffer contains gelatine or BSA under 1 or 0.1 mg/mL of concentration. The experiment was performed in triplicate. The results are presented in means ± S.E.M.

The data generated showed that the use of gelatine at 1 mg/mL was more suitable to the assay because it dramatically reduced the fluorescent background of the assay system.

The next component that needed to be assessed for its effect or background fluorescence was CPM itself. Reactions containing assay buffer only; 0.5 mM Na_2S; 40 μM cysteine; 40 μM cysteine and 0.5 mM Na_2S were set up and their fluorescence determined after addition of 25, 50 or 100 mg/mL CPM (Figure 3.14) (see section 2.5.9.4).

The buffer alone had little ($7.9x10^2$ to $1.3x10^3$ RFU) fluorescence while increased to $2.3x10^4$ - $3.3x10^4$ RFU when Na_2S was added to the reaction mixture.

Adding Cys alone resulted in an elevated fluorescence presumably due to complex formation between CPM and Cys further increased when both Na_2S

and Cys were present in the reaction mix (similar to earlier observations). The data show that the signal to noise is not significantly affected by the CPM concentration presumably because CPM at concentration of 25 μg/mL already saturates the assay system.

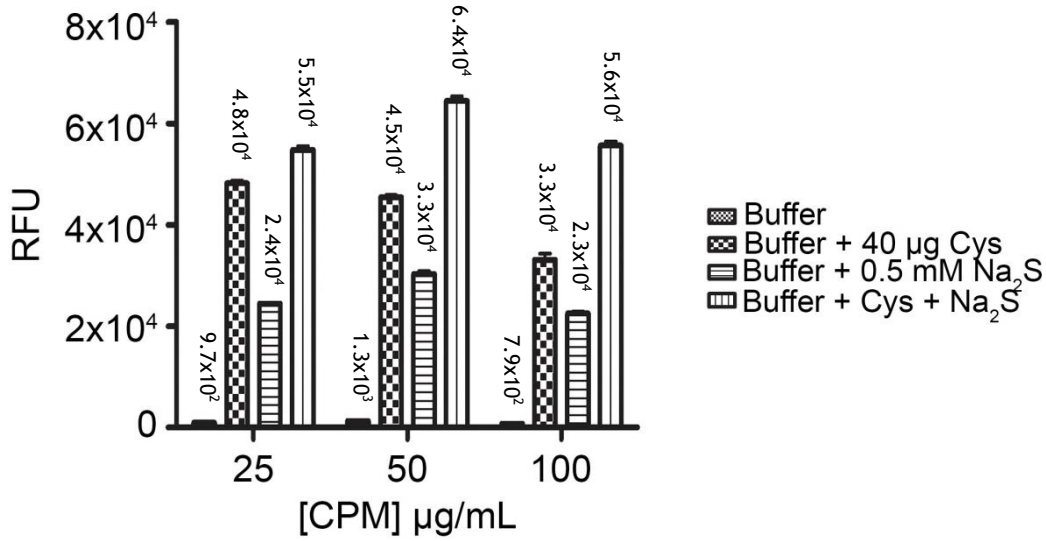

Figure 3.14 – Determination of the optimal CPM concentration.

The graph shows the variability of fluorescence generated by the assay buffer alone or in the presence of when 40 μM of cysteine, 0.5 mM of Na_2S or both, when incubated with different concentrations of CPM.

CPM is a light sensitive fluorochrome therefore it is important to assess the effect of storage in its stability. A reaction containing phosphate buffer pH 7.8 and 40 μM of cysteine was mixed with 100 μg/mL of CPM used on the same day of preparation or previously stored for 3 or 9 days at -20ºC (see section 2.5.9.3). Figure 3.15 shows that the fluorescence significantly (***, $P<0.001$) varies between storage periods. The fluorescence increases with storage length and therefore CPM should be prepared fresh.

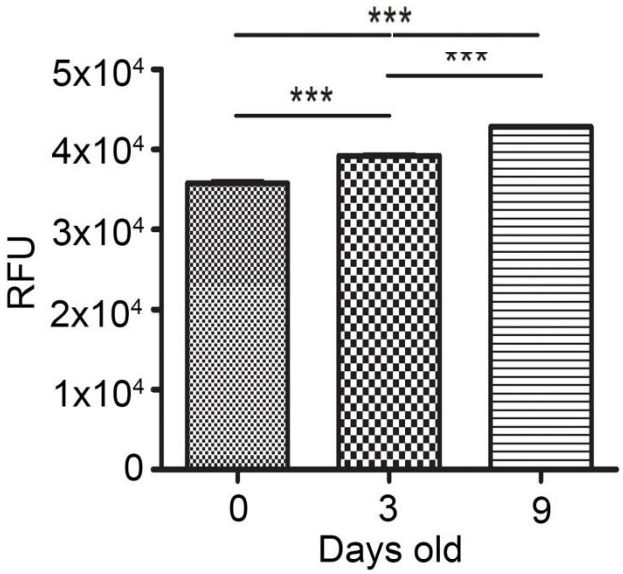

Figure 3.15 – Effect of storage on CPM fluorescence.

The stability of the CPM solution upon storage up to 9 days was assessed by mixing assay buffer, 40 µM of cysteine and 100 µg/mL of CPM. The relative fluorescence (λexcitation = 340 nm; λemission = 465 nm) was determined. The experiment was performed in triplicate and the results were analyzed using 1-way ANOVA with Tuckey post-test. The statistical results are represented as: ***, P<0.001.

3.8.2 Detection and quantification of cysteine synthesis

Having established the conditions for the CPM detection method, a standard curve was set up with increasing concentrations of cysteine (2-10 nmol) (Figure 3.16). Cysteine standards were prepared with 0.1 M potassium phosphate buffer pH 7.8, 1 mM EDTA, 0.5 mM Na_2S, 1 mg/mL gelatine, and 1 mM OAS (see section 2.5.9.5). An aliquot of each reaction was further mixed with 100 µg/mL CPM and the florescence was measured. The CPM assay showed a linear increase of RFU for a range of 0 to 10 nmol of cysteine (Figure 3.15). Variation of RFU increased with increasing cysteine concentrations. A regression curve was plotted and the resultant equation of the curve (RFU = 9171 x cysteine (nmol)) was used to determine cysteine synthesis in subsequent enzyme assays.

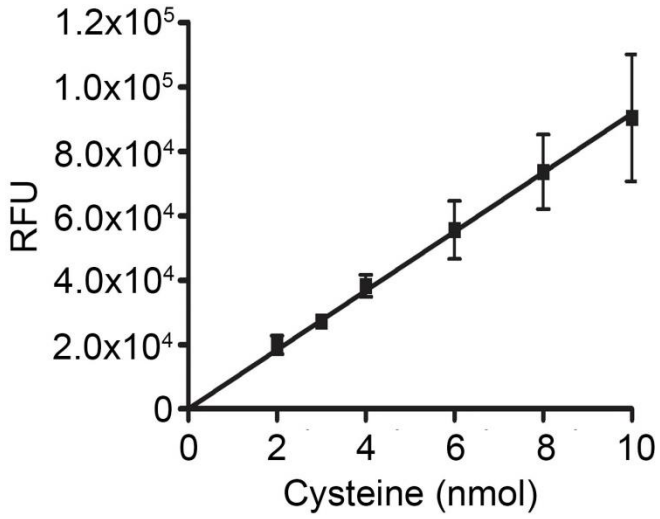

Figure 3.16 – Cysteine standard curve.

Cysteine (2 to 10 nmol) was mixed with assay buffer, 0.1 mg/mL gelatine and 100 µg/mL CPM and the fluorescence was measured (λexcitation = 340 nm; λemission = 465 nm). The experiment was performed six times (n=6) on different occasions and means ± S.E.M. are presented.

Three concentrations of N-r*Lmj*CS enzyme (25, 50 and 75 ng/mL) were tested (Figure 3.17) (see section 2.5.9.6). Cysteine synthesis was monitored every two minutes for a total of six minutes. All three concentrations resulted in cysteine being synthesised (Figure 3.17 and Table 3.6). The calculated rate (Table 3.7) shows that 50 ng/mL of N-r*Lmj*CS synthesed cysteine at the highest rate (0.7 nmol/min) in comparison with 25 ng/mL (0.1 nmol/min) and 75 ng/mL (0.5 nmol/min).

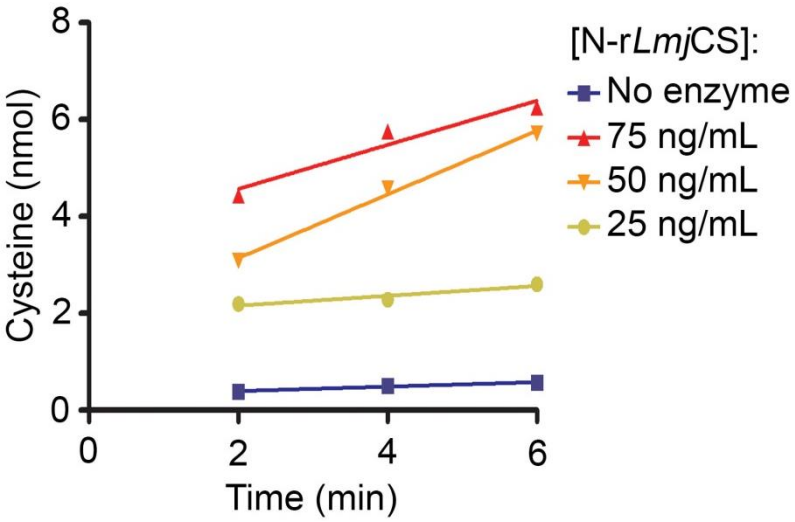

Figure 3.17 – Cysteine synthesis.

The graph illustrates the cysteine synthesis when different concentrations of N-r*Lmj*CS are tested. Three N-r*Lmj*CS enzyme concentrations were tested using 100 µg/mL of CPM and the fluorescence was measured (λexcitation = 340 nm; λemission = 465 nm).

Time (min)	25 ng/mL	50 ng/mL	75 ng/mL
2	1.9	2.8	4.2
4	1.8	4.2	5.4
6	2.1	5.3	5.9

Table 3.6 – Analysis of cysteine synthesis.

The table depicts the cysteine (nmol) values after the subtraction of the background (reaction with no N-r*Lmj*CS).

[N-r*Lmj*CS]	Rate (nmol/min)
25 ng/mL	0.1
50 ng/mL	0.7
75 ng/mL	0.5

Table 3.7 – Reaction rate.

Table showing the cysteine (nmol) synthetized per minute for each tested N-r*Lmj*CS concentration (25, 50 or 75 ng/mL).

3.8.2 Inhibition of N-r*Lmj*CS

The reaction described previously where 50 ng/mL of N-r*Lmj*CS were used to synthesise cysteine, was repeated this time in the presence of 50 μM DYVI (see section 2.5.9.7). As shown using the mercury chloride assay, DYVI is a potent inhibitor of *Lmj*CS; 0.1 mM DYVI inhibited 94% of N-r*Lmj*CS activity. The concentration CPM used was 50 μg/mL, and the DYVI concentration (50 μM) was reduced here. Cysteine synthesis was monitored every two minutes for a period of 6 minutes. Figure 3.18 shows that in the absence and presence of 50 μM DYVI, the results show that in the presence of 50 μM DYVI the CS activity was reduced by 86%; similar to the data presented in the previous section. This validated that the CPM assay has potential for further development.

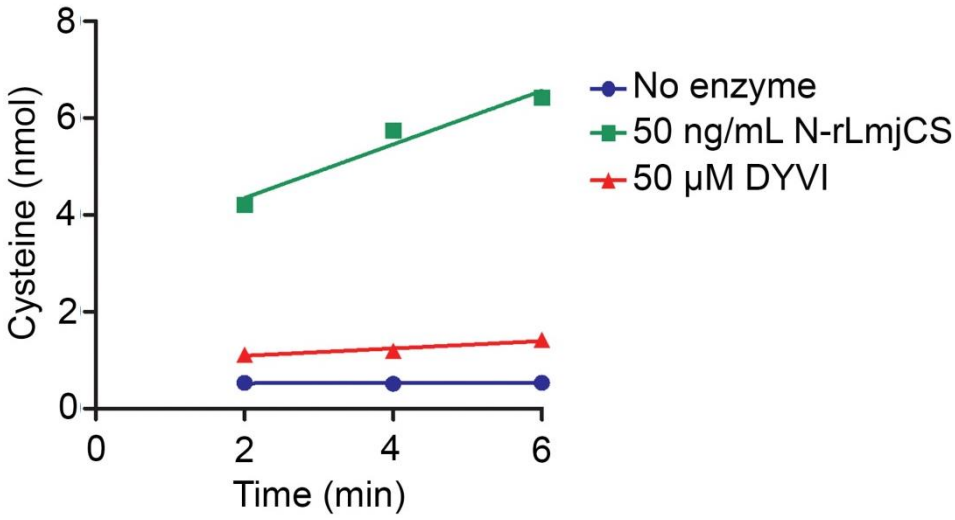

Figure 3.18 – Inhibition of N-r*Lmj*CS with 50 µM DYVI.

The graph illustrates the inhibition of N-r*Lmj*CS with 50 µM DYVI.

	Rate (nmol/min)
50 ng/mL N-r*Lmj*CS	0.6
50 µM DYVI	0.08

Table 3.8 – Rate of cysteine synthesis in the presence of 50 µM DYVI peptide.

The table shows the rates calculated for each reaction and the presence and absence of DYVI. The values are presented in cysteine (nmol) synthesised per minute.

The CPM assay was then also used to determine the IC_{50} of DYVI. The substrate (OAS) concentration was kept constant and increasing concentrations of DYVI were assayed. N-r*Lmj*CS activity was determined and the IC_{50} curve represented in Figure 3.18. The DYVI IC_{50} was determined to be 2 µM.

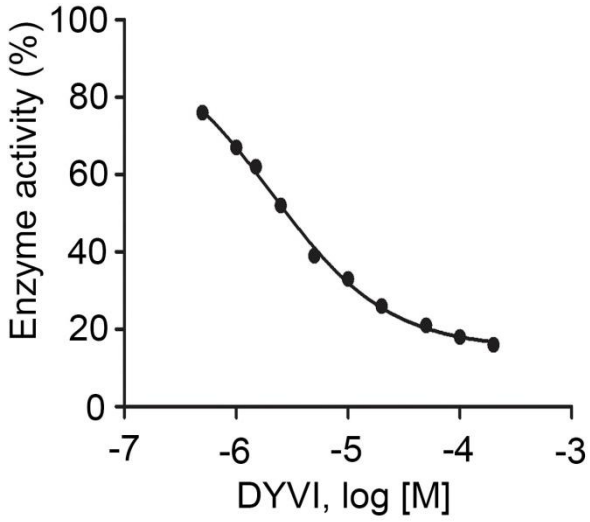

Figure 3.19 – Determination of DYVI IC_{50}.

The graph illustrates a sigmoidal dose-response curve from where DYVI IC_{50} value is extrapolated, 2 µM.

3.9 Results acquired from collaborators

The crystal structure of *Lmj*CS has been resolved by Dr Paul Fyfe from Professor William Hunter's research group at the University of Dundee. The generated construct pET15b-r*Lmj*CS (section 3.2) was sent and the r*Lmj*CS purified and crystallised at the referred facility. As illustrated on Figure 3.20, the *Lmj*CS is an asymmetric dimer. Each subunit contains two domains. The purified protein was yellow in colour consistent with the presence of PLP (previously observed on section 3.3), albeit crystals being colourless (Fyfe *et al.*, 2012). Further observations have revealed the presence of a polyglutamate (PGA) fragment attached to the same region on both subunits, and no PLP (Figure 3.21). The absence of PLP seems to be related to the presence of the PGA (Fyfe *et al.*, 2012). Additionally, *Lmj*CS has been found to have 47% structure conservation when compared with the *A. thaliana* cysteine synthase (*At*CS) (Fyfe *et al.*, 2012).

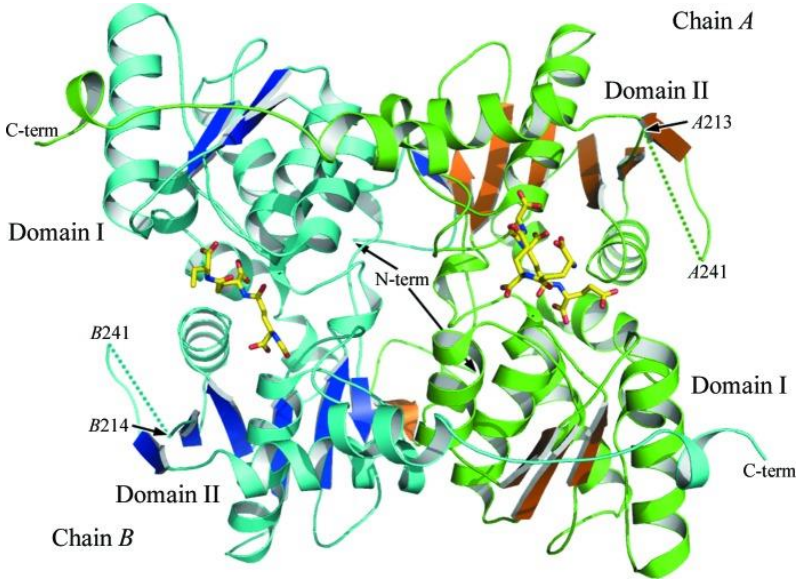

Figure 3.20 – Crystal structure of *Lmj*CS (Taken from (Fyfe *et al.*, 2012)).

Ribbon diagram of r*Lmj*CS enzyme as an asymmetric dimer. On subunit A helices are coloured green and strands are coloured brown; On subunit B helices are coloured cyan and strands are coloured blue; The PGA molecules are depicted in yellow (C atoms), red (O atoms) and blue (N atoms); the domains, and N- and C-terminals are illustrated.

Printed with permission from the Acta Crystallographica Section F.

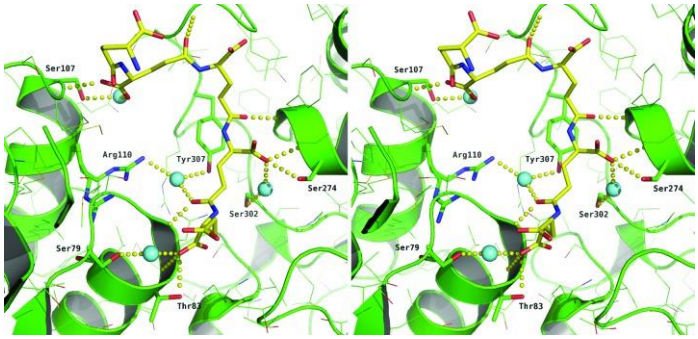

Figure 3.21 – Polyglutamate in the active site.

Stereo-view of PGA fragment bound to subunit A of *Lmj*CS enzyme. The *Lmj*CS in illustrated in green; N and O atoms from specific side chains are illustrated in blue and red, respectively; hydrogen bonds are depicted in yellow dots; water molecules are depicted in cyan (Fyfe *et al.*, 2012).

Printed with permission from the Acta Crystallographica Section F.

3.10 Summary

- C-r*Lmj*CS and N-r*Lmj*CS were successfully expressed and purified. r*Lmj*CS was generated by TEV protease digest from N-r*Lmj*CS.

- Kinetic analysis of the three forms of r*Lmj*CS show that the V_{max} of N-*Lmj*CS is higher than C-r*Lmj*CS and r*Lmj*CS; the N-r*Lmj*CS turnover (k_{cat}) is higher than the other two forms and this is reflected on the enzyme efficiency (lower k_{cat}/K_m), rendering a 2 times more efficient enzyme.

- The inhibition reaction testing peptides mimicking the C-terminal of SAT revealed that DYVI inhibits ~90 % of the enzymes activity of the three *Lmj*CS forms at a concentration of 0.1 mM. EGDGSGI inhibit 30-50% the enzyme's activity.

- The PGA found to be bound to the *Lmj*CS crystal structure tested as a putative inhibitor showed that only the enantiomer D-γEγEγEγE (0.1 mM) had a moderate inhibitor effect on C-r*Lmj*CS activity (20%). At 0.5 mM, D-γEγEγEγE did not showed higher inhibition of the C-r*Lmj*CS activity.

- The CPM detection method validation revealed that Na_2S and BSA highly contribute to the background fluorescence. While the pH of the buffer only marginally affected fluorescence, replacing the BSA with gelatine dramatically reduced the fluorescence background and increased the signal:noise ratio.

- CS activity was successfully detected using the CPM assay and it was shown to be suitable for the study of inhibition of enzyme activity. This provided some evidence that the CPM assay may be suitable for future

development into a HTS assay to test future inhibitors of CS from *Leishmania* or other organisms.

- The results acquired by collaborators showed that *Lmj*CS is an asymmetric dimer. Each dimer has two domains. PLP was absent in the crystal structure. The presence of PGA is believed to be the cause of its absence.

Characterization of a cysteine synthase knockout

4 Characterization of a cysteine synthase knockout

4.1 Introduction

Williams *et al*. 2009 have provided evidence for the existence of two cysteine biosynthetic pathways operating in *L. major*. Cysteine (Cys) is a building block of glutathione (GSH), which is itself a crucial component of trypanothione (TSH). TSH, as outlined in the introduction, is involved in the defence against oxidative stress and detoxification of drugs used against leishmaniasis (Ariyanayagam and Fairlamb, 2001; Oza *et al.*, 2005; Wyllie *et al.*, 2004). Thus, dissecting the cysteine biosynthetic mechanisms may reveal potential new targets exploitable for further anti-leishmanial drug discovery and development. Both cysteine synthase knockout (Δ*cs*) and cysteine synthase re-expressor (RE) cell lines have been previously generated in *L. donovani* (Dr Lesley McCaig PhD's thesis). These lines along with the wild-type (WT) line were used to infect hamsters before this work was commenced and at its outset these animals were available for me for assessment.

4.2 Results

4.2.1 Assessment of the ability of *L. donovani* WT, Δ*cs* and RE to infect hamsters

18 golden hamsters (*Mesocricetus auratus*) were infected by Dr Elmarie Myburgh with *L. donovani* wild type (WT), cysteine synthase knockout (Δ*cs*) and cysteine synthase re-expressor (RE). Six months after infection the hamsters were culled and their spleens and livers (target organs of *L. donovani*) were analyzed for signs of infection. The hamsters infected with *L. donovani* WT and with *L. donovani* Δ*cs* had parasites in both liver and

spleen. The organs of all animals were excised, measured and weighed (Tables 4.1 and 4.2) (see section 2.6.4).

The spleen of the infected animals had a higher parasitic burden than the liver as it was also observed by (Moreira *et al.*, 2012; Ott *et al.*, 1967) and more recently by Moreira *et al.*, 2012 (Table 4.1). Interestingly the parasitic burden was higher in animals infected with the Δ*cs* line than the WT line (Table 4.2). It is possible that there is a compensation mechanism that has been activated in those infected with the Δ*cs* line that allows the survival of these mutant parasites and therefore the maintenance of parasitic virulence in the absence of cysteine synthase. Surprisingly, none of the 6 hamsters infected with the RE line showed sign of parasitic infection. It was later found out (section 4.2.2) that the plasmid used to generate the RE line prior to hamster infection did not actually express the full-length CS which possibly rendered the recombinant protein inactive. Therefore it is possible that the expression of a truncated version of the CS had an adverse effect on the parasitic virulence. The spleen of the hamsters infected with the RE line was on average smaller than the ones infected with the other two lines (Table 4.2). This is consistent with the lack of parasites found in these hamsters. Conversely, the liver of the hamsters infected with the RE line was shown to be larger than the ones from the hamsters infected by the other two parasitic lines but this result could possibly be a negligible variation between hamsters (Table 4.2). The weight of the organs appeared to be unaffected regardless of the presence/absence of infection and parasite line used to infect them (Table 4.2).

Overall WT parasites were recovered in 4 out of 6 hamsters; Δ*cs* were infective to 2 out of 6 animals and RE did not infect hamsters at all.

Hamster	Organ	Number of parasites/g of organ
WT3	Spleen	18
WT3	Liver	2
WT4	Spleen	3
WT6	Spleen	12
Δ*cs*4	Spleen	306
Δ*cs*6	Spleen	31

Table 4.1 – *L. donovani* found in the liver and spleens of 6 hamsters infected.

The table shows the hamster group (WT/Δ*cs*/RE) and number (1-6) where the parasites were recovered. The number of parasites per gram of organ was determined by limiting dilution and the organ from where they were found is stated.

	Weight (g ± S.E.M.)		Size (cm ± S.E.M.)	
Group	Spleen	Liver	Spleen	Liver
WT	0.2 ± 0.0	3.5 ± 0.3	3.4 ± 0.2	2.7 ± 0.2
Δ*cs*	0.1 ± 0.0	3.6 ± 0.4	3.4 ± 0.1	2.7 ± 0.1
RE	0.1 ± 0.0	3.8 ± 0.2	2.5 ± 0.1	3.5 ± 0.1

Table 4.2 – Measurements of the infected organs recovered from the hamsters.

The table shows the size (cm ± S.E.M.) and weight (g ± S.E.M.) of the infected organs from where the three *L. donovani* lines were recovered.

4.2.2 Phenotypic and genotypic characterization of *L. donovani*

Two knockout cassettes were generated previously to replace both alleles of the *cs* coding region with two antibiotic resistant genes, hygromycin (*hyg*) and nourseothricin acetyltransferase (*sat*) (Figure 4.1A). A *cs* re-expressor plasmid (pGL102*Ldcs,* Figure 4.1B) was previously generated and transfected into the *cs* knockout line. The protein and gDNA of the parasitic lines were extracted and compared to the wild-type line (WT) (see sections 2.4.6 and 2.5.3). Figure 4.1C shows a western-blot probed with anti-CS and anti-EF-1α antibodies. The anti-CS antibody detected a band with 35.5 kDa in the WT lane while the protein detected in the RE lane appears smaller. No protein of this size was detected in the Δ*cs* lane confirming the absence of CS protein in the Δ*cs L. donovani*. The 49 kDa bands correspond to the EF-1α protein and it is used to ensure protein load. Figure 4.1C shows a southern-blot of restricted gDNA isolated from WT and Δ*cs L. donovani*. The membrane was probed with the *cs* ORF, *hyg* ORF and *sat* ORF. The blots revealed the 4.7 kb and 0.6 kb bands diagnostic to the presence of the CS gene in the WT lane while these bands are no longer present in the Δ*cs* lane where the two selectable marker bands are detected confirming the replacement of both CS alleles with sat and hyg. The RE lane confirms the presence of the episomal pGL102*Ldcs* in the CS genomic background.

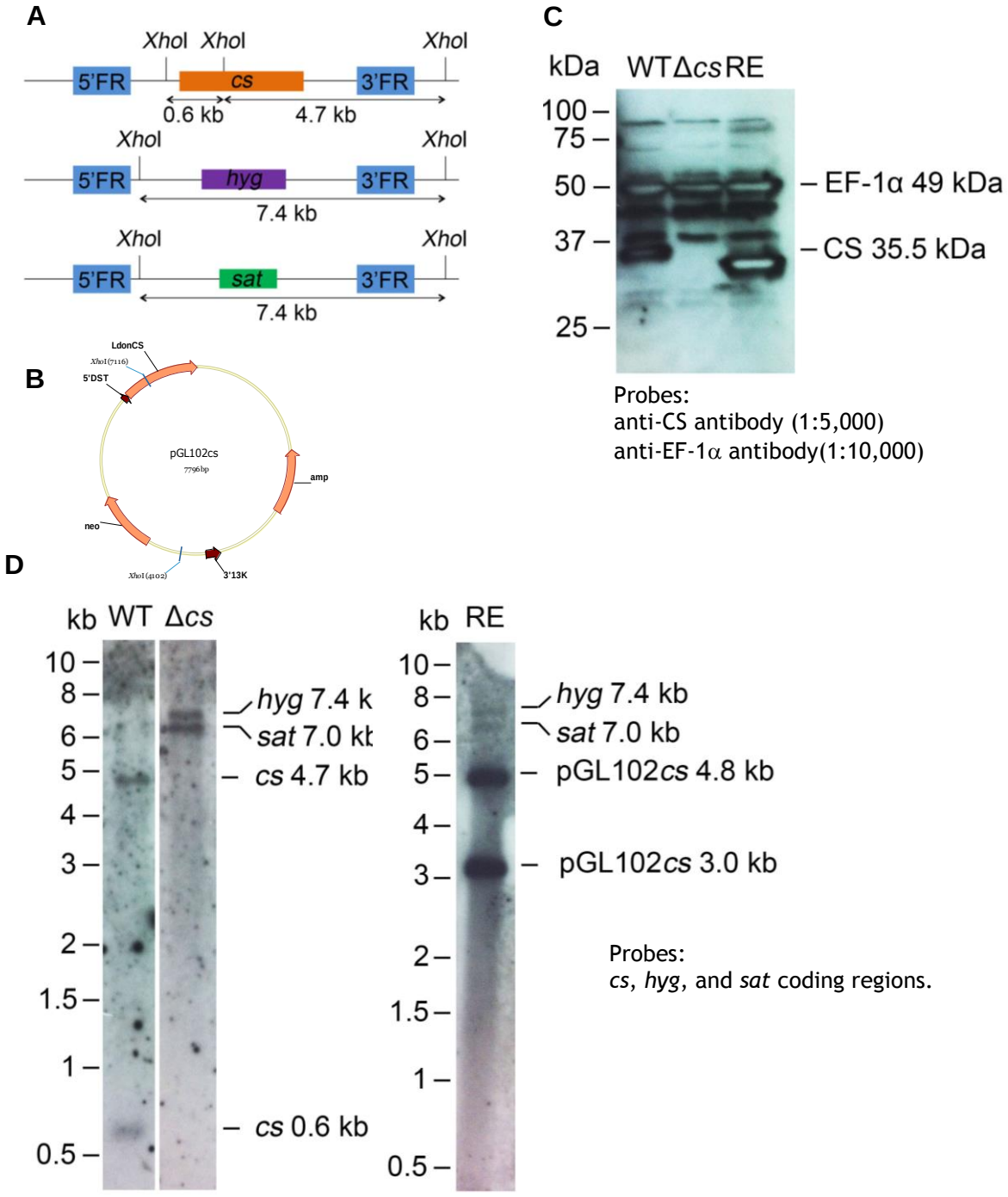

Figure 4.1 - Phenotypic and genotypic analysis of *L. donovani* WT, Δcs and RE parasitic lines.

(A) A schematic diagram showing the *cs* knockout cassette used previously to replace both alleles of the *cs* coding region (orange) with two antibiotic resistance genes, hygromycin phosphotransferase (*hyg*, purple) and nourseothricin acetyltransferase (*sat*, green), by homologous recombination. *Xho*I restriction enzymes are shown along with the expected sizes of resultant DNA fragments. (B) A schematic diagram of the pGL102*Ld*cs RE construct previously generated. The arrows indicates the *Xho*I restriction enzyme sites (0.7 kb and 3.7 kb) and the predicted sizes of resultant DNA fragments; (3'13K) 13 kb RNA; (5'DST) *Leishmania* splice acceptor; (FR) flanking region. (C) The previously generated Δ*cs*

and RE lines were analyzed by western blotting. 10 µg of total protein extract was separated by SDS-PAGE (10%) blotted onto nitrocellulose and probed with anti-CS antibody at 1:5,000 and anti-EF-1α antibody at 1:10,000 (loading control), and exposed for 5 seconds. (D) Southern blot analyses after diagnostic digestion with *Xho*I. 2 µg of genomic DNA was loaded in each lane and were probed against *cs*, *hyg* and *sat*.

4.2.3. Generation of a new pGL102*Ldcs* construct

The CS protein synthesised in the RE line appeared smaller than the protein detected in the WT line (Figure 4.1C). This finding prompted an investigation into the CS sequence used to generate the RE line. The previous plasmid was re-sequenced and revealed a 27 bp shorter CS gene. Upon re-analysis of the *L. donovani* CS sequence available on GeneDB (LdBPK_363750.1), a new now full-length CS construct was generated in pGL102. The *cs* gene (1,014 bp), amplified from *L. donovani* WT gDNA, was ligated to pSC-B-amp/kan intermediate vector (Stratagene). The *cs* gene was digested out and ligated to the digested pGL102 transfection vector, generating a new pGL102*Ldcs* transfecting plasmid (Figure 4.2).

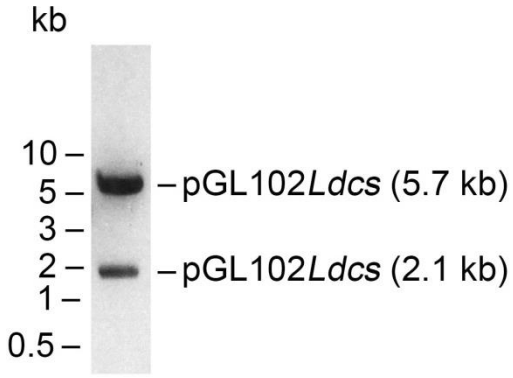

Figure 4.2 – Generation of the new pGL102*Ldcs* plasmid for transfection. *Nco*I restriction enzyme digest of pGL102*Ldcs* construct originates 2.1 kb and 5.7 kb fragments.

4.2.4. Phenotyping of WT, Δ*cs* and RE *L. donovani*.

The loss of CS activity clearly could impact on a variety of pathways operating in *L. donovani*. Therefore a number of phenotypic features of the three parasite lines available were performed.

4.2.4.1. Analysis of parasite growth

The growth of the WT, Δ*cs* and the new RE lines was monitored until the parasites reached the stationary phase (see section 2.6.3). The initial cell density was $5x10^5$ parasites/mL. The growth curves (Figure 4.3A) present four phases: the lag phase (days 1 and 2); the log phase (days 3 and 4); the late log phase (day 5); and the stationary phase (day 6). The experiment was performed in triplicate on several occasions. The results were statistically analyzed using one-way ANOVA with Dunnett's post-test using the WT line as a control. The cell densities (Figure 4.3B) reveal that the growth of the Δ*cs* line is significantly slower (***, $P<0.001$) from the WT line. This growth defect is not seen in the RE line which shows that the growth defect is a consequence of the absence of the *cs* gene.

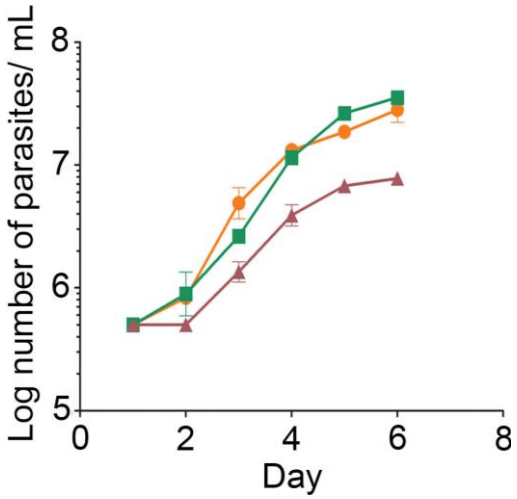

Day	WT	Δ*cs*	RE
1	$5.0x10^5 \pm 0$ (n=6)	$5.0x10^5 \pm 0$ (n=18)	$5.0x10^5 \pm 0$ (n=3)
2	$8.6x10^5 \pm 1.1x10^5$ (n=6)	$5.0x10^5 \pm 0$ (n=12)**	$1.1x10^6 \pm 2.1x10^5$ (n=3)
3	$6.9x10^6 \pm 2.4x10^6$ (n=8)	$1.9x10^6 \pm 5.4x10^5$ (n=14)***	$2.6x10^6 \pm 2.1x10^5$ (n=5)
4	$1.4x10^7 \pm 1.4x10^6$ (n=11)	$5.0x10^6 \pm 1.1x10^6$ (n=14)***	$1.1x10^7 \pm 6.6x10^5$ (n=8)
5	$2.0x10^7 \pm 2.5x10^6$ (n=6)	$6.8x10^6 \pm 4.8x10^5$ (n=6)***	$2.4x10^7 \pm 1.6x10^6$ (n=6)*
6	$3.2x10^7 \pm 7.0x10^6$ (n=6)	$7.9x10^6 \pm 8.1x10^5$ (n=3)***	$3.2x10^7 \pm 3.0x10^6$ (n=6)

Figure 4.3 – Growth curves of the *L. donovani* lines.

The graph and the table show the growth analysis of the *L. donovani* WT, Δ*cs* and RE lines. All the cultures were diluted to $5x10^5$ parasites/mL. Parasite density was recorded every 24 hours. The experiments were carried out in triplicate on multiple occasions (n, number of replicates) and the data is displayed as mean ± S.E.M. The data was analyzed with one-way ANOVA and Dunnett's post-test for multiple comparisons relative to WT control (please refer to the table).

4.2.4.2. Analysis of mRNA synthesis

To assess if this was the result of transcriptional or post-transcriptional events, the mRNA levels of expression of the *cs* and *cbs* genes were measured by QRT-PCR (see sections 2.4.1, 2.4.7 and 2.4.9). The results were analyzed using the $2^{-\Delta\Delta C_T}$ method (Livak and Schmittgen, 2001). Figure 4.4A shows the *cs* expression in the Δ*cs* and RE lines in comparison with the WT line. The results were statistically analyzed using one-way ANOVA with Dunnett's post-test using the WT line as a control. As expected, Δ*cs* line did not have a CS mRNA in accordance with the absence of the gene. In the RE line the *cs* expression was 27 times higher than in the WT line (***, P<0.001). Regarding the *cbs* gene, the expression was 22 times higher in the Δ*cs* line than in the WT line (*, 0.01<P<0.05), and it was reduced to near WT levels in the RE line. This suggests that *cbs* is over-expressed in the Δ*cs* line in response to the loss of CS.

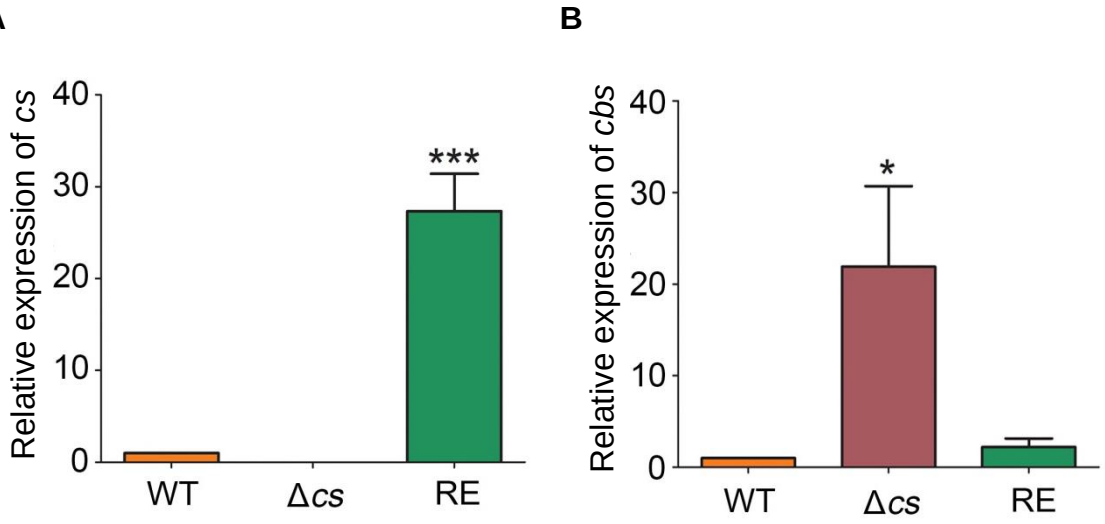

Gene	WT	Δ*cs*	RE
cs	1 ± 0.0 (n=3)	0 ± 0.0 (n=3)	27 ± 4.0 (n=3)***
cbs	1 ± 0.0 (n=3)	22 ± 9.0 (n=3)*	2 ± 0.9 (n=3)

Figure 4.4 – Expression of *cs* and *cbs* genes.

The expression of *cs* and *cbs* mRNA was determined by qRT-PCR relative to the expression of these genes in WT parasites. The data displayed are means ± S.E.M. of three independent determinations performed in triplicate (n, number of replicates); one-way ANOVA and Dunnett's test for multiple comparisons relative to WT control. Panel A: Relative

expression of *cs* gene. Panel B: Relative expression of *cbs* gene. (***) P<0.001; (*) 0.01<P<0.05.

4.2.4.3. Analysis of protein content

Figure 4.4 assessed weather the reverse transsulphuration pathway could potentially compensate for the loss of CS. A western blot of the 3 parasitic lines was done and probed with anti-CS and anti-CBS antibodies (Figure 4.5A) (see section 2.5.3). Anti-oligopeptidase B (OPB) was used as loading control. The western-blot confirms the absence of CS protein from the Δ*cs* line and the re-expression of the protein with the correct size in the new RE line. The RE line over-expressed CS presumably because it is expressed from an episome rather than a copy of the gene integrated into it, for instance in the rRNA locus of the parasites genome.

CBS shows a slight overexpression in both the Δ*cs* and RE lines suggesting a marginal up-regulation of the reverse-transsulphuration pathway on the protein level. However, enzyme activity determinations would be required to fully assess whether reverse transsulphuration is indeed upregulated in the Δ*cs* and RE lines.

A

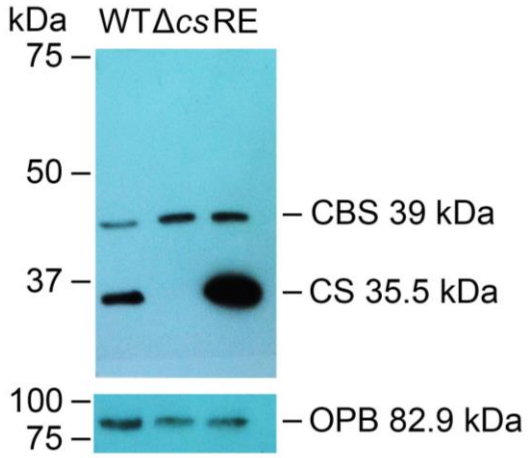

B

	WT	Δ*cs*	RE
CBS	1	2.3	1.5
CS	1	-	3.4

Figure 4.5 – Western blot of the WT and Δ*cs* recovered from the hamster samples and the newly generated RE line that did not went through hamster.

(A) Western blot analysis of the newly generated RE line in comparison with WT and Δ*cs* lines recovered from the hamster samples. 5 µg of total protein extracts were loaded in each lane and probed with anti-CS antibody at 1:5,000, anti-CBS antibody at 1:10,000 and lastly anti-OPB antibody at 1:10,000 to assess equal loading. (B) Band sizes relative to WT anti-OPB control, for each protein analyzed in the western blot. The means were determined with the image processing and analysis software package LabImage1D.

4.2.5. Susceptibility to oxidative stress and metal stress

Cysteine synthase is a key enzyme in the sulphydrylation pathway that leads to the formation of cysteine from *O*-acetyl serine (Williams *et al.*, 2009). Cysteine is the building block of glutathione (GSH) and trypanothione (TSH) (Figure 4.6). TSH is a low molecular thiol responsible for protecting *Leishmania* and other trypanosomatids against oxidative stress (Oza *et al.*, 2005). Thus a CS knockout line should be in theory more susceptible to oxidative stress if indeed the sulphydrylation pathway is the main supplier of cysteine for GSH and TSH biosynthetic pathways.

4.2.5.1 Susceptibility to pro-oxidants

The susceptibility of *L. donovani* lines to hydrogen peroxide, cumene hydroperoxide, and *tert*-butyl hydroperoxide was assayed (Figure 4.7) (see section 2.6.11). These are known to induce lipid peroxidase in cells (Cao *et al.*, 2013; Jovanovic and Jovanovic, 2013; Zavodnik *et al.*, 2013).

Half of the *L. donovani* WT were killed with 265 μM hydrogen peroxide. Both the Δ*cs* and RE lines did not significantly differ (324 μM and 300 μM, respectively) from the control WT line, albeit Δ*cs* being slightly more resistant.

All three lines were more sensitive to cumene hydroperoxide. 21 μM was enough to kill half of the WT parasites; for the Δ*cs* line, 16 μM were needed; for the RE line, 14 μM. Again, the absence of *cs* did not result in a significantly greater sensitivity to this pro-oxidant.

When testing the effect of *tert*-butyl hydroperoxide, the Δ*cs* line (44 μM) showed no significant difference compared with the WT line (51 μM) and the RE line (41 μM).

In other organisms glutathione peroxidase is responsible for the detoxification of hydroperoxides. This enzyme is however absent from trypanosomatids (Fairlamb and Cerami, 1992). In trypanosomatids, TSH is involved in the detoxification of peroxides via tryparodixyn (TXN)-mediated reactions (Flore and Milunsky, 2012). TXN is kept in a reduced state by TSH (Fairlamb and Cerami, 1992).

The absence of *cs* did not make the Δ*cs* line more sensitive for oxidative stress. On the contrary the line presented the same sensitivity as the WT line. As mentioned previously, cysteine is part of the backbone of TSH, thus it is possible that the reverse trans-sulphuration pathway is compensating for the absence of *cs* by supplying cysteine molecules to the GSH/TSH biosynthetic pathways (Figure 4.6).

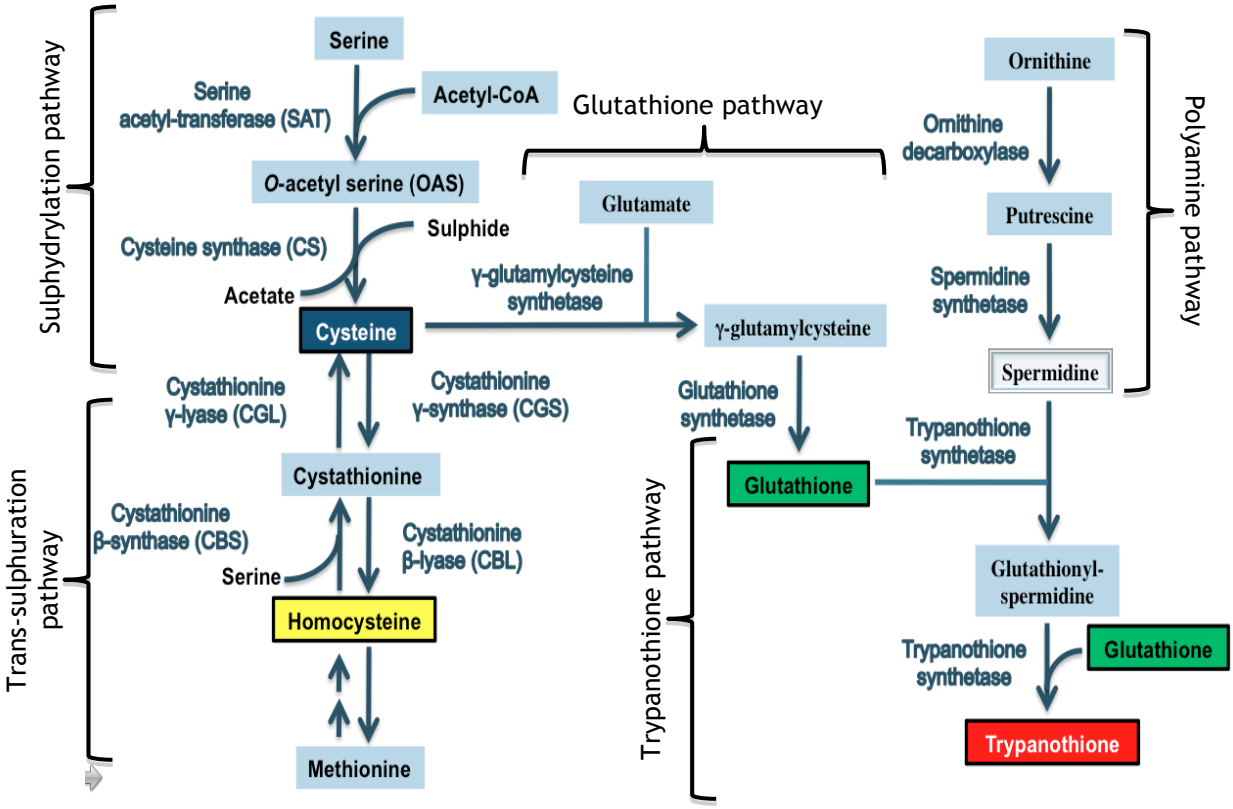

Figure 4.6 – Cysteine, glutathione and trypanothione biosynthetic pathways.

Cysteine (dark blue) can be synthesized by the sulphydrylation pathway or by the reverse trans-sulphuration pathway (RTS). Cysteine is used to synthesize glutathione (green) in the glutathione biosynthetic pathway. Glutathione along with spermidine, from the polyamine pathway, come together to generate trypanothione in the trypanothione pathway.

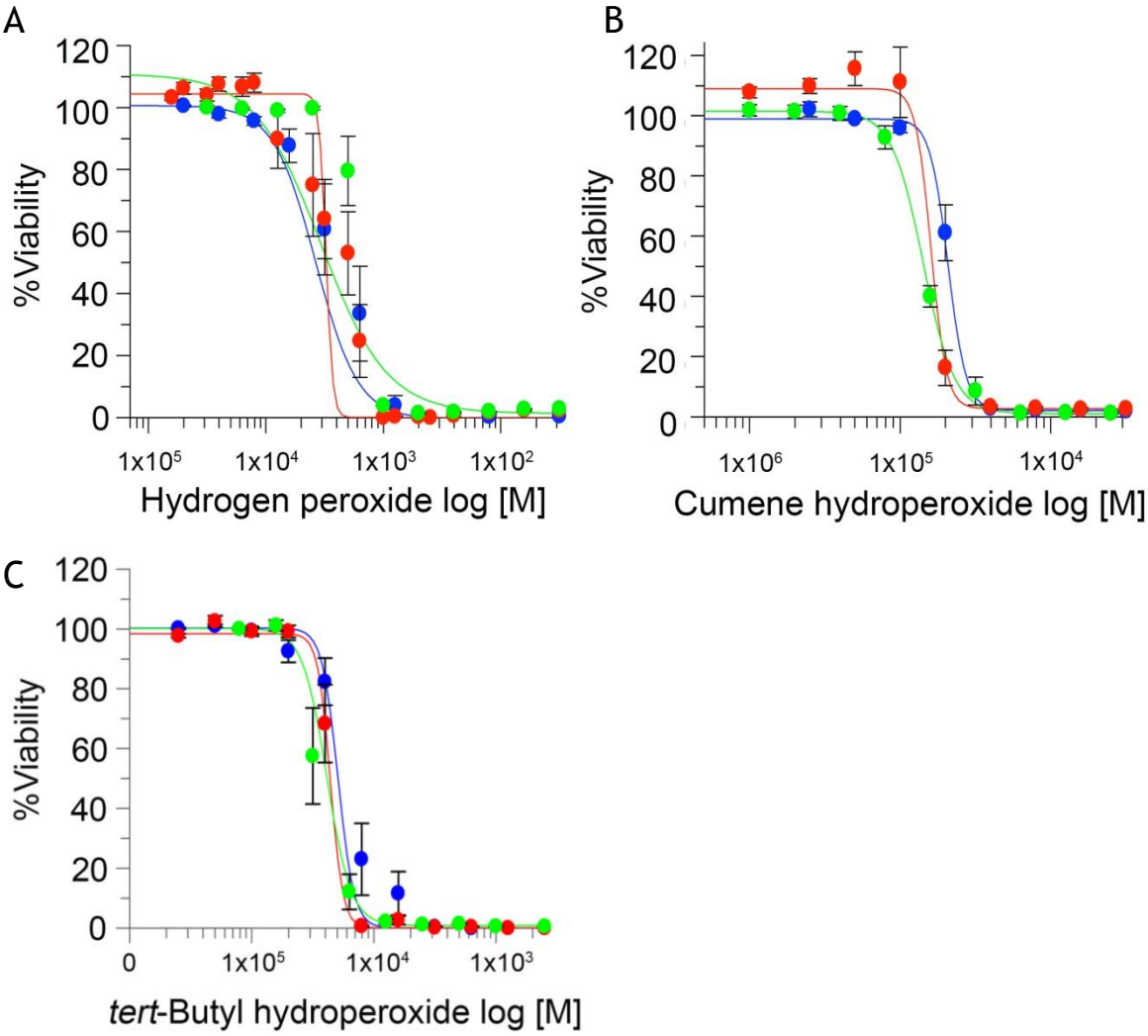

D

IC_{50} (μM)	WT	Δcs	RE
Hydrogen peroxide	265 ± 11 (n=7)	324 ± 44 (n=16)	300 ± 11 (n=8)
Cumene hydroperoxide	21 ± 1 (n=6)	16 ± 2 (n=6)	14 ± 0.3 (n=5)
tert-Butyl hydroperoxide	51 ± 6 (n=6)	44 ± 4 (n=8)	41 ± 8 (n=6)

Figure 4.7 – Susceptibility to oxidative stress.

Determination of *L. donovani* promastigotes IC_{50} for hydrogen peroxide (A), cumene hydroperoxide (B), and *tert*-butyl hydroperoxide (C). The table shows the IC_{50} value with S.E.M. determined by GraFit5 software. The experiments were performed on different days and the number of repeats (n) is indicated in the table. The concentrations ranged from 0.02 to 30 mM for hydrogen peroxide; from 1 μM to 1 mM for cumone hydroperoxide; and 1 μM to 1 mM for *tert*-butyl hydroperoxide.

4.2.5.2 Susceptibility to metal stress

Metal-containing drugs (*e.g.* pentavalent antimonial drugs) are used frequently in the treatment of visceral leishmaniasis. Trypanothione forms metal-TSH complexes that are extruded from the cells leading to reduction of the thiol buffering capacity of *Leishmania* (Decuypere *et al.*, 2012; Fairlamb and Cerami, 1992; Mittal *et al.*, 2007; Rai *et al.*, 2013). P-glycoprotein A (P-gpA), an ABC transporter of metal-thiol conjugates into the vacuole, is believed to be involved in this efflux (Rai *et al.*, 2013; Singh *et al.*, 2007). Elevated thiol levels have been used as markers of antimony and arsenite-resistance (Mukhopadhyay *et al.*, 1996; Rai *et al.*, 2013). This is accompanied by high levels of TSH and over-expression of its biosynthetic pathway enzymes (Ashutosh *et al.*, 2007; Mandal *et al.*, 2007; Mukhopadhyay *et al.*, 1996). Thus, it is expected that a putative thiol deficient *Leishmania* line would be more sensitive to metal stress.

Figure 4.8 shows a sensitivity study to metal stress in the three lines of *L. donovani* (see section 2.6.11). Surprisingly, the Δ*cs* line was significantly more resistant to potassium arsenate (255 μM; *, 0.01<P<0.05) than the WT line (148 μM). The sensitivity was recovered in the RE line (190 μM). Again the non-sensitivity of the Δ*cs* line to the stress points towards the existence of another mechanism of cysteine supply.

Regarding cadmium chloride there was a significant difference (*, 0.01<P<0.05) between the Δ*cs* (115 μM) and the WT line (241 μM). The RE line is significantly more resistant (547 μM; ***, P<0.001) to cadmium chloride than the WT line. So far there is no clear evidence that the high levels of CS results in resistance to pro-oxidants or high levels of stress generated by metals.

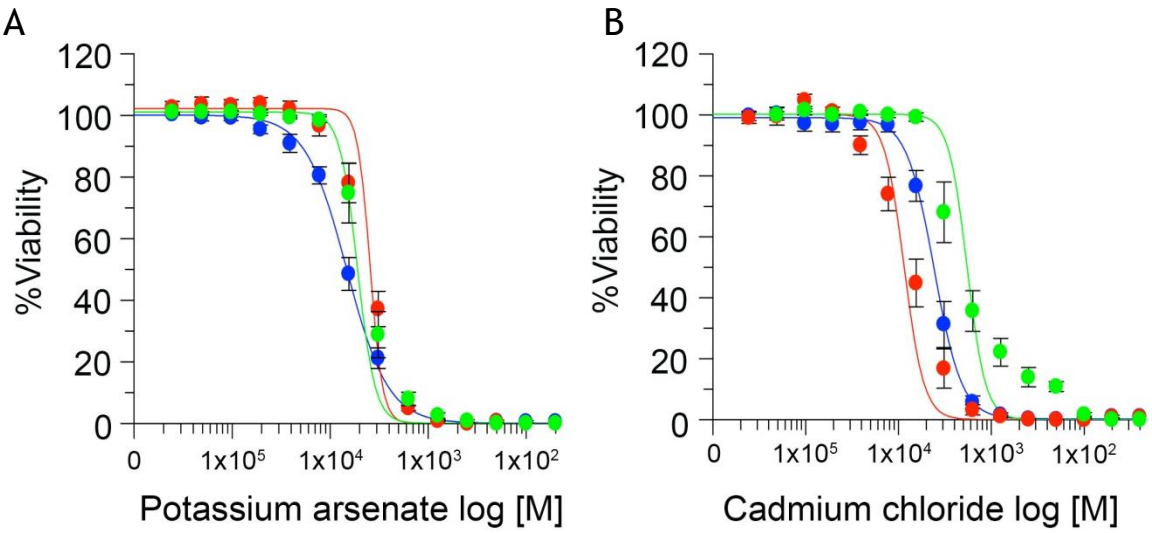

C

IC_{50} (μM)	WT	Δcs	RE
Potassium arsenate	148 ± 9 (N=13)	255 ± 42* (N=14)	190 ± 27 (N=8)
Cadmium chloride	241 ± 21 (N=17)	115 ± 17* (N=17)	547 ± 120 (N=8)***

Figure 4.8 – Susceptibility to metal stress.

Determination of *L. donovani* promastigotes IC_{50} of potassium arsente (A), and cadmium chloride (B). The table shows the IC_{50} value with S.E.M. determined by GraFit5 software. The experiments were performed on different days and the number of repeats (n) are indicated in the table. The concentrations ranged from 0.003 to 20 mM for potassium arsenate, and from 0.003 to 40 mM for cadmium chloride. (*) 0.01<P<0.05; (***) P<0.001.

4.2.6 Determination of thiol levels and the role of the trans-sulphuration pathway

Thiols are the major protectors against xenobiotic toxicity and oxidative damage (Decuypere *et al.*, 2012; Fairlamb and Cerami, 1992; Mittal *et al.*, 2007; Rai *et al.*, 2013). Previous data suggested that there could be a compensation mechanism being activated in the Δ*cs* line as a result of the lack of *cs*. This sub-chapter aims to address this question and to test this hypothesis by analysing the thiol content of the three cell lines.

4.2.6.1 Effect of cysteine synthase knockout on the thiol levels

Figure 4.9 shows a typical chromatogram of *L. donovani* WT harvested on day four after inoculation with a cell number of $2.7x10^8$ cells extracted (see section 2.5.10.1). In the first instance the HPLC system was calibrated using cysteine (Cys), homocysteine (HCys), trypanothione (TSH) and glutathione (GSH) (Figure 4.9A). The system allowed separation of these four thiols with retention times for Cys of 44 ± 0.3 min; HCys of 52 ± 0.2 min; TSH of 56 ± 0.3 min; GSH of 72 ± 0.5 min. The detection range for the detection of all the four thiols was between 50 and 500 pmol.

The next step was then to assess the parasitic cell number required to detect the thiols. It was found out that a minimum of $2.5x10^7$ cells were required to obtain reproducible peaks with peak areas within the detection range.

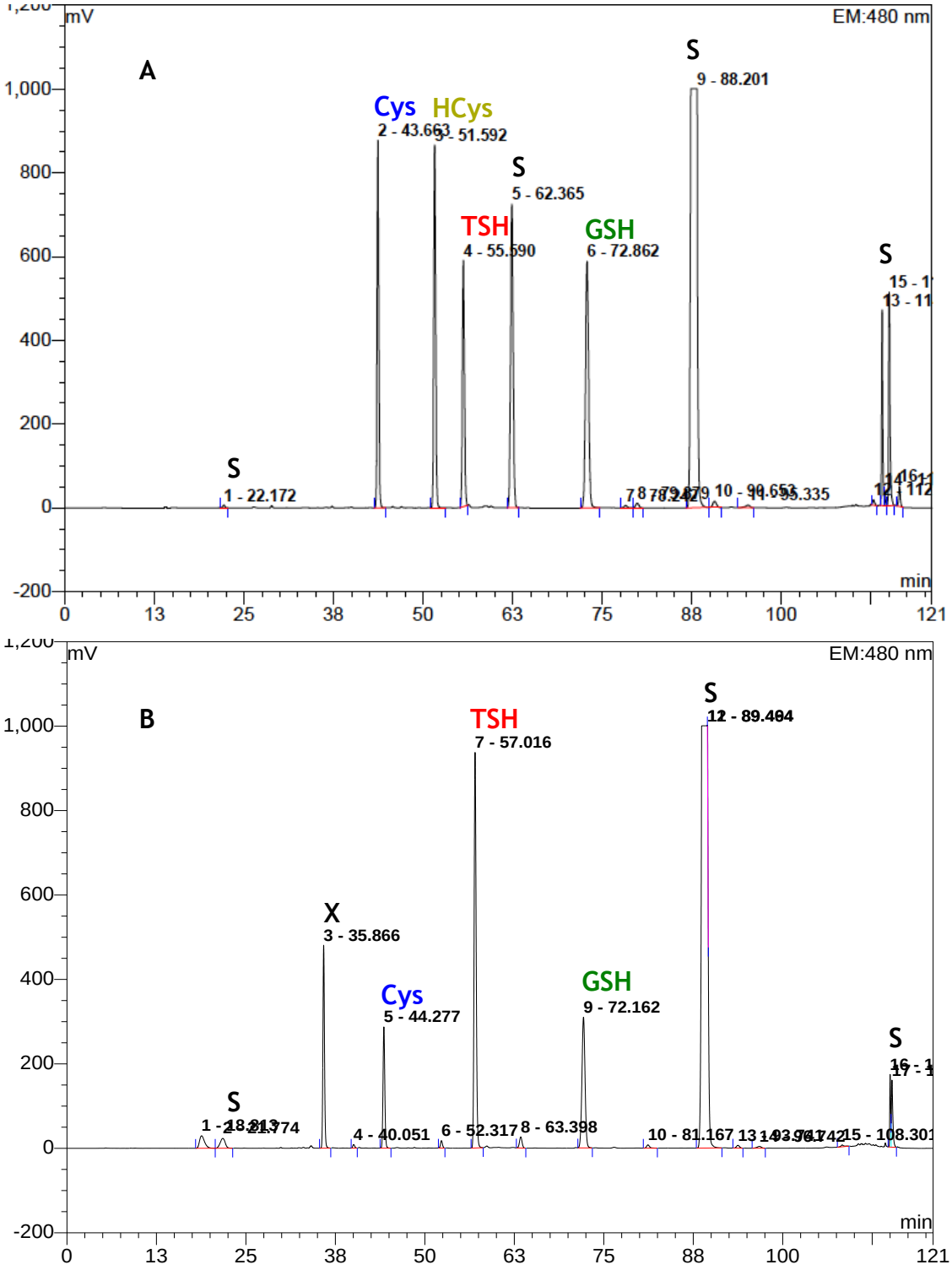

Figure 4.9 - Schematic diagram showing the correlation of the chromatograms of the standards (A) with the WT line (B) on day 4.

Chromatogram A shows the peaks of cysteine (Cys, blue), homocysteine (HCys, yellow), trypanothione (TSH, red), glutathione (GSH, green), and solvent (S, black). The lines connect the standard peaks with the homologue peak in the WT chromatogram. Only one peak was not identified and it was thus labelled as X.

Figure 4.10, 4.11 and Table 4.4 show the thiol levels of the three *L. donovani* lines measured by reverse-phase HPLC over a period of four days (day 3 to day 6 of growth). The data was statistically analyzed using the one-way ANOVA with Dunnett's post-test relative to WT control (Graphpad Prism5 software). The three major thiols present and detectable in *Leishmania* are Cys, GSH and TSH, while the levels of HCys were negligible.

In agreement with previous reports, the concentration of TSH (4-5 nmol/10^8 cells) does not vary during log phase (days 3 and 4) and decreases in stationary phase (days 5 and 6) (Ariyanayagam and Fairlamb, 2001; Weldrick *et al.*, 1999). The same behaviour is observed for Cys and GSH. TSH is the major thiol accounting for 67% of the total thiols on day 4; followed by GSH present at 21%; and Cys with 12% (day 4).

The WT thiol levels were compared with the Δ*cs* and RE lines from day 3 to day 6. On day 3, the absence of CS in the Δ*cs* line does not affect the total level of the thiols present. On day 3 the level of Cys is 0.8 nmol/10^8 cells in the Δ*cs* and WT lines; the level of TSH is 4.2 nmol/10^8 cells (WT line) and 4.8 nmol/10^8 cells (Δ*cs* line); and the level of GSH is 1.4 nmol/10^8 cells (WT line) and 2.3 nmol/10^8 cells (Δ*cs* line). The RE line behaves like an over-expressor with a significant higher level of total thiols (12.5 nmol/10^8 cells; ***, $P<0.001$) compared with the WT line (6.5 nmol/10^8 cells). This is reflected on a significantly higher level (*, $0.01<P<0.05$) of Cys (1.8 nmol/10^8 cells) and TSH (8.2 nmol/10^8 cells), but not GSH (2.3 nmol/10^8 cells), suggesting GSH is promptly used in the biosynthesis of TSH.

On day 4 the thiol levels in the Δ*cs* line decrease dramatically. Cys (0.2 nmol/10^8 cells), TSH (1.0 nmol/10^8 cells) and GSH (0.3 nmol/10^8 cells) are significantly (***, $P<0.001$) lower than WT line (Cys - 0.9 nmol/10^8 cells; TSH – 5.2 nmol/10^8 cells; GSH – 1.7 nmol/10^8 cells). This is obviously reflected in the total thiol level where the Δ*cs* line (1.5 nmol/10^8 cells) has significantly lower level of total thiols (***, $P<0.001$) than the WT line (7.8 nmol/10^8 cells). The total levels of thiol of the RE line decreases which is reflected in a reduction of TSH and GSH levels.

In late-log (day 5) and stationary phases (day 6) there is no significant difference between total and individual levels of thiols between the three *L. donovani* lines.

On day 5 (late-log phase) there is a drop in all thiol levels of WT. Cys droped from 0.9 nmol/10^8 cells (day 4) to 0.5 nmol/10^8 cells (day 5). Cys level decreases further on day 6 to 0.3 nmol/10^8 cells. TSH decreases from 5.2 nmol/10^8 cells (day 4) to 1.8 nmol/10^8 cells (day 5). TSH level increases to 3 nmol/10^8 cells on day 6. GSH levels reduce the same manner as seen in Cys. From day 4 to day 5, GSH levels lower from 1.7 nmol/10^8 cells to 1.0 nmol/10^8 cells, and continues to lower from day 5 to day 6 (0.7 nmol/10^8 cells).

In the Δcs line the lower level of thiols determined on day 4 are increasing on day 5. Cys increases from 0.2 nmol/10^8 cells (day 4) to 0.8 nmol/10^8 cells (day 5). TSH increase from 1.0 nmol/10^8 cells (day 4) to 3.9 nmol/10^8 cells (day 5). And GSH increase from 0.3 nmol/10^8 cells (day 4) to 1.3 nmol/10^8 cells (day 5). On day 6 (stationary phase) the level of Cys (0.5 nmol/10^8 cells), TSH (3.5 nmol/10^8 cells), and GSH (1.0 nmol/10^8 cells) are similar to day 5.

The RE line has similar level of Cys (0.6 nmol/10^8 cells) on day5 to day 4 (0.8 nmol/10^8 cells). TSH levels are also similar between both days 4 (3.4 nmol/10^8 cells) and day 5 (3.6 nmol/10^8 cells). The level of GSH drop to nearly half betwen day 4 (2.1 nmol/10^8 cells) and day 5 (1.5 nmol/10^8 cells). Between day 5 and day 6 the thiol levels almost half for Cys (0.3 nmol/10^8 cells), TSH (1.5 nmol/10^8 cells), and GSH 1.0 nmol/10^8 cells).

Overall, this data suggests that CS (and thus the sulphydrylation pathway) has an important role in maintaining thiol levels specially during the log phase of parasitic growth (*i.e.* day 4). The absence of CS resulted in reduced levels of Cys, TSH and GSH, suggesting that cysteine uptake or biosynthesis via the trans-sulphuration pathway were not suficient to supply enough cysteine for the GSH and TSH biosynthetic pathways. Correlating this effect of thiol level reduction with growth, suggests that the delayed growth of *L.*

donovani lacking CS activity is caused by a reduced ability to generate thiols. Nonetheless, higher levels of TSH and GSH were observed on day 5. This suggests that perhaps while on day 4 the available cysteine suppliers were not able to cope with the high cell division, where thiol synthesis is at its peak (according with data from the WT line). Whereas on day 5, where the cell division slows down to reach stationary phase on day 6, the alternative mechanisms available for cysteine synthesis are able to supply suffient amount to the GSH and TSH biosynthetic pathways.

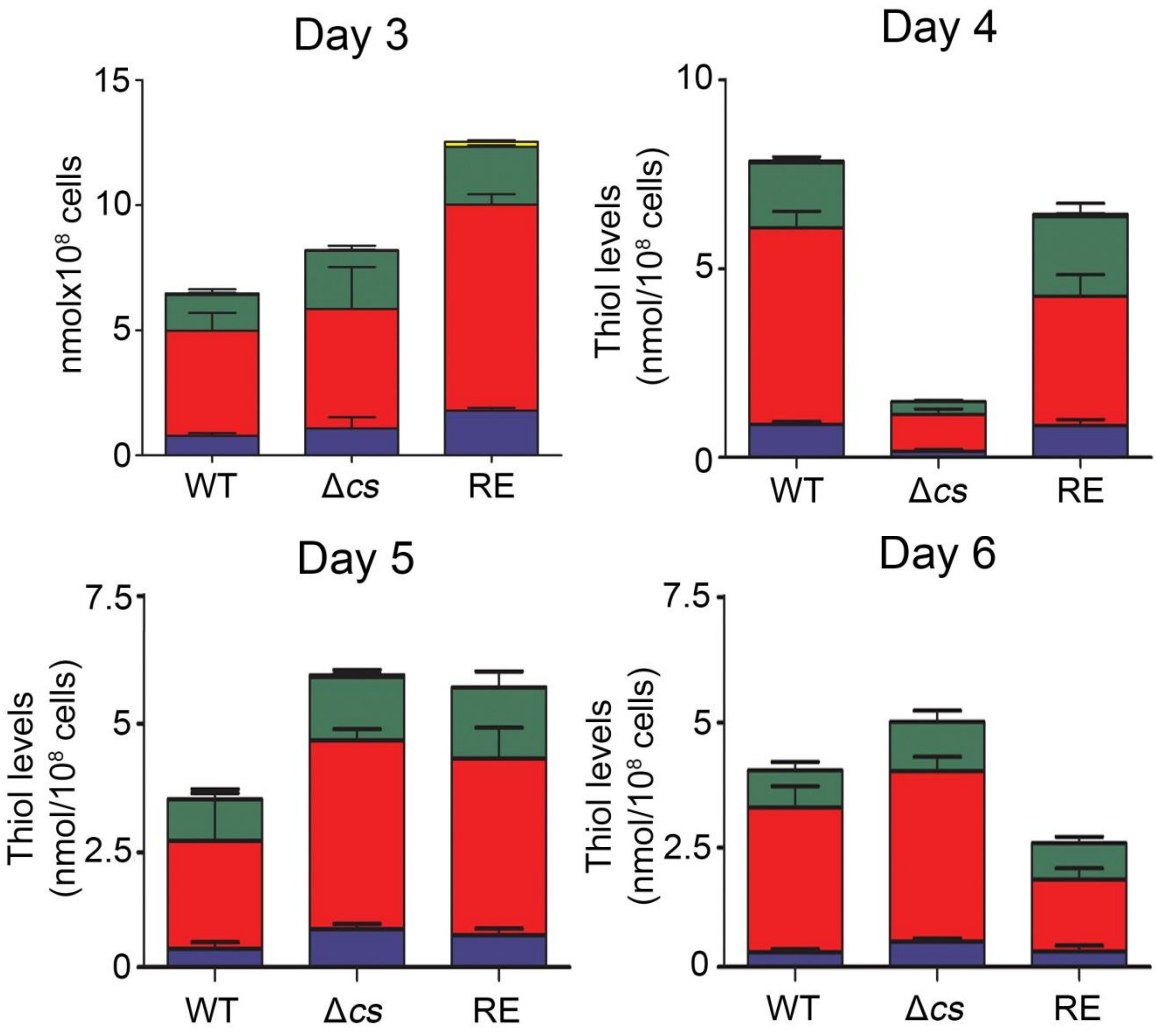

Figure 4.10 – Quantification of total thiols.

The level of cysteine (Cys, blue), trypanothione (TSH, red), glutathione (GSH, green), and homocysteine (HCys, yellow) were quantified by reverse-phase HPLC. Cultures were simultaneously diluted to $5x10^5$ cells/mL and at least $2.5x10^7$ cells/mL were harvested. Thiols were derivatized from day 3 to 6 for thiol analysis. The data is displayed in mean ± S.E.M. (please refer to Table 4.4).

		Thiol levels per day (nmol/10^8 cells ± S.E.M.)			
		3	4	5	6
WT	Cys	0.8 ± 0.1 (n=7)	0.9 ± 0.1 (n=10)	0.5 ± 0.1 (n=5)	0.3 ± 0.0 (n=5)
	TSH	4.2 ± 0.7 (n=7)	5.2 ± 0.4 (n=10)	1.8 ± 0.9 (n=5)	3.0 ± 0.4 (n=5)
	GSH	1.4 ± 0.2 (n=7)	1.7 ± 0.2 (n=10)	1.0 ± 2.2 (n=5)	0.7 ± 0.1 (n=5)
	HCys	0.1 ± 0.0 (n=7)	n.d. (n=10)	n.d. (n=5)	n.d. (n=5)
Total thiols		6.5	7.8	3.3	4
Δ*cs*	Cys	1.1 ± 0.5 (n=5)	0.2 ± 0.0 (n=10)***	0.8 ± 0.1 (n=6)	0.5 ± 0.1 (n=7)
	TSH	4.8 ± 1.7 (n=5)	1.0 ± 0.1 (n=10)***	3.9 ± 0.2 (n=6)	3.5 ± 0.3 (n=7)
	GSH	2.3 ± 0.2 (n=5)	0.3 ± 0.0 (n=10)***	1.3 ± 0.1 (n=6)	1.0 ± 0.2 (n=7)
	HCys	n.d. (n=5)	n.d. (n=10)*	n.d. (n=6)	n.d. (n=7)
Total thiols		8.2	1.5***	6	5
RE	Cys	1.8 ± 0.1 (n=6)*	0.8 ± 0.2 (n=11)	0.6 ± 0.1 (n=9)	0.3 ± 0.1 (n=5)
	TSH	8.2 ± 0.4 (n=6)*	3.4 ± 0.6 (n=11)*	3.6 ± 0.6 (n=9)	1.5 ± 0.2 (n=5)
	GSH	2.3 ± 0.1 (n=6)	2.1 ± 0.3 (n=11)*	1.5 ± 0.3 (n=9)	0.7 ± 0.1 (n=5)
	HCys	0.2 ± 0.1 (n=6)*	0.1 ± 0.0 (n=11)	n.d. (n=9)	n.d. (n=5)
Total thiols		12.5**	6.4	5.7	2.5

Table 4.4 - Analysis of the thiol quantification.

The table summarises the levels of cysteine (Cys), trypanothione (TSH) glutathione (GSH) and homocysteine (HCys) for the *L. donovani* WT, Δ*cs*, and RE lines. Levels were determined by reverse-phase HPLC from day 3 to day 6. Each thiol was analyzed separately and compared between the three lines using one-way ANOVA and Dunnett's post-test for multiple comparisons relative to WT control (n, number of replicates). (*) 0.01<P<0.05; (**) 0.001<P<0.01; (***) P<0.001; (n.d.) not detectable.

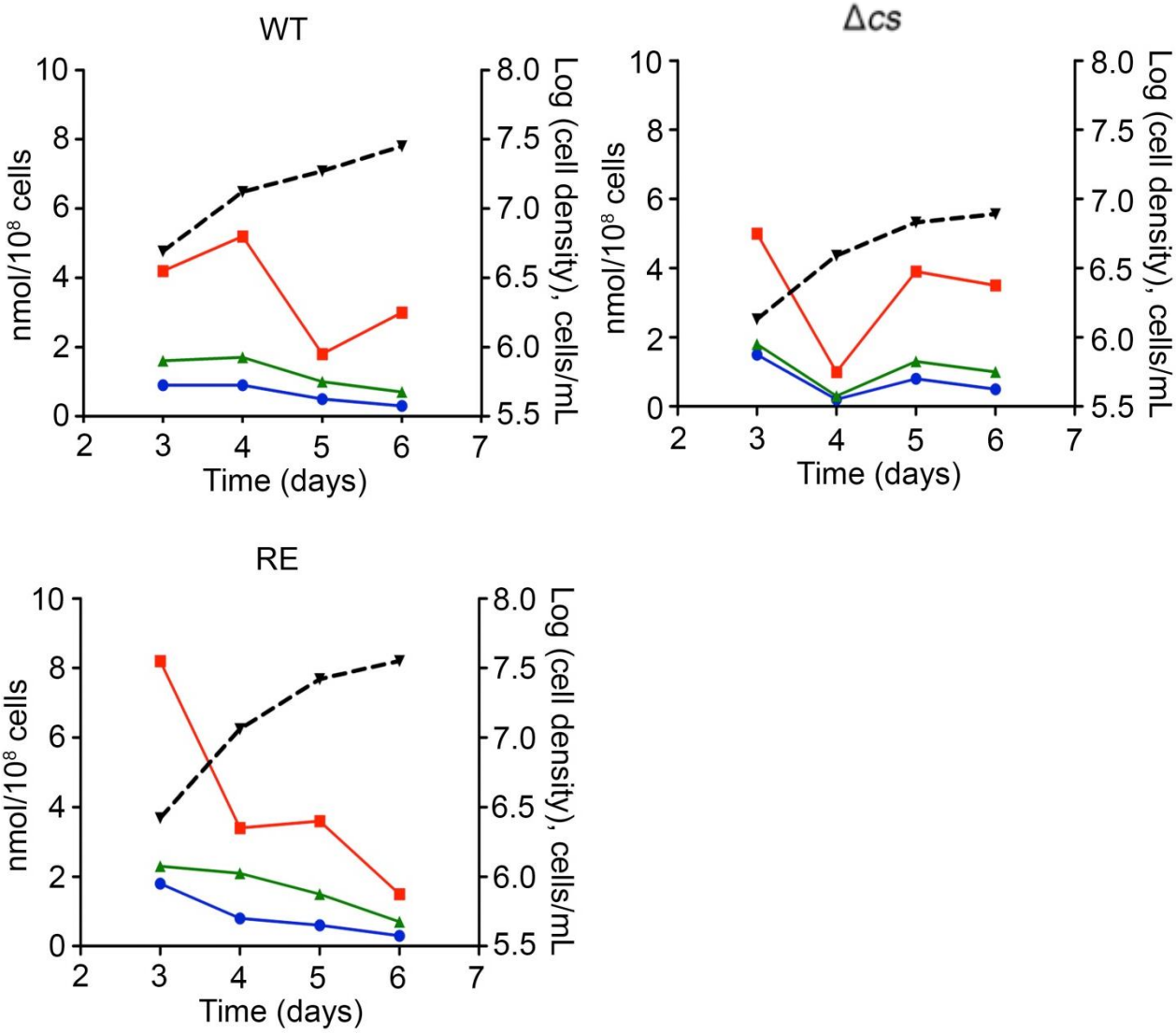

Figure 4.11- Analysis of individual thiol variation with the growth of *L. donovani*.

The thiol levels of the WT, Δ*cs*, and RE lines were plotted against the growth curve (black dashed line): TSH (red), GSH (green), and Cys (blue).

4.2.7 Effect of propargylglycine on the thiol balance

Propargylglycine (PAG) is an inhibitor of pyridoxal 5'-phosphate (PLP)-dependent enzymes. The pathways involved and linked to cysteine biosynthesis (Figure 4.6) have several PLP-dependent enzymes that can be targetted by this inhibitor. The enzymes are CS from the sulphydrylation pathway; and cystathionine γ-lyase (CGL), cystathionine β-synthase (CBS), cystathionine γ-synthase (CGS), and cystathionine β-liase (CBL) from the reverse trans-suphuration pathway; in addition to this, ornithine decarboxylase (ODC) from the polyamine pathway is also a PLP-dependent enzyme.

The sensitivity to PAG was analyzed by determination of PAG IC_{50} in the three *L. donovani* lines (Figure 4.12) (see section 2.6.11). Surprisingly, not only is the Δ*cs* line (215 μM) is more resistant to PAG than the WT line (102 μM), this difference is highly significant ($P<0.001$). The RE line is less resistant (195 μM) than the Δ*cs* line but still significantly (**, $0.001<P<0.01$) more resistant than the WT line.

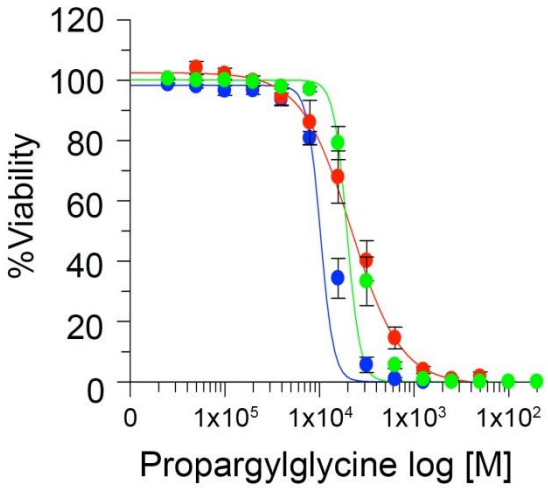

IC_{50} (μM)	WT	Δcs	RE
Propargylglycine (PAG)	102 ± 6 (n=10)	215 ± 17 (n=18)***	195 ± 23 (n=6)**

Figure 4.12 – IC_{50} determination of Propargylglycine.

Determination of propargylglycine (PAG) IC_{50} of *L. donovani* promastigotes. The table shows the IC_{50} value with S.E.M. determined by GraFit5 software (Erythacus). The experiments were performed on different days and the number of repeats (n) is indicated in the table. The concentrations ranged from 1 μM to 1 mM of PAG. (**) 0.001<P<0.01; (***) P<0.001.

To further analyze the contribution of the RTS pathway to the synthesis of Cys and thus other thiols, the three *L. donovani* lines were incubated for 24h with 0, 50 and 250 μM PAG during log phase (Figure 4.13 and Table 4.5).

The no drug control values include all the measurements performed on a non-treated line, hence being the same as the day 4 data presented in Table 4.4. A general overview shows that total thiol levels were most affected by 250 μM of PAG. Incubating with this concentration of PAG, resulted in a reduction of total thiols in the WT line to 2.8 nmol/10^8 cells in contrast with 7.8 nmol/10^8 cells (no drug) (***, P<0.001); the Δ*cs* line has a third of total thiol levels (0.5 nmol/10^8 cells) of the no drug control (1.5 nmol/10^8 cells) (**, 0.001<P<0.01); and in the RE line thiols were reduced by half (2.9

nmol/10^8 cells) compared to the no drug control (6.4 nmol/10^8 cells) (*, 0.01<P<0.05) (Table 4.5).

Looking at each individual thiol, at 5 μM PAG, the WT line presents similar levels of Cys (1.2 nmol/10^8 cells) and TSH (4.6 nmol/10^8 cells) to the no drug control (Cys 0.9 nmol/10^8 cells; TSH 5.2 nmol/10^8 cells). However the levels of GSH (2.6 nmol/10^8 cells) are significantly higher (*, 0.01<P<0.05) than the control (1.7 nmol/10^8 cells), possibly suggesting an accumulation of GSH that is not used for TSH synthesis. The same pattern is seen in the Δ*cs* line for the same PAG concentration. In the RE line the level of each thiol was unaffected by 5 μM PAG.

At 50 μM the level of GSH in the WT line is still significantly higher (2.7 nmol/10^8 cells, **, 0.01<P<0.05) than the control (1.7 nmol/10^8 cells). The levels of Cys and TSH are similar to the control. In the Δ*cs* line, the levels of Cys, TSH and GSH are similar to the control. 50 μM of PAG does not show significant effects in the thiol levels on this line. In the RE line the levels of Cys significantly decrease (0.4 nmol/10^8 cells, *, 0.01<P<0.05) in the presence of 50 μM PAG. TSH and GSH are not affected by this concentration.

As mentioned previously, 250 μM PAG has the most marked effect on the total thiol levels, particularly on TSH and GSH. On the WT line the TSH level significantly (P<0.001) drop from 5.2 nmol/10^8 cells (WT control) to 0.6 nmol/10^8 cells. Cys and GSH are not significantly affected. In the Δ*cs* line, both TSH (0.3 nmol/10^8 cells, **, 0.001<P<0.01) and GSH (0.2 nmol/10^8 cells, *, 0.01<P<0.05) are significantly lower that the Δ*cs* control (TSH 1.0 nmol/10^8 cells; GSH 0.3 nmol/10^8 cells). TSH (0.8 nmol/10^8 cells, ***, P<0.001) and GSH (1.4 nmol/10^8 cells, *, 0.01<P<0.05) are also significantly lower in the RE control line (TSH 3.4 nmol/10^8 cells; GSH 2.1 nmol/10^8 cells).

The fact that TSH and, to a lesser extent, GSH were significantly more affected by PAG, indicates that not only the enzymes from the cysteine biosynthetic pathways are being inhibited but also ODC from the polyamine

pathway may be limited to PAG. In fact PAG seemed to show negligible effects on the biosynthesis of cysteine - there was no significant loss of Cys in the presence of the drug for the treated parasites. The data implis that PAG may have inhibited ODC activity resulting in this remarkable reduction of TSH observed in all three parasite lines at 250 μM PAG.

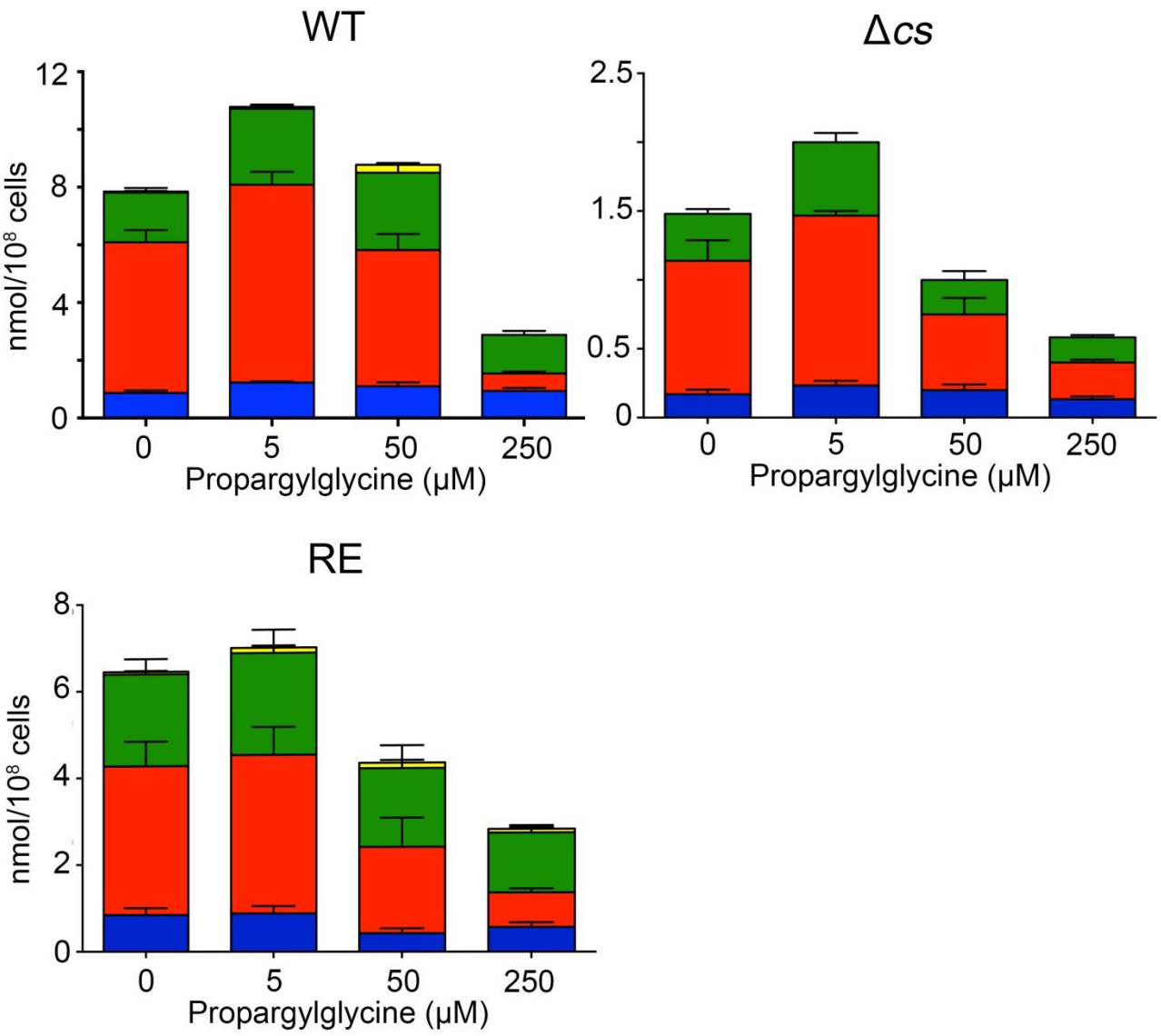

Figure 4.13 – Thiol quantification on day 4 in the presence of propargylglcyine.

The thiols quantified were cysteine (blue, Cys), trypanothione (red, TSH), glutathione (green, GSH) and Homocysteine (yellow, HCys). Cultures were simultaneously diluted to 5x10^5 cells/mL. Propargylglycine (PAG) was added to the cultures at different concentrations on day 3. No-drug cultures were used as controls. Thiols were derivatized with monobromobimane, which forms a fluorescent compound with the thiol-containing proteins (λemission = 480 nm; λexcitation = 365 nm). The thiol derivatives were separated by reverse-phase HPLC and data was collected in form of a chromatogram. The experiment was carried out in duplicates on several occasions.

Thiol levels (nmol/10^8 cells ± S.E.M.)					
Propargylglycine (µM)		**0 µM**	**5 µM**	**50 µM**	**250 µM**
WT	Cys	0.9 ± 0.1 (n=10)	1.2 ± 0.0 (n=3)	1.1 ± 0.1 (n=4)	0.9 ± 0.1 (n=5)
	TSH	5.2 ± 0.4 (n=10)	4.6 ± 2.3 (n=3)	4.7 ± 0.6 (n=4)	0.6 ± 0.1 (n=5)***
	GSH	1.7 ± 0.2 (n=10)	2.6 ± 0.1 (n=3)*	2.7 ± 0.3 (n=4)**	1.3 ± 0.1 (n=5)
	HCys	n.d. (n=10)	n.d. (n=3)	0.3 ± 0.1 (n=4)	n.d. (n=5)
Total		7.8	8.4	8.8	2.8***
Δ*cs*	Cys	0.2 ± 0.0 (n=10)	0.2 ± 0.0 (n=3)	0.2 ± 0.0 (n=4)	0.1 ± 0.0 (n=6)
	TSH	1.0 ± 0.1 (n=10)	1.2 ± 0.0 (n=3)	0.5 ± 0.1 (n=4)	0.3 ± 0.0 (n=6)**
	GSH	0.3 ± 0.0 (n=10)	0.5 ± 0.1 (n=3)*	0.2 ± 0.1 (n=4)	0.2 ± 0.0 (n=6)*
	HCys	n.d. (n=10)	n.d. (n=3)	n.d. (n=4)	n.d. (n=6)
Total		1.5	1.9	0.9	0.5**
RE	Cys	0.8 ± 0.2 (n=11)	0.9 ± 0.2 (n=5)	0.4 ± 0.1 (n=4)*	0.6 ± 0.1 (n=6)
	TSH	3.4 ± 0.6 (n=11)	3.6 ± 0.7 (n=5)	2.0 ± 0.7 (n=4)	0.8 ± 0.1 (n=6)***
	GSH	2.1 ± 0.3 (n=11)	2.3 ± 0.5 (n=5)	1.8 ± 0.5 (n=4)	1.4 ± 0.2 (n=6)*
	HCys	0.1 ± 0.0 (n=11)	0.1 ± 0.0 (n=5)	0.1 ± 0.1 (n=4)	0.1 ± 0.0 (n=6)
Total		6.4	6.9	4.3	2.9*

Table 4.5 – Analysis of the thiol levels measured on day 4 in the presence of propargylglycine.

The table depicts the numeric data from the comparative study on thiol levels in the presence of propargylglycine (PAG). The data are displayed in mean ± S.E.M. (n, number of replicates). Each thiol was analyzed separately and compared with the no-drug control using one-way ANOVA and Dunnett's test for multiple comparisons relative to WT control. (*) 0.01<P<0.05; (**) 0.001<P<0.01; (***) P<0.001; (n.d.) not detectable.

4.2.8 Characterization of the polyamine pathway

PAG had a pronounced effect on the levels of TSH while GSH and cysteine were only marginally or not affected at all by the inhibitor.

This suggests that the enzymes responsible for the synthesis of Cys may either not be inhibited or that an inhibitor of the Cys sulphydrylation or RTS pathways have no effect on Cys levels. Therefore it was surprising to see this significant reduction of TSH in all treated parasitic lines but particularly in the WT parasites (5.2 nmol/10^8 cells to 0.6 nmol/10^8 cells). One possible reason for this strong reduction could be that the synthesis of TSH may be affected by PAG. In fact, ODC, the rate-limiting enzyme of polyamine biosynthesis is also a PLP-dependant enzyme and may well be affected by PAG. Since TSH biosynthesis requires both GSH and the polyamine spermidine, it can be suggested that the strong reduction of TSH levels may be due to inhibition of its synthesis possibly due to ODC inhibition. Since the degree of TSH reduction was more pronounced in WT parasites than in the Δ*cs* line, the expression levels of ODC in the parasites was assessed by RT-PCR (see sections 2.4.1, 2.4.7 and 2.4.9). The results were analyzed using the $2^{-\Delta\Delta C_T}$ method using the WT levels as a reference (Livak and Schmittgen, 2001). The experiment was carried in triplicate on three separate occasions. The results were statistically analyzed using one-way ANOVA with Dunnett's post-test using the WT line as control.

Figure 4.14 shows that the level of *odc* expression in the Δ*cs* line is 7 times higher than in the WT line ($P<0.001$) (Figure 4.14) and the levels of *odc* expression in the RE line were 2 times higher than in the WT line. These results indicate that higher levels of *odc* expression observed in the Δ*cs* result from the absence of the *cs* gene. When the *cs* gene is episomally expressed in the RE line, the level of *odc* expression is lower, closer to the level seen on the WT line.

To assess how this affects the amount of ODC protein in these parasites western blots were performed (Figure 4.15) (see section 2.5.3). The

experiment was repeated on several occasions (Figure 4.17). 5 μg of protein extracted from the WT, Δ*cs* and RE lines was loaded onto a membrane. Four antibodies where sequentially tested to avoid superimposition of protein bands. The anti-ODC and anti-CS antibodies were applied first to the membrane (Figure 4.15A) and proteins with sizes matching that of ODC (77.2 kDa) and CS (35.5 kDa) proteins were detected in the WT and RE lanes. As expected, the CS (35.5 kDa) band was absent from the Δ*cs* line. Surprisingly, the ODC (77.2 kDa) band was nearly absent in Δ*cs* as well, which is opposed to the expectation given the increased mRNA levels detected by QRT-PCR (Figure 4.14). The membrane was subsequently stripped and then probed with anti-CBS antibody first and then anti-OPB as loading control (Figure 4.15B). OPB (82.9 kDa) and CBS (39 kDa) protein bands appeared in all three lanes, confirming equal loading in all three lanes of the western blot. As previously observed, the CBS (39 kDa) band was more intense in the Δ*cs* line than the other two lines.

These results suggest that the Δ*cs* line appears not to rely on polyamine biosynthesis since ODC levels appear to be low.

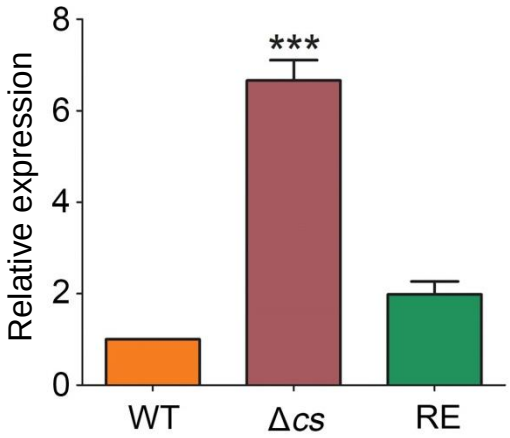

Gene	WT	Δcs	RE
odc	1 ± 0.0 (n=3)	7 ± 0.4 (n=3)***	2 ± 0.3 (n=3)

Figure 4.14 – Relative expression of *odc*.

The relative expression of *odc* was determined by quantitative real time PCR relative to WT. Data displayed as mean ± S.E.M. of three independent determinations (n, number of replicates); one-way ANOVA and Dunnett's post-test for multiple comparisons relative to WT control. (***) P<0.001.

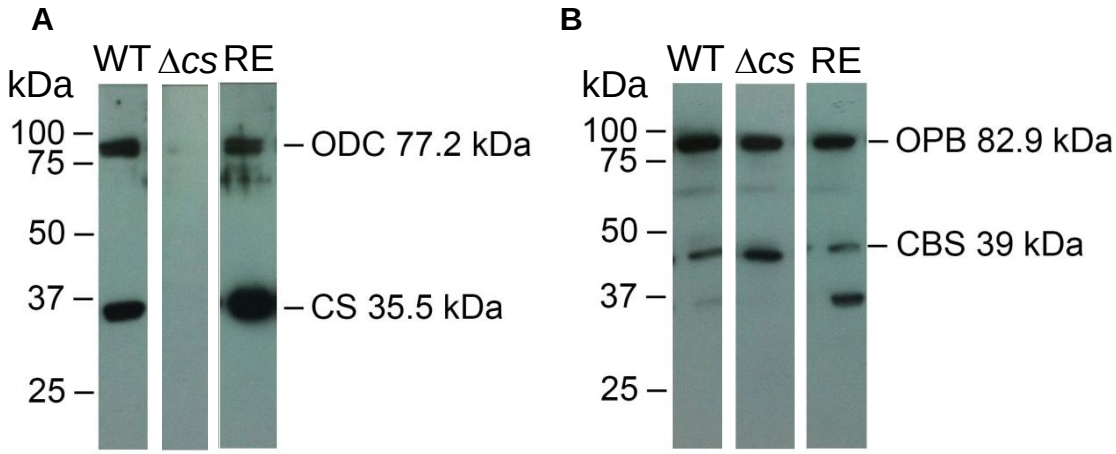

Figure 4.15 – Western blot analyses of the ODC protein expression.

Analyses of ODC expression by western blot. 5 µg of total protein extracts were loaded in each lane and probed with anti-ODC antibody at 1:5,000 and anti-CS antibody at 1:5,000 (panel A). The membrane was then stripped and probed with anti-CBS antibody at 1:10,000 and anti-OPB antibody at 1:10,000 for equal loading control (panel B). Anti-CS and anti-CBS antibodies are, in this case, also used as controls. ODC expression in the Δ*cs* line is reduced compared with the WT line. The ODC expression is recovered in the RE line. The 35.5 kDa band seen on lane RE corresponds to residual anti-CS antibody still bound to the CS protein.

ODC was further characterized by determining the IC_{50} of DFMO, a specific suicide inhibitor of the enzyme, for the three lines (Boitz *et al.*, 2009; Olenyik *et al.*, 2011).

The parasites were diluted to $1x10^6$ cells/mL and incubated for 72 h with increasing concentrations of DFMO (0.001 μM to 20 mM) (see section 2.6.11). To determine the cell viability, resazurin was added and the parasites were further incubated for 48 h and the fluorescence was measured (λemission = 549 nm; λexcitation = 590 nm). The experiment was carried out in duplicate or triplicate and performed on different occasions.

Figure 4.19 shows the sigmoidal dose-response curves for each line. The determined IC_{50} value for WT was 103 μM; for Δ*cs* it was not possible to determine the IC_{50} value even when in DFMO concentration of more than 10 mM were applied; the RE IC_{50} value was 77 μM for DFMO and thus in the same range as the determined for the WT parasites. This data suggests that the lack of Δ*cs* results in a severe down-regulation of ODC activity. The reasons for this are yet to be fully understood.

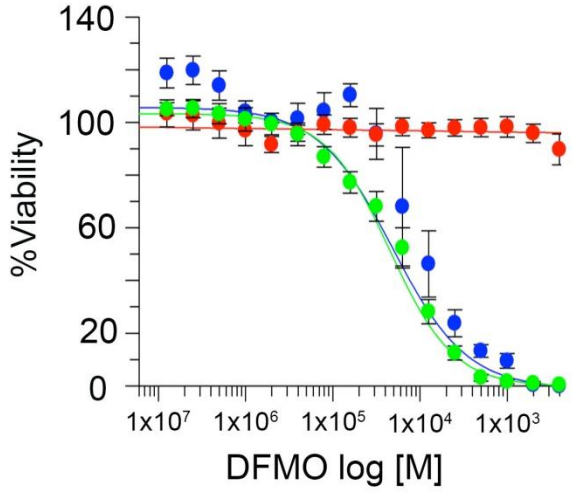

IC_{50} (µM ± S.E.M.)	WT	Δcs	RE
α-difluoromethylornithine (DFMO)	48 ± 6 (n=4)	>10 mM (n=7)	45 ± 4 (n=8)

Figure 4.16 – IC_{50} determination of DFMO.

IC_{50} determination of *L. donovani* promastigotes exposed α-difluoromethylornithine (DFMO). Cultures were diluted to 1x10^6 cells/mL and incubated with varying dilutions of DFMO, in a limiting dilution manner. The concentrations ranged from 0.001 µM to 20 mM. Metabolic activity was determined by the addition of resazurin sodium salt after 72 hours, and fluorescence (λemission = 549 nm; λexcitation = 590 nm) was measured after 48 hours. Graph – Sigmoidal dose-response curve showing the percentage of cell viability with the log of the molar concentration of DFMO. Table – Means of the IC_{50} values for each line with S.E.M. (n, number of replicates).

4.2.9 Validation of detection and quantification of polyamines

To better understand and characterise the effect of the Δ*cs* on ODC and presumably downstream metabolic processes, attemptes were made to determine the polyamine levels in *L. donovani* WT, Δ*cs* and RE lines by HPLC (see section 2.5.10.2). A number of different analysis techniques using HPLC are available in the literature and it was decided that suitability to the HPLC system available had to be assessed (Das Gupta *et al.*, 2005; Jiang *et al.*, 1999; Kabra *et al.*, 1986; Shim and Fairlamb, 1988; Wittich *et al.*, 1987). Two methods were tested, one using methanol/H_2O as a mobile phase and

one using the ion paring compound octane-1-sulfonate and acetonitrile as the mobile phase (Tables 4.6) Polyamine standards were derivatized with dansyl chloride (Das Gupta *et al.*, 2005; Jiang *et al.*, 1999; Kabra *et al.*, 1986; Shim and Fairlamb, 1988; Wittich *et al.*, 1987) and the dansylated polyamines were extracted from the reaction mixture using ethyl ether.

In polyamine analyses 1,6-diaminohexane (a diamine not naturally occurring) is used as the internal standard to test various derivatisation and separation techniques.

400 pmol of 1,6-diaminohexane was derivatized with dansyl-chloride and extracted in 4 mL of diethylether (Wittich *et al.*, 1987). After evaporating at 70°C to dryness, the derivatized diamine was resuspended in 250 μL 5% acetic acid in methanol, and 10 μL (20 pmol) were separated by HPLC using solvent gradients A and B and a 250 x 4.6 μm silica column. The peaks were detected using a Dionex Ultimate 2000 fluorescent detectors at λexcitation of 365 nm and λemission of 485 nm. As a control, 10% TCA was also derivatized and treated in the same way as 1,6-diamonohexane and separated (Jiang *et al.*, 1999).

Gradient A resulted in a chromatogram with no peaks. The 1,6-diamonohexane had to be washed off the column with 100% acetonitrile. Figure 4.17 shows a chromatogram of a buffer alone (Figure 4.17A) and the 20 pmol of 1,6-diaminohexane (Figure 4.17B). Comparing the two chromatograms suggested 1.6-diaminohexane eluted near a solvent peak at 34 min.

To test gradient C, 1 nmol of putrescine was tested instead of 20 pmol of 1,6-diaminohexane. It was intended that by changing the polyamine one would be able to clearly identify its peak from the solvent peaks. Also by increasing the injected quantity of polyamine from 20 pmol to 1 nmol would again facilitate its identification. Figure 4.18 shows a chromatogram of a derivatized buffer alone sample (Figure 4.18A) and 1 nmol putrescine (Figure 4.18C). Comparing both chromatograms suggests that putrescine co-eluted with a solvent peak. The putative putrescine peak is higher than the than solvent peak by 10 times. This also suggests that the limit of detection

is lower than 1 nmol. Another explanation for the lack of the presence of a specific peak could be that putrescine had bound to the column very tightly and was not actually eluted from it with the mobile phase used.

Gradient A:

Time (minutes)	0	25	37.5	46.25	50	52.5	62.5
% Solvent A	42.5	32.5	17.5	0	0	42.5	42.5
% Solvent B	57.5	67.5	82.5	100	100	57.5	57.5

Flow rate = 0.55 mL/ min
Solvent A – Methanol
Solvent B – ddH_2O

Gradient B:

Time (minutes)	0	13	18	29	32	51	56	62.5
% Solvent A	75	70	35	25	0	0	75	75
% Solvent B	25	30	65	75	100	100	25	25

Flow rate = 1 mL/ min
Solvent A – 75 % Octane-1-sulfonate (20mM) and 25 % acetonitrile
Solvent B – 20 % Octane-1-sulfonate (20mM) and 80 % acetonitrile

Gradient C:

Time (minutes)	0	15	45	62.5
% Solvent A	70	0	0	70
% Solvent B	30	100	100	30

Flow rate = 1 mL/ min
Solvent A – 75 % Octane-1-sulfonate (20mM) and 25 % acetonitrile
Solvent B – 20 % Octane-1-sulfonate (20mM) and 80 % acetonitrile

Tables 4.6 – Gradients and solvents tested for the separation of polyamines.

Tables containing the three gradients tested for the separation of polyamines. The gradients are identified as A, B and C. The solvent combination and flow rate applied is referred to below each table.

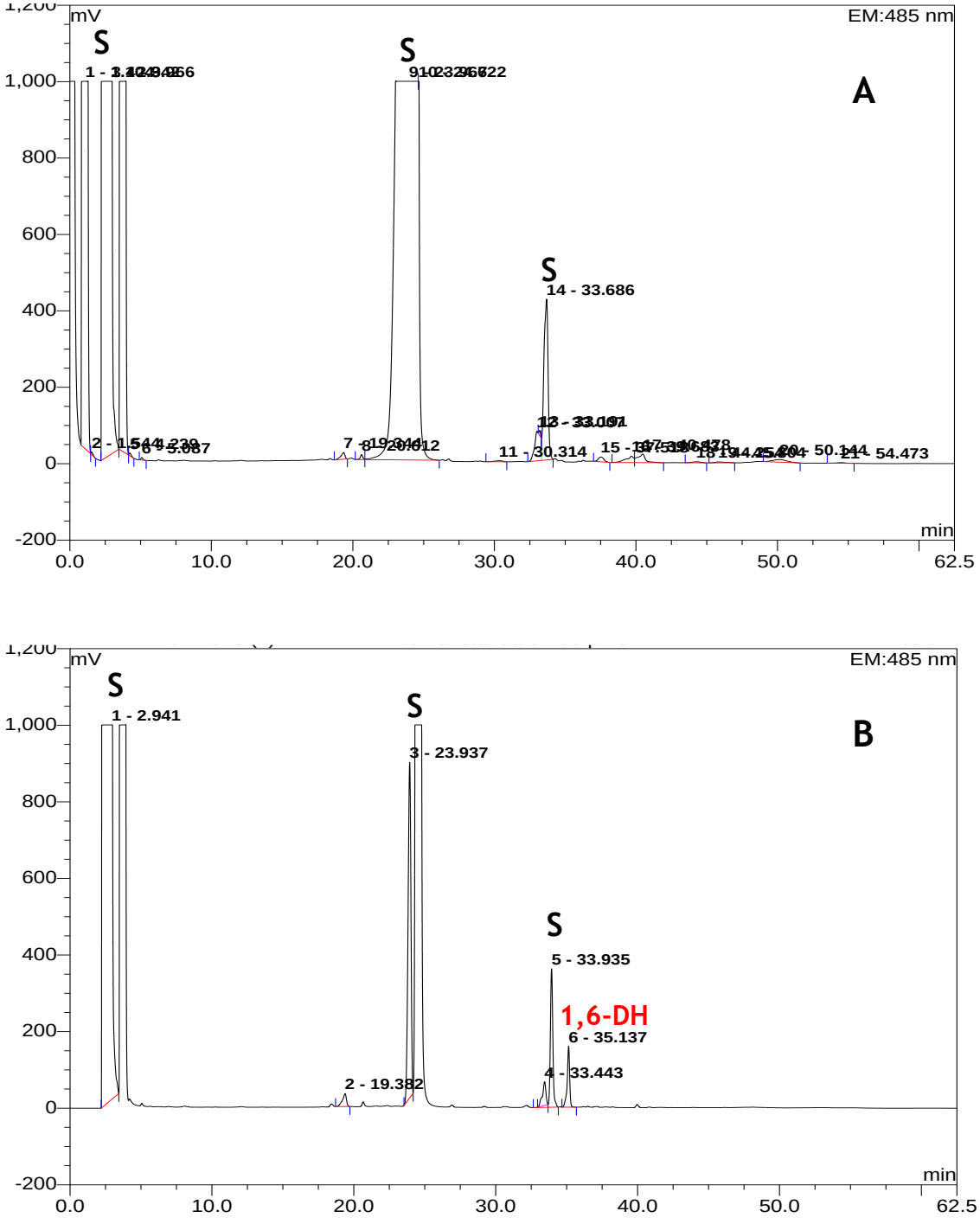

Figure 4.17- Chromatograms resultant from gradient B.

20 pmol of 1,6-diaminohexane were run using the gradient B. Panel A shows the chromatogram of a blank with solvent (S) peaks. Panel B shows the chromatogram of 1,6-diaminohexane (1,6-DH, red), which is eluted close to a solvent peak.

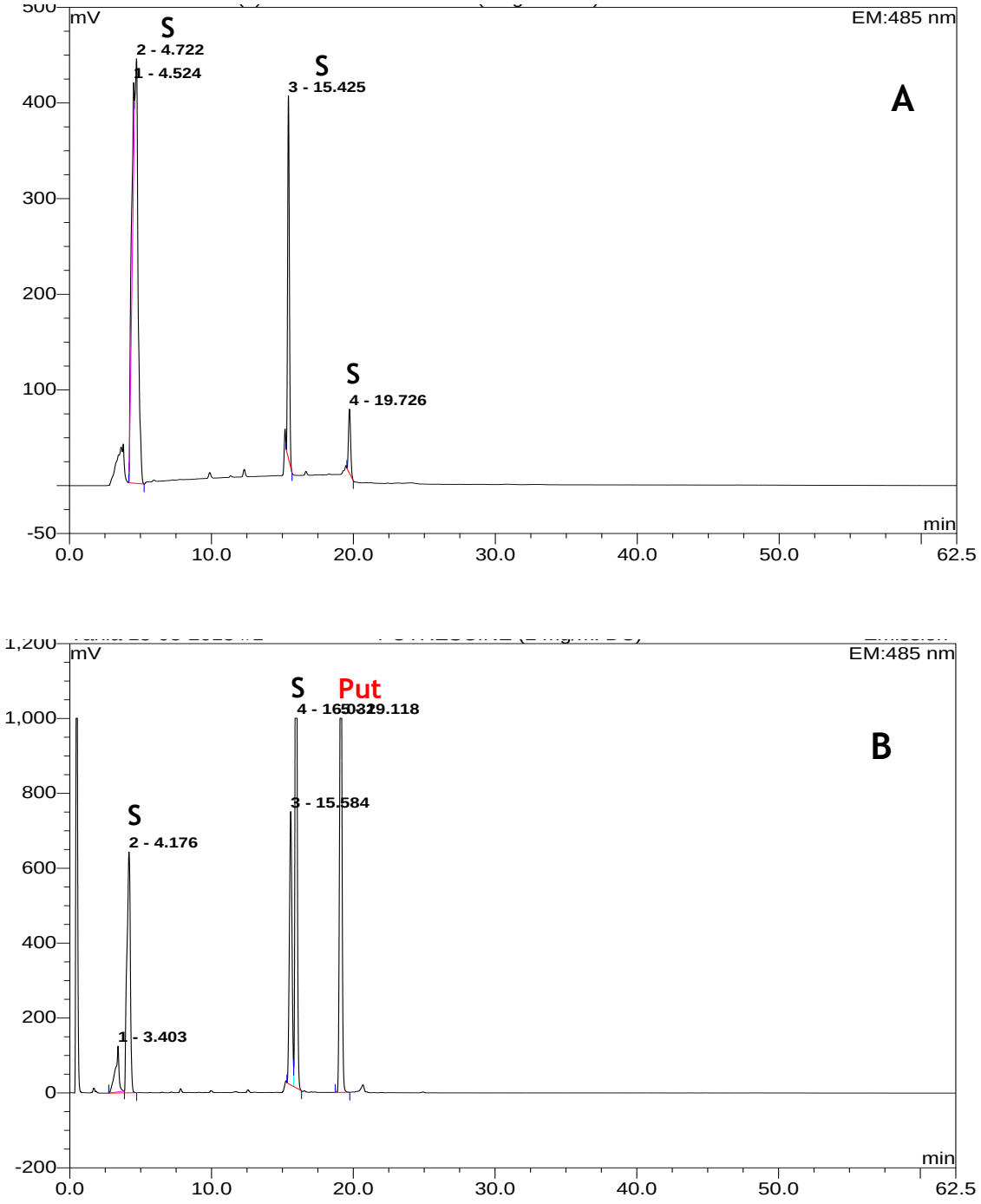

Figure 4.18 – Chromatograms resultant from gradient C.

1 nmol of putrescine was run using the gradient C. Panel A shows the chromatogram of a blank. Panel B shows the chromatogram of putrescine. (S) solvent peak; (Put) putrescine peak.

Having established that gradient C was the most appropriate for polyamine separation and identification, the concentration of dansylchloride was tested. The concentration of dansylchloride varied between 2 (Das Gupta *et al.*, 2005) and 10 mg/mL (Jiang *et al.*, 1999; Rojas-Chaves *et al.*, 1996) depending on the publication. Proline, used to quench the excess of dansylchloride, was used only when 10 mg/mL of dansylchloride were used. Three samples of 1 nmol/20 μL of putrescine were derivatized: the first one was derivatized with 2 mg/mL without proline (Figure 4.19A); the second one was derivatized with 10 mg/mL dansylchloride (Figure 4.19B); and the third one was derivatized with 10 mg/mL of dansylchloride following by quenching with 25% proline (Figure 4.19C).

Figure 4.19 shows the identification of the common peak, both from the buffer and the putrescine. Increasing the concentration of dansylchloride from 2 (Figure 4.19A) to 10 mg/mL (Figure 4.19B) resulted in an increase of the background peaks (buffer picks). Also the putative putrescine peak is two minutes apart between chromatograms, which might indicate that it does not correspond to putrescine. However, given the size of the peak it is likely to be putrescine. The background peaks were further reduced when 25% proline was used to quench the excess of dansyl chloride (Figure 4.19C). This also allowed the clear identification of the putrescine peak at 17.56 min (Figure 4.19C).

Gradient C and 10 mg/mL of dansylchloride with subsequent quenching with 25% proline was used to derivatise and separate the other polyamines. The standard curve of putrescine (125-500 pmol), spermidine (125-800 pmol), and spermine (250-800 pmol) were generated using 500 pmol 1,6-diaminohexane as an internal standard. An example of a standard chromatogram can be seen on Figure 4.20A). This internal standard was added to the parasitic extracts. The parasitic extracts (minimum of $5x10^7$ cells) of the WT and Δ*cs* lines were derivatized as established previously and the resultant chromatogram was compared with the standard chromatogram. The parasitic extract chromatograms of both WT and Δ*cs* lines (Figure 4.20B and Figure 4.21B, respectively) presented more peaks

than the standard chromatogram (Figure 4.20A and Figure 4.21A, respectively).

The same number of parasites ($7.6x10^7$ parasites) was derivatized for both lines. This experiment was performed once with only one replicate. The parasites were in stationary phase. Polyamines were quantified using the standard curves previously generated and the area of the peaks. Table 4.7 shows the quantification of the detected putrescine and spermidine. As expected, the spermine peak was not detected in the parasitic extract chromatograms. The level of putrescine in the WT line was 8.3 nmol/10^8 cells, whereas in the Δcs line it was 1.4 nmol/10^8 cells. The level of spermidine in the WT line was 6.1 nmol/10^8 cells, which is similar to the Δ*cs* line that has 5.9 nmol/10^8 cells.

This work could not be finalized due to time constraints. This preliminary data do however support the suggestion that ODC activity is reduced in Δcs (a strong reduction of putrescine levels) while spermidine levels appear to remain unaffected. This may be explained by the fact the TSH can be degraded by TSH synthase/amidase reduction of TSH levels in the Δ*cs* parasite line (Oza *et al.*, 2005).

Further studies aim to elucidate the link between Cys acquisition pathways and polyamine and TSH biosynthetic pathways to fully understand the impact on the parasite's metabolism of the CS deletion.

	nmol/10^8 cells	
Parasitic line	Putrescine	Spermidine
WT	8.3	6.1
Δ*cs*	1.4	5.9

Table 4.7 – Quantification of polyamines.

Polyamine levels of the WT and Δ*cs* lines when in stationary phase. The parasitic extracts were derivatized with 10 mg/mL of dansylchloride and subsequently quenched with proline. 1,6-diaminohexane was used as the internal standard. The polyamines were separated using gradient C conditions. These values are the results from one experiment with one replicate.

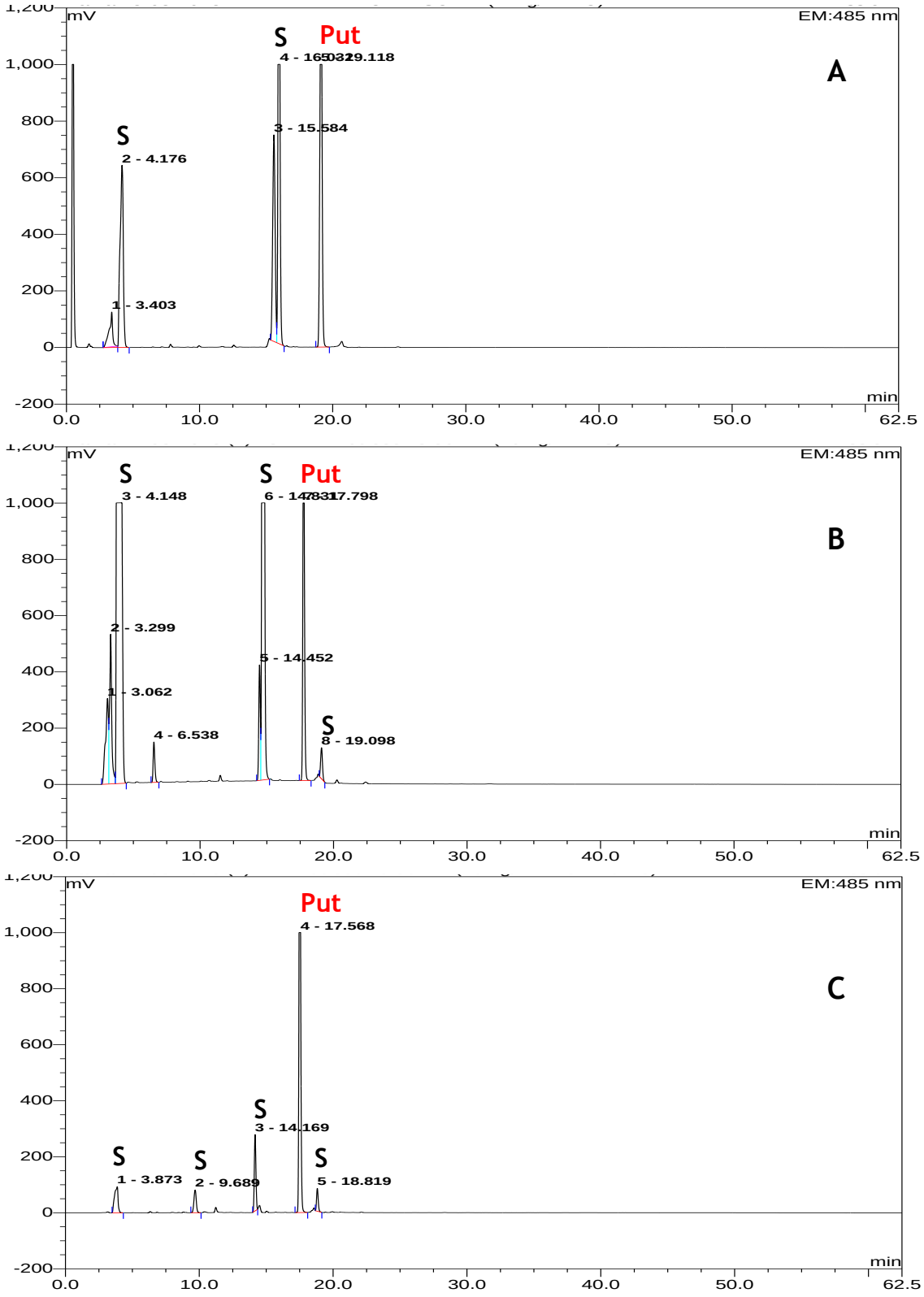

Figure 4.19 - Analysis of dansylchloride derivatisation.

Panel A – 1 nmol of putrescine derivatized with 2 mg/mL of dansylchloride; Panel B – 1 nmol of putrescine derivatized with 10 mg/mL of dansylchloride; Panel C – 1 nmol of putrescine derivatized with 10 mg/mL of dansylchloride with subsequent quenching with proline. (S) Solvent peak; (Put) putrescine peak.

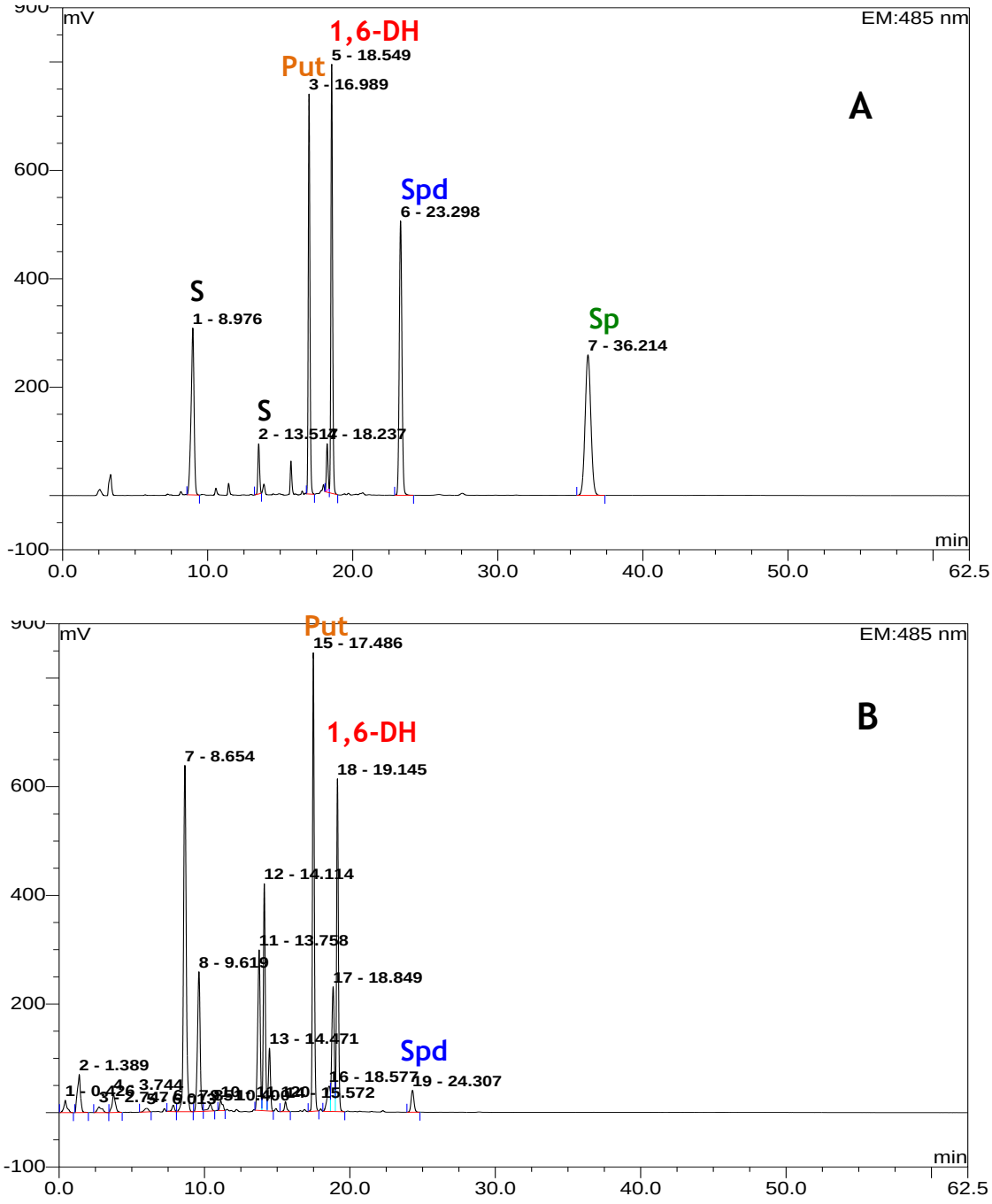

Figure 4.20 – Analysis of the homologous peaks between the standard and the parasitic extract chromatogram.

Panel A - Standard chromatogram. (Put, orange) 400 pmol putrescine; (1,6-HD, red) 500 pmol 1,6-diaminohexane; (Spd, blue) 400 pmol spermidine; (Sd, green) 400 pmol spermine; (Bf, black) buffer. Panel B - Parasitic extract of the WT line. Putrescine (Put, orange); 1,6-diaminohexane (1,6-HD, red); spermidine (Spd, blue); spermine (Sd, green).

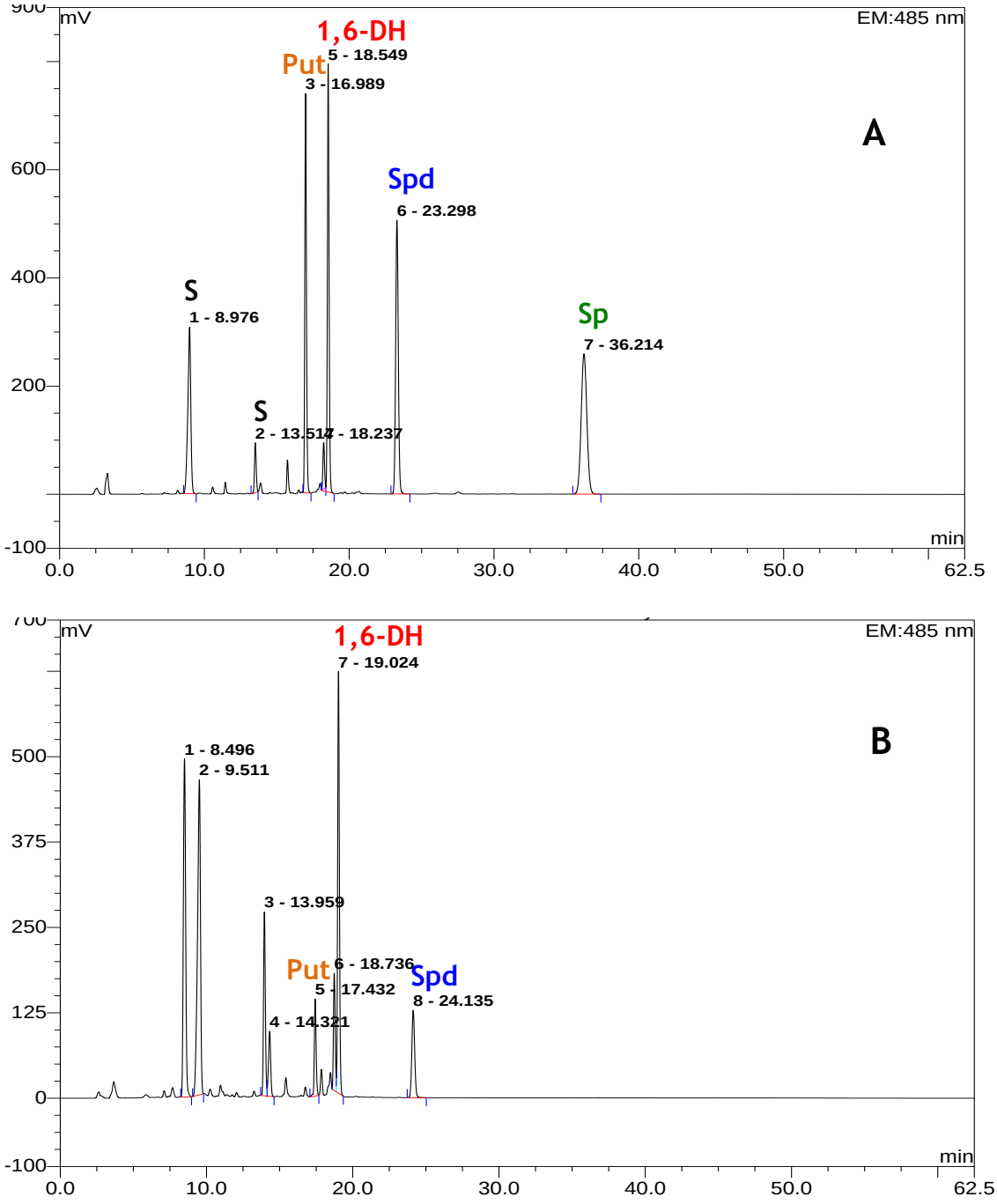

Figure 4.21 - Analysis of the homologous peaks between the standard and the parasitic extract chromatogram.

Panel A – Standard chromatogram. (Put) 400 pmol putrescine; (1,6-HD) 500 pmol 1,6-diaminohexane; (Spd) 400 pmol spermidine; (Sd) 400 pmol spermine; (S) solvent. Panel B – Parasitic extract of the Δ*cs* line. Putrescine (Put, orange); 1,6-diaminohexane (1,6-HD, red); spermidine (Spd, blue); spermine (Sd, green).

4.2.10 Summary

- Hamsters previously infected with *L. donovani* WT, Δ*cs* and RE lines were culled and parasites were recovered from the spleens and livers. None of the *L. donovani* RE were found to have infected the hamsters, while 2/6 animals infected with Δ*cs* contained parasites, suggesting that CS is not essential.

- Subsequent inspection revealed that the previously generated RE line did not re-express the full-length CS. Therefore a new RE line was generated in the Δ*cs* line isolated from hamsters. Thus I had a "full" set of WT, Δ*cs* and RE lines were able to be used for further analyses.

- Δ*cs* promastigotes had a growth defect. This line did not show susceptibility to external stressors.

- Analyses of relative gene expression of *cs* and *cbs* revealed that Δcs contained 22 times more *cbs* mRNA than WT.

- Re-expression of CS did reverse the effect on mRNA/protein levels observed in Δ*cs*.

- Thiol levels in WT, Δ*cs* and RE lines vary depending on their growth phase.

- The Δ*cs* line generally had reduced leves of thiols compared to WT.

- Inhibition of PLP-dependent enzymes (same as those involved in Cys biosynthesis or trans-sulphuration) showed a significant difference in

IC_{50} between WT and Δ*cs* lines. Surprisingly, Δ*cs* was less susceptible to inhibition by PAG than WT.

- Treatment with 250 μM PAG (~IC_{50}) thiols dropped dramatically in WT parasites with TSH being reduced by 70-90%.

- The synthesis of TSH requires spermidine. ODC, one of the rate-limiting steps of polyamine synthesis, is also PLP-dependent. Therefore its status was assessed. ODC mRNA levels showed a 7 fold increased in Δ*cs* compared to WT, while protein levels were drastically reduced as shown by the western blotting. This suggests that ODS mRNA translation is negatively affected in Δ*cs*.

- The lack of susceptibility (loss of sensitivity) against DFMO supports that Δ*cs* have an altered polyamine metabolism.

- Initial attempts were made to assess this hypothesis further by analyzing *L. donovani* polyamine levels.

Discussion

5 Discussion

Cysteine is the most important building block for the redox active low molecular weight thiols like glutathione, which is found almost ubiquitously, and trypanothione, which occurs in trypanosomatids (Oza *et al.*, 2005).

Most organisms rely on the supply of cysteine via the reverse transsulphuration pathway (see Figure 4.6) or on amino acid uptake (Nozaki *et al.*, 2001; Williams *et al.*, 2009). *Leishmania* have been shown to contain not only the reverse and forward transsulphuration pathways (Williams *et al.*, 2009) but also possess the cysteine *de novo* biosynthesis pathway. This provides them with at least two pathways to generate this important amino acid (Williams *et al.*, 2009). In addition, the parasites can take up cysteine from their environment, although the rate of transport determined is much lower than that found in another trypanosomatid *T. brucei* (Duszenko *et al.*, 1992), another trypanosomatid. These findings are in line with the lack of the cysteine *de novo* biosynthesis pathway in *T. brucei* (Duszenko *et al.*, 1992).

Given this unusual metabolic situation in *Leishmania*, it was postulated that in these organisms the *de novo* biosynthesis of cysteine in these organisms might have essential functions. In a number of other prokaryotes and eukaryotes such as *H. influenza, Mycobacterium tuberculosis, A. thaliana* and *S. cerevisiae,* the cysteine *de novo* biosynthesis pathway has been studied and found to offer potential for drug discovery (Huang *et al.*, 2005; Poyraz *et al.*, 2013; Schnell *et al.*, 2007; Thomas and Surdin-Kerjan, 1997).

The two key enzymes of the pathway are serine acetyltransferase (SAT) and cysteine synthase (CS). SAT and CS are known to form a complex that promotes SAT activity and inhibits CS activity (Berkowitz *et al.*, 2002; Francois *et al.*, 2006; Salsi *et al.*, 2010; Zhao *et al.*, 2006). Upon *O*-acetylserine (OAS) formation the complex dissociates releasing CS, which

then converts OAS to cysteine (Berkowitz *et al.*, 2002; Francois *et al.*, 2006; Salsi *et al.*, 2010; Zhao *et al.*, 2006). It was previously found that this interaction between the two enzymes also occurred between the *L. major* recombinant proteins (Williams *et al.*, 2009), this formed the basis of the hypothesis tested in this study that C-terminal peptides derived from the C-terminal amino acid sequences of a variety of SAT may have inhibitory activity on *Leishmania* CS.

To assess the essentiality of the sulphydrylation pathway and in particular CS for the survival of *L. donovani,* the gene encoding CS was knocked out by a previous member of the Müller lab and the parasites were used to inoculate hamsters with the aim to assess their virulence. Alongside *L. donovani* Δ*cs*, the re-expressing line and the wild type *L. donovani* were used to infect the animals. When I joined the lab, the hamsters had been infected about 6 months earlier and it was time to analyze their parasite load.

Overall, wild type *L. donovani* had successfully infected four out of six hamsters and the Δ*cs* line was found to have infected two out of six infected hamsters. Surprisingly, the re-expressing line had not infected any of the six hamsters. As outlined in chapter 4, the RE line was found not to express the full-length CS protein which could be one reason for the lack of the parasites to establish a successful infection in the animals. Another reason however could be that the episomal expression plasmid from which CS was expressed in the RE line was lost while in the animal – no selection for plasmid was carried out during the 6 months of incubation. However, the loss of CS re-expression should not have had a completely deleterious effect on parasite infectivity, given that the Δ*cs* line was able to successfully infect the hamsters (albeit at a lower efficiency than the wild type parasites, suggesting some reduction in virulence).

The results from the *in vivo* infectivity assays did not rule out that *L. donovani* CS has some importance in the infectivity and virulence of the

parasites in their mammalian host. In order to obtain a better understanding of the effect of the CS knockout on the physiology of *Leishmania* promastigotes, a number of assays were performed. First the thiol levels of wild type, Δ*cs* and RE were analyzed throughout their growth phases. The major thiol detected in all growth phases of *L. donovani* WT, Δ*cs* and RE (lag phase, logarithmic phase and stationary phase) was trypanothione followed by glutathione and cysteine. Other peaks were detected by the HPLC system used but their identity was not followed up. My data compared well with those previously published for *L. donovani* (Jiang et al. 1999), although Ariyanayagam and Fairlamb report much higher levels of trypanothione in stationary phase of *L. donovani* that are more similar to those that I determined during log phase of parasite growth (Ariyanayagam and Fairlamb, 2001). Thiol levels previously determined in other species of *Leishmania* showed some variability between *Leishamania* species and also between trypanosomdatid species (see Table 5.1).

Compared to the WT, the Δ*cs* line had a lower level of total thiols. This was most obvious during the early log phase of parasite growth. The RE line did not show this reduction of thiols during the log phase of growth suggesting that the decreased thiol levels in Δ*cs* is attributable to the loss of CS activity. In late log phase, the thiols in Δ*cs* appear to recover although they are still lower than those detected in WT and RE lines. The recovery of the thiol levels may be due to the activation of the reverse-transsulphuration pathway compensating for the loss of the sulphydrilation pathway, which was tested by analyzing the relative expression of CBS, the rate-limiting enzyme of the reverse-transsulphuration pathway. My results show a significant increase in *cbs* mRNA levels which translate to a ~3 fold increase in CBS protein levels in the Δ*cs* line, supporting the suggestion that CBS may compensate to some extent for the loss of CS activity. Also Williams *et al.* (2009) showed that *Lmj*CBS has *Lmj*CS activity and thus *Ld*CBS might in this case be replacing the activity of *Ld*CS.

			Thiol levels (nmol/10^8 cells)			
Specie	Life cycle stage	Growth stage	Cys	GSH	TSH	Reference
L. donovani [1]	Promastigotes	Log	0.8 ± 0.1	1.4 ± 0.2	4.2 ± 0.7	Section 4.2.6.1
L. donovani [1]	Promastigotes	Log	0.9 ± 0.1	1.7 ± 0.2	5.2 ± 0.4	Section 4.2.6.1
L. donovani [1]	Promastigotes	Late-log	0.5 ± 0.1	1.0 ± 2.2	1.8 ± 0.9	Section 4.2.6.1
L. donovani [1]	Promastigotes	Stationary	0.3 ± 0.0	0.7 ± 0.1	3.0 ± 0.4	Section 4.2.6.1
L. donovani [2]	Promastigotes	Late-log		2.15 ± 0.37	8.23 ± 1.08	(Jiang *et al.*, 1999)
L. donovani [3]	Promastigotes	Stationary		4.8 ± 1.0	6.3 ± 0.5	(Ariyanayagam and Fairlamb, 2001)
L. major [4]	Promastigotes	Late-log	1	2	6	(Williams *et al.*, 2009)
L. major [5]	Promastigotes	Stationary		0.6 ± 0.1	2.9 ± 0.9	(Ariyanayagam and Fairlamb, 2001)
L. tarentolae [6]	Promastigotes	Mid-log	0.13	0.09	0.1	(Mukhopadhyay *et al.*, 1996)
L. mexicana [7]	Promastigotes	Stationary		0.9 ± 0.1	3.5 ± 0.7	(Ariyanayagam and Fairlamb, 2001)
L. aethiopica [8]	Promastigotes	Stationary		0.7 ± 0.1	1.9 ± 0.2	(Ariyanayagam and Fairlamb, 2001)
L. tropica [9]	Promastigotes	Stationary		1.7 ± 0.3	1.5 ± 0.2	(Ariyanayagam and Fairlamb, 2001)
C. fasciculate [10]	Choanomastigote	Stationary		4.6 ± 0.5	7.8 ± 1.4	(Ariyanayagam and Fairlamb, 2001)
T. cruzi [11]	Epimastigote	Stationary		2.1 ± 0.2	6.4 ± 0.2	(Ariyanayagam and Fairlamb, 2001)
T. brucei [12]	Epimastigote	Stationary		2.1 ± 0.2	3.3 ± 0.5	(Ariyanayagam and Fairlamb, 2001)

Table 5.1 – Thiol levels in trypanosomatids.

The table shows the level of Cys, GSH and TSH in trypanosomatids in different stages of growth. Strain: (1) BPK206, (2) LV9 (MHOM/ET/67/HU3), (3) LV9 (MHOM/ET/67/HU3), (4) MHOM/IL/80/Fiedlin, (5) MHOM/SA/85/JISH118, (6) TarII WT, (7) MNYC/BZ/62/M379, (8) MHOM/ET/72/L100, (9) MHOM/SU/74/K27, (10) HS6, (12) MHOM/BR/78/Silvio, (12) S427 c118.

This work aimed to assess the essentiality of the cysteine synthase and its suitability as a putative drug target. *Leishmania* cysteine synthase can be inhibited and its inhibition should directly affect the synthesis of trypanothione, the main defense against xenobiotics and oxidants for these parasites.

The fact that the CS knockout had a negative effect on thiol levels in the Δ*cs* parasites, prompted me to test the effect of pro-oxidants and metal stressors on the parasite mutants in comparison to wild type *L. donovani*. The defense against oxidative and metal stress depends directly on the level of low-molecular thiols in *Leishmania* (Krauth-Siegel and Leroux, 2012). The WT, Δ*cs* and RE lines' susceptibilities to potassium arsenate and cadmium chloride were tested to assess the importance of CS in the mechanism of defense against these species.

Previous studies have shown that arsenite and antimonial resistance are both linked to overexpression of TSH, which results from the overexpression of γ-GCS (rate-limiting enzyme of GSH synthesis) and ODC (rate-limiting enzyme of polyamine synthesis). Together this leads to the overexpression of TSH, which forms conjugates with these species. As explained before, these conjugates are extruded from the parasites via efflux pumps (Haimeur *et al.*, 1999; Legare *et al.*, 2001; Mukhopadhyay *et al.*, 1996; Wyllie *et al.*, 2010). In the absence of CS the Δ*cs* line was more resistant to potassium arsenate. From the literature it would be expected that the Δ*cs* line would be more sensitive to potassium arsenate. The TSH-arsenite conjugate extrusion coupled with lower level of all thiols in this line should make this line more sensitive (Rai *et al.*, 2013). It is possible that the increased expression of the transsulphuration pathway may have compensatory effects particularly when stresses are applied to the parasites that explain this observation. To assess this, it would be interesting to analyze the level of *cbs* mRNA and CBS protein as well as the level of thiols in the presence of potassium arsenate.

Studies in plants have shown that cadmium stress is associated with increase of CS activity and expression of the serine acetyltransferase gene family (Fediuc *et al.*, 2005; Howarth *et al.*, 2003; Kawashima *et al.*, 2004). In the absence of CS the ∆*cs* line is more sensitive to cadmium chloride and the RE line is more resistant than the WT line. This result is in good agreement with what was observed in the plants.

The detoxification of peroxides in trypanosomatids depends on trypanothione, trypanothione reductase and tryparedoxin. These reduce 2-Cys-peroxiredoxin-type tryparedoxin peroxidases (Figure 1.10) (Castro *et al.*, 2002a; Lin *et al.*, 2005; Wilkinson *et al.*, 2003). The detoxification of hydrogen peroxide, cumene hydroperoxide, and *tert*-butyl hydroperoxide was assessed in the WT, ∆*cs* and RE lines. The absence of cysteine synthase had no significant effect on the resistance towards hydrogen peroxide and cumene hydroperoxide. The ∆*cs* line was more resistant to *tert*-butyl hydroperoxide. The cases of resistance to this species reported in the literature are associated with overexpression of the mitochondrial 2-Cys-peroxiredoxin-type tryparedoxin peroxidases in *L. amazonensis* (Castro *et al.*, 2002b; Lin *et al.*, 2005). It is not known whether the absence of cysteine synthase results in increased levels of these peroxidases. Further studies need to be done.

As an inhibitor of PLP-dependent enzymes, it was postulated that propagylglycine (PAG) might have a more pronounced effect on ∆*cs* line than WT and RE *L. donovani*. Surprisingly, my data suggests that the ∆*cs* line is significantly more resistant to PAG than the WT line. This is somewhat surprising although (Williams *et al.*, 2009) have shown in his study that the *L. major* recombinant CS protein is not sensitive to inhibition by PAG supporting the interpretation that the loss of CS should not necessarily affect the susceptibility to the this inhibitor. When incubating WT, ∆*cs* and RE lines with PAG for 24 hours at increasing concentrations and subsequently measuring the thiol level of the treated parasites, it was obviously that PAG generally led to the reduction of thiols in all three parasite lines. The most

severe effect was found in the WT line where trypanothione levels were reduced by 89 % when the parasites were treated with 250 μM PAG. Similarly the GSH levels were greatly reduced in these parasites. There are a number of possible explanations for these findings – (1) the levels of glutathione and trypanothione are severely affected because the source of cysteine is limiting and (2) the synthesis of trypanothione is affected because the source of glutathione may be negatively affected by CS deletion. Another possible explanation for the severe reduction of trypanothione levels may also be that PAG not only affects the activity of reverse transsulphuration and sulphydrylation pathways, but also inhibits ornithine decarboxylase (ODC, another PLP-dependent enzyme) therefore disturbing the supply of the polyamine spermidine, necessary for trypanothione biosynthesis (see Figure 4.6) in the parasites.

ODC is one of the rate-limiting enzymes for polyamine biosynthesis and is responsible for the conversion of ornithine into putrescine (Boitz *et al.*, 2009). ODC is inhibited by difluoromethylornithine (DFMO), an irreversible suicide inhibitor of this enzyme (Coons *et al.*, 1990; Kaur *et al.*, 1986; Poulin *et al.*, 1992). This drug has proven very effective against *T. b. gambiense* (Fairlamb *et al.*, 1987). This is primarily because the turnover of the ODC protein in Trypanosomatids is relatively slow which allows the irreversible inhibitor to exert its effects leading to a reduction in polyamines and consequently trypanothione levels. These alterations eventually affect the ability of the parasites to multiply and they differentiate into forms that no longer change their variant surface glycoprotein so that the human immune system can remove them. In addition, the parasites are unable to recover from the loss of ODC through polyamine uptake and without polyamines the level of trypanothione lowers leaving their antioxidant capability seriously compromised (Hanson *et al.*, 1992; Hasne and Ullman, 2005). DFMO in *Trypanosoma* forms a Schiff base with the PLP of one of ODC's monomers and forms a covalent bond to the Cys of the other monomer. This induces a 145° rotation of the Cys residue towards the active site (Grishin *et al.*, 1999). *Leishmania* has the ability of taking up polyamines from the media

and this is believed to be what makes this inhibitor not a suitable drug against these parasites. It does however affect cell growth in the absence of polyamines in the culture medium (Basselin *et al.*, 2000; Burchmore and Barrett, 2001). When assessing whether the levels of ODC are in anyway affected in the *L. donovani* ∆*cs* lines, I performed RT-PCR and discovered that ODC mRNA levels are greatly increased in the mutant parasites. However, this does not translate into the over-expression of the protein but the western blot analyses of ∆*cs* shows that the ODC protein is virtually absent from these parasites. It is not unusual to see this incongruence in trypanosomatids. The mRNA in trypanosomatids is transcribed as polycistronic units and it is not regulated at the level of transcription initiation. The gene expression is thus regulated post-transcriptionally through changes in message stability, protein stability or through translational regulation (Martinez-Calvillo *et al.*, 2010; Willert and Phillips, 2008). Despite this very low level of ODC protein, the mutant parasites must contain sufficient ODC to generate spermidine for the synthesis of their trypanothione that I detected albeit this synthesis may operate at reduced levels.

Protein extraction is usually carried at around day 5 when the cells are at the right density. The TSH levels on this day are about 4 nmol/10^8 cells. However on day 4 all the thiols are low (not only TSH) so this should not only be a result of low ODC, but also low cysteine synthesis. As outlined above, it is intriguing how Δ*cs* is able to survive on such a low levels of ODC, however it is known that this absence can be circumvented by polyamine uptake from the media (Jiang *et al.*, 1999). (Jiang *et al.*, 1999) have shown that Δ*odc* mutants are polyamine auxotrophs. The Δ*odc* mutants were able to take up putrescine from the medium and restore the polyamines pools, whereas spermidine by itself was not able to restore putrescine lavels. This is an indication of the absence of polyamine catabolism pathway in these parasites (Jiang *et al.*, 1999). However, the levels of conjugated spermidine and TSH were reduced with an accumulation of GSH. Interestingly this is not what I observe – the GSH levels are not accumulated in the Δ*cs* line, which

may well be a result of the loss of CS biosynthesis. In this situation *L. donovani* may be challenged as GSH may have roles in maintenance of redox homeostasis that do not allow its complete depletion for the cells. In order to achieve this it is possible that spermidine biosynthesis is reduced and that trypanothione degradation is increased in an effort to maintain redox homeostasis and spermidine provision for instance DNA stabilization. These are clearly speculations that need to be tested in future studies. To further assess my data I performed DFMO inhibiton studies on WT, Δ*cs* and RE lines. The *L. donovani* DFMO IC_{50} values vary between 30 and 125 μM (Basselin *et al.*, 1997; Coons *et al.*, 1990; Kaur *et al.*, 1986; Mukhopadhyay *et al.*, 1996).

The DFMO IC_{50} values for the WT and RE determined here are 48 and 45 μM, respectively. The Δ*cs* line appeared entirely resistant to DFMO, even at concentrations as high as 10 mM DFMO no inhibition of parasite growth was observed. One reason for this observation may be that there is a great reduction of ODC activity present in these parasites already - presumably they rely heavily on polyamine uptake to allow their survival. This however, was not tested in this study and is something to investigate in future work.

To assess whether the absence of ODC is affecting the polyamine levels in the Δ*cs* line, the level of polyamines should be determined. Unfortunately due to time constraints it was not possible to complete this part of my study. The preliminary data suggests however that the Δ*cs* line has lower polyamine levels than the WT line. The data are in general agreement with those previously determined in *L. donovani* and it would certainly be worth following these analyses up in future studies. Low levels of polyamines are linked with growth arrest of *L. donovani* parasites. Should the mutant line have lower levels of polyamines, this could certainly explain the growth defect observed.

Recombinant *L. major* cysteine synthase enzymes carrying N-terminal or C-terminal His-tags were expressed in *E. coli* and purified via Ni-agarose ion-affinity chromatography. The C-terminally His-tagged *Lmj*CS was previously

studied in detail by (Williams *et al.*, 2009) and it was readily available in the lab. A second *Lmj*CS construct with a cleavable N-terminal His-tag was generated and recombinantly expressed in order to assess the influence of the tag on the kinetic profile of the resulting recombinant protein and to utilize the non-tagged protein for crystallization trials.

The three *Lmj*CS enzymes (N-terminally His-tagged, C-terminally His-tagged and non-tagged CS) were generated in mg amounts and their kinetic parameters were analyzed.

The results show that the K_m values for OAS of the three *Lmj*CS enzymes are in the same range - 4 mM. The His-tag clearly did not affect the affinity of CS to one of its substrates. However, the turnover of the substrate by the enzyme is affected by the His-tag and I found that the V_{max} of N-terminally tagged r*Lmj*CS is double that of untagged r*Lmj*CS and C-terminally tagged r*Lmj*CS.

Table 5.2 shows the kinetic parameters of a variety of CS enzymes of other species in comparison with the data obtained in this study. If not mentioned, the biochemical assay used to determine these parameters was the one described by (Kredich and Tomkins, 1966). The enzymes characterized *T. vaginalis* and *A. pernix* have very high K_m values for OAS (39.6 and 28 mM, respectively). This is due to the fact that these organisms do not use OAS as a substrate for CS but their preferred substrate OPS which has a much more favorable K_m value of ~30 mM.

L. donovani (Raj *et al.*, 2012), *S. typhimurium* (Tai *et al.*, 1993) and *L. major* (Williams *et al.*, 2009) have been reported to have K_m values in the range of 15-18.2 mM, which is about four times higher than the K_m values that I determined for the three enzymes tested here. Often these variations can be attributed to different operators and emphasizes that the comparison of kinetic parameters showing only small variations may simply be within the experiential error rather than being physiologically and

biologically meaningful. A good example is the *S. typhimurium* where the K_m is five times higher in Becker *et al.* (1969) than in Tai *et al.* (1993). The calculated V_{max} (3,300 μmol/min/mg) based on the data provided in the `Williams *et al.* (2009) work, is three times higher than the highest V_{max} determined in this work (N-r*Lmj*CS – 1,192 μmol/min/mg), and the turnover number (2,047 sec^{-1}) is 2.5 times higher than the N-r*Lmj*CS's (751 sec^{-1}). The efficiency of the enzyme is not however affected as both have the same order of magnitude (~10^5 $M^{-1}sec^{-1}$).

Low K_m shows the specificity of the enzyme towards the substrate. The three *A. thaliana* CS enzymes have relatively low K_m values of ~0.5 mM.
The finding that the His-Tag (whether N- or C-terminal) has little if any effect on CS affinity to its substrate but may marginally affect catalytic efficiency of the enzyme. This is also in agreement with kinetic analyses reported for *At*CS enzymes.

Overall this study shows that the His-tag is not affecting the kinetics of the *Lmj*CS. Either recombinant His-tagged enzyme can be used in biochemical assays to characterize the native non-tagged *Lmj*CS without the need of extra His-tag digest and purification steps.

Species	His-tag	V_{max} (μmol/min/mg)	K_m (mM)	K_{cat} (sec^{-1})	K_{cat}/K_m ($M^{-1}sec^{-1}$)	Reference
L. major	N-terminal	1,192 ± 58	4 ± 0.3	751	$1.9x10^5$	Section 3.6.2
L. major	C-terminal	696 ± 24	4 ± 0.2	438	$1.1x10^5$	Section 3.6.2
L. major	-	630 ± 28	4 ± 0.3	373	$9.3x10^4$	Section 3.6.2
L. major	C-terminal	3,300[§]	17.5 ± 4.8	2,047	$1.2x10^5$	(Williams *et al.*, 2009)
*L. donovani**	C-terminal		18.2 ± 0.2			(Raj *et al.*, 2012)
A. thaliana (type A)[¶]	-	906 ± 39	0.7 ± 0.1			(Wirtz *et al.*, 2004)
A. thaliana (type B)[¶]	-	592 ± 8	0.3 ± 0.02			(Wirtz *et al.*, 2004)
A. thaliana (type C)[¶]	-	534 ± 9	0.4 ± 0.02			(Wirtz *et al.*, 2004)
A. thaliana[#]	C-terminal		1.4 ± 0.2	1,780 ± 280	$1.3x10^6$	(Bonner *et al.*, 2005)
S. oleacea (type A)[#]	-		1.33			(Warrilow and Hawkesford, 2002)
S. oleacea (type B)[#]	-		1.16			(Warrilow and Hawkesford, 2002)
A. pernix[#]			28	202		(Mino and Ishikawa, 2003)
T. vaginalis	C-terminal		39.5	153 ± 44		(Westrop *et al.*, 2006)
S. typhimyrium	-		5 1.0 ± 0.6			(Becker *et al.*, 1969) (Tai *et al.*, 1993)
*S. typhimurium**	-		15 ± 3			(Tai *et al.*, 1993)
E. coli			4.8	2,030		(Mino *et al.*, 2000b)
Spinach chloroplast			1.3			(Droux *et al.*, 1992)
Thermus thermophilus			4.8	493		(Mizuno *et al.*, 2002)

Table 5.2 – Kinetic characterization of the CS enzymes in difference species.

This table compares the CS enzymes in terms of maximum velocicy (V_{max}, μmol/min/mg), Michaelis-Menten constant (K_m, mM), turnover number (K_{cat}, sec^{-1}), and catalytic efficiency (K_{cat}/K_m, $M^{-1}sec^{-1}$). *Using 5-thio-2-nitrobenzoate (TNB, 412 nm) as an alternative substrate to sulphide. [§] Calculated. [¶] Reverse-phase HPLC. [#] Acid-ninhydrin reagent (546 nm).

As mentioned before, CS and SAT form a bimolecular complex where the C-terminus of SAT interacts directly with the active site of CS and leads to its inhibition (Berkowitz *et al.*, 2002; Raj *et al.*, 2012; Wirtz and Hell, 2006; Zhao *et al.*, 2006). Detailed analyses of the plant and also bacterial enzymes showed that the last 10 amino acids of *Mt*SAT and *At*SAT are sufficient to lead to CS inhibition and analyses of *Ec*SAT with *Ec*CS showed that the carboxyl group of the final Ile of the protein occupies the same position in CS as the carboxyl group of the aminoacrylate intermediate that is generated during the catalytic cycle of CS. Therefore it can be presumed that the C-terminal Ile of SAT blocks the CS active site and hinders PLP from binding to active site Lys residue (Francois *et al.*, 2006; Mino *et al.*, 2000a; Schnell *et al.*, 2007).

The non-tagged recombinant *Lmj*CS was used for crystallization trials resulting in the generation of crystals of the parasite protein. One important aspect of the analyses of these crystals was that polyglutamate (PGA) was found to have bound to the active site of *Lmj*CS while PLP was missing from the structure (Fyfe *et al.*, 2012). It was hypothesized that perhaps PGA may be an inhibitor for the CS activity in a similar way to small peptides. Therefore not only C-terminal peptides of SAT but also the PAG enantiomers were tested for their inhibitory activity towards *Lmj*CS. The results show that D-γEγEγEγE inhibited 20% of C-r*Lmj*CS's activity however it was non-concentration dependent. Five times increase in the inhibitor concentration should result in an increased inhibition which was not the case. Therefore this inhibition was considered negligible and may be due to variations in the assays performed. The PGA also failed to inhibit N-r*Lmj*CS and r*Lmj*CS. Overall it was therefore concluded that PGA does not inhibit *Lmj*CS and its presence in the active site might result from its high concentration in the crystallization buffer. Additionally this impeded co-crystallization studies with SAT C-terminal based peptides (Fyfe *et al.*, 2012).

Other peptides that were tested for their inhibitory effect on *Lmj*CS were the *A. thaliana* SAT C-terminal peptide DYVI and the *Leishmania* SAT C-

terminal peptide GDGSGI. Surprisingly, DYVI at 0.1 mM inhibited ~90% of *Lmj*CS in contract with only ~40% inhibition by EGDGSGI when used at the same concentration. The same is observed in *E. histolytica* where *Eh*SAT peptide SPSI inhibits 30% of *Eh*CS in contrast with DFSI peptide (*Mt*SAT C-terminal) that inhibits 50% of activity of *Eh*CS (Table 5.3) (Kumar *et al.*, 2011). A whole variety of peptides were tested against various CS proteins from different sources (summarised in Table 5.3). Clearly the length and the type of amino acid composition of these peptides affected their inhibitory efficiency and it becomes clear that cross-species inhibition seems to be a common theme (Fyfe *et al.*, 2012; Raj *et al.*, 2012; Wang and Leyh, 2012) (Table 5.3).

Salsi *et al.* (2010) demonstrated through a docking study the importance of the terminal Ile and the second and third last amino acids of the peptide. Replacing the third last amino acid of *Mt*SAT from phenylalanine to tryptophan (DWSI), both with large side chains, increased the inhibitory effect of the peptide from 50% to 54%. When phenylalanine was replaced by tyrosine (DYSI), also with a large side chain, the inhibitory effect was unchanged. On the other hand, when the second and third last amino acids were replaced by amino acids with small side chains (DPTI and DTTI), the ability to inhibit *Eh*CS decreased significantly (42.17% and 29.96% respectively) (Kumar *et al.*, 2011). The same is observed in *L. donovani* where peptides with large side chains (DFSI, DYSI and DWSI) inhibit ~50% of *Ld*CS in contrast with peptides with small side chains (DPTI and DTTI) that inhibit ~40% (Raj *et al.*, 2012). The authors have also demonstrated that larger side chains result in tighter interactions using binding dissociation studies. This clearly shows the potential of these peptides as future lead compounds to generate inhibitors acting against CS proteins.

Wang *et al.* (2012) demonstrated that the *E. coli* CS-SAT complex passes through a pre-steady state phase before reaching the final conformation. This pre-steady state conformation is similar to the one observed when a 10 amino acid peptide based on C-terminus of *Ec*SAT is used instead of the full

length *Ec*SAT (Wang and Leyh, 2012). This suggests that more than the last 4 or 5 amino acids of SAT are required to allow the full interaction of SAT with the CS active site; suggesting that longer peptides need to be considered and that their composition acquired by using peptide scans would be useful to dissect the required interactions (Wang and Leyh, 2012). For instance it was shown that *Lmj*CS is more sensitive to the 7 amino acids of *Lmj*SAT (EDGGSGI) than the last 4 amino acids (GSGI) (Fyfe *et al.*, 2012). The inhibition of *Ld*CS by the last 8 amino acids of *Ld*SAT (LERDGSGI), and *Lmj*CS by the last 7 amino acids of *Lmj*SAT (EGDGSGI) was comparable (48.8% and 40% respectively) (Fyfe *et al.*, 2012; Raj *et al.*, 2012). Additionally, Ile alone, although having a major role in the binding to the active site and impeding the formation of the aminoacrylate intermediate during the catalysis of CS, was not able to inhibit *Lmj*CS at a concentration of 4 mM (Fyfe *et al.*, 2012). This with the previous information highlights the role of all the interactions made by amino acids in preceding positions in the inhibition of CS.

The potential of these peptides has been proven to be immense and thus there is a need to develop non-toxic high-throughput screening biochemical assay that would allow the screening of several peptides in a 96-well plate. The present study demonstrates the potential of CPM as a detection method that allows high-throughput screening of small peptide inhibitors and also potential other chemical libraries against CS. One of the first challenges faced when testing this component was the background that is generated by the internal fluorescent of CPM and some of the essential components used in the enzyme assay. Na_2S had the most pronounced effect on fluorescent background generation, as did BSA. The thiol groups of the cysteines present in the BSA protein can form complexes with CPM generating high background, when BSA was used as protein stabilizer. Replacing BSA with gelatin significantly reduced this background. It was also not surprising that Na_2S caused background reaction with CPM given that the equilibrium between Na_2S <-> NaS^- <-> S^{2-} at pH 7-8 promotes complex formation of the ionized Na_2S with CPM generating fluorescence background. Lowering the pH

to 6.5 did not decrease the background (Wirtz *et al.*, 2004). The signal to noise ratio did not improve by lowering the CPM concentration from 100 μg/mol to 25 μg/mol and variation in the fluorescence was observed when CPM was stored. With the assay optimised, cysteine synthesis was successfully detected using CPM in a 96-well plate. Further, 94% *Lmj*CS activity inhibition was detected by the system. The *At*SAT based peptide (DYVI) IC_{50} was determined (2 μM), which is 3.5 times lower than the DYVI IC_{50} determine using the mercury-chloride assay (7 μM, Table 5.2) (Fyfe *et al.*, 2012).

Overall the CPM detection assay is a significantly less toxic assay system when compared with the mercury chloride assay. Far fewer steps and reagents allow a much swifter assay performance and the fact that it is amenable to reduced volumes such as microtitre plate volumes, makes it an attractive alternative to the conventional mercury chloride assay system. An improved assay system is not only an interesting development for the assessment of *Leishmania* CS activity but also for the testing of CS proteins from other sources i.e. plants and other microorganisms where the inhibition of this crucial enzyme may have a more pronounced effect than in *Leishmania*.

CS Specie	C-terminal SAT (Specie)	IC_{50}	K_i	% Inhibition	Reference
L. major	DYVI (*A. thaliana*)			~90	Section 3.7
L. major	EGDGSGI (*L. major*)			~40	Section 3.7
L. major	GSGI (*L. major*)	1.5 mM			(Fyfe *et al.*, 2012)
L. major	EGDGSGI (*L. major*)	270 μM			(Fyfe *et al.*, 2012)
L. major	DYVI (*A. thaliana*)	7 μM	4 μM		(Fyfe *et al.*, 2012)
L. major	I	> 4 mM			(Fyfe *et al.*, 2012)
L. major	N-blocked derivatives	250 μM			(Fyfe *et al.*, 2012)
L. donovani	DPTI			45.7 ± 3	(Raj *et al.*, 2012)
L. donovani	DTTI			37.3 ± 2	(Raj *et al.*, 2012)
L. donovani	DFSI (large side chains)			48.8 ± 2	(Raj *et al.*, 2012)
L. donovani	DYSI (large side chains)			52.9 ± 2	(Raj *et al.*, 2012)
L. donovani	DWSI (large side chains)			54.6 ± 1	(Raj *et al.*, 2012)
L. donovani	LERDGSGI (*L. donovani*)			48.8 ± 4	(Raj *et al.*, 2012)
H. influenza	GIDDGMNLNI (*E.coli*)	130 nM			(Huang *et al.*, 2005)
M. tuberculosis	DFSI (*M. tuberculosis*)		5 μM		(Schnell *et al.*, 2007)
E. histolytica	SPSI (derived from *Eh*SAT)			30.19 ± 1.6	(Kumar *et al.*, 2011)
E. histolytica	DFSI (*M. tuberculosis*)			50.41 ± 0.7	(Kumar *et al.*, 2011)
E. histolytica	DPTI			42.17 ± 5.7	(Kumar *et al.*, 2011)
E. histolytica	DTTI			29.96 ± 4.0	(Kumar *et al.*, 2011)
E. histolytica	DYSI (large side chains)			52.17 ± 0.9	(Kumar *et al.*, 2011)
E. histolytica	DWSI (large side chains)			54.64 ± 2.8	(Kumar *et al.*, 2011)

Table 5.3 – Analyses of the C-terminal of SAT as model for putative CS inhibitors.

This study is based on the cysteine synthase complex formation that results on the inhibition of cysteine synthase activity. The table presents the inhibition data collected from studies done in different species using SAT C-terminal as a base to design small peptide inhibitor of CS.

Conclusion and Future Work

6 Conclusion and Future work

There is certainly a need for finding new drug targets in *Leishmania* as more cases of resistance arise and people are left with drugs that cause serious toxic side effects. The present work has highlighted that the parasite's thiol metabolism in particular the generation of cysteine may be an exploitable way of interfering with the parasite's viability and virulence. However CS itself may not present the ideal drug target as its removal from the parasites had only led to the reduction of mammalian infectivity. This clearly means that the parasites equipped to compensate the lack of sulphydrylation pathway potentially by resorting to the reverse trans-sulphuration pathway. This was particularly seen in the exposure to pro-oxidants and metal stressors, where the Δ*cs* line did not show sensitivity to any stressors. Another good indication of this is the over-expression of CBS mRNA and protein. A double knockout would certainly help to test this hypothesis. From the thiol measurements it appears that the reverse trans-sulphuration pathway might not be sufficient to maintain the thiol levels throughout the growth phases of promastigotes. Perhaps this has an effect on associated pathways such as the polyamine biosynthesis pathway as shown by the down-regulation of ODC. Low level of GSH resultant from low levels of cysteine, would possibly lead to an accumulation of spermidine in the cell. Also if no cysteine is converted into methionine by the forward trans-sulphuration pathway also operating in the parasites, the decarboxylated S-adenosylmethionine will be possibly lacking for the polyamine biosynthesis. Although (Williams *et al.*, 2009) has shown that *L. major* can uptake methionine from the medium and increase the thiol pool by RTS pathway the methionine levels may be limiting in the culture conditions and it should be tested whether an increase in external methionine (or in fact its withdrawal) affects parasite thiol and polyamine pools as well as their survival.

Because this study was carried in promastigotes it is not known whether the two pathways generating cysteine are operating in all parasite stages. It is essential that the pathway to be impaired by a putative drug would also affect the amastigote stage. Despite the fact that the *in vivo* experiments

suggest that the CS mutants are infective to the vertebrate host it would still be informative to assess this infectivity using macrophage infections *in vitro*.

The CS can be inhibited by small molecule peptides. The promising results from the CPM assay shows that high-throughput screening of small peptide inhibitors is possible with low toxicity. It would be interesting to develop an inhibitor of PLP-dependent enzymes that would have affinity for both CS and CBS enzymes. This study together with (Williams *et al.*, 2009), shows how regulated the cysteine biosynthetic pathway is in these parasites, which is a strong indication of its essentiality.

References

Agren, D., Schnell, R., Oehlmann, W., Singh, M., and Schneider, G. (2008). Cysteine synthase (CysM) of *Mycobacterium tuberculosis* is an *O*-phosphoserine sulfhydrylase: evidence for an alternative cysteine biosynthesis pathway in mycobacteria. J Biol Chem *283*, 31567-31574.

Agren, D., Schnell, R., and Schneider, G. (2009). The C-terminal of CysM from *Mycobacterium tuberculosis* protects the aminoacrylate intermediate and is involved in sulphur donor selectivity. FEBS Lett *583*, 330-336.

Alphey, M.S., Williams, R.A., Mottram, J.C., Coombs, G.H., and Hunter, W.N. (2003). The crystal structure of *Leishmania major* 3-mercaptopyruvate sulfurtransferase. A three-domain architecture with a serine protease-like triad at the active site. J Biol Chem *278*, 48219-48227.

Ariyanayagam, M.R., and Fairlamb, A.H. (2001). Ovothiol and trypanothione as antioxidants in trypanosomatids. Mol Biochem Parasitol *115*, 189-198.

Ariyanayagam, M.R., Oza, S.L., Guther, M.L., and Fairlamb, A.H. (2005). Phenotypic analysis of trypanothione synthetase knockdown in the African trypanosome. Biochem J *391*, 425-432.

Ashutosh, Sundar, S., and Goyal, N. (2007). Molecular mechanisms of antimony resistance in *Leishmania*. J Med Microbiol *56*, 143-153.

Bachrach, U., Don, S., and Wiener, H. (1973). Polyamines and tumor cells: effect of transformation of chick embryo fibroblasts by Rous sarcoma virus on polyamine levels. Biochem Biophys Res Commun *55*, 1035-1041.

Banerjee, R., and Zou, C.G. (2005). Redox regulation and reaction mechanism of human cystathionine-beta-synthase: a PLP-dependent hemesensor protein. Arch Biochem Biophys *433*, 144-156.

Basselin, M., Badet-Denisot, M.A., Lawrence, F., and Robert-Gero, M. (1997). Effects of pentamidine on polyamine level and biosynthesis in wild-type, pentamidine-treated, and pentamidine-resistant *Leishmania*. Exp Parasitol *85*, 274-282.

Basselin, M., Coombs, G.H., and Barrett, M.P. (2000). Putrescine and spermidine transport in *Leishmania*. Mol Biochem Parasitol *109*, 37-46.

Basselin, M., Lawrence, F., and Robert-Gero, M. (1996). Pentamidine uptake in *Leishmania donovani* and *Leishmania amazonensis* promastigotes and axenic amastigotes. Biochem J *315 (Pt 2)*, 631-634.

Basu, M.K., and Ray, M. (2005). Macrophage and *Leishmania*: an unacceptable coexistence. Crit Rev Microbiol *31*, 145-154.

Becker, M.A., Kredich, N.M., and Tomkins, G.M. (1969). The purification and characterization of *O*-acetylserine sulfhydrylase-A from *Salmonella typhimurium*. J Biol Chem *244*, 2418-2427.

Ben Salah, A., Buffet, P.A., Morizot, G., Ben Massoud, N., Zaatour, A., Ben Alaya, N., Haj Hamida, N.B., El Ahmadi, Z., Downs, M.T., Smith, P.L., *et al*. (2009). WR279,396, a third generation aminoglycoside ointment for the treatment of Leishmania major cutaneous leishmaniasis: a phase 2, randomized, double blind, placebo controlled study. PLoS Negl Trop Dis *3*, e432.

Berkowitz, O., Wirtz, M., Wolf, A., Kuhlmann, J., and Hell, R. (2002). Use of biomolecular interaction analysis to elucidate the regulatory mechanism of the cysteine synthase complex from *Arabidopsis thaliana*. J Biol Chem *277*, 30629-30634.

Besteiro, S., Williams, R.A., Coombs, G.H., and Mottram, J.C. (2007). Protein turnover and differentiation in *Leishmania*. Int J Parasitol *37*, 1063-1075.

Birke, H., Haas, F.H., De Kok, L.J., Balk, J., Wirtz, M., and Hell, R. (2012). Cysteine biosynthesis, in concert with a novel mechanism, contributes to sulphide detoxification in mitochondria of *Arabidopsis thaliana*. Biochem J *445*, 275-283.

Birkholtz, L.M., Williams, M., Niemand, J., Louw, A.I., Persson, L., and Heby, O. (2011). Polyamine homoeostasis as a drug target in pathogenic protozoa: peculiarities and possibilities. Biochem J *438*, 229-244.

Bogdanova, N., and Hell, R. (1997). Cysteine synthesis in plants: protein-protein interactions of serine acetyltransferase from *Arabidopsis thaliana*. Plant J *11*, 251-262.

Boitz, J.M., Yates, P.A., Kline, C., Gaur, U., Wilson, M.E., Ullman, B., and Roberts, S.C. (2009). *Leishmania donovani* ornithine decarboxylase is indispensable for parasite survival in the mammalian host. Infect Immun *77*, 756-763.

Bonner, E.R., Cahoon, R.E., Knapke, S.M., and Jez, J.M. (2005). Molecular Basis of Cysteine Biosynthesis in Plants: structural and functional analysis of o-acetylserine sulfhydrylase from *Arabidopsis thaliana*. Journal of Biological Chemistry *280*, 38803-38813.

Bradford, M.M. (1976). A rapid and sensitive method for the quantitation of microgram quantities of protein utilizing the principle of protein-dye binding. Anal Biochem *72*, 248-254.

Braunstein, A.E., Goryachenkova, E.V., Tolosa, E.A., Willhardt, I.H., and Yefremova, L.L. (1971). Specificity and some other properties of liver serine sulphhydrase: evidence for its identity with cystathionine β-synthase. Biochim Biophys Acta *242*, 247-260.

Bray, P.G., Barrett, M.P., Ward, S.A., and de Koning, H.P. (2003). Pentamidine uptake and resistance in pathogenic protozoa: past, present and future. Trends Parasitol *19*, 232-239.

Burchmore, R.J., and Barrett, M.P. (2001). Life in vacuoles-nutrient acquisition by *Leishmania* amastigotes. Int J Parasitol *31*, 1311-1320.

Cao, L., Waldon, D., Teffera, Y., Roberts, J., Wells, M., Langley, M., and Zhao, Z. (2013). Ratios of biliary glutathione disulphide (GSSG) to glutathione (GSH): a potential index to screen drug-induced hepatic oxidative stress in rats and mice. Anal Bioanal Chem *405*, 2635-2642.

Carter, K.C., Sundar, S., Spickett, C., Pereira, O.C., and Mullen, A.B. (2003). The in vivo susceptibility of *Leishmania donovani* to sodium stibogluconate is drug specific and can be reversed by inhibiting glutathione biosynthesis. Antimicrob Agents Chemother *47*, 1529-1535.

Castro, H., Budde, H., Flohe, L., Hofmann, B., Lunsdorf, H., Wissing, J., and Tomas, A.M. (2002a). Specificity and kinetics of a mitochondrial peroxiredoxin of *Leishmania infantum*. Free Radic Biol Med *33*, 1563-1574.

Castro, H., Sousa, C., Santos, M., Cordeiro-da-Silva, A., Flohe, L., and Tomas, A.M. (2002b). Complementary antioxidant defense by cytoplasmic and mitochondrial peroxiredoxins in *Leishmania infantum*. Free Radic Biol Med *33*, 1552-1562.

CDC. Centers for Disease Control and Prevention - Leishmaniasis, Center for Disease Control and Prevention.

Chibale, K., Visser, M., Yardley, V., Croft, S.L., and Fairlamb, A.H. (2000). Synthesis and evaluation of 9,9-dimethylxanthene tricyclics against trypanothione reductase, *Trypanosoma brucei*, *Trypanosoma cruzi* and *Leishmania donovani*. Bioorg Med Chem Lett *10*, 1147-1150.

Chung, C., Ohwaki, K., Schneeweis, J., Stec, E., Varnerin, J., Goudreau, P., Chang, A., Cassaday, J., Yang, L., Yamakawa, T., *et al.* (2008). A fluorescence-based thiol quantification assay for ultra-high-throughput

screening for inhibitors of coenzyme A production. Assay and Drug Development Technologies *6*.

Coelho, A.C., Messier, N., Ouellette, M., and Cotrim, P.C. (2007). Role of the ABC transporter PRP1 (ABCC7) in pentamidine resistance in *Leishmania amastigotes*. Antimicrob Agents Chemother *51*, 3030-3032.

Comini, M.A., Krauth-Siegel, R.L., and Flohe, L. (2007). Depletion of the thioredoxin homologue tryparedoxin impairs antioxidative defence in African trypanosomes. Biochem J *402*, 43-49.

Coombs, G.H., Hart, D.T., and Capaldo, J. (1983). *Leishmania mexicana*: drug sensitivities of promastigotes and transforming amastigotes. J Antimicrob Chemother *11*, 151-162.

Coombs, G.H., Westrop, G.D., Suchan, P., Puzova, G., Hirt, R.P., Embley, T.M., Mottram, J.C., and Muller, S. (2004). The amitochondriate eukaryote *Trichomonas vaginalis* contains a divergent thioredoxin-linked peroxiredoxin antioxidant system. J Biol Chem *279*, 5249-5256.

Coons, T., Hanson, S., Bitonti, A.J., McCann, P.P., and Ullman, B. (1990). Alpha-difluoromethylornithine resistance in *Leishmania donovani* is associated with increased ornithine decarboxylase activity. Mol Biochem Parasitol *39*, 77-89.

Cornish-Bowden, A. (2004). Fundamentals of Enzyme Kinetics (Portland Press).

Croft, S.L., and Coombs, G.H. (2003). Leishmaniasis - current chemotherapy and recent advances in the search for novel drugs. Trends Parasitol *19*, 502-508.

Croft, S.L., and Engel, J. (2006). Miltefosine - discovery of the antileishmanial activity of phospholipid derivatives. Trans R Soc Trop Med Hyg *100 Suppl 1*, S4-8.

Croft, S.L., and Olliaro, P. (2011). Leishmaniasis chemotherapy - challenges and opportunities. Clin Microbiol Infect *17*, 1478-1483.

Croft, S.L., Sundar, S., and Fairlamb, A.H. (2006). Drug resistance in leishmaniasis. Clin Microbiol Rev *19*, 111-126.

Croft, S.L., Yardley, V., and Kendrick, H. (2002). Drug sensitivity of *Leishmania species*: some unresolved problems. Trans R Soc Trop Med Hyg *96 Suppl 1*, S127-129.

Cunningham, M.L., and Fairlamb, A.H. (1995). Trypanothione reductase from *Leishmania donovani*. Purification, characterisation and inhibition by trivalent antimonials. Eur J Biochem *230*, 460-468.

Cunningham, M.L., Zvelebil, M.J., and Fairlamb, A.H. (1994). Mechanism of inhibition of trypanothione reductase and glutathione reductase by trivalent organic arsenicals. Eur J Biochem *221*, 285-295.

Das Gupta, R., Krause-Ihle, T., Bergmann, B., Muller, I.B., Khomutov, A.R., Muller, S., Walter, R.D., and Luersen, K. (2005). 3-Aminooxy-1-aminopropane and derivatives have an antiproliferative effect on cultured *Plasmodium falciparum* by decreasing intracellular polyamine concentrations. Antimicrob Agents Chemother *49*, 2857-2864.

Decuypere, S., Vanaerschot, M., Brunker, K., Imamura, H., Muller, S., Khanal, B., Rijal, S., Dujardin, J.C., and Coombs, G.H. (2012). Molecular mechanisms of drug resistance in natural *Leishmania* populations vary with genetic background. PLoS Negl Trop Dis *6*, e1514.

Droux, M., Martin, J., Sajus, P., and Douce, R. (1992). Purification and characterization of *O*-acetylserine (thiol) lyase from spinach chloroplasts. Arch Biochem Biophys *295*, 379-390.

Droux, M., Ruffet, M.L., Douce, R., and Job, D. (1998). Interactions between serine acetyltransferase and *O*-acetylserine (thiol) lyase in higher plants - structural and kinetic properties of the free and bound enzymes. Eur J Biochem *255*, 235-245.

Dumas, C., Ouellette, M., Tovar, J., Cunningham, M.L., Fairlamb, A.H., Tamar, S., Olivier, M., and Papadopoulou, B. (1997). Disruption of the trypanothione reductase gene of *Leishmania* decreases its ability to survive oxidative stress in macrophages. EMBO J *16*, 2590-2598.

Duszenko, M., Muhlstadt, K., and Broder, A. (1992). Cysteine is an essential growth factor for *Trypanosoma brucei* bloodstream forms. Mol Biochem Parasitol *50*, 269-273.

Escobar, P., Matu, S., Marques, C., and Croft, S.L. (2002). Sensitivities of *Leishmania* species to hexadecylphosphocholine (miltefosine), ET-18-OCH(3) (edelfosine) and amphotericin B. Acta Trop *81*, 151-157.

Fairlamb, A.H., Blackburn, P., Ulrich, P., Chait, B.T., and Cerami, A. (1985). Trypanothione: a novel bis(glutathionyl)spermidine cofactor for glutathione reductase in trypanosomatids. Science *227*, 1485-1487.

Fairlamb, A.H., and Cerami, A. (1985). Identification of a novel, thiol-containing co-factor essential for glutathione reductase enzyme activity in trypanosomatids. Mol Biochem Parasitol *14*, 187-198.

Fairlamb, A.H., and Cerami, A. (1992). Metabolism and functions of trypanothione in the Kinetoplastida. Annu Rev Microbiol *46*, 695-729.

Fairlamb, A.H., Henderson, G.B., Bacchi, C.J., and Cerami, A. (1987). In vivo effects of difluoromethylornithine on trypanothione and polyamine levels in bloodstream forms of *Trypanosoma brucei*. Mol Biochem Parasitol *24*, 185-191.

Faundez, M., Pino, L., Letelier, P., Ortiz, C., Lopez, R., Seguel, C., Ferreira, J., Pavani, M., Morello, A., and Maya, J.D. (2005). Buthionine sulfoximine increases the toxicity of nifurtimox and benznidazole to *Trypanosoma cruzi*. Antimicrob Agents Chemother *49*, 126-130.

Fediuc, E., Lips, S.H., and Erdei, L. (2005). O-acetylserine (thiol) lyase activity in Phragmites and Typha plants under cadmium and NaCl stress conditions and the involvement of ABA in the stress response. J Plant Physiol *162*, 865-872.

Flore, L.A., and Milunsky, J.M. (2012). Updates in the genetic evaluation of the child with global developmental delay or intellectual disability. Semin Pediatr Neurol *19*, 173-180.

Folcarelli, S., Venerini, F., Battistoni, A., O'Neill, P., Rotilio, G., and Desideri, A. (1999). Toward the Engineering of a Super Efficient Enzyme. Biochemical and Biophysical Research Communications *256*, 425-428.

Francois, J.A., Kumaran, S., and Jez, J.M. (2006). Structural Basis for Interaction of *O*-Acetylserine Sulfhydrylase and Serine Acetyltransferase in the *Arabidopsis* Cysteine Synthase Complex. The Plant Cell Online *18*, 3647-3655.

Frank, N., Kent, J.O., Meier, M., and Kraus, J.P. (2008). Purification and characterization of the wild type and truncated human cystathionine beta-synthase enzymes expressed in *E. coli*. Arch Biochem Biophys *470*, 64-72.

Fyfe, P.K., Westrop, G.D., Ramos, T., Muller, S., Coombs, G.H., and Hunter, W.N. (2012). Structure of *Leishmania major* cysteine synthase. Acta Crystallographica Section F *68*.

Gorman, J., and Shapiro, L. (2004). Structure of serine acetyltransferase from *Haemophilus influenzae* Rd. Acta Crystallogr D Biol Crystallogr *60*, 1600-1605.

Grishin, N.V., Osterman, A.L., Brooks, H.B., Phillips, M.A., and Goldsmith, E.J. (1999). X-ray structure of ornithine decarboxylase from *Trypanosoma brucei*: the native structure and the structure in complex with alpha-difluoromethylornithine. Biochemistry *38*, 15174-15184.

Haimeur, A., Guimond, C., Pilote, S., Mukhopadhyay, R., Rosen, B.P., Poulin, R., and Ouellette, M. (1999). Elevated levels of polyamines and trypanothione resulting from overexpression of the ornithine decarboxylase gene in arsenite-resistant *Leishmania*. Mol Microbiol *34*, 726-735.

Hanson, S., Adelman, J., and Ullman, B. (1992). Amplification and molecular cloning of the ornithine decarboxylase gene of *Leishmania donovani*. J Biol Chem *267*, 2350-2359.

Harhay, M.O., Olliaro, P.L., Costa, D.L., and Costa, C.H. (2011). Urban parasitology: visceral leishmaniasis in Brazil. Trends Parasitol *27*, 403-409.

Hasne, M.P., and Ullman, B. (2005). Identification and characterization of a polyamine permease from the protozoan parasite *Leishmania major*. J Biol Chem *280*, 15188-15194.

Haughan, P.A., Chance, M.L., and Goad, L.J. (1992). Synergism in vitro of lovastatin and miconazole as anti-leishmanial agents. Biochem Pharmacol *44*, 2199-2206.

Heeg, C., Kruse, C., Jost, R., Gutensohn, M., Ruppert, T., Wirtz, M., and Hell, R. (2008). Analysis of the *Arabidopsis O*-Acetylserine(thiol)lyase Gene Family Demonstrates Compartment-Specific Differences in the Regulation of Cysteine Synthesis. The Plant Cell Online *20*, 168-185.

Hell, R., Jost, R., Berkowitz, O., and Wirtz, M. (2002). Molecular and biochemical analysis of the enzymes of cysteine biosynthesis in the plant *Arabidopsis thaliana*. Amino Acids *22*, 245-257.

Howarth, J.R., Dominguez-Solis, J.R., Gutierrez-Alcala, G., Wray, J.L., Romero, L.C., and Gotor, C. (2003). The serine acetyltransferase gene family in *Arabidopsis thaliana* and the regulation of its expression by cadmium. Plant Mol Biol *51*, 589-598.

Huang, B., Vetting, M.W., and Roderick, S.L. (2005). The Active Site of *O*-Acetylserine Sulfhydrylase Is the Anchor Point for Bienzyme Complex Formation with Serine Acetyltransferase. Journal of Bacteriology *187*, 3201-3205.

Hunter, K.J., Le Quesne, S.A., and Fairlamb, A.H. (1994). Identification and biosynthesis of N1,N9-bis(glutathionyl)aminopropylcadaverine (homotrypanothione) in *Trypanosoma cruzi*. Eur J Biochem *226*, 1019-1027.

Husain, A., Jeelani, G., Sato, D., and Nozaki, T. (2011). Global analysis of gene expression in response to L-Cysteine deprivation in the anaerobic protozoan parasite *Entamoeba histolytica*. BMC Genomics *12*, 275.

Jha, T.K. (1983). Evaluation of diamidine compound (pentamidine isethionate) in the treatment resistant cases of kala-azar occurring in North Bihar, India. Trans R Soc Trop Med Hyg *77*, 167-170.

Jha, T.K., Sundar, S., Thakur, C.P., Felton, J.M., Sabin, A.J., and Horton, J. (2005). A phase II dose-ranging study of sitamaquine for the treatment of visceral leishmaniasis in India. Am J Trop Med Hyg *73*, 1005-1011.

Jiang, Y., Roberts, S.C., Jardim, A., Carter, N.S., Shih, S., Ariyanayagam, M., Fairlamb, A.H., and Ullman, B. (1999). Ornithine decarboxylase gene deletion mutants of *Leishmania donovani*. J Biol Chem *274*, 3781-3788.

Jovanovic, Z., and Jovanovic, S. (2013). Comparison of the effects of cumene hydroperoxide and hydrogen peroxide on Retzius nerve cells of the leech *Haemopis sanguisuga*. Exp Anim *62*, 9-17.

Kabra, P.M., Lee, H.K., Lubich, W.P., and Marton, L.J. (1986). Solid-phase extraction and determination of dansyl derivatives of unconjugated and acetylated polyamines by reversed-phase liquid chromatography: improved separation systems for polyamines in cerebrospinal fluid, urine and tissue. J Chromatogr *380*, 19-32.

Kamhawi, S. (2006). Phlebotomine sand flies and *Leishmania* parasites: friends or foes? Trends Parasitol *22*, 439-445.

Kandpal, M., and Tekwani, B.L. (1997). Polyamine transport systems of *Leishmania donovani* promastigotes. Life Sci *60*, 1793-1801.

Kaur, K., Emmett, K., McCann, P.P., Sjoerdsma, A., and Ullman, B. (1986). Effects of DL-alpha-difluoromethylornithine on *Leishmania donovani* promastigotes. J Protozool *33*, 518-521.

Kawashima, C.G., Noji, M., Nakamura, M., Ogra, Y., Suzuki, K.T., and Saito, K. (2004). Heavy metal tolerance of transgenic tobacco plants over-expressing cysteine synthase. Biotechnol Lett *26*, 153-157.

Kaye, P., and Scott, P. (2011). Leishmaniasis: complexity at the host-pathogen interface. Nat Rev Microbiol *9*, 604-615.

Krauth-Siegel, R.L., and Comini, M.A. (2008). Redox control in trypanosomatids, parasitic protozoa with trypanothione-based thiol metabolism. Biochim Biophys Acta *1780*, 1236-1248.

Krauth-Siegel, R.L., and Leroux, A.E. (2012). Low-molecular-mass antioxidants in parasites. Antioxid Redox Signal *17*, 583-607.

Kredich, N.M., Becker, M.A., and Tomkins, G.M. (1969). Purification and characterization of cysteine synthetase, a bifunctional protein complex, from *Salmonella typhimurium*. J Biol Chem *244*, 2428-2439.

Kredich, N.M., and Tomkins, G.M. (1966). The Enzymic Synthesis of l-Cysteine in Escherichia coli and *Salmonella typhimurium*. Journal of Biological Chemistry *241*, 4955-4965.

Kulshrestha, A., Bhandari, V., Mukhopadhyay, R., Ramesh, V., Sundar, S., Maes, L., Dujardin, J.C., Roy, S., and Salotra, P. (2013). Validation of a simple resazurin-based promastigote assay for the routine monitoring of miltefosine susceptibility in clinical isolates of *Leishmania donovani*. Parasitol Res *112*, 825-828.

Kumar, S., Raj, I., Nagpal, I., Subbarao, N., and Gourinath, S. (2011). Structural and biochemical studies of serine acetyltransferase reveal why the parasite *Entamoeba histolytica* cannot form a cysteine synthase complex. J Biol Chem *286*, 12533-12541.

Kumaran, S., and Jez, J.M. (2007). Thermodynamics of the interaction between *O*-acetylserine sulfhydrylase and the C-terminus of serine acetyltransferase. Biochemistry *46*, 5586-5594.

Laemmli, U.K. (1970). Cleavage of structural proteins during the assembly of the head of bacteriophage T4. Nature *227*, 680-685.

Ledent, P., Duez, C., Vanhove, M., Lejeune, A., Fonzé, E., Charlier, P., Rhazi-Filali, F., Thamm, I., Guillaume, G., Samyn, B., *et al.* (1997). Unexpected influence of a C-terminal-fused His-tag on the processing of an enzyme and on the kinetic and folding parameters. FEBS Letters *413*, 194-196.

Legare, D., Richard, D., Mukhopadhyay, R., Stierhof, Y.D., Rosen, B.P., Haimeur, A., Papadopoulou, B., and Ouellette, M. (2001). The *Leishmania* ATP-binding cassette protein PGPA is an intracellular metal-thiol transporter ATPase. J Biol Chem *276*, 26301-26307.

Lin, Y.C., Hsu, J.Y., Chiang, S.C., and Lee, S.T. (2005). Distinct overexpression of cytosolic and mitochondrial tryparedoxin peroxidases results in preferential detoxification of different oxidants in arsenite-resistant *Leishmania amazonensis* with and without DNA amplification. Mol Biochem Parasitol *142*, 66-75.

Livak, K., and Schmittgen, T. (2001). Analysis of relative gene expression datausinf real-time quantitative PCR and the 2-DDCT method. Applied Biosystems Methods, 402-408.

Lopez-Martin, C., Perez-Victoria, J.M., Carvalho, L., Castanys, S., and Gamarro, F. (2008). Sitamaquine sensitivity in *Leishmania* species is not mediated by drug accumulation in acidocalcisomes. Antimicrob Agents Chemother *52*, 4030-4036.

Mandal, G., Wyllie, S., Singh, N., Sundar, S., Fairlamb, A.H., and Chatterjee, M. (2007). Increased levels of thiols protect antimony unresponsive *Leishmania donovani* field isolates against reactive oxygen species generated by trivalent antimony. Parasitology *134*, 1679-1687.

Martinez-Calvillo, S., Vizuet-de-Rueda, J.C., Florencio-Martinez, L.E., Manning-Cela, R.G., and Figueroa-Angulo, E.E. (2010). Gene expression in trypanosomatid parasites. J Biomed Biotechnol *2010*, 525241.

McCall, L.I., Zhang, W.W., and Matlashewski, G. (2013). Determinants for the development of visceral leishmaniasis disease. PLoS Pathog *9*, e1003053.

McConville, M.J., de Souza, D., Saunders, E., Likic, V.A., and Naderer, T. (2007). Living in a phagolysosome; metabolism of *Leishmania amastigotes*. Trends Parasitol *23*, 368-375.

Meier, M., Janosik, M., Kery, V., Kraus, J.P., and Burkhard, P. (2001). Structure of human cystathionine beta-synthase: a unique pyridoxal 5'-phosphate-dependent heme protein. EMBO J *20*, 3910-3916.

Mikus, J., and Steverding, D. (2000). A simple colorimetric method to screen drug cytotoxicity against *Leishmania* using the dye Alamar Blue. Parasitol Int *48*, 265-269.

Miles, E.W., and Kraus, J.P. (2004). Cystathionine beta-synthase: structure, function, regulation, and location of homocystinuria-causing mutations. J Biol Chem *279*, 29871-29874.

Milman, N., Motyka, S.A., Englund, P.T., Robinson, D., and Shlomai, J. (2007). Mitochondrial origin-binding protein UMSBP mediates DNA replication and segregation in trypanosomes. Proc Natl Acad Sci U S A *104*, 19250-19255.

Mino, K., Hiraoka, K., Imamura, K., Sakiyama, T., Eisaki, N., Matsuyama, A., and Nakanishi, K. (2000a). Characteristics of serine acetyltransferase from *Escherichia coli* deleting different lengths of amino acid residues from the C-terminus. Biosci Biotechnol Biochem *64*, 1874-1880.

Mino, K., and Ishikawa, K. (2003). Characterization of a novel thermostable *O*-acetylserine sulfhydrylase from *Aeropyrum pernix* K1. J Bacteriol *185*, 2277-2284.

Mino, K., Yamanoue, T., Sakiyama, T., Eisaki, N., Matsuyama, A., and Nakanishi, K. (2000b). Effects of bienzyme complex formation of cysteine synthetase from *Escherichia coli* on some properties and kinetics. Biosci Biotechnol Biochem *64*, 1628-1640.

Mishra, B.B., Singh, R.K., Srivastava, A., Tripathi, V.J., and Tiwari, V.K. (2009). Fighting against Leishmaniasis: search of alkaloids as future true potential anti-Leishmanial agents. Mini Rev Med Chem *9*, 107-123.

Mittal, M.K., Rai, S., Ashutosh, Ravinder, Gupta, S., Sundar, S., and Goyal, N. (2007). Characterization of natural antimony resistance in *Leishmania donovani* isolates. Am J Trop Med Hyg *76*, 681-688.

Mizuno, Y., Miyashita, Y., Yamagata, S., Iwama, T., and Akamatsu, T. (2002). Cysteine synthase of an extremely thermophilic bacterium, *Thermus thermophilus* HB8. Biosci Biotechnol Biochem *66*, 549-557.

Moreira, N., Vitoriano-Souza, J., Roatt, B.M., Vieira, P.M., Ker, H.G., de Oliveira Cardoso, J.M., Giunchetti, R.C., Carneiro, C.M., de Lana, M., and Reis, A.B. (2012). Parasite burden in hamsters infected with two different strains of *Leishmania* (*Leishmania*) *infantum*: "Leishman Donovan units" versus real-time PCR. PLoS One *7*, e47907.

Mukhopadhyay, R., Dey, S., Xu, N., Gage, D., Lightbody, J., Ouellette, M., and Rosen, B.P. (1996). Trypanothione overproduction and resistance to antimonials and arsenicals in *Leishmania*. Proc Natl Acad Sci U S A *93*, 10383-10387.

Muller, S., Liebau, E., Walter, R.D., and Krauth-Siegel, R.L. (2003). Thiol-based redox metabolism of protozoan parasites. Trends Parasitol *19*, 320-328.

Müller, S., Wittich, R.-M., and Walter, R.D. (1988). The Polyamine Metabolism of Filarial Worms as Chemotherapeutic Target. In Progress in Polyamine Research, V. Zappia, and A. Pegg, eds. (Springer US), pp. 737-743.

Myler, J., Fasel, N. (2008). *Leishmania* - After the Genome (Caister Academic Press).

Naderer, T., and McConville, M.J. (2008). The *Leishmania*-macrophage interaction: a metabolic perspective. Cell Microbiol *10*, 301-308.

Nozaki, T., Asai, T., Kobayashi, S., Ikegami, F., Noji, M., Saito, K., and Takeuchi, T. (1998). Molecular cloning and characterization of the genes encoding two isoforms of cysteine synthase in the enteric protozoan parasite *Entamoeba histolytica*. Mol Biochem Parasitol *97*, 33-44.

Nozaki, T., Asai, T., Sanchez, L.B., Kobayashi, S., Nakazawa, M., and Takeuchi, T. (1999). Characterization of the gene encoding serine acetyltransferase, a regulated enzyme of cysteine biosynthesis from the protist parasites *Entamoeba histolytica* and *Entamoeba dispar*. Regulation and possible function of the cysteine biosynthetic pathway in Entamoeba. J Biol Chem *274*, 32445-32452.

Nozaki, T., Shigeta, Y., Saito-Nakano, Y., Imada, M., and Kruger, W.D. (2001). Characterization of transsulfuration and cysteine biosynthetic pathways in the protozoan hemoflagellate, *Trypanosoma cruzi*. Isolation and molecular characterization of cystathionine beta-synthase and serine acetyltransferase from *Trypanosoma*. J Biol Chem *276*, 6516-6523.

Oda, Y., Mino, K., Ishikawa, K., and Ataka, M. (2005). Three-dimensional structure of a new enzyme, *O*-phosphoserine sulfhydrylase, involved in l-cysteine biosynthesis by a hyperthermophilic archaeon, *Aeropyrum pernix* K1, at 2.0A resolution. J Mol Biol *351*, 334-344.

Olenyik, T., Gilroy, C., and Ullman, B. (2011). Oral putrescine restores virulence of ornithine decarboxylase-deficient *Leishmania donovani* in mice. Mol Biochem Parasitol *176*, 109-111.

Olsen, L.R., Huang, B., Vetting, M.W., and Roderick, S.L. (2004). Structure of serine acetyltransferase in complexes with CoA and its cysteine feedback inhibitor. Biochemistry *43*, 6013-6019.

Onn, I., Milman-Shtepel, N., and Shlomai, J. (2004). Redox potential regulates binding of universal minicircle sequence binding protein at the kinetoplast DNA replication origin. Eukaryot Cell *3*, 277-287.

Ott, K.J., Hanson, W.L., and Stauber, L.A. (1967). Course of infection of *Leishmania donovani* in hamsters inoculated by the intraperitoneal route. J Parasitol *53*, 641-645.

Oza, S.L., Shaw, M.P., Wyllie, S., and Fairlamb, A.H. (2005). Trypanothione biosynthesis in *Leishmania major*. Mol Biochem Parasitol *139*, 107-116.

Peacock, C.S., Seeger, K., Harris, D., Murphy, L., Ruiz, J.C., Quail, M.A., Peters, N., Adlem, E., Tivey, A., Aslett, M., *et al.* (2007). Comparative genomic analysis of three *Leishmania* species that cause diverse human disease. Nat Genet *39*, 839-847.

Perez-Victoria, F.J., Sanchez-Canete, M.P., Seifert, K., Croft, S.L., Sundar, S., Castanys, S., and Gamarro, F. (2006). Mechanisms of experimental resistance of *Leishmania* to miltefosine: Implications for clinical use. Drug Resist Updat *9*, 26-39.

Pham, T.T., Loiseau, P.M., and Barratt, G. (2013). Strategies for the design of orally bioavailable antileishmanial treatments. Int J Pharm *454*, 539-552.

Pompella, A., Visvikis, A., Paolicchi, A., De Tata, V., and Casini, A.F. (2003). The changing faces of glutathione, a cellular protagonist. Biochem Pharmacol *66*, 1499-1503.

Poulin, R., Lu, L., Ackermann, B., Bey, P., and Pegg, A.E. (1992). Mechanism of the irreversible inactivation of mouse ornithine decarboxylase by alpha-difluoromethylornithine. Characterization of sequences at the inhibitor and coenzyme binding sites. J Biol Chem *267*, 150-158.

Poyraz, O., Jeankumar, V.U., Saxena, S., Schnell, R., Haraldsson, M., Yogeeswari, P., Sriram, D., and Schneider, G. (2013). Structure-guided design of novel thiazolidine inhibitors of *O*-acetyl serine sulfhydrylase from *Mycobacterium tuberculosis*. J Med Chem *56*, 6457-6466.

Rai, S., Bhaskar, Goel, S.K., Nath Dwivedi, U., Sundar, S., and Goyal, N. (2013). Role of Efflux Pumps and Intracellular Thiols in Natural Antimony Resistant Isolates of *Leishmania donovani*. PLoS One *8*, e74862.

Raj, I., Kumar, S., and Gourinath, S. (2012). The narrow active-site cleft of O-acetylserine sulfhydrylase from *Leishmania donovani* allows complex formation with serine acetyltransferases with a range of C-terminal sequences. Acta Crystallogr D Biol Crystallogr *68*, 909-919.

Reguera, R.M., Balana-Fouce, R., Showalter, M., Hickerson, S., and Beverley, S.M. (2009). *Leishmania major* lacking arginase (ARG) are auxotrophic for polyamines but retain infectivity to susceptible BALB/c mice. Mol Biochem Parasitol *165*, 48-56.

Renslo, A.R., and McKerrow, J.H. (2006). Drug discovery and development for neglected parasitic diseases. Nat Chem Biol *2*, 701-710.

Roberts, S.C., Jiang, Y., Jardim, A., Carter, N.S., Heby, O., and Ullman, B. (2001). Genetic analysis of spermidine synthase from *Leishmania donovani*. Mol Biochem Parasitol *115*, 217-226.

Rojas-Chaves, M., Hellmund, C., and Walter, R.D. (1996). Identification of N-acetylspermidine in *Leishmania amazonensis*. Mol Biochem Parasitol *75*, 261-264.

Sakthianandeswaren, A., Foote, S.J., and Handman, E. (2009). The role of host genetics in leishmaniasis. Trends Parasitol *25*, 383-391.

Salsi, E., Bayden, A.S., Spyrakis, F., Amadasi, A., Campanini, B., Bettati, S., Dodatko, T., Cozzini, P., Kellogg, G.E., Cook, P.F., *et al.* (2009). Design of O-Acetylserine Sulfhydrylase Inhibitors by Mimicking Nature. Journal of Medicinal Chemistry *53*, 345-356.

Salsi, E., Campanini, B., Bettati, S., Raboni, S., Roderick, S.L., Cook, P.F., and Mozzarelli, A. (2010). A two-step process controls the formation of the bienzyme cysteine synthase complex. J Biol Chem *285*, 12813-12822.

Sangraula, H., Sharma, K.K., Rijal, S., Dwivedi, S., and Koirala, S. (2003). Orally effective drugs for kala-azar (visceral leishmaniasis): focus on miltefosine and sitamaquine. J Assoc Physicians India *51*, 686-690.

Schnell, R., Oehlmann, W., Singh, M., and Schneider, G. (2007). Structural Insights into Catalysis and Inhibition of *O*-Acetylserine Sulfhydrylase from *Mycobacterium tuberculosis*: crystal structures of the enzyme α-aminoacrylate intermediate and an enzyme-inhibitor complex. Journal of Biological Chemistry *282*, 23473-23481.

Segel, I. (1993). Enzyme kinetics (Wiley Classics Library).

Seifert, K., Escobar, P., and Croft, S.L. (2010). In vitro activity of anti-leishmanial drugs against *Leishmania donovani* is host cell dependent. J Antimicrob Chemother *65*, 508-511.

Seifert, K., Matu, S., Javier Perez-Victoria, F., Castanys, S., Gamarro, F., and Croft, S.L. (2003). Characterisation of *Leishmania donovani* promastigotes resistant to hexadecylphosphocholine (miltefosine). Int J Antimicrob Agents *22*, 380-387.

Shim, H., and Fairlamb, A.H. (1988). Levels of polyamines, glutathione and glutathione-spermidine conjugates during growth of the insect trypanosomatid *Crithidia fasciculata*. J Gen Microbiol *134*, 807-817.

Singh, N., Almeida, R., Kothari, H., Kumar, P., Mandal, G., Chatterjee, M., Venkatachalam, S., Govind, M.K., Mandal, S.K., and Sundar, S. (2007). Differential gene expression analysis in antimony-unresponsive Indian kala azar (visceral leishmaniasis) clinical isolates by DNA microarray. Parasitology *134*, 777-787.

Singh, N., Kumar, M., and Singh, R.K. (2012). Leishmaniasis: current status of available drugs and new potential drug targets. Asian Pac J Trop Med *5*, 485-497.

Smirnova, G.V., and Oktyabrsky, O.N. (2005). Glutathione in bacteria. Biochemistry (Mosc) *70*, 1199-1211.

Smith, P.K., Krohn, R.I., Hermanson, G.T., Mallia, A.K., Gartner, F.H., Provenzano, M.D., Fujimoto, E.K., Goeke, N.M., Olson, B.J., and Klenk, D.C. (1985). Measurement of protein using bicinchoninic acid. Anal Biochem *150*, 76-85.

Stauch, A., Duerr, H.P., Dujardin, J.C., Vanaerschot, M., Sundar, S., and Eichner, M. (2012). Treatment of visceral leishmaniasis: model-based analyses on the spread of antimony-resistant *L. donovani* in Bihar, India. PLoS Negl Trop Dis *6*, e1973.

Sundar, S. (2001). Drug resistance in Indian visceral leishmaniasis. Trop Med Int Health *6*, 849-854.

Sundar, S., Arora, R., Singh, S.P., Boelaert, M., and Varghese, B. (2010). Household cost-of-illness of visceral leishmaniasis in Bihar, India. Trop Med Int Health *15 Suppl 2*, 50-54.

Sundar, S., and Chatterjee, M. (2006). Visceral leishmaniasis - current therapeutic modalities. Indian J Med Res *123*, 345-352.

Sundar, S., Jha, T.K., Thakur, C.P., Bhattacharya, S.K., and Rai, M. (2006). Oral miltefosine for the treatment of Indian visceral leishmaniasis. Trans R Soc Trop Med Hyg *100 Suppl 1*, S26-33.

Tai, C.H., Nalabolu, S.R., Jacobson, T.M., Minter, D.E., and Cook, P.F. (1993). Kinetic mechanisms of the A and B isozymes of *O*-acetylserine sulfhydrylase from *Salmonella typhimurium* LT-2 using the natural and alternative reactants. Biochemistry *32*, 6433-6442.

Thakur, C.P., Dedet, J.P., Narain, S., and Pratlong, F. (2001). *Leishmania* species, drug unresponsiveness and visceral leishmaniasis in Bihar, India. Trans R Soc Trop Med Hyg *95*, 187-189.

Thakur, C.P., Kanyok, T.P., Pandey, A.K., Sinha, G.P., Messick, C., and Olliaro, P. (2000). Treatment of visceral leishmaniasis with injectable paromomycin (aminosidine). An open-label randomized phase-II clinical study. Trans R Soc Trop Med Hyg *94*, 432-433.

Thomas, D., and Surdin-Kerjan, Y. (1997). Metabolism of sulphur amino acids in *Saccharomyces cerevisiae*. Microbiol Mol Biol Rev *61*, 503-532.

Tovar, J., Cunningham, M.L., Smith, A.C., Croft, S.L., and Fairlamb, A.H. (1998a). Down-regulation of *Leishmania donovani* trypanothione reductase

by heterologous expression of a trans-dominant mutant homologue: effect on parasite intracellular survival. Proc Natl Acad Sci U S A *95*, 5311-5316.

Tovar, J., Wilkinson, S., Mottram, J.C., and Fairlamb, A.H. (1998b). Evidence that trypanothione reductase is an essential enzyme in *Leishmania* by targeted replacement of the *tryA* gene locus. Mol Microbiol *29*, 653-660.

Wang, T., and Leyh, T.S. (2012). Three-stage assembly of the cysteine synthase complex from *Escherichia coli*. J Biol Chem *287*, 4360-4367.

Warrilow, A.G., and Hawkesford, M.J. (2002). Modulation of cyanoalanine synthase and *O*-acetylserine (thiol) lyases A and B activity by beta-substituted alanyl and anion inhibitors. J Exp Bot *53*, 439-445.

Weldrick, D.P., Chodacka, B., Vogt, R., and Steenkamp, D.J. (1999). The effect of buthionine sulfoximine on the growth of *Leishmania donovani* in culture. FEMS Microbiol Lett *173*, 139-146.

Westrop, G.D., Goodall, G., Mottram, J.C., and Coombs, G.H. (2006). Cysteine Biosynthesis in *Trichomonas vaginalis* Involves Cysteine Synthase Utilizing *O*-Phosphoserine. Journal of Biological Chemistry *281*, 25062-25075.

WHO. WHO (World Health Organization) Web site on leishmanisis. Last assessed 27 November 2013.

Wilkinson, S.R., Horn, D., Prathalingam, S.R., and Kelly, J.M. (2003). RNA interference identifies two hydroperoxide metabolizing enzymes that are essential to the bloodstream form of the african trypanosome. J Biol Chem *278*, 31640-31646.

Willert, E.K., and Phillips, M.A. (2008). Regulated expression of an essential allosteric activator of polyamine biosynthesis in African trypanosomes. PLoS Pathog *4*, e1000183.

Williams, R., Westrop, G., and Coombs, G. (2009). Two pathways for cysteine biosynthesis in *Leishmania major*. Biochemical Journal 420.

Williams, R.A., Kelly, S.M., Mottram, J.C., and Coombs, G.H. (2003). 3-Mercaptopyruvate sulfurtransferase of *Leishmania* contains an unusual C-terminal extension and is involved in thioredoxin and antioxidant metabolism. J Biol Chem *278*, 1480-1486.

Wirtz, M., Beard, K.F., Lee, C.P., Boltz, A., Schwarzlander, M., Fuchs, C., Meyer, A.J., Heeg, C., Sweetlove, L.J., Ratcliffe, R.G., *et al.* (2012). Mitochondrial cysteine synthase complex regulates *O*-acetylserine biosynthesis in plants. J Biol Chem *287*, 27941-27947.

Wirtz, M., Berkowitz, O., Droux, M., and Hell, R. (2001). The cysteine synthase complex from plants. Mitochondrial serine acetyltransferase from *Arabidopsis thaliana* carries a bifunctional domain for catalysis and protein-protein interaction. Eur J Biochem *268*, 686-693.

Wirtz, M., and Droux, M. (2005). Synthesis of the sulphur amino acids: cysteine and methionine. Photosynth Res *86*, 345-362.

Wirtz, M., Droux, M., and Hell, R. (2004). *O*-acetylserine (thiol) lyase: an enigmatic enzyme of plant cysteine biosynthesis revisited in Arabidopsis thaliana. J Exp Bot *55*, 1785-1798.

Wirtz, M., and Hell, R. (2006). Functional analysis of the cysteine synthase protein complex from plants: structural, biochemical and regulatory properties. J Plant Physiol *163*, 273-286.

Wittich, R.M., Kilian, H.D., and Walter, R.D. (1987). Polyamine metabolism in filarial worms. Mol Biochem Parasitol *24*, 155-162.

Wyllie, S., Cunningham, M.L., and Fairlamb, A.H. (2004). Dual action of antimonial drugs on thiol redox metabolism in the human pathogen Leishmania donovani. J Biol Chem *279*, 39925-39932.

Wyllie, S., Mandal, G., Singh, N., Sundar, S., Fairlamb, A.H., and Chatterjee, M. (2010). Elevated levels of tryparedoxin peroxidase in antimony unresponsive *Leishmania donovani* field isolates. Mol Biochem Parasitol *173*, 162-164.

Wyllie, S., Patterson, S., Stojanovski, L., Simeons, F.R., Norval, S., Kime, R., Read, K.D., and Fairlamb, A.H. (2012). The anti-trypanosome drug fexinidazole shows potential for treating visceral leishmaniasis. Sci Transl Med *4*, 119re111.

Wyllie, S., Vickers, T.J., and Fairlamb, A.H. (2008). Roles of trypanothione S-transferase and tryparedoxin peroxidase in resistance to antimonials. Antimicrob Agents Chemother *52*, 1359-1365.

Zavodnik, I.B., Dremza, I.K., Cheshchevik, V.T., Lapshina, E.A., and Zamaraewa, M. (2013). Oxidative damage of rat liver mitochondria during exposure to *tert*-butyl hydroperoxide. Role of Ca(2)(+) ions in oxidative processes. Life Sci *92*, 1110-1117.

Zhao, C., Moriga, Y., Feng, B., Kumada, Y., Imanaka, H., Imamura, K., and Nakanishi, K. (2006). On the interaction site of serine acetyltransferase in the cysteine synthase complex from *Escherichia coli*. Biochem Biophys Res Commun *341*, 911-916.

Zocher, G., Wiesand, U., and Schulz, G.E. (2007). High resolution structure and catalysis of *O*-acetylserine sulfhydrylase isozyme B from *Escherichia coli*. FEBS J *274*, 5382-5389.